Perturbations to nutrient and carbon cycles by river damming

by

Taylor Maavara

A thesis
presented to the University of Waterloo
in fulfillment of the
thesis requirement for the degree of
Doctor of Philosophy
in
Earth Sciences (Water)

Waterloo, Ontario, Canada, 2017

Examining committee membership

The following served on the Examining Committee for this thesis. The decision of the Examining Committee is by majority vote.

External Examiner   Dr. Christiane Zarfl
                                     Assistant Professor

Supervisor   Dr. Philippe Van Cappellen
                                     Professor, Canada Excellence Research Chair

Co-supervisor   Dr. Hans Dürr
                                     Research Assistant Professor

Internal Member   Dr. Brian Kendall
                                     Assistant Professor

Internal-external Member   Dr. Merrin Macrae
                                     Associate Professor

Other Member(s)   Dr. Jens Hartmann
                                     Professor

AUTHOR'S DECLARATION

This thesis consists of material all of which I authored or co-authored: see Statement of Contributions included in the thesis. This is a true copy of the thesis, including any required final revisions, as accepted by my examiners.

I understand that my thesis may be made electronically available to the public.

Statement of Contributions

This thesis consists of a series of co-authored papers. As first author on each paper, I was primarily responsible for the study designs and execution. The following summarizes the contributions of the co-authors of each paper.

Chapter 2

I developed the research questions and performed the core PRSi extractions. I analyzed the data, with input from Jennifer L.A. Hood (JLAH), Chris T. Parsons (CTP), Lorne Doig (LD) and Rebecca North (RN). JLAH and I wrote the paper, with input from CTP, RN, LD, and Philippe Van Cappellen (PVC). All other authors conducted laboratory and/or field research, or provided feedback on data interpretation.

Chapter 3

PVC and I designed the research; I developed the model and performed all data analysis, with input from PVC and Hans H. Dürr (HHD), and PVC and I wrote the paper.

Chapter 4

PVC and I designed the research and the model. Helen R. Powley (HRP), CTP and I performed the literature review, Severin Stojanovic (SS) and I wrote the computer code, all authors analyzed model results, and PVC and I wrote the paper, with input from CTP.

Chapter 5

PVC and I designed the research questions and overall modelling approach. Ronny Lauerwald (RL) and I developed and coded the model, with input from PVC and Pierre Regnier (PR). All authors contributed to writing the paper.

Chapter 6

Zahra Akbarzadeh (ZA) and I developed the nitrogen model that generated results used in this chapter. PVC and I developed research questions and I performed the data analysis and wrote the paper, with input from PVC.

Abstract

The damming of rivers represents one of the most far-reaching human modifications to the flows of water and associated matter from land to sea. Globally there are over 70 000 large dams whose reservoirs store more than seven times as much water as natural rivers. Due to increasing demands for energy, irrigation, drinking water, and flood control, the construction of dams will continue into the foreseeable future. Indeed, there is currently an ongoing boom in dam construction, particularly focused in emerging economies, which is expected to double the fragmentation of rivers on Earth. Essential nutrient elements such as phosphorus (P), nitrogen (N), silicon (Si), and carbon (C) are transported and transformed along the land-ocean aquatic continuum (LOAC), forming the basis for freshwater food webs in lakes, rivers, wetlands, reservoirs, and floodplains, and ultimately for marine food webs in estuarine and coastal environments. The dam-driven fragmentation of the rivers along the LOAC will significantly modify global nutrient and C fluxes via elimination from the water column in reservoirs.

In this thesis, I quantify in-reservoir elimination and transformation fluxes for phosphorus (P), silicon (Si), and organic carbon (OC), with the goal of determining (1) how much Si, P, and organic C (OC) are retained or eliminated globally due to river damming, (2) how damming modifies the balance of productivity (heterotrophy vs. autotrophy) in river systems worldwide, (3) to what extent damming changes nutrient speciation or reactivity along the LOAC, and (4) if reservoirs retain or eliminate certain nutrients more efficiently than others, and if so, how this decoupling changes nutrient ratios delivered to coastal zones. I address these research questions at the reservoir scale, by quantifying nutrient elimination in Lake Diefenbaker, Saskatchewan, and through the development of spatially explicit global nutrient and carbon models.

In Chapter 2, I present a reservoir-scale field study of reactive silicon dynamics in Lake Diefenbaker, a reservoir in Canada's central prairie province of Saskatchewan. I use a year-round dataset of surface water samples and sediment cores to construct a Si budget for the reservoir, including an estimation of the amount of Si buried in the reservoir annually. I use this study to illustrate the differences in retention of Si relative to N and P, and put forth the hypothesis that river damming results in a decoupling of nutrient cycling. This study acts as an introduction to the concept of differential nutrient retention in reservoirs, which I go on to show at the global scale for Si, P, and C in reservoirs in Chapters 3, 4, and 5.

Following Chapter 2, I address my research questions by developing a mechanistic approach to global scale biogeochemical modelling. This approach yields spatially explicit results, which allows for the quantification of regional watershed and coastal trends, as well as lumped continental changes. In Chapter 3, the modelling approach itself is introduced, through application to the Si cycle. I show, via a meta-analysis comparing the distribution of physical and chemical parameters of published reservoir Si budgets to reservoirs worldwide, that the existing literature Si budgets are severely limited in their ability to represent the dataset of global reservoirs. I then introduce the mechanistic approach by developing a biogeochemical box model representing Si dynamics in reservoirs. I assign rate expressions to transformation fluxes and input/output fluxes, which are constrained as uniform distributions between limits that encapsulate possible global ranges. Using a Monte Carlo approach, I allow the model to randomly select each rate constant independently for 6000 iterations, generating a database of hypothetical Si dynamics in reservoirs worldwide. I use this generated dataset to establish expressions relating Si retention to water residence time, which I apply to an existing database of global reservoirs. Ultimately I develop a global estimate of dissolved and reactive Si burial in reservoirs for year 2000.

Chapters 4 and 5 use the same modelling approach presented in Chapter 3, but applied to riverine P and organic carbon (OC) fluxes. Because the cycles of P and OC have been studied in more detail than Si in the literature, it is possible to constrain higher order probability density functions (PDFs) for many rate constants. In the case of OC, it also becomes possible to use a statistically significant semi-empirical approach to calculate a number of fluxes, as expressions to predict OC dynamics have been established from globally applicable datasets. Using the upstream-catchment area-normalized Global-NEWS model's watershed yields as input to each reservoir, I use the 1970, 2000, 2030 and 2050 model predictions to estimate historical and predict future P and OC elimination by dams. In Chapter 4, I show that damming retains 12% of the global total P load to watersheds in year 2000, potentially rising to 17% by 2030. In Chapter 5, I show that global OC mineralization in reservoirs exceeds carbon fixation ($P<R$); the global P/R ratio, however, varies significantly, from 0.20 to 0.58 because of the changing age distribution of dams. I further estimate that at the start of the 21st Century, in-reservoir burial plus mineralization eliminated 4.0 ± 0.9 Tmol yr^{-1} (48 ± 11 Tg C yr^{-1}) or 13% of total OC carried by rivers to the oceans. Because of the ongoing boom in dam building, in particular in emerging economies, this value could rise to 6.9 ± 1.5 Tmol yr^{-1} (83 ± 18 Tg C yr^{-1}) or 19% by 2030.

Chapter 6 ties the previous global scale P and Si model together, plus a global scale N model (Akbarzadeh et al., in preparation), to predict changes to nutrient ratios delivered by rivers to the coastal zones. I use this analysis, in combination with anthropogenic nutrient loading data, to contextualize the role of river damming as a driver of changing nutrient limitation in the coastal shelf zones of the world. Results indicate that dams preferentially eliminate P over Si, and Si over N, from the water column. I show that while damming drives riverine N:P ratios up, anthropogenic nutrient loading is shifting these ratios down, increasing the prominence of N-limitation in river water discharged to the coasts. Because of the preferential elimination of Si over N, the net rise in N-limitation increases the prominence of Si-limitation in coastal river discharge, potentially creating conditions suitable for harmful algal blooms to develop.

My results show that damming is driving a severe reorganization of global nutrient cycles along the entire LOAC. By quantifying the changes to multiple nutrient cycles, I show that a multi-nutrient management approach is needed in heavily dammed watersheds, as deliberate reduction of one nutrient species flux can have unintended consequences on other nutrient elements. These alterations persist from the reservoir to the river's discharge into coastal zones. The effects of damming on nutrient cycling, in combination with other human pressures and management strategies, therefore have the potential to affect ecosystems worldwide.

Acknowledgements

I am grateful to the Natural Sciences and Engineering Research Council of Canada (NSERC), Ontario Graduate Scholarships (OGS), and the University of Waterloo for funding this research.

I am indebted to Philippe Van Cappellen, my mentor and friend, who took me on as an undergraduate and taught me how to be a scientist. My PhD experience was consistently a joy, a challenge, and an endless series of new, exciting opportunities. I owe this to Philippe.

To my thesis committee and collaborators, thank you for your guidance and support, your criticism and your encouragement. Pierre Regnier and Ronny Lauerwald, thanks for many great discussions and your exceptional feedback. Thanks to Lorne Doig and Rebecca North for involving me in the Lake Diefenbaker project, and for your hard work and support with the silicon budget.

To my friends and colleagues in Ecohydrology and at UW, you are an outstanding community of scientists and researchers. I am especially grateful to Christina Smeaton, Chris Parsons, Sana Louie, Amanda Niederkorn, Radmila Kovac, Adrian Mellage, James Telford, Steph Slowinski, Fereidoun Rezanezhad, Kim Van Meter, Erin Jones, Jen Hood, Raoul-Marie Couture, Xu Zhang, Helen Powley, Zahra Akbarzadeh, Geertje Pronk, Marianne Vandergriendt, and Shuhuan Li. Thanks for great days in the field and lab, productive scientific discussions, after-work drinks, and office cardboard box forts. You have all helped me grow as a scientist.

To my climbing partners, thanks for keeping me focused and catching my falls (literal and figurative). Derek, Helen, Karn, Bharat, Sean, Paul, Katie, Wynona, and everyone else I have roped up with over the years, I couldn't have climbed this mountain without you. To Katharine and Danielle, thanks for sitting next to me on the train to Hogwarts.

Dedication

To my parents, for your unwavering support and guidance. Thank you for teaching me to appreciate both arts and sciences, for igniting my love of wilderness, which in turn drives my passion for environmental research, and for exemplifying how to work hard and live full lives.

To my brothers, Scott and Alec, for committing to your dreams in the most enthusiastic ways imaginable.

Table of Contents

xi

List of Figures

List of Tables

"The best thing for being sad," replied Merlyn, beginning to puff and blow, "is to learn something. That is the only thing that never fails. You may grow old and trembling in your anatomies, you may lie awake at night listening to the disorder of your veins, you may miss your only love, you may see the world about you devastated by evil lunatics, or know your honour trampled in the sewers of baser minds. There is only one thing for it then—to learn. Learn why the world wags and what wags it. That is the only thing which the mind can never exhaust, never alienate, never be tortured by, never fear or distrust, and never dream of regretting. Learning is the thing for you. Look at what a lot of things there are to learn—pure science, the only purity there is. You can learn astronomy in a lifetime, natural history in three, literature in six. And then, after you have exhausted a milliard lifetimes in biology and medicine and theocriticism and geography and history and economics—why, you can start to make a cartwheel out of the appropriate wood, or spend fifty years learning to begin to learn to beat your adversary at fencing. After that you can start again on mathematics, until it is time to learn to plough."

<div align="right">- T. H. White, The Once and Future King</div>

Chapter 1

Introduction

1.1 Rivers in the Anthropocene

Rivers are the great connectors of the freshwater cycle. They provide essential services to humans and ecosystems alike, including drinking water, transportation channels, food security, waste assimilation, water purification, and nutrient cycling. River systems have supported human settlements for millennia, since humans progressed from nomadism to sedentarism (P'yankova, 1994). Rivers and their associated riparian areas and floodplains harbour a plethora of habitats that sustain rich biodiversity. Essential nutrient elements such as phosphorus (P), nitrogen (N), silicon (Si), and carbon (C) are transported and transformed along the land to ocean aquatic continuum (LOAC), forming the basis for freshwater food webs in lakes, rivers, wetlands, impoundments, and floodplains, and ultimately for marine food webs in estuarine and coastal environments. The current geological era has been referred to as the Anthropocene due to the dramatic and irreversible changes made by humans to the Biogeosphere (Crutzen, 2006). Enhanced nutrient loading, river damming, channelization, urbanization, and land use change all alter river biogeochemistry. The resulting changes to nutrient fluxes along the LOAC are thus funneled throughout the global aquatic ecosystems with important consequences for water quality and ecosystem services. This thesis will focus on two modifications that seemingly have inverse effects on the magnitude of riverine nutrient fluxes: anthropogenic nutrient loading and river damming.

1.1.1 Nutrient enrichment

Humans have profoundly modified global riverine N and P fluxes, by increasing nutrient loading, primarily in the form of agricultural fertilizer and manure application, and wastewater discharge (Galloway et al., 2004; Meybeck, 1982; Ruttenberg, 2003). Increased nutrient loading can result in the development of eutrophic conditions in water bodies, with increases in algal growth and biomass, which may lead to the occurrence of harmful algal blooms (HABs). In their worst manifestation, HABs are characterized by the abundance of algal species that release harmful toxins, which result in fish, sea life, and occasionally, human mortality (Heisler et al., 2008). HABs and nuisance algal blooms tend to promote anoxia in bottom waters, due to aerobic bacterial decomposition of dead algae (Anderson et al., 2002). It is estimated that nearly every coastal nation, and virtually all nations with freshwater bodies, suffer from eutrophication to some degree (Anderson et al., 2008;

1

Hallegraeff, 1993; Smith et al., 2006). In the United States, coastal HABs alone have an estimated economic impact of $50 million USD annually (Anderson et al., 2000). With rising populations, and consequent agricultural intensification and wastewater production, nutrient loading to rivers continues to rise despite management efforts.

It is estimated that both N and P loads delivered to the coastal ocean have doubled or tripled since pre-Industrial times (Compton et al., 2000; Filippelli, 2002; Galloway et al., 2004). Carbon loads to river systems, meanwhile, have increased by approximately 70%, due largely to increased soil erosion following deforestation and land use changes (Houghton et al., 1999; Regnier et al., 2013). Riverine Si fluxes, comparatively, have decreased due to anthropogenic interference. Plants, including trees and crops, uptake Si, and are subsequently removed from the landscape due to deforestation or harvesting, thereby reducing the stores of reactive Si (Struyf et al., 2010).

Phytoplankton assimilate inorganic C, P and N according to the following generalized reaction for photosynthesis to generate soft tissue organic matter:

$$106 \; CO_2 + 16 \; NO_3^- + HPO_4^{2-} + 122 \; H_2O + 18 \; H^+ \rightarrow C_{106}H_{263}O_{110}N_{16}P + 138 \; O_2 \qquad (1.1)$$

The C:N:P ratio of 106:16:1 in the organic matter produced is called the Redfield ratio, and represents the average composition in most marine and many freshwater phytoplankton assemblages (Redfield, 1934; Teubner and Dokulil, 2002). If an aquatic system's N:P ratio is greater than 16:1, the system tends to be P-limited, and if N:P is below 16:1, N-limited. Existing research has shown that by reducing the load of the limiting nutrient, eutrophication can be mitigated, particularly if the bioavailable forms of the nutrient are reduced (Schindler, 1977; Schindler et al., 2008). The Redfield ratio has been expanded to include Si and is referred to as the Redfield-Brzezinski ratio. The C:N:P:Si ratio for photosynthesis is approximately 106:15:1:16 for marine diatoms and, for freshwater diatoms, varies between 106:15:1:14 and 106:15:1:84 (Brzezinski, 1985; Conley et al., 1989; Struyf et al., 2009). Due to these photosynthetic uptake ratios, the C, N, P and Si cycles are strongly coupled along the LOAC, particularly in unperturbed environments.

1.1.2 River damming

The damming of river systems has been ongoing for millennia, with the first dams built before 2000 BCE to store drinking and irrigation water in the Egyptian empire (ICOLD, 2007). Global dam construction continued steadily over time, but it was not until following the Second World War that humans began systematically damming rivers worldwide. This boom in dam construction peaked in

the 1960s and 1970s, with most dams built in North America, primarily Canada and the United States, and in Western Europe (Figure 1.1). Dams are built for one or more purposes, which include flood or ice control, hydropower generation, irrigation and drinking water supply, navigation, and recreation. In 2015, 16.6% of the world's electricity was generated by hydropower (REN21, 2016), while at the end of the 20th Century dam reservoirs supplied around 30-40% of irrigation water globally (WCD, 2000). A comprehensive list of ecosystem and societal services provided by river dams is summarized in Table 1.1.

We are currently in the midst of a second boom in dam construction, with over 3700 hydroelectric dams with generating capacities of 1 MW or greater planned or under construction worldwide (Zarfl et al., 2015). The total cost of these dam projects is estimated as around $2 trillion USD worldwide (Hermoso, 2017). There is a distinct geographic shift in the locations of these new dams compared with those constructed in the 20th century (Figure 1.1). South America, China, Southeast and Central Asia, and the Balkans emerge as the major hotspots for dam construction, largely driven by the need to reduce greenhouse gas emissions worldwide while simultaneously providing energy for growing economies. At present, hydroelectricity accounts for 80% of the energy produced by renewable sources, which together account for 20% of the global energy production (Zarfl et al., 2015). The 3700 new dams will increase the global hydroelectric generating capacity by 73%. Despite the anticipated reduction in greenhouse gas emissions provided by these dams, the consequences to freshwater and coastal ecosystems have the potential to be severe.

Freshwater ecosystems have been referred to as the "biggest losers" of the 2016 Paris Agreement on climate change, due to the global push to construct more dams to offset greenhouse gas emissions (Hermoso, 2017). Based on their River Fragmentation Index, Grill et al. (2015) estimate that following the current dam building boom, 93% of the rivers on Earth will be moderately to severely fragmented. One of the major consequences of damming is the homogenization of seasonally variable river flows and spatial differences along the LOAC (Poff et al., 2007). River biodiversity is directly related to flow heterogeneity, the reduction of which makes ecosystems more susceptible to pathogens, pests or subsequent disturbances, natural or otherwise (Landres et al., 1999). Declining fish populations, particularly salmon, is most often cited as a major consequence of river damming, due to the salmon's inability to return to its upstream spawning habitat (Kareiva et al., 2000). Following the completion of the planned dams on the Mekong, Congo, and Amazon River basins, up to a third of all freshwater fish species globally could become threatened (Winemiller et al., 2016).

Table 1.1: Positives and negatives of river damming.

Benefits of river damming	Perceived or potential negatives of damming
Flood control	Reduction in fish populations; fish species extinction
Ice control	Sediment accumulation and reservoir infilling
Drinking water storage	Evaporation and loss of water due to stagnation
Irrigation water storage	Flooding of sacred land and/or artifacts during reservoir infilling
Hydroelectricity production	Retention or elimination of nutrients from rivers
Transportation and trade channels	Increased seismic activity
Recreation	Increased prevalence of disease (e.g. schistosomiasis)
Aquaculture	Ecosystem fragmentation
Retention or elimination of nutrients	Flood risk, property damage if not maintained
Potential to settle transboundary water disputes	Increased greenhouse gas emissions in reservoirs
Potential to reduce the spread of invasive species (e.g. Asian carp, sea lamprey)	Forced relocation of local communities by dam construction
Increased job opportunities	Potential to galvanize transboundary water disputes
Construction of new infrastructure (e.g. roads)	Low economic rate of return on investment
Reduction of greenhouse gas emissions from energy production	Loss of fertile land
	Flooding of high quality timber
	Loss of revenue
	Cost overruns during construction (averaging 96%) are the norm and are usually shouldered by taxpayers (Ansar et al., 2014)
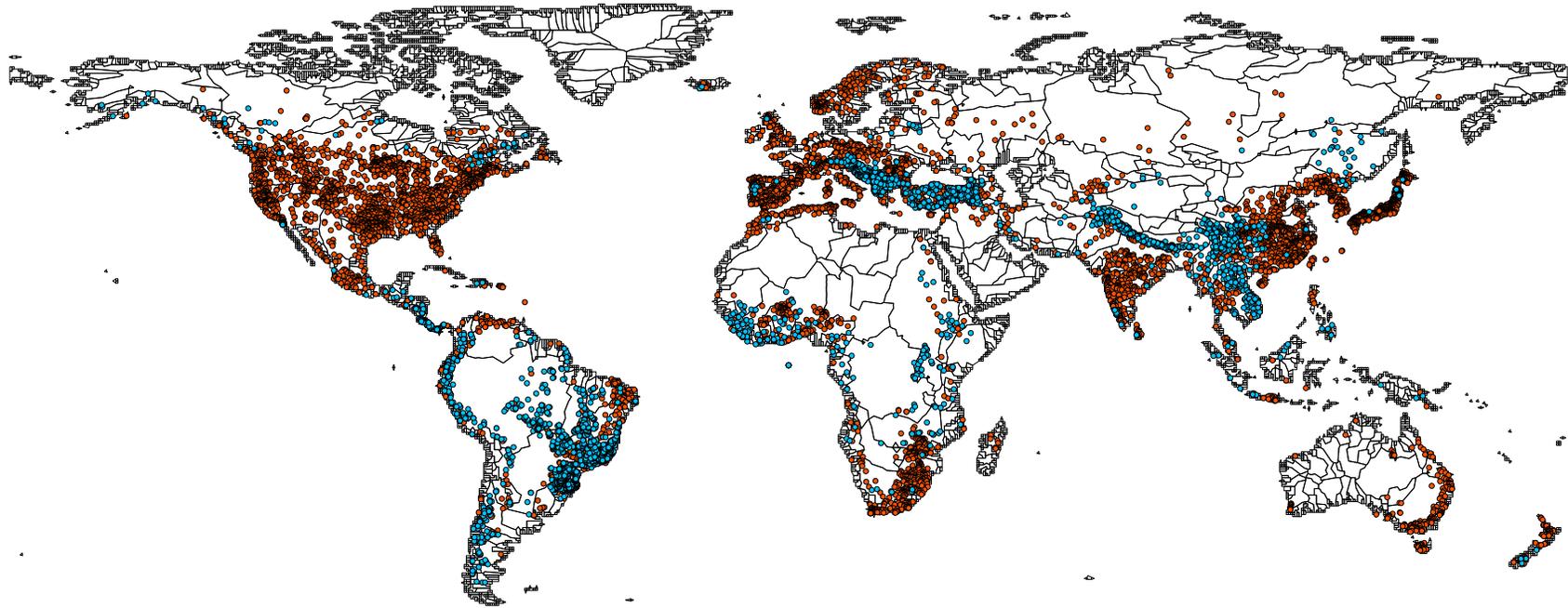
Figure 1.1: Existing dams (in red) and planned or under construction dams (in blue), according to the Global Reservoirs and Dams (GRanD) database (Lehner et al., 2011) and the database assembled by Zarfl et al. (2015). Grey lines indicate major watershed boundaries in STN-30p database (Fekete et al., 2001).

Flooding of formerly riparian or terrestrial ecosystems also results in species population decline, while often simultaneously promoting the propagation of unwanted or invasive species (McManus et al., 2010; Nilsson and Berggren, 2000).

1.2 Damming and biogeochemical cycling

This thesis focuses on quantifying the damming-driven modifications to the C, Si, P and, to a lesser extent, N cycles. By advancing our understanding of the large-scale impacts of dam construction on nutrient cycles, watershed managers may be able to take a step closer to responsible dam construction and operation. C and the macronutrients P and N serve as the basis for all life on Earth, while Si is an important auxiliary nutrient used primarily by plants, diatoms, radiolaria, and sponges. Undammed rivers act as conduits for nutrient transport from the continents to the oceans, with limited "vertical" fluxes such as burial or gas exchanges with the atmosphere (Cole et al., 2007). By installing a dam, the river's flow is impeded and the water residence time in the impounded reach lengthens. Water residence time, τ_r, is defined as:

$$\tau_r = \frac{V}{Q}$$
(1.2)

where V is the volume of the water body [L^3] and Q is the discharge or flow through the water body [$L^3 T^{-1}$]. A system that was previously fluvial in nature transitions to a more lentic environment, though typically retains fluvial properties and thus is not a typical lake (Figure 1.2).

Reservoirs typically display a continuum of fluvial-to-lentic hydrodynamics from their upstream to downstream zones, with upper reaches more turbid and shallower, and with lower water residence time and higher nutrient availability (Hayes et al., 2017; Thornton et al., 1996). Sediment and sediment-associated nutrient deposition takes place when a particle's sinking velocity exceeds the advective upwelling in the reservoir (Friedl and Wüest, 2002). In the fluvial portion of a reservoir, advective upwelling remains high and so particle settling and burial are minor. Moving downstream, the water residence time increases, advective upwelling decreases, and suspended sediment is deposited from the water column, reducing turbidity and increasing light availability, which, in turn, promotes biological productivity drawing down dissolved nutrient concentrations through assimilation into biomass. The lentic region of reservoirs close to dams therefore tends to have low turbidity, low nutrient availability, and high water residence times. Total reservoir nutrient retention or elimination, R_X, is calculated as:

$$R_X = \frac{(F_{in} - F_{out})}{F_{in}}$$
(1.3)

where F_{in} is the influx of nutrient X to the reservoir [M T^{-1}], F_{out} is the efflux through the dam [M T^{-1}] and R_X is a unitless value, usually less than 1.

Anthropogenic changes to nutrient loads operate in conjunction with losses from damming. Existing evidence suggests that in general in-reservoir elimination of P and N is relatively small compared with the magnitude of anthropogenic nutrient emissions to river systems, which would seem to suggest that river damming plays a relatively minor role in riverine nutrient fluxes. However, regional studies have shown that river damming can promote HABs in coastal ecosystems (Billen and Garnier, 2007; Conley et al., 1993; Humborg et al., 2000; Humborg et al., 1997). The current paradigm indicates that reservoirs eliminate bioavailable P, N, and Si from the water column through burial (and denitrification in the case of N), reducing the overall loads transported downstream. However, P and N are replaced through anthropogenic activities while Si, which has few anthropogenic sources, is not replenished, compounding anthropogenic Si removal from deforestation and agriculture (Struyf et al., 2010). The global P:Si and N:Si ratios delivered to coastal zones may therefore be significantly higher than in pre-human conditions. The Si-limiting conditions can result in diatoms being outcompeted by species more characteristic of HABs (Figure 1.3) (Billen et al., 1991). HABs arising from dam-driven Si-limitation have been observed in the Baltic Sea, and their drivers have been modeled for coastal zones globally (Garnier et al., 2010; Humborg et al., 2008). Given that diatoms account for up to a quarter of global primary productivity, and 40% of the primary productivity in the oceans (Buchan et al., 2014; Falkowski et al., 1998), this shift has the potential to greatly alter coastal oceanic food chains, and as a result, global carbon cycling (Tréguer and Pondaven, 2000).

The situation described in Figure 1.3 implies Si-excess as a desirable scenario in coastal ecosystems (Billen and Garnier, 2007; Billen et al., 1991; Garnier et al., 2010; Strokal et al., 2017). However, it is important to note that Si-excess may also lead to toxic diatom blooms. In the diatom genus *Pseudo-nitzschia*, more than a dozen species can produce the neurotoxin domoic acid (Fryxell et al., 1997). In 1987, three residents of Prince Edward Island, Canada, died due to ingestion of shellfish contaminated with domoic acid, which was found to originate from a bloom of *Pseudo-nitzschia multiseries* (Bates et al., 1989; Perl et al., 1990). The California coast has been a hotspot for *Pseudo-nitzschia* blooms since the 1920s (Fryxell et al., 1997), with recorded instances of sea lion mortality and sea bird poisoning (Bargu et al., 2012; Scholin et al., 2000). One such instance of

seagull domoic acid poisoning, characterized by thousands of birds pelting into buildings and the ground and regurgitating anchovies in Monterey, California, inspired Alfred Hitchcock to make the
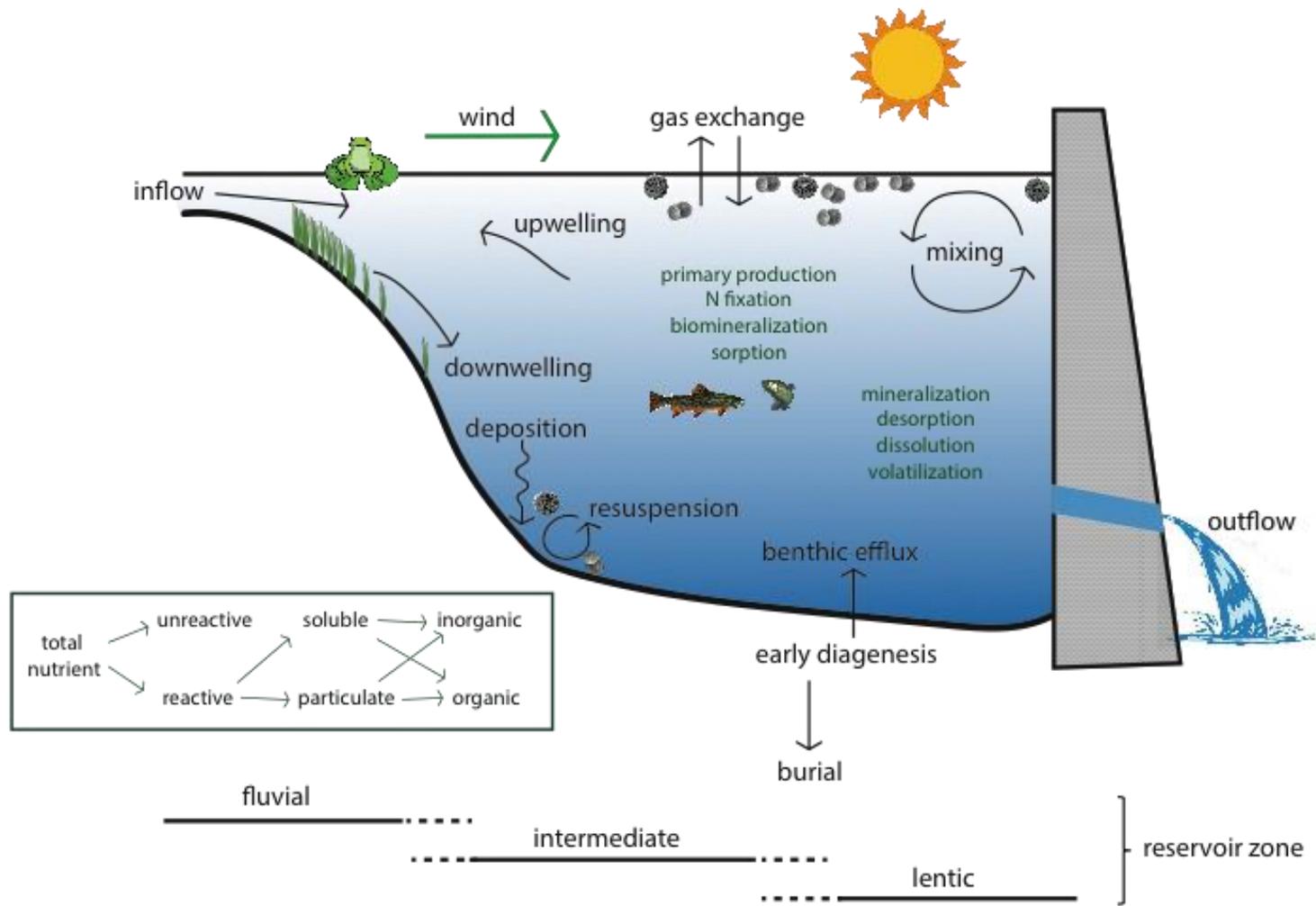
Figure 1.2: Generalized in-reservoir physical and biogeochemical processes. Modified from Van Cappellen and Maavara (2016).
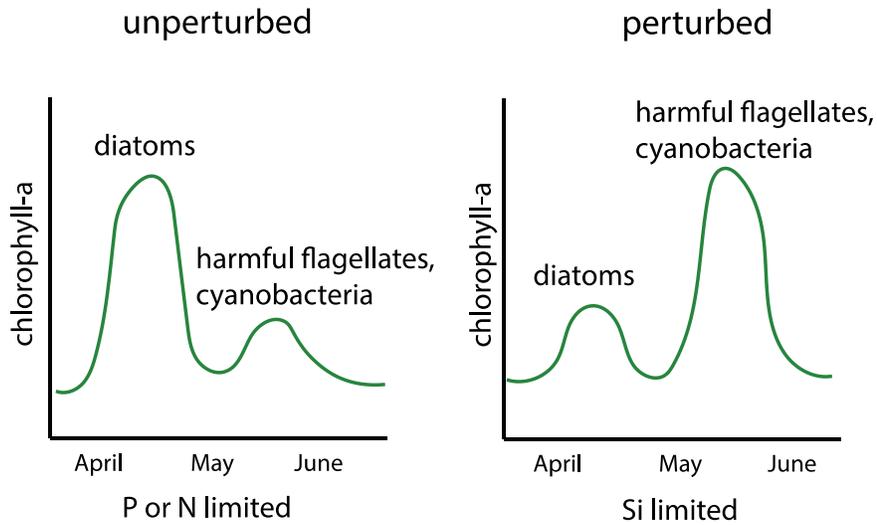
Figure 1.3: Typical coastal phytoplankton succession scenarios in temperate areas of the Northern Hemisphere, based on nutrient availability. In the unperturbed scenario, Si concentrations are in excess and spring diatom populations reduce P and N concentrations, preventing subsequent harmful flagellate or cyanobacteria blooms later in the year. In the perturbed scenario, Si concentrations are limiting to diatoms: sufficient N and P concentrations remain following the diatom bloom for a HAB to form in late spring or early summer. Modified from Billen et al. (1991).

film *The Birds* (Bargu et al., 2012). Though *Pseudo-nitzschia* blooms have never been explicitly correlated with river damming, these case studies provide a reminder that changing nutrient delivery to coastal areas can result in varied, often unexpected, consequences to ecosystem health.

A key question that arises when considering damming is whether dams are a responsible solution for water and energy issues. In other words, do the societal, economic, and environmental services outweigh the detriments? It is difficult to answer this question simply, and is usually only relevant at the scale of individual dams. Broad questions such as "are dams good or bad?" generally cannot be answered in a meaningful way, as each dam presents a unique set of circumstances, with its own advantages and disadvantages. The reasons for proposing the dam, the values and interests of the parties impacted by the dam construction, and the quantity and quality of the data available all must be weighed. There are few cases where dams are unquestionably the answer to a problem, just as there are few cases where dams are a perfect solution.

For example, the Three Gorges Dams on the Yangtze River in China is one of the most controversial dam construction projects in history. On the one hand, the hydroelectricity provided has in part allowed China to reduce its dependence on more polluting energy sources like coal, which has resulted in the country's recent slowing down of the growth in their greenhouse gas emissions (Le Quéré et al., 2016). On the other hand, the dam has been referred to as an "environmental catastrophe," having resulted in the displacement of 1.3 million people, widespread eutrophication in the reservoir's tributaries, increased prevalence of the snail-borne disease schistosomiasis, potentially increased seismic activity in the region, and bringing a local dolphin species to the brink of extinction (Hvistendahl, 2008; Wu et al., 2003). As the negative effects of greenhouse gas emissions on global climate worsen, the obvious question arises of whether the environmental, economic, and social costs of the Three Gorges Dam are outweighed by the reduction in China's greenhouse gas emissions.

Such discussions weighing the pros and cons of river damming could be conducted regarding any dam worldwide. However, in many cases, these discussions are lacking, and the dams are being constructed with insufficient environmental assessments or understanding of the consequences of damming. In developing countries, hydroelectric construction projects with generating capacities <10 MW are often exempt from environmental assessment (Hermoso, 2017). A classic example of a dam built with a severe misunderstanding of the environmental consequences is the Balbina Dam in Amazonas, Brazil, where it is estimated that it would take 114 years of hypothetical emissions from coal or natural gas for the same energy production as the dam to equal those from the degradation of the forest flooded following dam closure (Figure 1.4) (Fearnside, 1995). In the United States, 38.4%
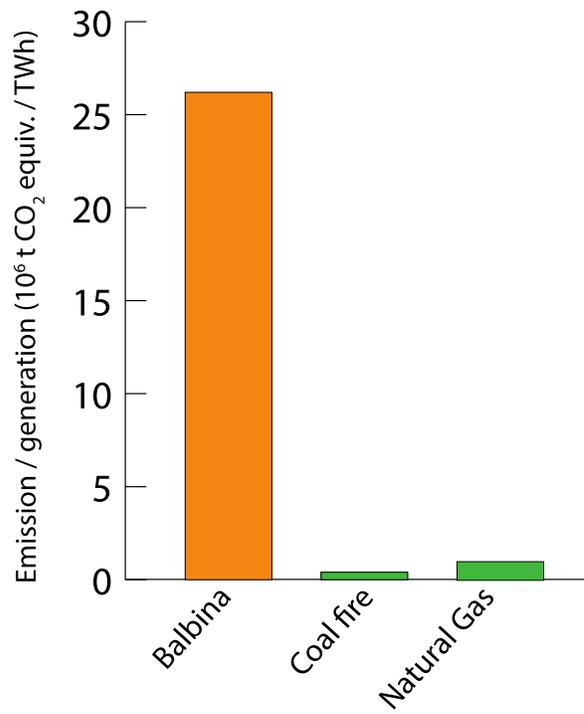
Figure 1.4: CO_2 emissions normalized by amount of energy generation for Balbina Dam compared with coal fire and natural gas. Data from Fearnside (1995).

of dams exist for recreational purposes, while 3.8% of dams have "undetermined" purposes (FEMA, 2016). Given the ecological detriment suffered by rivers to provide a superficial, non-essential service, one suspects that these dams were built with little consideration of the ecological consequences.

Factors such as the impacts of nutrient retention or elimination by reservoirs on river ecosystem health remain poorly understood and so are rarely included as part of environmental assessments. In addition, environmental assessments rarely extend beyond the immediate ecosystem surrounding the location of dam construction. The science dedicated to constraining the role of damming in global nutrient fluxes along the entire LOAC remains in its infancy. The existing estimates have high uncertainties and are calibrated using equations derived empirically from small, statistically non-significant datasets. Often the same equation is used to predict reservoir elimination for multiple nutrient elements, and so any potential preferential retention of one nutrient over another is not considered. The effects of river damming on global nutrient cycles, therefore, remain poorly quantified at the present time and the implications for ecosystem health along the LOAC and in the coastal ocean are difficult to predict. Given the global impact that dams have on river systems, a comprehensive global study is needed to predict how humans have and will continue to reorganize riverine nutrient fluxes.

1.3 On the importance of global scale biogeochemical modelling

A key value of global models lies in their ability to integrate findings across many spatial and temporal scales. They provide the only means of addressing an entire category of research questions concerned with quantifying the repercussions of human modifications to one aspect of a biogeochemical cycle on the rest of the cycle, no matter how far spatially or temporally removed. Global models allow for the quantification of a worldwide perturbation, such as anthropogenic nutrient loading or river damming, on the fluxes delivered along the entire LOAC. Mechanistic or process-based global models, in particular, are exceptionally useful in their ability to make predictions to regions of the world where data are sparse. This process in turn can enable scientists and policy makers to identify further research directions. Global biogeochemical models have demonstrated their usefulness to cycles such as those of C and N, which include greenhouse gases among their species. These models provide crucial information to climate models. As the world economy responds to climate change, global biogeochemical models become relevant when developing policies like carbon cap and trade and nutrient credit trading (Betsill and Hoffmann, 2011; Lal, 2010).

When developing a global model, the modeler is forced to determine which parameters are the most important drivers of the processes being considered. By assigning a hierarchy to the relative significance of biogeochemical drivers, global models also enable researchers to, say, identify whether a given watershed is an outlier among the global dataset. This process can guide the establishment of management plans or formulation of research questions at smaller scales. By relying only on local studies, one runs the risk of collecting data that are not statistically representative or misidentifying the dominant processes.

1.4 Modelling the global biogeochemical impacts of damming

The initial work on lake P retention by Vollenweider (1975) serves as a starting point for reservoir nutrient modelling. Vollenweider identified water residence time as a master variable controlling lake P retention using a mass balance approach to express the burial of P in sediments (see Appendix C for full derivation). A similar approach can be applied to dam reservoirs, which is justified given the high statistical correlation observed between water residence time and the magnitudes of in-reservoir fluxes (Brunskill et al., 1971; Hejzlar et al., 2006; Mulholland and Elwood, 1982). The landmark study by Vörösmarty et al. (1997) quantifies the continental "ageing" of water due to damming. They predict that freshwater in impounded basins spends an average of 27 more days before reaching the oceans than for unimpounded basins. Using a similar approach quantifying changes to water residence times, Vörösmarty et al. (2003) predict that reservoirs trap 30% of the sediment in regulated basins, or 16% of the total sediment transported along rivers worldwide.

Reservoir nutrient retention has been quantified at scales ranging from the individual reservoir to all reservoirs worldwide, with most efforts focused on total P (TP), total N (TN), and selected C fluxes (e.g. gaseous CO_2 and CH_4 emissions). Global modelling efforts have been largely empirical; that is, relationships generated from individual reservoir datasets are applied to global databases of reservoirs. Most existing estimates of reservoir nutrient elimination are built into lumped models designed to predict nutrient loading to watersheds, or in earth system box models representing major pools and fluxes within global nutrient cycles. As a result, reservoir nutrient retention is typically predicted using a single empirical calculation, derived based on a small dataset of nutrient burial in previously published studies. In the following sections, I will discuss existing global reservoir nutrient retention models, with particular emphasis on the Global-NEWS model, which is utilized in Chapters 3-6.

1.4.1 Global-NEWS

The Global Nutrient Exports from WaterSheds (Globel-NEWS) model is a lumped, semi-empirical model that predicts nutrient loading to coastal zones worldwide (Mayorga et al., 2010; Seitzinger et al., 2005). Specifically, it predicts sediment, organic C (OC) and nutrient (N, P, and Si) yields based on land use and land cover (e.g., wetlands, cropland, and grasslands), climate variables (including temperature and precipitation), geomorphological parameters (including slope and lithology), and anthropogenic alterations (including consumptive water usage). The Global-NEWS model differentiates between dissolved and particulate nutrient and OC species, as well as organic and inorganic nutrient species, it implicitly accounts for in-stream nutrient and OC losses, and it has been used to hindcast nutrient loads to watersheds in the years 1970 and 2000, and to forecast the 2030 and 2050 loads according to the Millennium Ecosystem Assessment (MA) scenarios (Seitzinger et al., 2010).

The model includes an empirical damming correction factor for dissolved inorganic nutrient species and particulate species (Beusen et al., 2005; Harrison et al., 2005). The empirical equation for reservoir dissolved inorganic P (DIP) retention was originally derived by Wilhelmus et al. (1978), using water residence time as the independent variable. The equation for dissolved inorganic N (DIN) retention was developed empirically based on both hydraulic residence time and water depth (i.e. hydraulic load), using lake and river data from eight locations, mainly first order streams (Dumont et al., 2005; Seitzinger et al., 2002). These equations were then applied to a worldwide database of 714 reservoirs with dams taller than 15m (Lehner and Döll, 2004). The Global-NEWS output has additionally been used as a foundation for more thorough lake and reservoir N and dissolved Si (DSi) retention models, called the NiRReLa and SiRReLa models (Nitrogen or Silicon Retention in Reservoirs and Lakes) (Harrison et al., 2012; Harrison et al., 2009). The developers of these models use the Global-NEWS watershed area-normalized loads (i.e. yields) to predict nutrient input to lakes and reservoirs in the Global Lakes and Watersheds Database (GLWD) (Lehner and Döll, 2004), and then apply empirical retention equations to these loads to predict reservoir N and DSi removal. I evaluate the approach used for DSi in more detail in Chapter 3. Because of the separation of yields by nutrient species, as well as the spatially explicit model output, the Global-NEWS output, with its damming correction factor excluded, is well suited to use as an input to the models I develop in Chapters 3-5.

1.4.2 Other global retention models

The IMAGE-Global Nutrient Model (GNM) predicts TN and TP loads and retention in freshwater systems (lakes, wetlands, rivers and reservoirs) and soils on an annual timescale and at a 0.5°x0.5° grid cell spatial scale (Beusen et al., 2015; Beusen et al., 2016). The GNM component is an immensely complicated hydrology-based module within the IMAGE integrated assessment model, which incorporates the Earth system (e.g. changes to land, ocean, and atmosphere) with the human system (e.g. changes to population, economy, and development) (Stehfest et al., 2014). The model uses a global drainage network, which incorporates the GRanD dams (Lehner et al., 2011), to predict N and P removal using a first-order relationship with hydraulic load and uptake velocity. Uptake velocity is predicted by empirically modifying an average literature value based on temperature and nutrient concentration within the water column. The IMAGE-GNM model allows for important questions related to sustainability to be addressed, and the approach of using a single, global hydrological network incorporating all types of surface water bodies is an important advancement in global nutrient modelling (see Chapter 7 for more discussion related to this point). However, the model suffers from the same shortcoming as Global-NEWS of using an over-simplified, empirically derived damming retention factor. Furthermore, the IMAGE-GNM is not calibrated, and the validation is done only on a few arbitrarily selected sites on major rivers worldwide. This approach does not lend confidence to the validity of the model output at the high-resolution global scale that the authors suggest their model predicts.

Other estimates of reservoir nutrient and C elimination are built into global nutrient box models. Laruelle et al. (2009) developed a global box model of the Si cycle, with an assessment of the effects of river damming on riverine fluxes delivered downstream. Frings et al. (2014) generated the first estimate of biogenic Si (BSi) burial in reservoirs worldwide, by averaging the BSi deposition fluxes calculated using sediment cores from a limited number of reservoirs, and then multiplying this value by the global reservoir surface area. The Terrestrial-Ocean-aTmosphere Ecosystem Model (TOTEM) similarly represents N, P, C and sulfur (S) fluxes, and includes a lumped lake and reservoir burial flux for each nutrient (Mackenzie et al., 2002; Ver et al., 1999). With regard to the C cycle, the majority of studies on global reservoir dynamics focus on predicting greenhouse gas emissions (Barros et al., 2011; Deemer et al., 2016; Mendonça et al., 2012b; Raymond et al., 2013). Though estimates of C burial in reservoirs do exist, they are outdated first-order estimates incorporated into global models (see Chapter 6 for more details). Like Global-NEWS's damming correction factor and the NiRReLa

and SiRReLa models, these estimates are made with empirical approaches, based on small datasets of reservoirs that are statistically unrepresentative of the global reservoir distributions.

1.5 Thesis structure

In this thesis, I address the following research questions.

1. How much Si, P, and OC are retained or eliminated globally due to river damming worldwide?

2. How does damming modify the balance of productivity (heterotrophy vs. autotrophy) in river systems worldwide?

3. To what extent does damming change nutrient speciation or reactivity along the LOAC?

4. Do dam reservoirs retain or eliminate certain nutrients more efficiently than others, and if so, how does this decoupling change nutrient ratios delivered to coastal zones?

I begin the research portion of this thesis (Chapters 2-6) with a reservoir-scale field study of reactive silicon dynamics in Lake Diefenbaker, a reservoir in Canada's central prairie province of Saskatchewan (Maavara et al., 2015a). I use this study to illustrate the differences in retention of Si relative to N and P, and present the hypothesis that river damming results in a decoupling of nutrient cycling (Research Questions 3 and 4).

Following Chapter 2, I address my research questions by developing a mechanistic approach to global scale biogeochemical modelling that does not rely on empirical equations derived from small, statistically non-significant datasets. I introduce the mechanistic approach in Chapter 3 by developing a biogeochemical box model of reservoir Si dynamics, to predict global dissolved and reactive Si burial in reservoirs (Research Question 1).

Chapters 4 and 5 use the same modelling approach presented in Chapter 3, but applied to riverine P and OC fluxes. Using the upstream-catchment area-normalized Global-NEWS model's watershed yields as input to each reservoir, I use the 1970, 2000, 2030 and 2050 model predictions to estimate historical and predict future P and OC elimination by dams (Research Questions 1-3).

Chapter 6 links the P and Si models together with a global scale N model (Akbarzadeh et al., in preparation), to predict changes to nutrient ratios delivered by rivers to the coastal zones. I analyze to what extent the damming of rivers worldwide alters nutrient limitation, between Si, P and N, in river water discharged to continental margins. I use this analysis, in combination with anthropogenic

nutrient loading data, to contextualize the role of river damming as a driver of changing nutrient limitation in the coastal shelf zones of the world (Research Question 4).

Chapter 7 summarizes the major conclusions to the four Research Questions, and elaborates on the research directions that should be pursued following the work in this thesis. In particular, I discuss the need for a nutrient-loading and retention model that includes the entire river continuum, and our growing understanding of the role of nutrient elimination in small reservoirs (<0.1 km^2). I conclude with a brief discussion of the management challenges and opportunities that dam construction presents.

Chapter 2

Reactive silicon dynamics in a large prairie reservoir (Lake Diefenbaker, Saskatchewan)

This chapter is modified from:

Maavara, T., Hood, J.L.A., North, R.L., Doig, L.E., Parsons, C.T., Johansson, J., Liber, K., Hudson, J.J., Lucas, B.T., Vandergucht, D.M. and Van Cappellen, P. (2015) Reactive silicon dynamics in a large prairie reservoir (Lake Diefenbaker, Saskatchewan). Journal of Great Lakes Research 41, 100-109.

2.1 Summary

There is an up-coming global surge in dam construction. River damming impacts nutrient cycling in watersheds through transformation and retention in the reservoirs. The bioavailability of silicon (Si) relative to nitrogen (N) and phosphorus (P) concentrations, in combination with light environment, controls diatom growth and therefore influences phytoplankton community compositions in most freshwater aquatic ecosystems. In this study, I quantified reactive Si cycling and annual Si retention in Lake Diefenbaker, a 394 km^2 prairie reservoir in Saskatchewan, Canada. Retention estimates were derived from 7 sediment cores combined with high-resolution spatiotemporal sampling of water column dissolved Si (DSi). Current annual DSi retention in the reservoir is approximately 30% of the influx, or 2.7 x 10^8 mol yr^{-1}. The relative retention of DSi is higher than that of bioavailable N, but lower than that of bioavailable P, indicating a decoupling of the P, N, and Si cycles in the reservoir. The largest accumulation of reactive particulate Si (PRSi) is found in sediments deposited in the mid-reservoir region, which corresponds to the region of highest epilimnetic DSi decrease during the 2013 open water season. This region corresponds to the fluvial-to-lacustrine transition zone, and represents a hot spot for Si retention. Differences in retention efficiencies of macronutrients may not only affect the in-reservoir ecology and water quality, but also modifies the N:P:Si ratios exported downstream, which has the potential to alter ecosystem processes in receiving water bodies.

2.2 Introduction

Rivers and streams are being dammed worldwide for flood control, crop irrigation, hydroelectric power generation, and drinking water supply. Reservoirs resulting from dam construction act as sinks (and on long time scales potentially as sources) of nutrients, because of increased sedimentation and burial of allochthonous and autochthonous particulate matter (Friedl and Wüest, 2002; Humborg et al., 2006; Vörösmarty et al., 1997). Damming reduces the downstream delivery of nutrients and alters nutrient ratios in receiving water bodies, including the coastal zone (Garnier et al., 2010).

The relative availabilities of phosphorus (P), nitrogen (N), and silicon (Si) influence the phytoplankton community composition of aquatic ecosystems (Sferratore et al., 2008; Teubner and Dokulil, 2002; Triplett et al., 2012). In freshwater environments, including dammed reservoirs, diatoms are usually present as a large component of the phytoplankton biomass when Si is available in relative excess to the N and P requirements of siliceous algae (Billen et al., 1991; Brzezinski, 1985; Malone et al., 1996). Dissolved silicon (DSi), the most bioavailable pool, is almost entirely in the form of monomeric silicic acid (H_4SiO_4), with ionized forms and polymers representing only a small

portion in most freshwater bodies (Iler, 1979). In many aquatic systems, diatomaceous silica (SiO_2) comprises the majority of reactive particulate Si (PRSi) (Sauer et al., 2006; Triplett, 2008). PRSi refers to all particulate-associated Si that may dissolve in the water column or be transported out of the reservoir prior to burial in the sediment. PRSi can include amorphous biogenic or pedogenic Si, mineral-sorbed Si, and poorly crystalline aluminosilicates (Davis et al., 2002; Saccone et al., 2007; Sauer et al., 2006).

The formation and dissolution of diatom frustules are the major transformation fluxes between DSi and PRSi in reservoir environments (Frings et al., 2014). Diatom production is seasonal and controlled by the availability of major macronutrients (DSi, N, and P), temperature, photic depth, and water column hydrodynamics (Hecky et al., 2010; Schelske, 1985). Upon death or senescence, diatoms sink to the bottom of the reservoir and a fraction of the frustules are buried in the sediments, removing reactive Si from the water column, while the remainder is re-dissolved to the water column (Humborg et al., 2008; Triplett, 2008). Abiotic removal of DSi by sorption and (co-) precipitation are of minor importance in Si-rich water bodies compared to DSi uptake by diatoms (Saccone et al., 2007). Due to the longer residence times than their previous riverine state, and lake-like hydrodynamics characteristic of many reservoirs, PRSi burial represents a significant Si sink, which is introduced to the watershed after reservoir construction.

Despite the important role of Si in aquatic ecosystems, it is a relatively under-studied nutrient element, particularly in reservoir environments, with fewer than 20 Si budgets available globally (refer to Chapter 3, or Maavara et al. (2014)). The quantification of reservoir Si retention and the consequences to downstream environments is made difficult by the lack of literature and robust datasets. Given the global surge in dam construction (Zarfl et al., 2015), the need to quantify reservoir Si dynamics in a variety of climatic and morphological zones is critical to alleviating the knowledge gap.

This study focuses on quantifying the Si dynamics of a northern prairie reservoir, Lake Diefenbaker, in Saskatchewan, Canada. Lake Diefenbaker represents an ideal location to quantify seasonal changes in spatiotemporal Si cycling, particularly under-ice Si cycling, given the northern climate's dramatic seasonal differences. The nearly 200 km long reservoir is additionally well suited to quantify Si cycling and retention throughout the transition from the up-reservoir riverine environment to the down-reservoir lacustrine environment. The objectives of this study are to (1) analyze and establish the drivers of the spatiotemporal trends in DSi and PRSi in Lake Diefenbaker,

and (2) estimate the present-day annual DSi retention and PRSi accumulation in the reservoir. This study, the first to quantify Si cycling in Lake Diefenbaker, provides a firm basis for future hypothesis-driven studies of reactive Si cycling in the basin and the effects of Si retention on downstream ecosystems.

2.3 Materials and Methods

2.3.1 Site description

Lake Diefenbaker is a dimictic reservoir located on the South Saskatchewan River (SSR), in Canada's central prairie province of Saskatchewan (WSA, 2012). Trophic status varies spatially in the reservoir, with oligo-mesotrophic waters down-reservoir and meso-eutrophic waters up-reservoir (Dubourg et al., 2015). The watershed area of the reservoir is approximately 120,000 km^2, with 67% of the area under agriculture use and the remainder predominantly native grassland (WSA, 2012). The reservoir was created in 1967 by the construction of two large embankment dams, the Gardiner Dam on the SSR, and the Qu'Appelle Dam on the Qu'Appelle River (Figure 2.1). The Gardiner Dam drains 99% of the outflow of the reservoir with hypolimnetic withdrawal. The reservoir is used for irrigation, recreation, flood and ice control, hydroelectricity production, and as a source supply for potable water in local and downstream communities.

The water residence time in the reservoir is on average 1.1 years (Donald et al., 2015) the mean depth is 22 m, the maximum depth is 59 m near the Gardiner Dam, the volume is approximately 9.03 km^3, and the total surface area is 394 km^2 (Sadeghian et al., 2015). For the purposes of this study, four reservoir sections have been identified (Figure 2.1). The up-reservoir region extends from Highway 4 to Core 2 and is 48 km^2. The mid-reservoir extends from Core 2 to Elbow and is 228 km^2. The down-reservoir Gardiner and Qu'Appelle arms have surface areas of 72 km^2 and 46 km^2 respectively.

2.3.2 Field sampling

To establish a DSi budget, water samples were manually collected in 20-L polyethylene bottles every two weeks from June to October of 2013 and once monthly from November 2013 to May 2014, from the two inflowing rivers, SSR and Swift Current Creek (SCC), and the outflows below the two dams (Figure 2.1). In order to quantify in-reservoir DSi dynamics, monthly water sampling was conducted during the open water season (June–October) of 2013 at 11 stations distributed along the entire length of Lake Diefenbaker (Figure 2.1). Water samples were collected with a Van Dorn sampler from 2
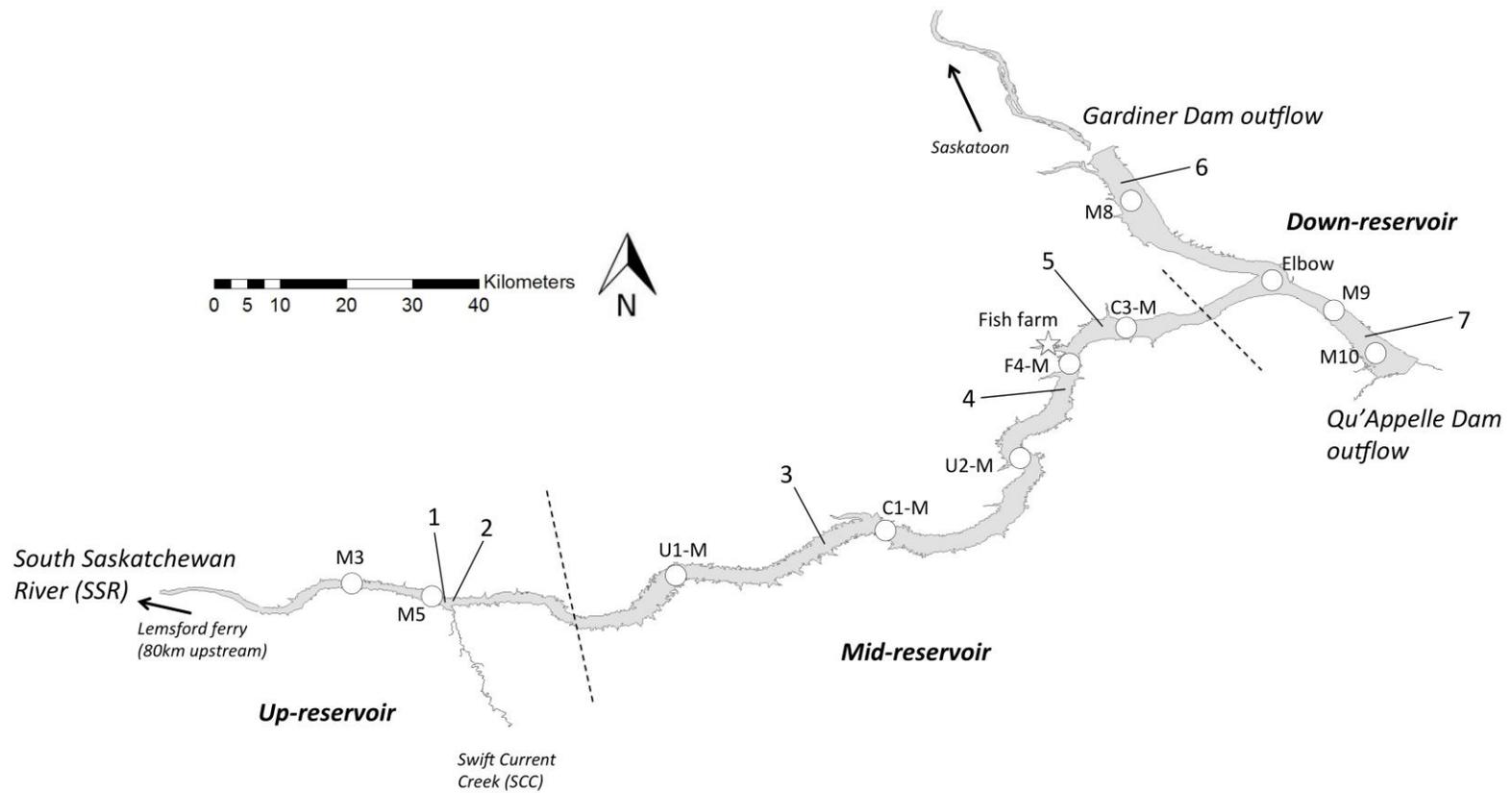
Figure 2.1: Map of Lake Diefenbaker, including 11 water column sampling sites (circles), 7 core locations (numbered), and fish farm (star). Dashed lines separate up-, mid-, and down-reservoir areas. Also note that water samples are collected on the two inflowing rivers (South Saskatchewan River and Swift Current Creek) and at the two dam outflows (Gardiner Dam and Qu'Appelle Dam).

depths, representative of the mixed layer, except during periods of stratification when hypolimnetic samples were also collected (Table 2.1). Stratification was inferred from the presence of a thermocline (gradient > 0.5°C m^{-1}) using a temperature sensor (YSI, model 6600 V2). The water samples were transported to the University of Saskatchewan where they were stored in an environmental chamber at *in situ* lake temperature until filtration the following day.

Seven cores were collected in 7.5-cm inner-diameter Lucite tubes using a Glew gravity corer and transported to the University of Saskatchewan, where the cores were sectioned at 1-cm intervals and the sediment was freeze-dried (for details, see Lucas et al. (2015b)). Two cores were collected in the up-reservoir region before (Core 1) and at the confluence (Core 2) of SSR and SCC. Three cores were collected between the SSR-SCC confluence and the town of Elbow (Cores 3-5). One core was collected in the Gardiner arm (Core 6) and one in the Qu'Appelle arm (Core 7). Cores 1, 2, 4, 5, and 6 were collected in September 2011, Cores 3 and 7 in July 2012. All cores were obtained from mid-channel locations (Figure 2.1).

2.3.3 Analytical methods

2.3.3.1 Water column DSi

Samples were filtered through 0.2 μm pore size polycarbonate filters and DSi concentrations were determined colorimetrically with the heteropoly blue method (Standard Method 4500 - SiO$_2$ D; APHA, 1989). The detection limit was 11.2 μM, with a standard error for duplicate samples of ±0.9 μM. The detection limit was calculated as the standard deviation of the blank absorbances times the number of blanks analyzed (Method 3 from Apostol et al. (2009)). Standard errors were determined using an outside SiO$_2$ standard from Ricca Chemical Company (cat. no. 6750-16).

2.3.3.2 Sediment PRSi

Concentrations of reactive particulate Si (PRSi) were determined on freeze-dried sediments using the alkaline extraction procedure described by Ohlendorf and Sturm (2008): 50 ± 15 mg ground sample was digested in 10 mL of 1M NaOH for 3 hours at 100°C in Teflon digestion bombs. The hot NaOH extraction solution was filtered through 0.2 μm pore size polyethersulfone filters and the Si and Al concentrations were analyzed by inductively coupled plasma optical emissions spectroscopy (ICP-OES, Thermo Scientific iCAP 6000). The total extracted Si was corrected for the contribution of silicate minerals assuming an Si:Al ratio of 2:1, as in Ohlendorf and Sturm (2008). Samples extracted

Table 2.1: DSi concentrations (μM) at sampling sites throughout Lake Diefenbaker, sampled at biweekly-monthly intervals between June and October 2013, and additionally once monthly at inflow and outflow locations from November to May 2014. Inflow and outflow surface samples were taken at depth 0m, epilimnion at depth 2m, and hypolimnion varied depending on location and extent of stratification of water column (depth ranged between 13.5 and 46.5m). All means are unweighted and arithmetic.

Location	Site	Depth	Max	Mean	Min	n
Upstream	Lemsford Ferry (inflow)	Surface	112	73	17	21
Up-reservoir	M3	Epilimnion	103	82	63	4
	M5	Epilimnion	115	82	63	5
		Hypolimnion	93	90	86	2
Tributary	Swift Current Creek inflow (SCC)	Surface	281	157	61	19
Mid-reservoir	U1-M	Epilimnion	104	83	80	5
		Hypolimnion	113	96	69	4
	C1-M	Epilimnion	99	86	57	5
		Hypolimnion	91	74	52	4
	U2-M	Epilimnion	101	75	43	6
		Hypolimnion	77	55	38	4
	F4-M	Epilimnion	97	76	41	5
		Hypolimnion	85	61	40	4
	C3-M	Epilimnion	87	63	28	6
		Hypolimnion	73	57	42	5
Down-reservoir	Elbow	Epilimnion	75	58	27	5
		Hypolimnion	74	63	49	4
Gardiner arm (down-reservoir)	M8	Epilimnion	63	47	24	5
		Hypolimnion	57	51	38	3
	Gardiner Dam (outflow)	Surface (below dam)	236	63	33	19
Qu'Appelle arm (down-reservoir)	M9	Epilimnion	69	54	36	5
		Hypolimnion	78	63	47	2
	M10	Epilimnion	92	61	25	5
		Hypolimnion	88	75	67	3
	Qu'Appelle Dam (outflow)	Surface (below dam)	339	92	31	19

in triplicate gave an average standard error of 15%. The method detection limit for the extractions was 0.08 mol kg⁻¹ PRSi (Ohlendorf and Sturm, 2008), and the analytical detection limit was 0.007 mol kg⁻¹ (Apostol et al., 2009). Average standard deviation for the ICP-OES analyses was 3%, based on triplicate measurements of the samples plus Certified Reference Materials (QCS-27, lot 1224831, High Purity Standards, Charleston, SC; Phenova WP Silica 74.0ppm SiO_2 [1232 μM], lot 9051-17, Golden, CO; Phenova WP Silica 112.0ppm SiO_2 [1862 μM], lot 8131-21, Golden, CO).

The Si:Al ratio of 2:1 used to correct for the contribution of aluminosilicate dissolution to the extracted Si concentrations is assumed to be representative of common clays minerals found in lacustrine sediments, such as montmorillonite. Measurements performed on individual aluminosilicate grains in a scanning electron microscope equipped with X-ray microanalysis (SEM/EDS) all yielded Si:Al ratios close to 2. The procedure for determining PRSi was further tested on 3 of the samples from the inter-laboratory comparison coordinated by Conley (1998) and 2 samples characterized by Saccone et al. (2007). The results deviated on average by 9% from the PRSi values quoted in the original literature (for details, refer to Appendix A, Table AB1).

2.3.4 DSi fluxes and retention

The annual DSi fluxes into and out of the reservoir were estimated using flow-weighted DSi concentrations for the inflows (SSC and SSR) and outflows (SSR and Qu'Appelle River). At each influx and efflux location, the Beale's ratio estimator equation (Beale, 1962; Quilbé et al., 2006) was used to determine annual DSi fluxes, F_{DSi}:

$$F_{DSi} = \overline{CQ} \cdot \frac{\mu_Q}{\bar{Q}} \cdot n \cdot \left(\frac{1 + \frac{1}{n_d} \frac{S_{CQ}}{\overline{CQ} \cdot \bar{Q}}}{1 + \frac{1}{n_d} \frac{S_{Q^2}}{\bar{Q}^2}} \right) \tag{2.1}$$

with

$$\mu_Q = \frac{\sum_{i=1}^{n} Q_i}{n}$$

where F_{DSi} is the flux (mol yr⁻¹), $\overline{CQ}$ is the arithmetic average of the fluxes calculated on days where concentration (C) and discharge (Q) were both measured (mol day⁻¹), Q_i is the discharge (km³ day⁻¹) on day i (Figure 2.2), $\bar{Q}$ is the arithmetic mean discharge for the days Q and C are both measured (mol day⁻¹), n is the total number of days over the period of flux estimation, i.e., 365 days, n_d is number of days C and Q were both measured, S_{CQ} is the covariance between $\overline{CQ}$ and $\bar{Q}$, and S_{Q^2} is the variance

26

of $\bar{Q}$. This ratio estimator is an unbiased calculation of flux that adjusts for the covariance between flux and discharge. Flow-weighted concentration averages can be back-calculated by dividing F_{DSi} by the total annual discharge at the relevant inflow or outflow location. For a detailed discussion of the ratio estimator method and a comparison with other flux calculations, refer to Appendix A.

To estimate the outflow through the Gardiner Dam, discharge values for downstream Saskatoon were used. Pomeroy and Shook (2012) show that the discharge through the Gardiner Dam is linearly related to the discharge in Saskatoon with less than 8% difference, assuming a delay of one calendar day. Discharge values collected at half-hour intervals for Saskatoon and the Elbow Diversion Canal, which receives the outflow through the Qu'Appelle Dam, were obtained from Environment Canada's Water Office (2014). Inflow for 2013 was estimated from discharge values measured on SCC and on the SSR at the upstream town of Medicine Hat and the Red Deer River before its confluence with the SSR near the Alberta-Saskatchewan border. Discharges were adjusted for the lag time to the reservoir, which depends on volume of flow (data provided by D. Lazowski, Environment Canada). Upstream discharge data for the SSR were not available at the time of writing from January to May, 2014. Daily discharge for this period was estimated by taking the average discharges from the same calendar days in 2011–2013.

The annual DSi retention (R_D) was calculated using:

$$R_D = \frac{DSi_{in} - DSi_{out}}{DSi_{in}} \tag{2.2}$$

where DSi_{in} and DSi_{out} represent the influx and efflux of DSi in mol yr^{-1}, respectively. Net retentions calculated using location-specific water discharges and Equation 2.2 include both biogeochemically-driven retention processes (e.g. uptake and burial) and hydrologically-driven processes (e.g., loss and gain of DSi due to reservoir volume change associated with fluctuating water levels).

2.3.5 Sediment and PRSi accumulation

Several methods are used to estimate average sediment accumulation rates, S_{acc} (cm yr^{-1}). Sediment depth at year of reservoir formation (1967) was determined by noting the absence of diatom frustules; this depth occurred at 15 cm in Core 4 and 27 cm in Core 6 (Lucas et al., 2015a). The non-zero quantity of PRSi below 27 cm depth in Core 6 may be the result of dissolution of non-biogenic PRSi in the extraction procedure, possibly pedogenic amorphous Si washed in during reservoir in-filling. S_{acc} over the history of the reservoir at the location of Cores 4 and 6 was calculated by dividing the depth

of sediment by the years over which it accumulated, yielding S_{acc} of 0.61 cm yr^{-1} at Core 6 and 0.34 cm yr^{-1} at Core 4.

The bottoms of the remaining cores did not capture the 1967 transition from river to reservoir. S_{acc} at Cores 1 and 2, found using recent and historical cross-sectional and bathymetric data (Sadeghian et al., 2015) indicate an S_{acc} of 4 cm yr^{-1} at the location of both cores. Diatom stratigraphies were similar among cores 4–7, indicating that diatom communities along the length of the reservoir were similar since its creation. For the following calculations, I will assume Cores 4, 6, and 7 capture 44 to 45 years of historical sediment deposition in the reservoir (Lucas et al., 2015a). Comparison of the magnetic susceptibility stratigraphic profiles of the Core 5 (2011) and an additional core collected in 2012 (analyzed for chironomid remains) demonstrated that Core 5 profile represented 1976 to 2011. Since I did not capture the full depositional history at Core 3, it is impossible to calculate an S_{acc}. However, one can be estimated. Given that Core 3 is greater than 50 cm deep, and assuming at most 45 years of accumulation, S_{acc} must exceed 1.1 cm yr^{-1}. Sadeghian et al. (2015) report decreasing sediment accumulation with distance down-reservoir, with a rate of 2 cm yr^{-1} approximately 15 km down-reservoir of SCC. Linear interpolation between this location and Core 4 yields an average sediment accumulation rate at Core 3 of approximately 1.3 cm yr^{-1}. These calculated S_{acc} allow for the evaluation of trends in PRSi deposition.

To convert S_{acc} in cm yr^{-1} to average mass accumulation rates, M_{acc}, in kg yr^{-1}, a dry bulk density of 0.29 g cm^{-3} (dry weight/wet volume) was calculated by averaging dry bulk densities from Cores 1, 2, 4, 5, and 7 at two depths per core. Cores 6 and 7 were used to represent the accumulation in the Gardiner and Qu'Appelle arms, yielding M_{acc} of 1.3 x 10^8 kg yr^{-1} and 4.6 x 10^7 kg yr^{-1}, respectively. Cores 1 and 2 were used to represent the area up-reservoir of SCC, with an M_{acc} of 5.6 x 10^8 kg yr^{-1}. Two estimation methods are used to determine a range of M_{acc} for the mid-reservoir. The first is the arithmetic mean of the mass accumulation rates of mid-reservoir cores (Cores 3–5) as applied to the reservoir area from SCC to Elbow, yielding 5.6 x 10^8 kg yr^{-1}. The second estimate assumes a linear change in rates between SCC, the location 15 km down-reservoir of SCC, Core 3, 4 and 5, and assuming no change in accumulation perpendicular to the core transect, yielding 9.3 x 10^8 kg yr^{-1} accumulation. M_{acc} for the entire reservoir is estimated to be between 1.3 x 10^9 – 1.7 x 10^9 kg yr^{-1}.

The fluxes of PRSi to sediment, $PRSi_{acc}$, in each section of the reservoir (mol yr^{-1}) were calculated by multiplying M_{acc} (kg yr^{-1}) by core PRSi concentrations (mol kg^{-1}). The PRSi concentrations in the most recent five years of deposition in each core were averaged to approximate present-day annual

fluxes. Cores 1 and 2 were averaged to estimate PRSi concentration up-reservoir of Swift Current Creek until the first sampling site (M3). Core 3 was used to estimate PRSi concentrations from SCC to U2-M, Core 4 from down-reservoir of U2-M to F4-M, and Core 5 from down-reservoir of F4-M to Elbow. Cores 6 and 7 were used to estimate PRSi concentration in each arm of the reservoir.

2.4 Results

2.4.1 Discharge

The year 2013 was a wet year, with spring flooding occurring throughout the watershed (greater than 50-year floods in some locations). The total annual flow for the June 2013 – May 2014 sampling period into the reservoir via the SSR was 10.3 km^3, with an additional 0.1 km^3 flowing in through SCC. Total flow through the Gardiner and Qu'Appelle dams was 11.8 km^3 and 0.07 km^3, respectively. Instantaneous discharge through the Gardiner Dam peaked on June 26 at 2057 m^3 s^{-1}. Discharge on the SSR was lowest while ice-covered in winter, maintaining an average flow of approximately 100 m^3 s^{-1} from mid-December through March. Flow out of the Qu'Appelle arm peaked at a value close to, but less than 10 m^3 s^{-1} on June 22 during a downstream channel conveyance test, and averaged 2.4 m^3 s^{-1} (Water Office, 2014).

2.4.2 Water column DSi

The flow-weighted average DSi inflow concentration (Equation 2.1) at the upstream Lemsford Ferry sampling site was 87 μM. The annual flow-weighted average outflow concentrations through the Gardiner and Qu'Appelle dams were 56 and 78 μM, respectively. Concentrations of DSi varied spatially and temporally throughout the reservoir (Figure 2.3). On average, epilimnetic DSi concentration showed a decreasing trend with distance down-reservoir. Peaks in epilimnion DSi concentration were observed in the mid-reservoir from mid-July to early August, and from late September to early-October. Peak concentrations shifted progressively to later times with distance down-reservoir. In the mid-reservoir, epilimnetic DSi concentrations over the sampling period ranged from 24 to 115 μM, with a mean of 69 μM (Table 2.1). The Qu'Appelle arm exhibited the highest concentrations throughout the monitoring period, averaging 91 μM with a peak concentration of 339 μM on September 10. The highest hypolimnetic DSi concentrations during water column stratification were observed in the up-reservoir to mid-reservoir transition at the end of August. The mean hypolimnion DSi concentration (67 μM) was similar to the epilimnion (66 μM). However, the same
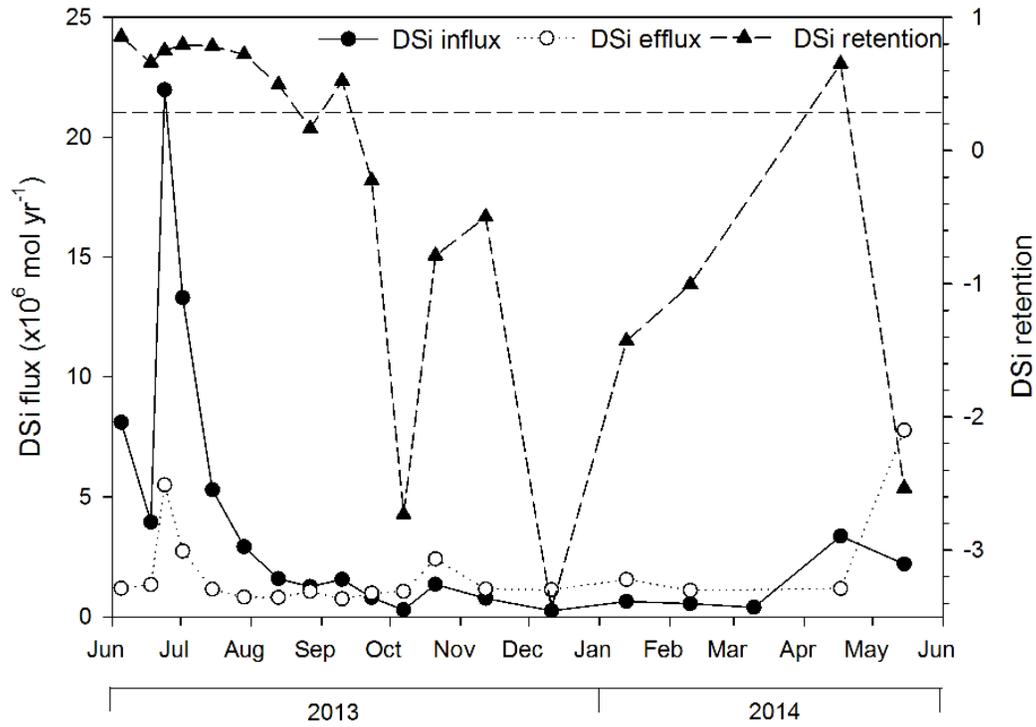
Figure 2.2: Total time-specific DSi influxes and effluxes. Retention (unitless) is calculated as the difference between the influx and the efflux, divided by the influx (Equation 2.2). Horizontal dashed line indicates annual average DSi retention of 0.30.
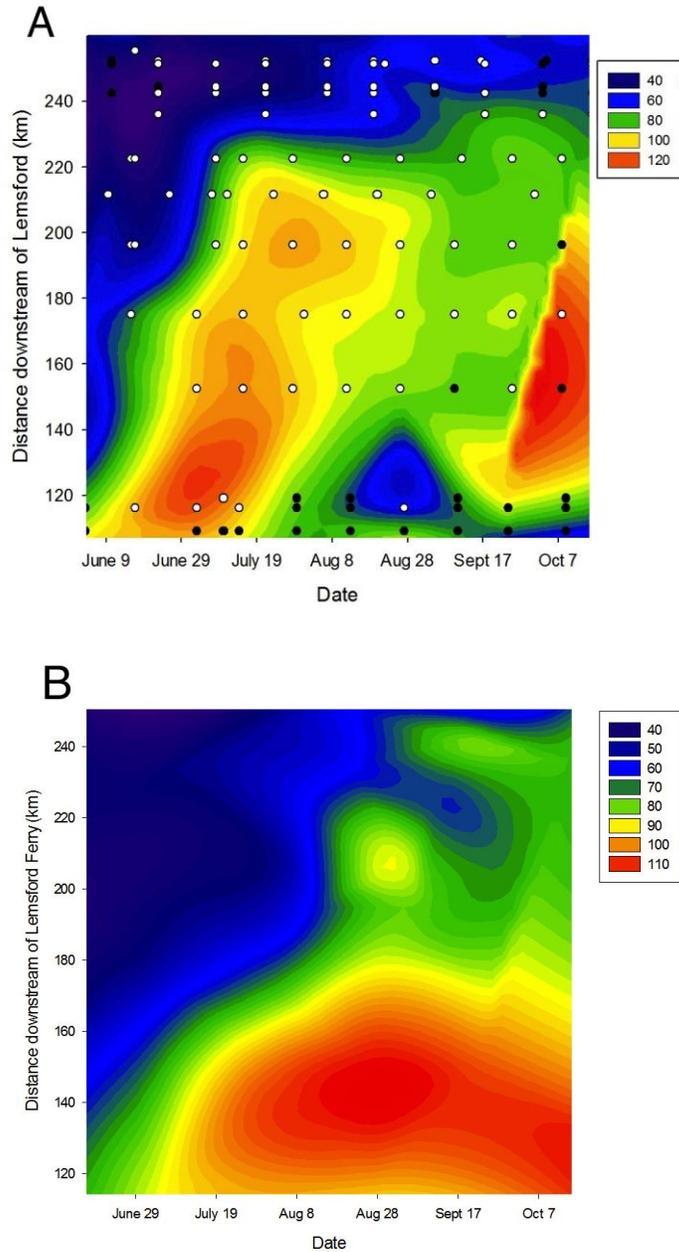
Figure 2.3: Open water season spatial and temporal variability of DSi concentrations (in μM) in (a) epilimnion and (b) hypolimnion, from the M3 sampling site to the Gardiner Dam (epilimnion) or to M8 (hypolimnion). The Qu'Appelle arm accounts for only 1% of outflow and is not shown. Distances are relative to upstream Lemsford ferry. Epilimnion DSi contours are based on 58 data points, hypolimnion contours on 32 data points. Hypolimnion DSi concentrations were only collected during periods of thermal stratification. Overlain circles identify temperature measurements used to determine thermal stratification; white circles indicate stratification, black circles indicate a well-mixed water column. See text for details. Note that sampling times and locations of temperature and DSi measurements do not always correspond.

31

down-reservoir movement of the peak DSi concentration water over time, as observed for the epilimnion, was not seen in the hypolimnion.

With the spatiotemporal distribution of the DSi concentrations, 4 distinct periods during the open water season are visually identified; a spring low DSi period (June 5 – June 18), an early-summer high DSi period (June 19 – July 16), a DSi late summer low (July 17 – August 28) followed by increasing DSi in the fall (August 29 – October 15) (Figure 2.3a). Analysis of variance (ANOVA) analysis confirmed that DSi concentrations differed significantly among these periods ($F_{3,42}$ = 6.552, $p < 0.001$). For the hypolimnion, only 2 periods could be distinguished; a spring low DSi period (June 17 – July 16) and a high DSi summer/fall period (July 17 – October 15; Figure 3b). The DSi concentrations in these 2 periods were statistically different ($F_{1,31}$ = 20.85, $p < 0.001$).

2.4.3 DSi retention

In the year of study, DSi retention, R_D, (Equation 2.2) in Lake Diefenbaker was 0.30 (Figure 2.4). The reservoir experienced a large inflow volume due to heavy rain in southern Alberta in late June of 2013. Two retention estimates were calculated for the sampling year, R_D as described in the methods, and an adjusted R_D, which is closer to a more typical year. To calculate an adjusted R_D, selected outlier peak flows were removed from the flow dataset. Outliers were determined by comparing the inflow discharge at SSR to a 52-year historical average inflow discharge (Water Office, 2014), and by comparing the yearly flow profile of both the inflow at SSR and outflow discharge at the Gardiner Dam to the preceding year (Hudson and Vandergucht, 2015). The average inflow discharge was 10.3 km^3 yr^{-1} for the June 2013 – May 2014 sampling year, while the 52 year historical average was 7.1 km^3 yr^{-1}. The preceding year, 2012, had a more typical average discharge of 8.1 km^3 yr^{-1}. In 2013, only three days were in excess of the peak discharge of the previous year at both the Gardiner Dam and at the SSR inflow: June 24-26. The annual DSi_{in} without these outliers is 9.2 x 10^8 mol yr^{-1} and DSi_{out} is 7.5 x 10^8 mol yr^{-1}. These values differ by 1% and 17% respectively, from the fluxes obtained by using all the flow data from the 2013–2014 sampling year, 9.1 x 10^8 mol yr^{-1} and 6.4 x 10^8 mol yr^{-1}. The adjusted R_D excluding outliers is 0.18, which may be more typical of an average flow year, while the unadjusted R_D for the 2013–2014 sampling year is 0.30. The small change in influx and larger efflux as a result of outlier removal indicates there is greater DSi retention in a reservoir during a flood event, particularly if reservoirs like Lake Diefenbaker operate by reducing discharge through the dam in response to flooding.

In addition to the annual calculations, separate R_D values were calculated for the open water season (June – October, 2013) and the winter (November 2013 – May 2014). The open water season
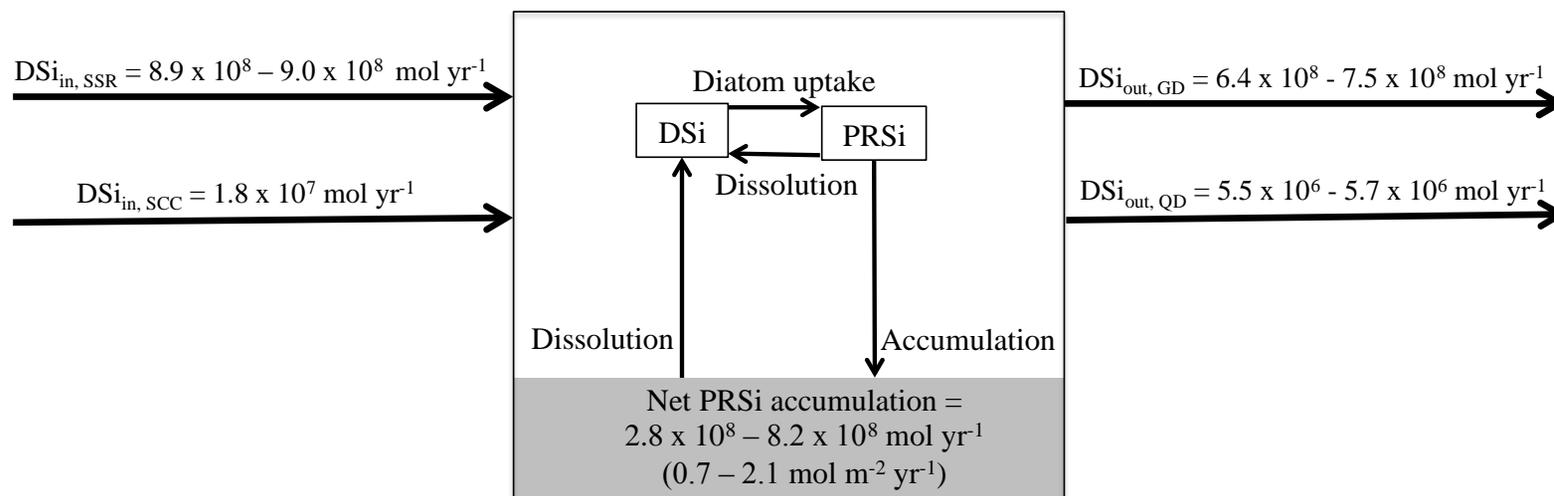
Figure 2.4: Annual reactive Si fluxes in Lake Diefenbaker for study period. GD = Gardiner Dam, QD = Qu'Appelle Dam, SSR = South Saskatchewan River, SCC = Swift Current Creek. Refer to text for assumptions related to each flux.

R_D including the June flood was 0.68, and 0.64 without flood data. Throughout the remainder of the year, R_D was equal to -1.3, indicating a net export.

2.4.4 Reactive particulate silicon

The PRSi concentration for the 7 cores averaged 0.38 mol kg^{-1} (2.3 dry wt% SiO$_2$) (Figure 2.5). The highest PRSi concentrations were observed in the mid-reservoir Cores 3, 4 and 5, which peaked at 0.88 mol kg^{-1} in the top 1 cm of Core 5. Concentrations in Cores 1 and 2 were much lower, averaging 0.22 and 0.29 mol kg^{-1}, respectively. Core 3 had the highest overall PRSi concentration, averaging 0.62 mol kg^{-1} with consistently high concentrations > 0.5 mol kg^{-1} at all depths. Sediments from the down-reservoir arms (Cores 6 and 7) had intermediate PRSi concentrations, averaging 0.53 and 0.46 mol kg^{-1} in the most recent 5 years of deposition. While there was little change in PRSi concentration with depth in Cores 1, 2, and 3, all cores down-reservoir of Core 3 show decreasing PRSi trends with depth (Figure 2.5).

2.5 Discussion

2.5.1 Sediment PRSi records

The down-core trend in PRSi concentration in Cores 3 to 7 can indicate changes in reservoir silica dynamics over time (Figure 2.5). Down-core trends in PRSi concentration differed among cores, indicating that temporal changes in diatom biomass varied spatially throughout the reservoir. Up-reservoir of SCC there was no apparent change in PRSi concentration with depth, indicating no change during the period captured by these cores (approximately 8 and 13 years) at this location. PRSi concentrations were below 0.36 mol kg^{-1} up-reservoir of SCC in Cores 1 and 2, but were highest overall at Core 3 (about 0.62 mol kg^{-1} PRSi on average), indicating a hotspot for Si deposition throughout the period of time represented by the core profile (approximately 38 to 39 years). Top-core concentrations of PRSi suggest that the current region of highest siliceous algal biomass is currently between Cores 3 and 5. Abirhire et al. (2015) observed the reservoir's highest diatom biomass in this location, further indicating that high PRSi concentrations are derived from diatom frustules. Down-core PRSi concentrations were similar among all cores, suggesting more uniform diatom biomass and *PRSi$_{acc}$* throughout the reservoir in its earlier history. This is also indicated by Lake Diefenbaker down-core diatom community structure (Lucas et al., 2015a). The recent increase in PRSi concentration mid-reservoir suggests increases in algal biomass or changes in phytoplankton community composition favouring an increased abundance of diatoms.

34
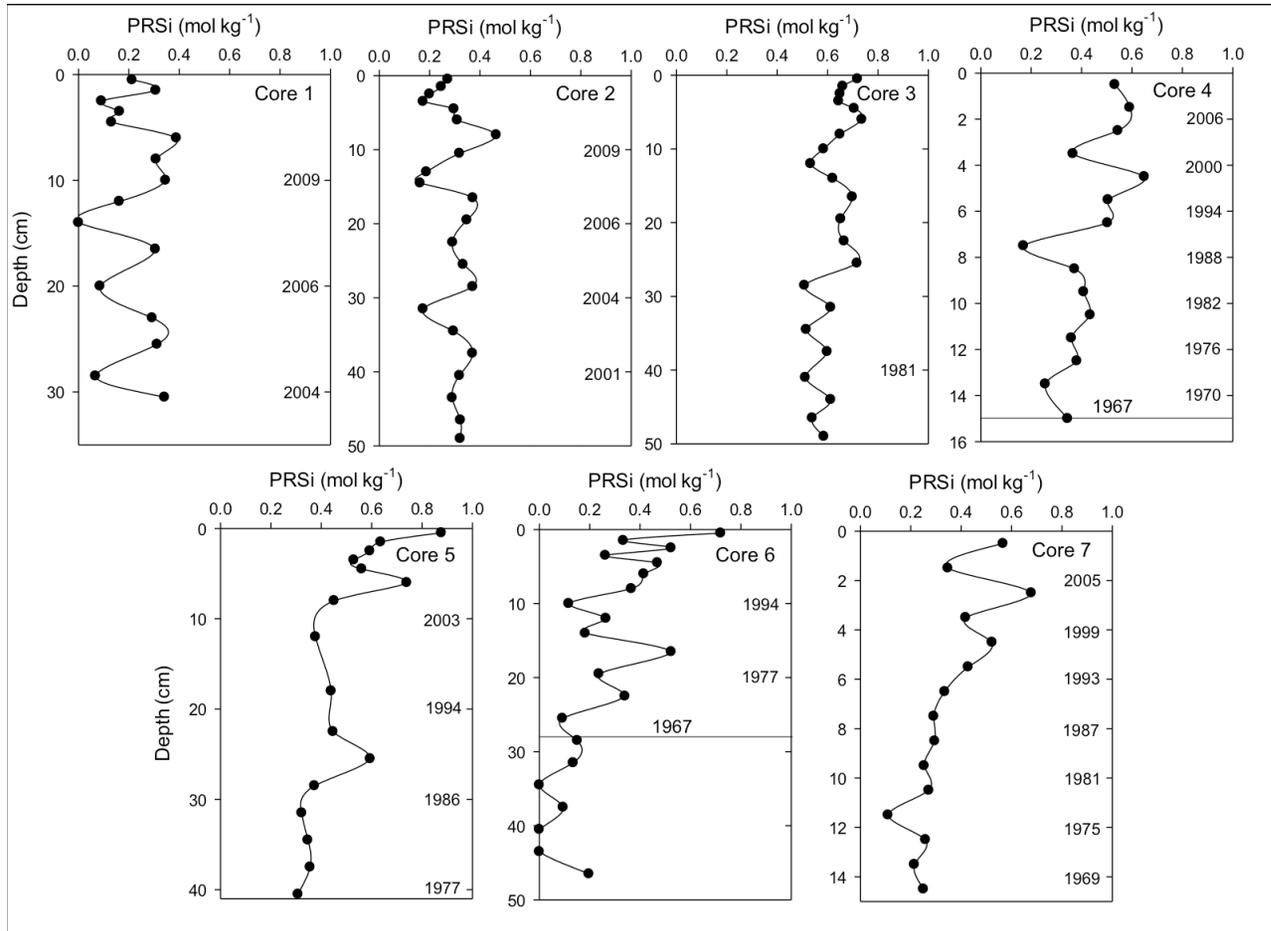
Figure 2.5: PRSi concentration (mol kg^{-1}) for sediment cores within Lake Diefenbaker. Core bottoms (1967) are marked for Cores 4 and 6. Approximate dates are given on a secondary y-axis where applicable. 0 cm depth represents 2011 for Cores 1–2 and 4–6, and 2012 for Cores 3 and 7.

The perceived higher diatom production mid-reservoir between Cores 3 and 5 could have resulted from slower current velocity, leading to decreased turbidity (Soballe and Kimmel, 1987), while still maintaining relatively high DSi and other nutrient concentrations that enter the reservoir with the inflow water. Decreased turbidity results in increased light availability, which may stimulate diatom and other algal production, leading to increased biomass. The increased algal biomass may drawdown water column nutrient concentrations, resulting in lower dissolved nutrient concentrations available further down the reservoir. A turbidity gradient down-reservoir of SCC is supported by a shift in algal community from upstream diatom species (e.g., *Stephanodiscus)* to high-light species (e.g., *Aulacoseira*; Lucas et al. (2015a)). These dynamics are consistent with established hydrodynamic zonation of dammed river valley reservoirs, which can be subdivided into longitudinal fluvial, transition, and lacustrine zones (Kimmel and Groeger, 1986; Thornton et al., 1996). Cores 3 to 5 capture Lake Diefenbaker's transition zone, characterized by higher light and nutrient availability (Dubourg et al., 2015), thus enabling higher algal productivity and biomass. The down-reservoir lacustrine zone, represented in the Gardiner and Qu'Appelle arms, is characterized by slightly lower nutrient availability and lower light availability, likely due to higher maximum depths. These characteristics are reflected by the lower PRSi concentrations observed in the sediment cores. Similar DSi reductions have been observed in the tributaries and upstream lakes of the Yangtze River, where diatom uptake draws down DSi concentrations before waters reach the main river (Duan et al., 2007).

2.5.2 In-reservoir DSi dynamics

DSi concentrations in the epilimnion and the hypolimnion vary seasonally and spatially within the reservoir, but are high enough not to be limiting for diatom production (i.e., less than 16:1:17 N:P:Si; Hecker et al. (2012); Teubner and Dokulil (2002)). Changes in epilimnetic DSi concentration can result from changes to DSi inflow concentrations and from diatom uptake. During a diatom bloom event, DSi concentrations are often drawn down (Hofmann et al., 2002; Opfergelt et al., 2011) and assuming no major changes to inflow concentrations, patterns in epilimnetic DSi concentration may reflect patterns in diatom biomass.

The four distinct DSi concentration periods track from up-reservoir to down-reservoir, moving with the water current, and coincide with stratification, mixing, and high discharge from the spring melt (Figure 2.3). Low DSi concentrations in the spring may coincide with a peak in diatom biomass, a phenomenon observed in many temperate reservoirs, lakes, and rivers (Ferris and Lehman, 2007; Goedkoop and Johnson, 1996; Müller et al., 2005). The low spring concentrations, averaging 47 μM, appear first further down-reservoir, but, as we have observed that concentration highs and lows move

36

from upstream to downstream over time, it is possible that the low period extended up-reservoir earlier than the sampling period of this study. The observations of high diatom biomass by Dubourg et al. (2015) throughout the mid-reservoir support the inference of a spring peak in diatoms.

The DSi concentration increased in early summer, after stratification, to an average of 81 μM in the epilimnion (Figure 2.3). This may indicate the end of the spring diatom biomass peak, which also coincides with yearly peak discharge, and therefore peak turbidity, at the end of June. Although the DSi low concentration period extends down-reservoir, the period of higher DSi concentration does not; this is likely a result of DSi uptake, indicating that diatoms control water column DSi concentrations even in the summer, after the spring bloom. This interpretation would seem to be supported by observations of high diatom biomass in the Gardiner arm during this time (Dubourg et al., 2015). This is also the period associated with the highest DSi retention (Figure 2.2). Spatially, the decline in DSi concentration mid-reservoir coincides with the locations of Cores 3 to 5, supporting the finding that PRSi is higher in the mid-reservoir cores due to biological uptake and subsequent sedimentation. Together, these observations indicate that the fluvial-to-lacustrine transition zone mid-reservoir is a hotspot for DSi uptake and Si retention, exhibiting disproportionately high reaction rates relative to the rest of the reservoir (McClain et al., 2003). We can further conclude that diatom uptake is the most dominant control on DSi concentrations in Lake Diefenbaker during the open water season throughout the reservoir.

Late summer DSi concentration lows reflect low inflow concentrations and lower phytoplankton biomass (Dubourg et al., 2015). After a bloom event, diatoms sink below the thermocline and become buried in the sediment, but any increase in DSi resulting from partial dissolution of frustules cannot be brought back to the surface until fall turnover. The increase in DSi in the mid-reservoir region in late-September is most likely the result of delivery of DSi from the hypolimnion during fall turnover, and evidence suggests this supported a small increase in phytoplankton biomass, which included diatoms (Dubourg et al., 2015). The timing of fall turnover for the mid-reservoir location (between U1-M and F4-M) is supported by observations of water column mixing (Figure 2.3a). This period coincides with negative DSi retention, or apparent DSi export (Figure 2.2). DSi concentrations were less variable and relatively high in the hypolimnion throughout the summer and fall, suggesting sediment Si dissolution. Note that net PRSi preservation in the cores indicates that only a fraction of PRSi is dissolved during this time.

Changes in DSi concentration represent the net effect of both uptake and remineralization or dissolution, and the high DSi concentrations observed in the hypolimnion of Lake Diefenbaker indicate sediment Si dissolution. During stratification, DSi originating from the sediment cannot easily enter the mixed layer to subsequently be taken up by diatoms, leading to hypolimnetic DSi concentration build-up over the summer. Rapid PRSi dissolution and recycling has been observed in other lakes and reservoirs, including Marne Reservoir, Three Gorges Reservoir, and Lough Neagh (Garnier et al., 1999; Gibson et al., 2000; Ran et al., 2013). Results from these studies indicate that sediment dissolution can take place over relatively small timescales (i.e., on the order of days to weeks), leading to Si changes seasonally within the reservoir, rather than slowly as the reservoir ages.

2.5.3 DSi retention

The majority of Lake Diefenbaker's retention occurred in the open water season from June to September when diatom productivity facilitated the transformation of DSi into PRSi. R_D during this time was 0.64–0.66, indicating efficient transformation of inflowing DSi to PRSi. Through the ice-covered winter, the reservoir was a source of DSi to the downstream watershed, indicated by the R_D of -1.3. The reservoir is drawn down in the winter, and so from a mass-balance approach a portion of the net DSi loss is due to a decrease in the volume of water present in the reservoir. During the reservoir drawdown period from October to March, the reservoir level dropped approximately 4.6 m. We can use this drawdown to calculate the approximate change in reservoir volume during this period (1.8 km^3). By then multiplying this volume loss by the average reservoir outflow DSi concentration, the approximate mass lost due to reservoir drawdown is calculated. Using an average concentration of 65.6 µM at the Gardiner Dam, I estimate that approximately 1.2 x 10^8 mol of DSi is exported from the reservoir via drainage alone, or 34% of the net export. The remainder of the efflux presumably arises due to the dissolution of previously deposited PRSi to the water column, and delivery from the hypolimnion after fall turnover. These vastly different seasonal results provide compelling evidence for the need to quantify year-round Si fluxes in reservoir budgets in order to determine the effect of the reservoir on the Si cycle of downstream environments.

Lake Diefenbaker's 2013–2014 R_D value of 0.30 is somewhat higher than the retention found in other reservoirs, while the 0.18 retention calculated without flood outliers is more typical of reservoirs of this size. Maavara et al. (2014) estimated that globally, reservoirs have an average R_D of 0.13 and rarely exceed 0.3 except when residence time approaches 5 years or more. Lake Diefenbaker's high R_D in 2013 may be driven by reservoir operation protocol (i.e., a reduction in

discharge through the dam as a result of the need for flood control), while the adjusted R_D (0.18) is more similar to the average global retention estimate. This finding suggests high flow years and years with large flood events, may have higher DSi retention, and dam operation protocol has an impact on reservoir DSi retention, and thus, the DSi cycle in downstream environments.

There are few studies on Si dynamics for large reservoirs with similar residence times with which to compare my findings. Falcon Reservoir on the Rio Grande in Texas is hydrodynamically similar to Lake Diefenbaker with a residence time of 0.8 years and a surface area of 339 km^2 (Kelly, 2001). R_D in Falcon Reservoir is 0.17, the same as Lake Diefenbaker's adjusted R_D. Falcon Reservoir also has an excess of DSi relative to N and P, and comparable turbidity (typically <10 NTU) (Hudson and Vandergucht, 2015). It is likely that there is considerable annual and seasonal variability governing retention in each of these reservoirs, as there is for Lake Diefenbaker. However, whether the seasonal trends in DSi retention are similar in all reservoirs has yet to be determined. Long-term evolution of Si transformations in reservoirs additionally may be critical to the amount of retention that takes place annually. Reservoir ageing hypotheses suggest that over time, water column turbidity and sediment accumulation decrease (Holz et al., 1997; Kimmel and Groeger, 1986). The combined effects of these changes on primary productivity and PRSi re-dissolution to the water column remain unclear and may be key variables governing long-term Si retention in reservoirs.

2.5.4 Annual PRSi accumulation

The R_D estimates for the 2013–2014 sampling year indicates that the reservoir is a net sink for Si and it promotes the transformation of DSi to PRSi, mainly driven by diatom uptake. The reservoir's $PRSi_{acc}$ values support this observation. Using the most recent 5 years of deposition for each core and applying the M_{acc} range, a $PRSi_{acc}$ of 5.8 x 10^8 – 8.2 x 10^8 mol yr^{-1} was calculated. Frings et al. (2014) have shown that using one sediment core to represent cross-sectional deposition in lacustrine water bodies can lead to overestimation of $PRSi_{acc}$. Sediment focussing tends to result in the majority of accumulation taking place in the deepest section of a water body, corresponding to the mid-channel locations where Lake Diefenbaker cores were collected. Cross-sections reconstructed for Lake Diefenbaker's mid-reservoir location show that the sediment depositional area may represent as little as 50% of the overall reservoir surface area (Sadeghian et al., 2015). Halving yields a revised $PRSi_{acc}$ of 2.9 x 10^8 – 4.1 x 10^8 mol yr^{-1}.

The most recently deposited PRSi may not have yet undergone seasonal dissolution to the water column. The high values in the top 1 cm of Cores 5 and 6 may be indicators of pre-seasonal

diagenesis. Including these values in the top-core concentration averages could lead to an over-estimation of the net annual $PRSi_{acc}$. I have therefore calculated a $PRSi_{acc}$ that excludes the top 1 cm in the calculation of all average top-core PRSi concentrations. Overall reservoir $PRSi_{acc}$ decreases to $5.6 \times 10^8 - 8.0 \times 10^8$ mol yr^{-1} using reservoir surface area, or $2.8 \times 10^8 - 4.0 \times 10^8$ mol yr^{-1} using a 50% sediment depositional area.

My overall range of $PRSi_{acc}$ estimates, $2.8 \times 10^8 - 8.2 \times 10^8$ mol yr^{-1} (normalized by surface area to $0.7 - 2.1$ mol m^{-2} yr^{-1}) is lower than $PRSi_{acc}$ of Si-rich reservoirs, including the Iron Gates Reservoir on the Danube River (2.6 mol m^{-2} yr^{-1}) (Friedl et al., 2004; Teodoru and Wehrli, 2005), St. Croix on the Mississippi River (2.9 mol m^{-2} yr^{-1}) (Triplett, 2008), and Amance and Champaubert Reservoirs in the Seine River basin (3.4 and 4.5 mol m^{-2} yr^{-1} respectively) (Garnier et al., 1999). The disparity of low $PRSi_{acc}$ and average-to-high R_D values relative to other reservoirs may be accounted for by the water column PRSi fluxes, specifically, large PRSi effluxes via the dams. Future research quantifying water column PRSi fluxes would be beneficial to enhance Lake Diefenbaker's Si budget, as well as help contextualize Si budgets for other reservoirs.

In contrast to Si retention, the Lake Diefenbaker phosphorus and nitrogen budgets indicate near-complete retention of P in the reservoir (North et al., 2015), and low N retention, with net export in some years (Donald et al., 2015). The difference between Si, P, and N retention suggests a de-coupling of the nutrient cycles, and indicates that the mechanisms of retention are not the same for Si, P, and N. This feature of reservoir nutrient retention has not been explored in the literature and future research should focus on assessing the impact of preferential P retention on both reservoir ecosystems and downstream aquatic and marine environments, in both Si and P- or N- deficient systems.

2.6 Conclusions

This study represents the first report of Si dynamics in Lake Diefenbaker. Analysis of Lake Diefenbaker water column samples (DSi concentrations), sediment cores (PRSi concentrations), and sediment accumulation rates revealed that DSi retention is 0.30 for the 2013–2014 sampling year. The mechanisms responsible for the high DSi retention in Lake Diefenbaker may likely be related to high water column DSi concentration relative to N and P, long water residence times, and flood control operation of the reservoir. The majority of Si retention takes place in the mid-reservoir region in the transition zone from fluvial to lacustrine hydrodynamics, which represents a hotspot in Si cycling. This may be a feature unique to river-influenced reservoirs and highlights their importance in

landscape biogeochemical cycling. Temporally, high diatom productivity during the open water season (June – October) results in the transformation of DSi to PRSi, and a net flux of PRSi to the sediment. In winter, PRSi is dissolved to the water column, leading to net DSi export from the reservoir. The near-complete retention of P, low N retention, and moderate Si retention represents de-coupling of the phosphorus, nitrogen, and silicon cycles and has the potential to influence downstream, coastal, and marine ecosystems. Future reservoir Si budgets should assess the role of nutrient retention in Lake Diefenbaker in the context of downstream ecosystem health. In addition, long-term multi-year data, including water column PRSi, should be collected in order to assess internal variability in Si retention, and the time-dependent evolution of the reservoir's Si budget.

Chapter 3

Worldwide retention of nutrient silicon by river damming: From sparse dataset to global estimate

This chapter is modified from:

3.1 Summary

Damming of rivers represents a major anthropogenic perturbation of the hydrological cycle, with the potential to profoundly modify the availability of nutrient silicon (Si) in streams, lakes and coastal areas. A global assessment of the impact of dams on river Si fluxes, however, is limited by the sparse data set on Si budgets for reservoirs. To alleviate this limitation, I use existing data on dissolved Si (DSi) retention by dams to calibrate a mechanistic model for the biogeochemical cycling of DSi and reactive particulate Si (PSi) in reservoir systems. The model calibration yields a relationship between the annual in-reservoir siliceous primary productivity and the external DSi supply. With this relationship and an estimate of catchment Si loading, the model calculates the total reactive Si (RSi = DSi + PSi) retention for any given reservoir. A Monte Carlo analysis accounts for the effects of variations in reservoir characteristics, and generates a global relationship that predicts the average reactive Si retention in reservoirs as a function of the water residence time. This relationship is applied to the GRanD database to estimate Si retention by damming worldwide. According to the results, dams retain 163 Gmol yr^{-1} (9.8 Tg SiO$_2$ yr^{-1}) of DSi and 372 Gmol yr^{-1} (22.3 Tg SiO$_2$ yr^{-1}) of RSi, or 5.3% of the global RSi loading to rivers.

3.2 Introduction

Silicon (Si) is an essential nutrient element for numerous aquatic organisms, foremost diatoms (Conway et al., 1977; Tréguer et al., 1995; Van Cappellen, 2003). The availability of Si is therefore a key variable controlling the ecology and health of many aquatic environments, including rivers, lakes and the coastal zone (Billen et al., 1991; Conley et al., 1993; Koszelnik and Tomaszek, 2008; Schelske and Stoermer, 1971; Tavernini et al., 2011). A growing number of studies have highlighted the effects of human modifications of stream and river systems, in particular the building of dams, on Si retention and the resulting consequences for regional to global scale nutrient cycling and ecological processes (Beusen et al., 2009; Conley et al., 1993; Garnier et al., 2010; Harrison et al., 2012; Hartmann et al., 2011; Humborg et al., 2000; Laruelle et al., 2009; Teodoru and Wehrli, 2005; Thieu et al., 2009). As ongoing construction of dams continues to increase the global volume of reservoirs, it is important to develop a predictive understanding of the accompanying impacts on Si fluxes along the river continuum.

Silicon is supplied to reservoirs under both dissolved and particulate forms. While diatoms and other siliceous organisms can directly take up dissolved Si, many Si-containing solid phases, including quartz and silicate minerals, are unavailable for biological utilization (Cornelis et al., 2011;

43

Dürr et al., 2011; Iler, 1979). A fraction of particulate Si, however, is supplied as reactive solid and solid-bound forms that can potentially act as a source of soluble Si in reservoirs. Diatoms and riparian plants further contribute to the particulate reactive Si pool of a reservoir through the production of biogenic silica (Sauer et al., 2006; Triplett, 2008; Znachor et al., 2013). Silicon retention is thus the net result of the interactions between the external supply of reactive Si, in-reservoir formation of biogenic silica, plus the dissolution and ultimate preservation of particulate reactive Si (Lauerwald et al., 2012; Teodoru et al., 2006; Van Cappellen, 2003).

A number of recent studies have addressed global Si retention by river damming. Beusen et al. (2009) used the Global-NEWS-DSi model, in which dissolved Si retention is assumed to correlate with global trends in phosphorus and sediment retention. Laruelle et al. (2009) introduced a correction factor in their global Si box model to simulate increased reactive Si retention on the continents under various damming scenarios. Harrison et al. (2012) took a step further with the development of the Silica Retention in Reservoirs and Lakes (SiRReLa) model. The SiRReLA model was statistically calibrated using a dataset of 12 lakes and 15 reservoirs. Harrison and coworkers proposed that the effects of trophic status and hydraulic load on the particle settling velocity represent the primary factors modulating Si retention in reservoirs. As with the work of Beusen et al. (2009), the SiRReLa model only accounts for the retention of dissolved Si. More recently, Frings et al. (2014) derived an average accumulation rate of biogenic silica in reservoirs, based on data from 18 reservoirs. By multiplying this rate by the total reservoir surface area, they then computed the mass of reactive Si retained annually by dams. A major source of uncertainty in the work of both Harrison et al. (2012) and Frings et al. (2014) is the small size of the data sets on which the global estimates are based.

Here, I re-evaluate worldwide reactive Si retention by man-made river dams, by combining existing data on dissolved Si retention with a mechanistic model of biogeochemical Si cycling in reservoirs. The proposed approach is designed to compensate for the sparse data on Si budgets in artificial reservoirs. The process-based model accounts for the fate of both reactive dissolved and particulate Si in reservoir systems. The model is calibrated with existing data on dissolved Si retention in reservoirs, while a Monte Carlo analysis accounts for the effects of the statistical variability of reservoir characteristics on the model-predicted retention of reactive Si. Based on the results, I then derive a relationship between reactive Si retention and water residence time, and use it to estimate global accumulation of reactive Si in reservoirs.

3.3 Terminology

In this chapter, reactive Si (RSi) refers to the sum of dissolved reactive Si and reactive particulate Si. Dissolved reactive Si (DSi) consists almost entirely of monomeric silicic acid or silicon hydroxide (H_4SiO_4). In most freshwaters, ionized forms of silicic acid and silica dimers and polymers only contribute minute fractions of DSi (Iler, 1979). Reactive particulate Si (PSi) comprises all particle-associated Si that can potentially dissolve prior to removal by burial in bottom sediments or river outflow. The distinction between reactive and unreactive particulate Si is somewhat subjective and depends on the reservoir under consideration. The input of PSi to a reservoir includes soil- and river-derived amorphous silica (SiO_2) and hydrous, poorly crystalline aluminosilicates, as well as Si sorbed to minerals, for example ferric oxyhydroxides (Davis et al., 2002), and natural organic matter. For many reservoirs, the PSi input likely consists largely of biogenically produced SiO_2, that is, structural siliceous deposits produced by plants (phytoliths), diatoms and other organisms (Barão et al., 2014; Saccone et al., 2007; Sauer et al., 2006; Struyf and Conley, 2009; Teodoru et al., 2006; Van Cappellen, 2003). Production of siliceous frustules by diatoms within the reservoir or lake further adds to the PSi pool.

Retention of RSi refers to its removal by processes in the reservoir. The main sink for RSi is burial of PSi in bottom sediments. Because data on PSi burial fluxes in artificial reservoirs are fairly scarce (Frings et al., 2014), RSi retention is generally estimated from the difference between measured input and output fluxes:

$$R_R = \frac{RSi_{in} - RSi_{out}}{RSi_{in}} \tag{3.1}$$

where R_R is the relative retention of RSi (unitless), and RSi_{in} and RSi_{out} are the input and output fluxes of reactive Si in units of mass per unit time. Equation 3.1 assumes that, on an annual basis, the reservoir's RSi budget is close to steady state. In most studies, the inputs and outputs of reactive Si are assumed to occur entirely via the river network, hence neglecting potential contributions to the RSi budget by atmospheric deposition or groundwater flow.

Because data sets on Si budgets for reservoirs usually only include measurements of DSi, but not PSi, usually only the retention of DSi is calculated from

$$R_D = \frac{DSi_{in} - DSi_{out}}{DSi_{in}} \tag{3.2}$$

45

where R_D is the relative retention of DSi (unitless), and DSi_{in} and DSi_{out} are the input and output fluxes of DSi. The values of R_D and R_R converge when DSi dominates RSi inputs and outputs. The latter is in fact an implicit assumption in most existing studies on Si retention in reservoirs and lakes. The input of DSi_{in} is typically calculated as the product of inflow discharge (Q_{in}) and the inflow DSi concentration (C_{in}). In reservoirs that discharge all water through the dam (e.g., hydroelectric reservoirs), DSi_{out} is similarly the product of outflow discharge (Q_{out}) and outflow DSi concentration (C_{out}). For storage reservoirs (e.g., reservoirs used for irrigation or municipal water supply), DSi_{out} is split between the water flow pumped out of the reservoir and that discharged through the dam. In order to maintain a water balance, the sum of the water flows pumped out of the reservoir and discharged through the dam is assumed to equal Q_{in}, that is, losses through groundwater recharge and evaporation are neglected. Unless available information indicates otherwise, I assume that the DSi concentrations in the pumped and discharged water flows are the same. In what follows, water fluxes, concentrations and retentions refer to annual averages.

3.4 Dataset

An exhaustive literature search yielded only 20 reservoirs for which R_D was provided or could be estimated (Table 3.1). (Note: I focus on DSi retention, because of the general lack of PSi measurements.) For comparative purposes, a dataset of 24 natural lakes was also assembled (Table AB1, Appendix B). The reservoir data set in Table 3.1 extends those of Harrison et al. (2012) and Frings et al. (2014). I only included artificial reservoirs associated with constructed dams. Thus, causeways, such as Lake Lugano, and natural impoundments, such as Lake Pepin, were not considered as reservoirs. For each reservoir or lake, the following information was collected: (1) surface area, (2) volume, (3) average water depth, (4) river discharge, (5) hydraulic load, (6) annual DSi influx and (7) efflux, (8) water residence time, (9) trophic status, (10) bedrock lithology of the catchment, (11) pH, and (12) climate (that is, temperature and precipitation). In addition, for the reservoirs I included the (13) primary function and (14) age of the reservoir.

The effects on DSi retention of the reservoir and lake properties included in the database were assessed through analysis of variance (ANOVA), t-tests, and regression models. The statistical analyses aimed at identifying the key variables to be included in the mechanistic Si reservoir model (section 3.5). A complete description of the results of the statistical analyses can be found in Appendix B and Table AB2. Local bedrock lithology was obtained from the various countries' national geological maps, and crosschecked against the Global Lithology Map (GLiM) database

46

(Hartmann and Moosdorf, 2012). Water residence time (τ_r) was calculated as $\tau_r = V/Q_{in}$, where V is the lake or reservoir volume, and Q_{in} the combined river inflow. In the absence of information on trophic status, or when it was poorly supported, I relied on Carlson and Simpson (1996)'s trophic status index approach. When not stated in the reference(s) listed in Table 3.1, the primary reservoir function (e.g. hydroelectricity production, irrigation, drinking water supply, or other) was extracted from the Global Reservoirs and Dams (GRanD) database (Lehner et al. 2011). Average annual precipitation and temperature were obtained for the nearest town or city from the World Climate database (worldclimate.com) and Environment Canada for Canadian lakes; for Toolik Lake, Alaska, climate data were retrieved from the Toolik Field Station website (http://toolik.alaska.edu/). The age of a reservoir is the number of years between dam closure and the date of data collection as stated in the original literature source. In those cases where data covered a range of years (e.g., Lake Alexandrina), the mid-point age was used. The age reported for the recently completed Suofenying Reservoir is "0 years" (Wang et al., 2010). In order to include this reservoir in the statistical analyses, I arbitrarily assigned a reservoir age of 0.1 years.

While originally data for 22 reservoirs were found, detailed analysis of the literature sources revealed that in a few of the studies major river inflows to the reservoir were neglected, thus introducing significant uncertainty in the estimated DSi retention. The most notable examples are Amistad Reservoir and the Lower Columbia Basin, for which the available data yielded large negative DSi retentions (-0.20 and -0.67, respectively). These reservoirs were all together removed from further analysis. Additionally, three reservoirs (Ardleigh, Suofenying, and Masinga) were excluded from the mechanistic model calibration (for justifications, see caption of Table 3.1). Thus, in total, 20 reservoirs were included in the statistical tests and 17 reservoirs in the calibration of the mechanistic model.

Comparison of the 20 reservoirs in Table 3.1 to the GRanD database (Lehner et al., 2011) (Figure 3.1) reveals a lack of reservoirs in Table 3.1 with water residence times over 3 years, which account for 21% of the GRanD reservoirs. They further point to a possible bias of my dataset towards reservoirs in areas dominated by limestone and, thus, towards more alkaline pH, which may increase the dissolution and decrease the preservation of biogenic silica (Ryves et al., 2006; Van Cappellen and Qiu, 1997). My dataset provides a reasonably good climatic distribution, with the majority of reservoirs located in temperate and subtropical latitudes, although no DSi retentions were obtained for arctic and subarctic reservoirs, which account for 8% of the GRanD

47
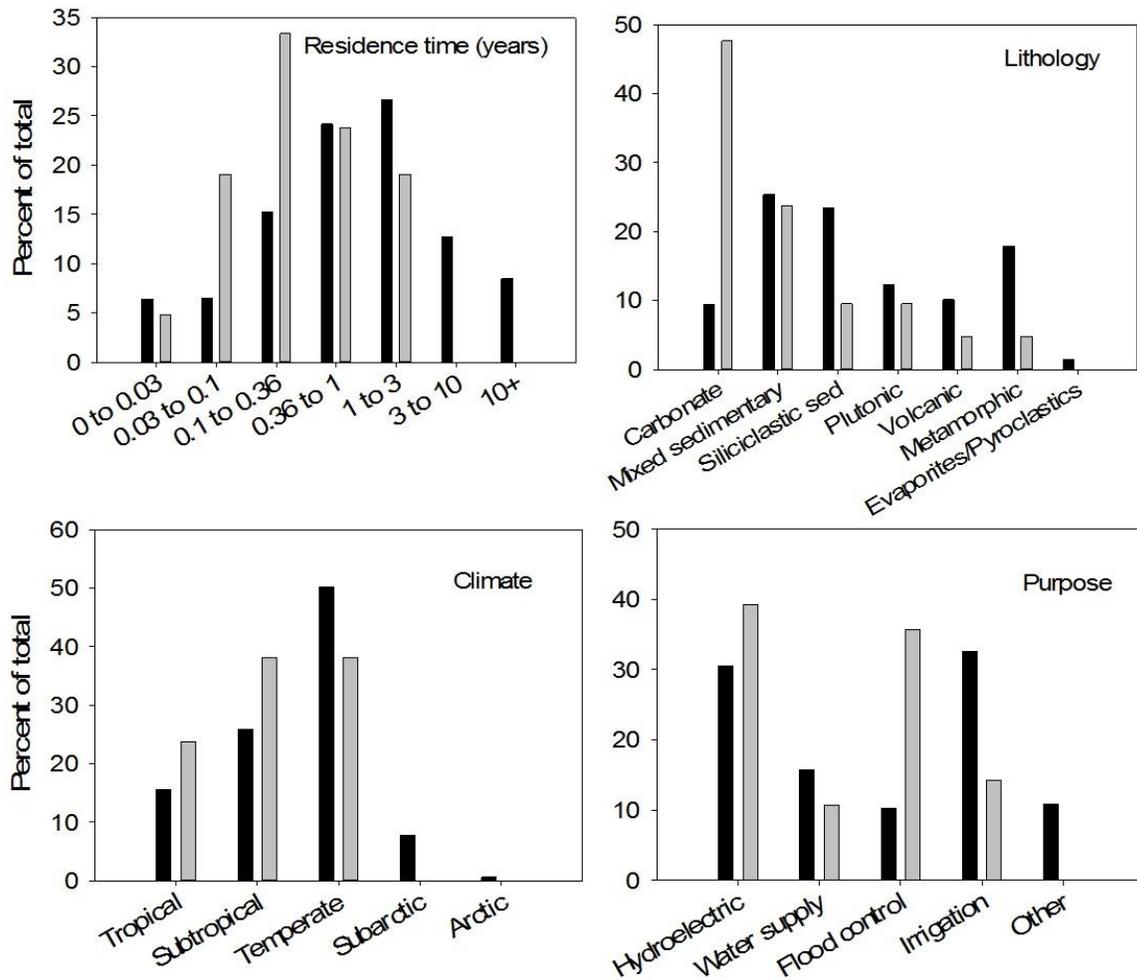
Figure 3.1: Comparison of reservoirs included in the calibration dataset (gray bars), described in section 3.4 and Table 3.1, and those of the GRanD database (black bars), according to residence time (in units of years), bedrock lithology, climate, and reservoir purpose. "Other" reservoir purposes include fisheries, navigation and recreation.

Table 3.1: Reservoir data set: see text for details. Oligo = oligotrophic, meso = mesotrophic, and eu = eutrophic. *Indicates reservoirs excluded from the calibration of the mechanistic model, but included in the statistical analyses (Ardleigh's water budget was unbalanced, Masinga was missing DSi flux information, and initial conditions for Suofenying could not be reconstructed).

Latitude	Reservoir name	Location	Bedrock lithology	Trophic status	Surface area (km^2)	Mean depth (m)	pH	Climate	Residence time (years)	DSi influx (mol yr^{-1})	R_D	Primary usage	Age (yrs)	Ref.
26.97	Suofenying*	China	Carbonate	Meso	5.7	23.5	8.06	Subtropical	0.016	4.56 x 10^8	-0.072	Hydroelectric	0	1
26.9	Dongfeng	China	Carbonate	Oligo	19.7	52	8.06	Subtropical	0.1	3.99 x 10^8	-0.055	Hydroelectric	12	1
27.3	Wujiangdu	China	Carbonate	Eu	47.5	48.4	8.06	Subtropical	0.14	5.41 x 10^8	0.23	Hydroelectric	27	1
36.9	Lake Powell	USA	Sandstone	Oligo	658	40	8.5	Subtropical	2.3	4.81 x 10^9	0.081	Irrigation	29	2
36.4	Lake Mead	USA	Sandstone	Meso	640	40	8.3	Subtropical	2.6	4.94 x 10^9	0.13	Irrigation	62	2, 21
26.6	Falcon	USA	Mixed sedimentary	Eu	338.5	11.52	7.9	Subtropical	1	7.02 x 10^8	0.17	Irrigation	44	2
44.6	Iron Gate	Romania	Mixed sed, carbonate	Eu	156.4	17.3	8.0	Temperate	0.03	1.41 x 10^{10}	0.040	Hydroelectric	29	3, 4, 5
48.2	Amance	France	Carbonate	Eu	0.5	4.5	N/A	Temperate	0.03	5.39 x 10^7	0.089	Flood control	4	6
48.2	Seine	France	Carbonate	Eu	23	7.6	N/A	Temperate	0.62	5.45 x 10^7	0.43	Flood control	28	6, 7
48.2	Aube	France	Carbonate	Eu	21	8.9	N/A	Temperate	0.4	2.32 x 10^7	0.57	Flood control	4	6
48.3	Marne	France	Carbonate	Eu	48	7.2	N/A	Temperate	0.46	5.39 x 10^7	0.48	Flood control	20	6
48.3	Champaubert	France	Carbonate	Eu	0.5	3.5	N/A	Temperate	0.11	2.32 x 10^7	0.158	Flood control	20	6
21.7	Thac Ba	Vietnam	Gneiss, carbonate	Meso	235	58	7.5	Tropical	2.2	7.19 x 10^9	0.012	Hydroelectric	31	8, 9
20.5	Hoa Binh	Vietnam	Mixed sed, carbonate	Meso	208	46	5.57	Tropical	0.09	8.07x10^9	0.16	Hydroelectric	9	8, 9, 20
30.8	Three Gorges	China	Carbonate	Eu	1100	35.5	8.04	Subtropical	0.097	4.65 x 10^{10}	0.038	Hydroelectric	4	10, 11
-6.9	Saguling	Indonesia	Volcanic	Eu	56	18.4	7.6	Tropical	0.23	1.49 x 10^9	0.382	Hydroelectric	18	13
-0.9	Masinga*	Kenya	Mixed igneous/ metamorphic	Meso	120	13.3	8.2	Tropical	0.25	N/A	0.4	Hydroelectric	27	14
-35.5	Lake Alexandrina	Australia	Carbonate	Eu	580.6	2.86	8.6	Subtropical	0.3	9.29 x 10^8	0.39	Irrigation	47.5	15, 16, 17
51.5	Ardleigh*	England	Mixed sedimentary	Eu	0.57	3.8	8.2-9.4	Temperate	0.36	1.39 x 10^6	0.79	Water supply	13	18
49.2	Solina-Myczowce	Poland	Mixed Sedimentary	Meso	24	22	6.4-6.8	Temperate	0.61	3.25 x 10^7	0.20	Hydroelectric	36	19

References: (1) Wang et al. (2010); (2) Kelly (2001); (3) Teodoru and Wehrli (2005); (4) Friedl et al. (2004); (5) McGinnis et al. (2006); (6) Garnier et al. (1999); (7) Thieu et al. (2009); (8) Le Thi Phuong et al. (2005); (9) Tran (1995); (10) Müller et al. (2012); (11) Ran et al. (2013); (13) Wakatsuki and Masunaga (2009); (14) Hughes et al. (2012); (15) Cook et al. (2010); (16) Geddes (1984); (17) Mosley et al. (2012); (18) Redshaw et al. (1988); (19) Koszelnik and Tomaszek (2008); (20) ISAG (2000); (21) Hoffman et al. (1967).

reservoirs. All major reservoir functions, particularly, hydroelectricity generation and flood control, are represented in Table 3.1.

A key outcome of the statistical analyses is that R_D significantly differs between reservoirs and lakes (p<0.0001) with, on average, 42% more DSi retention in lakes compared to reservoirs. In addition, reservoirs typically exhibit lower water residence times (τ_r) and higher hydraulic loads than lakes. The statistical analyses further imply that grouping lakes and reservoirs together may generate spurious results. For example, when combining lakes and reservoirs, a significant (p<0.05) dependence of R_D on the catchment lithology is found, with metamorphic and crystalline felsic rocks yielding the highest DSi retention, and carbonate rocks the lowest. However, when lakes are removed from the dataset, the trend is no longer apparent, suggesting that the relationship between R_D and lithology may be representative of lakes, but not of reservoirs. Reactive Si cycling in reservoirs is thus statistically distinct from that in lakes, which argues against merging data from both types of systems into a single dataset when estimating global lentic Si retention, as done by Harrison et al. (2012). Therefore, in what follows, only the data from the artificial reservoirs are considered. The non-linear regressions further implied that, for reservoirs, R_D is most closely related to τ_r.

Although the 20 reservoirs in Table 3.1 encompass a fairly broad range of settings and reservoir characteristics, as can be seen in Figure 3.1, it is important to emphasize that they represent less than 0.03% of the more than 75,000 reservoirs with a surface area $\geq$0.1 km^2 (Lehner et al., 2011). The limited dataset is thus unlikely to be statistically representative of reservoirs worldwide. For this reason, the primary function of the dataset is to calibrate a mechanistic model of Si cycling in reservoirs, which incorporates well-understood processes and parameter values constrained through an extensive literature review. The model then provides the means to extrapolate the sparse dataset to the global scale.

3.5 Mechanistic Si cycling model

3.5.1 Model description

A 4-box biogeochemical model is used to simulate annual reactive Si (RSi) cycling in reservoirs (Figure 3.2). In the model, the inputs to and outputs from the reservoir occur under the form of both reactive particulate (PSi) and DSi. Note that the model does not distinguish between different input and output pathways. Thus, the input flux of DSi for instance includes river inflow as well as potential contributions by atmospheric deposition and groundwater discharge. Within the reservoir, dissolution of PSi generates additional DSi, while siliceous organisms, primarily diatoms, transform

DSi into biogenic silica (BSi). The BSi pool represents silica deposits within living or recently deceased biomass, that is, silica still surrounded by protective organic membranes. Upon the degradation of the organic membranes, BSi integrates into the PSi pool and is, from then on, exposed to dissolution (Loucaides et al., 2012). The PSi that does not dissolve is exported downstream or accumulates in the sediments. In order to account for the fairly rapid loss in reactivity of particulate Si (i.e., ageing), as well as the build-up of pore water DSi, the sediment Si pool (SSi) is assigned a much lower rate constant of dissolution than PSi (Van Cappellen et al., 2002). The fraction of SSi that escapes dissolution is permanently removed by burial in the reservoir's sediments.

The annual input fluxes of DSi and PSi to the reservoir are imposed in the model. As a default value, I assume that the PSi influx equals 10% of the DSi influx, based on the global estimate of riverine PSi by Conley (1997) and supported by data of Ran et al. (2013) and Triplett et al. (2012). With one exception, all internal and outflow fluxes are assigned first-order rate expressions with respect to the source reservoirs (Laruelle et al., 2009). The exception is siliceous productivity, F_{12}, which is calculated assuming parabolic saturation kinetics (Valiela, 2013):

$$F_{12} = \frac{R_{max} \times [DSi]}{K_s + [DSi]} \tag{3.3}$$

where R_{max} is the maximum rate of BSi production, [DSi] the DSi concentration, and K_s the half-saturation constant for DSi uptake by siliceous organisms. The value of R_{max} represents the reservoir's mean annual carrying capacity for biological Si fixation.

In the model, the reservoir is treated as a well-mixed reactor; the rate constants for the outflow fluxes of DSi and PSi (i.e., $F_{1,out}$ and $F_{3,out}$) are therefore equal to the inverse of the water residence time. Default values for the other linear rate constants and for K_s were derived from in-depth reviews of the literature (Table 3.2). The values of R_{max} are reservoir-specific and were determined as explained in the next section. The mass balance equations were solved in Matlab for time steps of 0.01 year using Runge-Kutta 4 integration. Reservoir age was incorporated by running the models for the number of years since river damming; e.g. for a 20-year-old reservoir, the model was run for 2000 time steps.
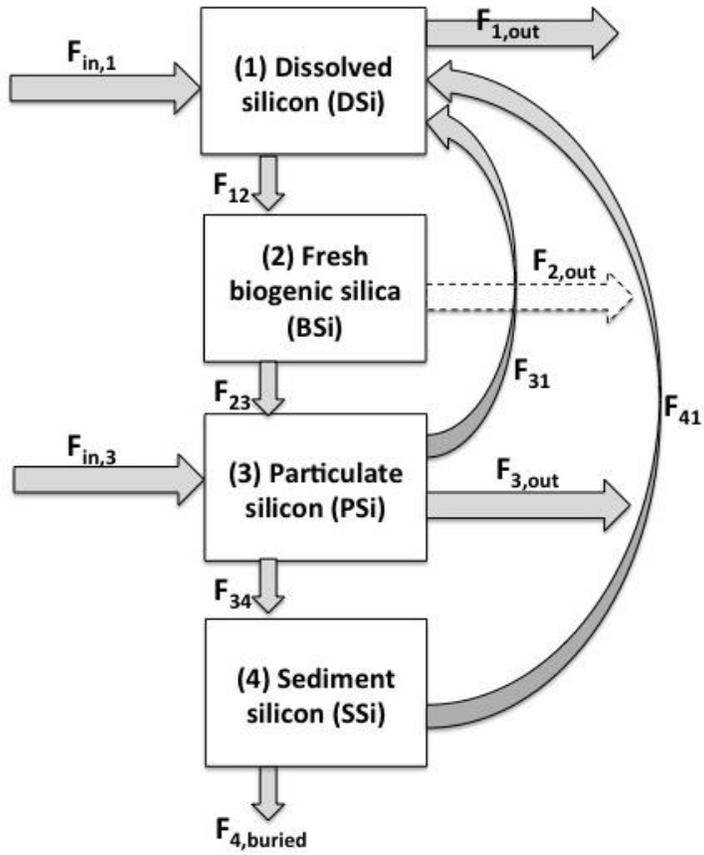
Figure 3.2: Mechanistic model of biogeochemical silicon cycling in reservoirs. See text for details.

The mechanistic model provides a highly simplified description of Si cycling, in line with the sparse database on reactive Si budgets for reservoirs. Some processes are not included, for example the direct incorporation of DSi into the SSi pool via clay mineral formation, while other processes are merged into a single flux. For instance, the fluxes F_{23} and F_{34} on Figure 3.2 combine reactive silica transformations and vertical transport. In addition, the model does not resolve seasonal effects on Si cycling in reservoirs, such as diatom blooms, flow variability or water column stratification. The model thus represents a first step in the knowledge-based scaling up of the limited data on Si dynamics in reservoirs.

3.5.2 Siliceous production: calibration

The mass balance Si model was applied to the 17 reservoirs of the calibration dataset described in section 3.4. For each reservoir the corresponding river discharge, reservoir volume, water residence time (τ_r), DSi influx and age (i.e., years since dam closure) were imposed. After assigning the default parameter values of Table 3.2, the only remaining free model parameter was the maximum siliceous production rate, R_{max}. For each of the reservoirs, the value of R_{max} was adjusted until the calculated DSi retention, R_D, matched the observed value.

The model-derived R_{max} values fall between 0.5 and 14.7 mol Si m^{-2} yr^{-1} (Table 3.3), that is, values consistent with observed diatomaceous production rates. Reservoirs receiving inflow with low DSi concentrations (15–70 μM, Dongfeng, Marne, Aube and Solina reservoirs) exhibit R_{max} values comparable to mean open ocean diatom productivities (0.6-0.8 mol Si m^{-2} yr^{-1}) (Krause et al., 2011; Nelson et al., 1995). The other model-derived R_{max} values are similar to silicon uptake rates measured in lakes and reservoirs. For example, siliceous productivities reported for Lake Michigan, Lake Ontario, Lake Superior, Lake Myvatn (Iceland) and two natural impoundments on the Mississippi River (Pepin and St. Croix) range from 0.5 to 7.1 mol Si m^{-2} yr^{-1} (Opfergelt et al., 2011; Schelske, 1985; Triplett, 2008), while for the Three Gorges Reservoir they fall between 1.6 and 2.7 mol Si m^{-2} yr^{-1} (Ran et al., 2013). The highest R_{max} values ($\geq$10 mol Si m^{-2} yr^{-1}, Amance, Champaubert and Saguling reservoirs) are within the range of siliceous productivities measured in coastal upwelling areas, where values can be as high as 416 mol Si m^{-2} yr^{-1} (Brzezinski et al., 1997; Nelson et al., 1995).

Non-linear regression indicates that the R_{max} values most strongly correlate with the input fluxes of DSi into the reservoirs. The following power relationship predicts R$_{max}$ across more than three orders of magnitude (Figure 3.3):

$$R_{max} = 10.837 \times DSi_{in}^{0.8126} \quad (R^2 = 0.83) \tag{3.4}$$

Table 3.2: Fluxes and parameters of the mechanistic Si reservoir model (Figure 3.2). Details on the fluxes and assumptions are given in the text (section 3.5). Ranges are compiled from diverse literature sources.

	Flux	Default value	Range	Reference
$F_{in,1}$	DSi influx	Reservoir specific	$2.32 \times 10^7 - 4.65 \times 10^{10}$ mol yr^1	See Table 3.1
$F_{in,3}$	PSi influx	10% of DSi influx	0–54% DSi influx	Conley (1997); Harrison et al. (2012); Ran et al. (2013); Triplett et al. (2012)
F_{12}	Biological DSi uptake	R_{max} = calculated using equation 6. $K_s = 0.005$mol m^{-2}	R_{max} see Table 3.3 K_s: $5 \times 10^{-7} - 0.05$ mol m^{-2}	Brzezinski et al. (1997); Donk and Kilham (1990); Michel et al. (2006); Znachor et al. (2013)
F_{31}	Fresh PSi dissolution	$k_{31} = 3$ yr^{-1}	$0.2 - 40$ yr^{-1}	Loucaides et al. (2012); Van Cappellen et al. (2002)
F_{23}	Decay siliceous biomass	$k_{23} = 25$ yr^{-1}	5-250 yr^{-1}	Dai et al. (2009); Wetz et al. (2008)
F_{34}	PSi ageing plus sedimentation	$k_{34} = 10$ yr^{-1}	5 - 45 yr^{-1}	Horn and Horn (2000)
$F_{1,out}$	DSi efflux from reservoir	$k_{tr} = 1/\tau_r$, where τ_r is residence time in years.	$F_{1,out}$:$1 \times 10^7 - 4.47 \times 10^{10}$ mol yr^{-1}	See Table 3.1; volume data from Lehner et al. (2011)
$F_{3,out}$	PSi efflux from reservoir	$k_{tr} = 1/\tau_r$.	Same as above	Same as above
F_{41}	Dissolution deposited SSi	$k_{41} = 0.01$ yr^{-1}	$0.002 - 0.16$ yr^{-1}	Loucaides et al. (2012); Van Cappellen et al. (2002)
$F_{4,buried}$	Permanent burial SSi	$k_{4,buried} = 0.002$ yr^{-1}	NA	Laruelle et al. (2009)

Table 3.3: Maximum siliceous primary productivity (R_{max}) and predicted RSi retention (R_R) for reservoirs in the dataset. See text for detailed discussion.

Reservoir	R_{max} (mol m^{-2} yr^{-1})	Predicted R_R
Iron Gate	5.43	0.02
Amance	11.40	0.04
Hoa Binh	8.27	0.11
Lake Alexandrina	1.16	0.29
Dongfeng	0.51	0.04
Champaubert	10.60	0.11
Wujiangdu	4.00	0.15
Saguling	14.73	0.29
Aube	0.84	0.48
Marne	0.84	0.41
Solina-Myczowce	0.54	0.22
Seine	1.74	0.40
Falcon	0.81	0.21
Thac Ba	2.87	0.10
Lake Powell	1.45	0.16
Lake Mead	3.13	0.19
Three Gorges	2.64	0.06

where R_{max} and DSi_{in} are both given in mol yr^{-1}. (Note: the R_{max} values in Table 3.3 are converted to units of mol yr^{-1} through multiplication with the corresponding reservoir surface areas given in Table 3.1). A positive correlation between R_{max} and DSi_{in} is not surprising: the higher the supply of bioavailable Si to a reservoir, the more siliceous production can be sustained. Other factors are expected to affect R_{max}, however. These include temperature, light intensity, turbidity, the availability of other essential nutrients, such as phosphorus and nitrogen, and reservoir hydrodynamics. These factors may in part explain the scatter seen in Figure 3.3.

3.5.3 Sensitivity analysis

In order to analyze parameter sensitivity of the mechanistic model, I define the following hypothetical, average reservoir, based on the information in Table 3.1. The reservoir is 10 years old and has a volume of 6 km^3, a surface area of 210 km^2 and a river discharge of 35 km^3 yr^{-1} (i.e., $\tau_r =$ 0.17 years). The inflow to the reservoir is assigned the global average river DSi concentration of 162.5 μM, according to the GloRiCh database of world river nutrient concentrations (Jens Hartmann, University of Hamburg, pers. comm.). From Equation (3.4), an R_{max} value of 6.0×10^8 mol yr^{-1} is obtained. All other parameters are assigned the default values listed in Table 3.2. Parameter values are then doubled and halved in turn and the effects on the predicted R_D and R_R values quantified. The results of the sensitivity analysis are summarized in Table 3.4. They reveal that R_{max} is the most sensitive parameter governing the model-predicted values of R_D and R_R. Doubling (halving) R_{max} yields a percent increase (decrease) of R_D by 68% (138%). Thus, not unexpectedly, RSi retention in reservoirs is highly sensitive to biological Si fixation.

In the above example, the computed DSi and RSi retentions are not sensitive to the age of the reservoir in the range tested (5-20 years). The latter range, however, far exceeds the water residence time of the reservoir (0.17 years). In fact, right after dam closure, R_D and R_R are quite sensitive to the age of the reservoir (Figure 3.4). When sediment starts to accumulate, retention of reactive Si is initially relatively high. As the sediment builds up, dissolution of the SSi pool returns increasing amounts of DSi to the water column, hence causing R_D and R_R to decrease. After about 1.5 years, the R_D and R_R values stabilize. (Note: for reservoirs with longer water residence times, it takes longer for R_D and R_R to stabilize).

3.5.4 Monte Carlo analysis

The statistical and sensitivity analyses imply that RSi retention by river damming is most strongly related to reservoir hydraulics and siliceous productivity. To account for the large variability in these

Table 3.4: Local sensitivity analysis responses of R_D and R_R to doubling and halving of parameters in mechanistic model. Default parameters are listed in section 3.6.3. Default R_D = 0.056 and R_R = 0.086. Percent change calculated as (default retention – sensitivity retention)/(default retention), and so negative values indicate an increase in retention compared with the default.

Parameter	Parameter description	% change from default R_D (doubling, halving)	% change from default R_R (doubling, halving)
k_{23}	Decay siliceous biomass rate constant (yr^{-1})	0.02, -0.03	0.01, -0.02
k_{34}	PRSi ageing plus sedimentation rate constant (yr^{-1})	-14.0, 14.6	-30.7, 32.0
K_s	Biological DSi uptake (half-saturation constant) (mol m^{-2})	0.16, -0.09	0.06, -0.03
k_{31}	Fresh PRSi dissolution rate constant (yr^{-1})	38.2, -24.0	13.7, -8.6
k_{41}	Dissolution deposited SSi rate constant (yr^{-1})	15.5, -8.3	9.2, -4.9
$k_{4,buried}$	Permanent burial SSi rate constant (yr^{-1})	-0.16, 0.08	-0.10, 0.05
R_{max}	Biological DSi uptake maximum rate constant (mol m^{-2} yr^{-1})	-137.9, 68.5	-49.6, 24.6
$F_{in,3}$	PRSi influx (mol yr^{-1})	37.0, -18.5	54.8, -27.4
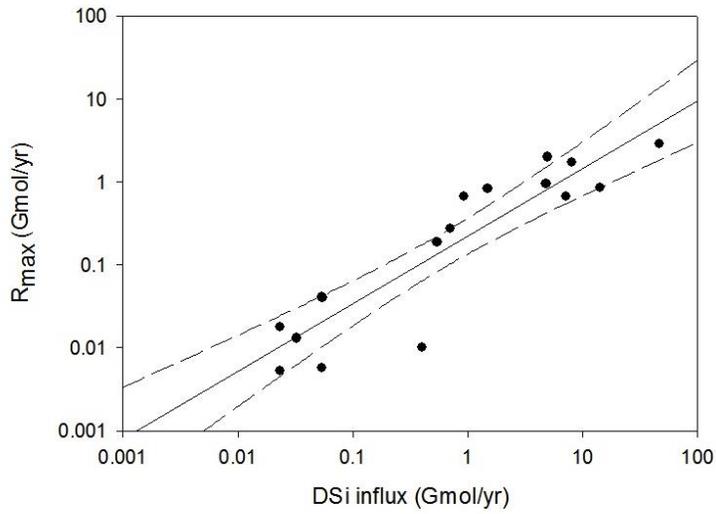
Figure 3.3: Maximum siliceous productivity, R_{max}, for the 17 reservoirs used to calibrate the mechanistic model, plotted against the DSi input. The solid line corresponds to Equation 3.4. Dashed lines are 95% confidence intervals. The R_{max} values are listed in Table 3.3.
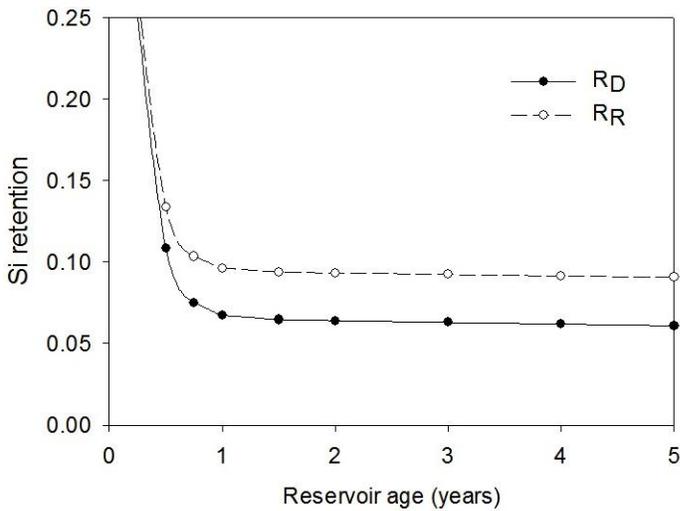
Figure 3.4: Retentions of DSi and RSi as a function of reservoir age, for the hypothetical "average" reservoir defined in section 3.5.3.

reservoir characteristics, a Monte Carlo analysis of the mechanistic Si cycling model was performed by randomly varying the following variables within prescribed ranges:

- volume (0.001 – 180 km^3),
- reservoir age (0.5 – 100 years),
- discharge (0.01 – 40 km^3 yr^{-1}),
- DSi inflow concentration (30 – 1500 µM),
- PSi influx (0.5 – 30% of DSi influx),
- R_{max} (Equation 3.4 ± one order of magnitude).

The above ranges were selected based on reported values in the literature, excluding obvious outliers. Only variables for which parameter ranges could be quantitatively constrained were included in the Monte Carlo analysis. The variables were further assumed to vary independently from one another, although some of the variables may be weakly correlated. Once the values of reservoir volume and discharge were selected, the water residence time was calculated as $\tau_r = V/Q_{in}$. The simulations further allowed for the possibility of BSi export from the reservoir via the dam outflow. (Note: in the baseline version of the model only DSi and PSi are exported from the reservoir.) The BSi efflux was calculated by multiplying the BSi concentration with the inverse of the water residence time (as for the DSi and PSi effluxes) and a randomly generated coefficient ranging from 0 to 1. All other model parameters were assigned their default values listed in Table 3.2. The analysis was carried out on 6000 model realizations.

The results of the Monte Carlo analysis are illustrated in Figure 3.5. As expected, for any given water residence time the computed total reactive Si retention, R_R, values cover a wide range (Figure 3.5A). The outlying values typically correspond to combinations of extreme reservoir characteristics. For example, R_R values approaching 1 at the lower residence times are primarily associated with very small reservoirs exhibiting extremely high productivities (i.e., much higher than predicted with Equation 3.4). Overall, most R_R values tend to fall between 0.03 and 0.5, with average values increasing with increasing water residence time.

The Monte Carlo analysis further reveals a systematic variation of the relative contributions of dissolved and particulate Si to total reactive Si retention, with increasing water residence time (Figure 3.5b). Short residence times result in a more efficient downstream export of PSi produced by in-reservoir siliceous production. Hence, at low τ_r, reactive Si retention tends to be dominated by the removal of inflowing DSi. As τ_r increases, however, there is more time for the PSi and SSi pools to

dissolve back to DSi. The relative contribution of R_D to the total retention of reactive Si then decreases, as seen for the model-predicted average R_D: R_R ratios (Figure 3.5b).

The general trend of R_R with respect to the water residence time was fitted to various standard curves (Figure AB1 in Appendix B). The following power law relationship yielded the best fit:

$$R_R = 0.1746 \times \tau_r^{0.2973} \quad (R^2 = 0.31, p{<}0.0001) \tag{3.5}$$

where τ_r is expressed in units of years. For consistency, a similar power law equation was fitted to the DSi retention values generated by the Monte Carlo simulations:

$$R_D = 0.0938 \times \tau_r^{0.4066} \quad (R^2 = 0.12, p{<}0.0001) \tag{3.6}$$

(Note: The R_D values are shown in Figure AB2 of Appendix B.)

3.6 Global Si retention by river damming

3.6.1 Approach

The estimation of the global retentions of RSi and DSi by river damming assumes that Equations (3.5) and (3.6) offer a reliable representation of reactive Si dynamics in reservoirs. I emphasize that the equations are not necessarily good predictors for any specific individual reservoir, but rather that they provide a meaningful representation of the average behaviour of Si when considering a large ensemble of reservoirs. The equations are then applied to the GRanD database (Lehner et al., 2011), which comprises information on 6862 reservoirs and their associated dams. Note that the previous global estimate of DSi retention in reservoirs by Harrison et al. (2012) was based on the earlier, smaller subset of 822 reservoirs presented by Lehner and Döll (2004). The GRanD database classifies several natural lakes as reservoirs if they are used as a primary water supply (e.g. Lake Ontario and Lake Victoria). In order to ensure no natural lakes are included in the estimates given below, the GRanD database was overlain with Lehner and Döll's Global Lakes and Wetlands Databases (GLWD) levels 1 and 2 (large and small lakes). Water bodies appearing in both datasets were removed from the calculations.

For each reservoir, the DSi input from the corresponding watershed was obtained from the Global-NEWS-DSi model, using the pre-dam scenario (Beusen et al., 2009):

$$DSi_{in} = W \times SiY \tag{3.7}$$

where DSi_{in} is given in units of mol yr^{-1}, W is the upstream watershed area (km^2) listed in the GRanD database, and SiY is the DSi yield of the watershed in units of mol Si km^{-2} yr^{-1}. Equation (3.7) assumes a uniform DSi yield throughout a given catchment (Harrison et al., 2012; Hartmann et al., 2010; Jansen et al., 2010). The amount of DSi retained annually in the reservoir was then obtained as (see Equation 3.2):

$$DSi_{ret} = DSi_{in} - DSi_{out} = R_D \times DSi_{in} \qquad (3.8)$$

where R_D was calculated with Equation 3.6. Because Global-NEWS only provides DSi yields, it was assumed that, globally, the river supply of PSi equals 10% of that of DSi (see above). Thus, the amount of reactive silica retained annually in a reservoir was computed as:

$$RSi_{ret} = RSi_{in} - RSi_{out} = R_R \times 1.1 \times DSi_{in} \qquad (3.9)$$

where R_R was calculated using Equation 3.5, and the 1.1 factor accounts for the 10% reactive PSi input. The water residence time used in Equations 3.5 and 3.6 was derived from the discharge and volume given in GRanD.

The frequency distribution of the R_R values calculated with Equation 3.5 for the GRanD reservoirs are shown in Figure 3.6. The distribution shows a positive skew towards lower retentions, with over 3000 reservoirs with RSi retentions between 0.1 and 0.2, followed by about 1600 reservoirs with retentions between 0.2 and 0.3. The arithmetic mean for the R_R value is 0.20, that for R_D is 0.13. The mean R_D:R_R ratio (0.13:0.20 = 0.65) is plotted as the solid horizontal line in Figure 3.5b. As can be seen, reservoirs with water residence times less than 0.1 year tend to have R_D:R_R ratios exceeding the mean value, while the opposite is true for reservoirs with water residence times larger than 0.1 year.

The GRanD database accounts for at least 76% of the estimated global volume of reservoirs worldwide, with the bulk of the remaining 24% volume mainly including reservoirs less than 1 km^2 in size (Lehner et al., 2011). The latter are typically associated with low RSi retentions (Figure 3.5). If we assume that the reservoirs not included in the GRanD database receive on the order of 24% of the global *RSi* input and exhibit, on average, only half the retention efficiency of the GRanD reservoirs (i.e., 10% rather than 20%,), then the missing reservoirs account for 12% of RSi retention by river damming. A 12% extra contribution was therefore added to the total RSi retention computed for the GRanD reservoirs.
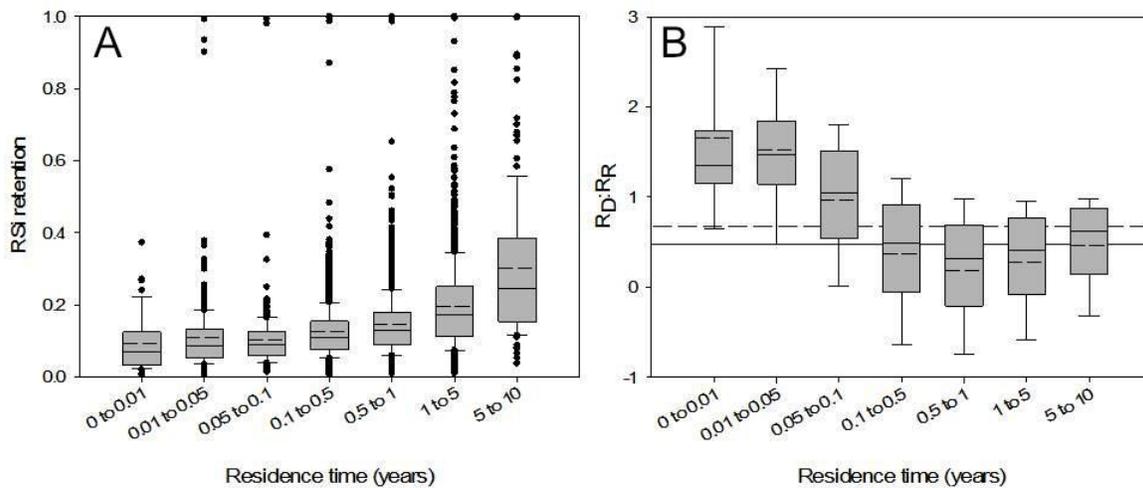
Figure 3.5: Monte Carlo analysis of the mechanistic model: a) RSi retention (R_R) values for 6000 model realizations versus the water residence time; b) R_D:R_R ratios for the same 6000 model realizations versus the water residence time. The dashed horizontal line on panel b corresponds to the (arithmetic) mean R_D:R_R ratio (0.65), the solid horizontal line to the globally weighted R_D:R_R ratio (0.45). See text for more details. Inside each box on both panels, the solid line indicates the median, the dashed line the mean value. The edges of each box represent the 1st and 3rd quartiles, and the whiskers are standard deviations. Note that outliers are not shown in panel B.
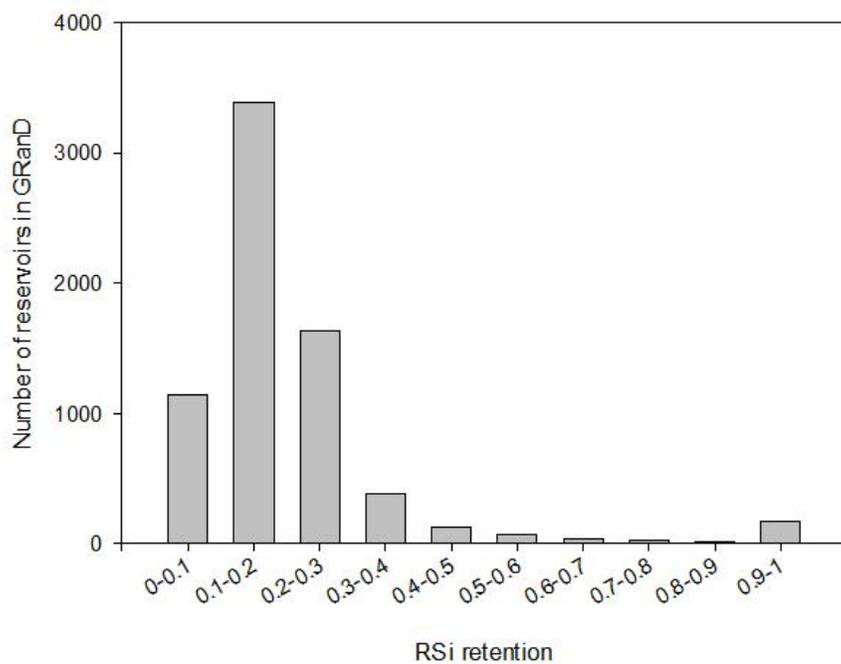
Figure 3.6: Distribution of model-derived RSi values for the reservoirs of the GRanD database. Arithmetic mean = 0.20, median = 0.17, standard deviation = 0.16.

3.6.2 Global estimates

With the approach described in the previous section, global RSi and DSi retentions in reservoirs are estimated to be equal to 372 Gmol yr^{-1} (22.3 Tg SiO$_2$ yr^{-1}), and 163 Gmol yr^{-1} (9.8 Tg SiO$_2$ yr^{-1}), respectively. The Global-NEWS model yields a global DSi loading to watersheds of 6325 Gmol yr^{-1} for the pre-dam scenario (Beusen et al. 2009). Assuming that PSi loading equals 10% that of DSi, a corresponding RSi loading of 6957 Gmol yr^{-1} is obtained. Thus, according to my estimates, 2.6% of the DSi and 5.3% of the RSi loadings to the world's river network are retained in dam reservoirs.

The 95% confidence interval of the power law for R_R as a function of water residence time (i.e., Equation 3.5) yields an error on the global RSi retention on the order of 1 Gmol yr^{-1}. This relatively small error indicates that the Monte Carlo analysis used to scale up the mechanistic model does not in itself introduce a large uncertainty on the global estimation of reactive Si retention. The main sources of uncertainty on the global estimates are associated with the calibration of the mechanistic model, the inputs of dissolved Si predicted by the Global-NEWS model, and the relative contribution of PSi to the total RSi input to reservoirs.

The globally weighted R_D:R_R ratio equals 0.45 (= 163/3001:372/3301), that is, a value markedly different from the mean R_D:R_R ratio (0.65 = 0.13:0.20). The reason is that global RSi retention is skewed toward reservoirs with higher water residence times, which, in turn, favour PSi retention (Figure 3.5B). Little data are available to confirm the dominant role of PSi in global reactive Si retention. To my knowledge, only the Si budgets for the Three Gorges Reservoir (Ran et al., 2013), Lake St. Croix and Lake Pepin (Triplett et al., 2008) account for both DSi and PSi. For these three water bodies, the budgets imply that PSi retention exceeds DSi retention, in line with our global estimates.

My estimated DSi retention is about one quarter lower than the global reservoir DSi retention of 516 Gmol yr^{-1} (31 Tg SiO$_2$ yr^{-1}) proposed by Harrison et al. (2012). One major reason for the difference is that Harrison and coworkers used a combined dataset including both lakes and reservoirs. My analysis, however, shows that reservoirs are less efficient in retaining Si than lakes (section 3.4). Combining both lentic systems may thus lead to an overestimation of Si retention in reservoirs. In a recent study, Frings et al. (2014) derived PSi accumulation rates for 30 lakes and reservoirs from mass balance considerations. By multiplying the mean accumulation rate for the reservoirs only with the global reservoir surface area, these authors obtained a RSi retention of 230 Gmol yr^{-1}, that is, a value significantly lower than my estimate. The RSi retention proposed by Frings

and coworkers, however, depends on the extent to which the average PSi accumulation rate of 18 reservoirs is representative of worldwide PSi retention in reservoirs.

With the mechanistic model presented in section 3.5 it is possible to make additional global-scale estimations. For example, application of the model to the GRanD database yields a global biological Si production in reservoirs of 516 Gmol yr^{-1}. Combined with the total surface area of reservoirs (3.7 x 10^5 km^2, Lehner et al, 2011) this translates into a mean siliceous productivity of 1.4 mol m^{-2} yr^{-1}. This value is higher than the average open ocean diatom productivity (0.6-0.8 mol m^{-2} yr^{-1}; Nelson et al., 1995), but similar to Si fixation in mesotrophic Lake Michigan (1.16 mol m^{-2} yr^{-1}; Schelske et al., 1985). Furthermore, according to the model, globally 62% of the external input plus in-reservoir production of PSi redissolves to DSi (Table 3.5). The latter estimate was obtained by calculating the reactive Si recycling efficiency (*RE*) for each of the reservoirs in the GRanD data set as follows:

$$RE = \frac{F_{31} + F_{41}}{F_{in,3} + F_{12}} \times 100\% \tag{3.10}$$

The 62% estimate is of the same order of magnitude as reported Si recycling efficiencies for individual lakes and reservoirs, including 65% for Lough Neagh (Dickson, 1975; Gibson et al., 2000), 66% for a dam reservoir on the Marne River (Garnier et al., 1999), and 55% for the Three Gorges Reservoir (Ran et al., 2013).

3.7 Conclusions

The global impact of dams on river Si fluxes is estimated via a new approach that merges biogeochemical modeling of reactive Si (RSi) cycling with data on reservoir Si budgets. A Monte Carlo analysis of the biogeochemical model yields a predictive relationship between reservoir RSi retention and water residence time, which, when applied to the GRanD data set, allows us to estimate global RSi retention by river damming. Although the construction of dams represents a major perturbation of the water cycle on the continents, the estimated retention of RSi in reservoirs is relatively small, on the order of 5% of the RSi loading to the world's river network. Nonetheless, with the global rise in phosphorus and nitrogen loadings to surface waters even a small reduction in the worldwide riverine flux of RSi may exacerbate ecological changes that can lead to eutrophication of streams, lakes and the coastal zone. The modeling results further imply that the building of dams may turn former river stretches into hotspots for siliceous productivity, fuelled by the efficient recycling of biogenic silica in reservoirs. By incorporating mechanistic knowledge of Si cycling, the proposed approach optimizes the extrapolation of the sparse data set on RSi retention in reservoirs to the global

scale. Global retention in reservoirs of other nutrients, for example phosphorus, could in principle be evaluated using a similar approach.

Table 3.5: Output of global silica retention model (Note: global reservoir surface area = 3.7×10^5 km^2, Lehner et al., 2011).

Description	Value
DSi retention (Gmol yr^{-1})	163.5 ± 2.2
DSi retention (Tg SiO$_2$ yr^{-1})	9.79 ± 0.13
DSi retention rate (mol m^{-2} yr^{-1})	0.44
Global average R_D (arithmetic)	0.13
RSi retention (Gmol yr^{-1})	372 ± 21
RSi retention (Tg SiO$_2$ yr^{-1})	22.29 ± 1.26
RSi retention rate (mol m^{-2} yr^{-1})	0.99
Global average R_R (arithmetic)	0.20
Siliceous productivity (Gmol yr^{-1})	516
Siliceous productivity (mol m^{-2} yr^{-1})	1.4
Recycling efficiency (%)	62

Chapter 4

Global phosphorus retention by river damming

This chapter is modified from:

Maavara, T., Parsons, C.T., Ridenour, C., Stojanovic, S., Dürr, H.H., Powley, H.R. and Van Cappellen, P. (2015) Global phosphorus retention by river damming. Proc Natl Acad Sci U.S.A. 112, 15603-15608.

4.1 Summary

More than 70,000 large dams have been built worldwide. With growing water stress and demand for energy, this number will continue to increase in the foreseeable future. Damming greatly modifies the ecological functioning of river systems. In particular, dam reservoirs sequester nutrient elements and, hence, reduce their downstream transfer to floodplains, lakes, wetlands and coastal marine environments. Here, I quantify the global impact of dams on the riverine fluxes and speciation of the limiting nutrient phosphorus (P), using a mechanistic modeling approach that accounts for the in-reservoir biogeochemical transformations of P. According to the model calculations, the mass of total P (TP) trapped in reservoirs nearly doubled between 1970 and 2000, reaching 42 Gmol yr^{-1}, or 12% of the global river TP load in 2000. Because of the current surge in dam building, I project that by 2030 about 17% of the global river TP load will be sequestered in reservoir sediments. The largest projected increases in TP and reactive P (RP) retention by damming will take place in Asia and South America, especially in the Yangtze, Mekong and Amazon drainage basins. Despite the large P retention capacity of reservoirs, the export of RP from watersheds will continue to grow unless additional measures are taken to curb anthropogenic P emissions.

4.2 Introduction

The systematic damming of rivers began with the onset of the Industrial Revolution and peaked in the period 1950-1980 (Vörösmarty et al., 1997; Zarfl et al., 2015). After slowing down during the 1990s, the pace of dam building has recently risen again sharply (Grill et al., 2015). As a consequence, the number of hydroelectric dams with generating capacity >1 MW is expected to nearly double over the next two decades (Zarfl et al., 2015). The current surge in dam construction will increase the proportion of rivers that are moderately to severely impacted by flow regulation from about 50% at the end of the 20th century to over 90% by 2030 (Grill et al., 2015). Homogenization of river flow regimes resulting from damming is a growing, worldwide phenomenon and has been invoked as one of the reasons for the decline in freshwater biodiversity (Poff et al., 2007).

Another major global driver of environmental change of river systems is enrichment by anthropogenic nutrients, in particular phosphorus (P) (Correll, 1998; Smil, 2000). Fertilizer use, soil erosion and the discharge of wastewater have more than doubled the global P load to watersheds compared to the inferred natural baseline (Compton et al., 2000; Filippelli, 2002; Meybeck, 1993; Ruttenberg, 2003). Because P limits or co-limits primary productivity of many aquatic ecosystems, increased river fluxes of P have been identified as a main cause of eutrophication of surface water

bodies, including lakes and coastal marine environments (Conley et al., 2009; Correll, 1998; Schindler, 1977). River damming and P enrichment are interacting anthropogenic forcings, because sediments accumulating in reservoirs trap P and, thus, reduce the downstream transfer of P along the river continuum (Friedl and Wüest, 2002; Harrison et al., 2010; Teodoru and Wehrli, 2005). This raises the question to what extent P retention by dams may offset anthropogenic P enrichment of rivers.

The number of published studies from which P retention efficiencies in dam reservoirs can be obtained is small: an extensive literature search only yields useable data for 155 reservoirs (Dataset S1, Appendix C), that is, less than 0.2% of the approximately 75,000 dam reservoirs larger than 0.1 km^2 (Lehner et al., 2011). The existing data nonetheless clearly show that even a single dam can significantly alter the flow of P along a river. For example, dam-impounded Lake Kariba (Zambezi River), Lake Diefenbaker (South Saskatchewan River), and Lac d'Orient (Seine River) sequester approximately 87%, 94% and 71% of their total P inflows, respectively (Donald et al., 2015; Garnier et al., 1999; Kunz et al., 2011). For the 1 million km^2 Lake Winnipeg watershed, 28 reservoirs and lakes accumulate over 90% of the total P load (Donald et al., 2015). The global retention of P by dams, however, remains poorly constrained (Lerman et al., 2004; Mayorga et al., 2010; Van Cappellen and Maavara, 2016). Previous estimations have simply applied a correction factor to river P loads to represent retention by dams (Beusen et al., 2005; Harrison et al., 2005; Mackenzie et al., 2002). This approach does not distinguish between the various chemical forms of P, nor does it account for differences in reservoir hydraulics, or provide information about uncertainties on retention estimates.

Here, I follow a mass balance modeling approach developed in Chapter 3 to calculate the global retention of nutrient silicon by dams (Maavara et al., 2014). The mass balance model represents the key biogeochemical processes controlling P cycling in reservoirs (Figure 4.1). The model separates total phosphorus (TP) into the following pools: total dissolved P (TDP); particulate organic P (POP); exchangeable P (EP); and unreactive particulate P (UPP). UPP consists mostly of crystalline phosphate minerals that are inert on reservoir-relevant timescales (≤ 100 years); TDP comprises inorganic and organic forms of P, while EP includes orthophosphate and organic P molecules sorbed to or co-precipitated with oxides, clay minerals and organic matter. Reactive P (RP) is defined as the sum of TDP, EP and POP; it represents the potentially bioavailable fraction of TP.
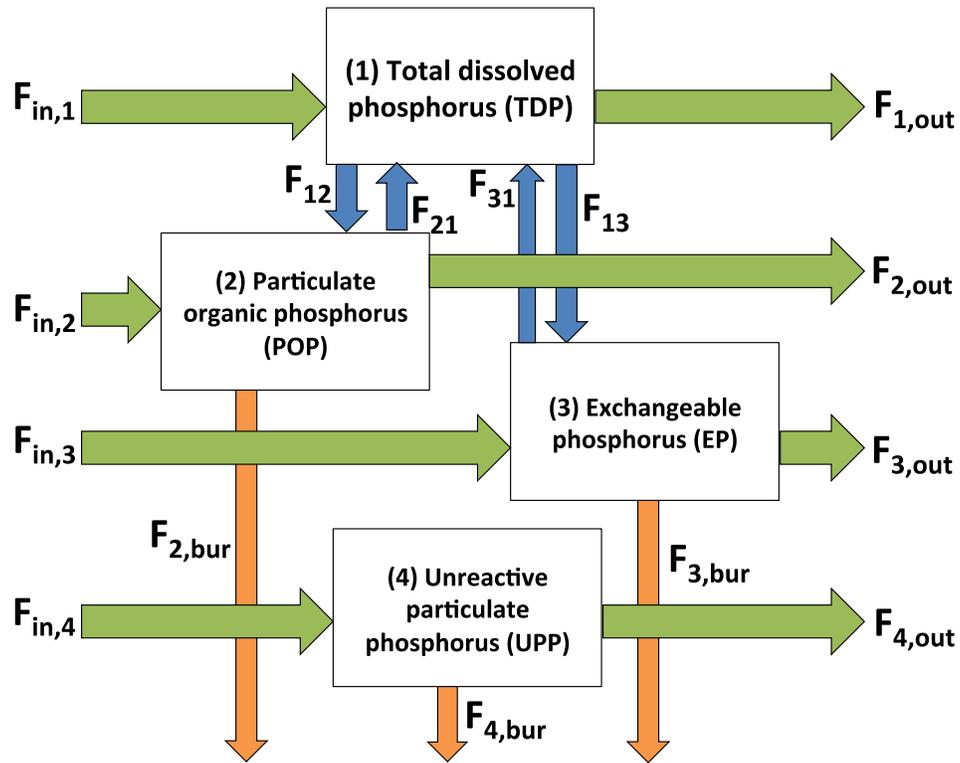
Figure 4.1: Mass balance model used to estimate retention of P in reservoirs. $F_{in,i}$, is the influx of the i-th P pool into the reservoir, $F_{i,out}$ the corresponding efflux out of the reservoir; F_{12} represents P fixation by primary productivity; F_{21} represents mineralization of POP; F_{13} and F_{31} are the sorption and desorption rates of dissolved P; $F_{i,bur}$ is the permanent burial flux of the i-th particulate P pool in the reservoir's sediments.

Global predictive relationships for the retention of TP and RP in reservoirs are derived from a Monte Carlo analysis of the model, which accounts for parameter variability within expected ranges. The relationships are applied to the reservoirs in the Global Reservoirs and Dams (GRanD) database (Lehner et al., 2011), in order to estimate the sequestration of TP and RP by dams in each of the major river basins of the world. Throughout, P retention efficiencies in a reservoir are defined as:

$$R_X = \frac{X_{in} - X_{out}}{X_{in}} \qquad\qquad (4.1)$$

where R_X is the fractional retention of TP or RP, and X_{in} and X_{out} are the input and output fluxes of TP or RP in units of mass per unit time. Annual amounts of TP and RP retained in a reservoir are then calculated by multiplying the R_X values with the corresponding TP and RP input fluxes from the dam's upstream watershed. The latter are obtained from the Global-NEWS model, which estimates emission yields for dissolved inorganic P (DIP), dissolved organic P (DOP), and particulate P (PP), of which 20% is assumed to be reactive (Compton et al., 2000; Meybeck, 1982). The Global-NEWS yield estimates are based on the biogeophysical characteristics, population density, socioeconomic status, land use and climatic conditions within the drainage basin (Mayorga et al., 2010).

Because the biogeochemical mass balance model explicitly represents the in-reservoir transformations between the different forms of P, it allows us to estimate how dams modify both the total and reactive fluxes of P along rivers. With the proposed approach, I reconstruct global TP and RP retentions by dams in 1970 and 2000, and make projections for 2030. For the latter, I apply the nutrient P loading trends developed for the four Millennium Ecosystem Assessment (MEA) scenarios (Seitzinger et al., 2010). The results illustrate the evolving role of damming in the continental P cycle and, in particular, the ongoing geographical shift in P retention resulting from the current boom in dam construction.

4.3 Results

4.3.1 P retention in dam reservoirs

Phosphorus retention in lakes and reservoirs correlates with the hydraulic residence time (τ_r) (Brett and Benjamin, 2008; Hejzlar et al., 2006; Kõiv et al., 2011). Accordingly, τ_r explains more than 45% of the variability of the R_{TP} and R_{RP} values generated by 6000 Monte Carlo iterations of the P mass balance model. The model-derived R_{TP} and R_{RP} values follow the equation originally proposed by Vollenweider (1975) for P retention in natural lakes:

$$R_X = 1 - \frac{1}{1 + \sigma \times \tau_r} \tag{4.2}$$

where σ is a first-order rate constant describing P loss from the water column (see supplementary material for a derivation of Equation 4.2). For TP retention in lakes σ has been related to the relative thickness of the photic zone and the average particle settling velocity (30, 32, 33). Non-linear least squares regressions yield the following statistically significant average values of σ: 0.801 yr^{-1} for R_{TP} (p<0.05) and 0.754 yr^{-1} for R_{RP} (p<0.05). The higher σ value for TP reflects the more efficient retention of UPP delivered to reservoirs, compared to the reactive P pools. The resulting difference between R_{TP} and R_{RP} is highest for hydraulic residence times between 0.5 and 1 year.

Preferential accumulation of UPP in reservoirs or, conversely, enhanced relative export of RP from reservoirs, is supported by observations. Salvia-Castellvi et al. (2001) found that cascades of small dams in Luxembourg exhibit higher TP retention efficiencies than soluble reactive P, leading to the stepwise increase in TP reactivity after each consecutive dam passage. For 11 out of 16 reservoirs in the Lake Winnipeg drainage basin, Donald et al. (2015) similarly found that retention of TP exceeded that of TDP, suggesting that the presence of dams increases the reactive fraction of the riverine P flux.

4.3.2 Global P retention by dams: 1970-2000

The global, model-predicted retention of TP for 2000 is 42 Gmol yr^{-1}, equivalent to 12% of the worldwide river TP load of 349 Gmol yr^{-1} (Table 4.1). The corresponding retention of RP amounts to 18 Gmol yr^{-1}. The global annual mass of TP retained in 2000 is almost double that in 1970 (22 Gmol TP yr^{-1}), although global TP loading to rivers only increased by 12% over the same time interval. Thus, the growth in TP (and RP) retention during the last three decades of the 20th century primarily reflects the increasing number of dams. The volume of dam reservoirs rose from about 3000 in 1970 to almost 6000 km^3 in 2000 (Lehner et al., 2011), while the mean reservoir retention efficiencies stayed nearly constant ($R_{TP} \approx 44\%$, $R_{RP} \approx 43\%$).

During the 1970-2000 period, the 3.2 million km^2 drainage basin of the Mississippi River remained the top P retaining catchment in the world (Figures 4.2a and 4.2b, Table 4.2, Dataset S2 in Appendix C). In 2000, the 700 reservoirs of the Mississippi River watershed accounted for 5.2 and 5.4% of the global amounts of TP and RP retention by dams, respectively. Other drainage basins with high TP and RP retentions included those of the Zambezi, Nile, Yangtze (Chang Jiang), Volga, and Paraná rivers. The high retentions in the drainage basins of the Zambezi and Volga are explained by a

Table 4.1: Global retentions of total phosphorus (TP) and reactive phosphorus (RP) by dams, in years 1970, 2000 and 2030. The 2030 retentions are calculated by including the new hydraulic dams (>1 MW generating capacity) planned to be completed by 2030, and using the projected 2030 TP and RP river loads for the four Millennium Ecosystem Assessment (MEA) scenarios: AM = Adapting Mosaic, GO = Global Orchestration, OS = Order from Strength, and TG = TechnoGarden.

	1970	2000	2030AM	2030GO	2030OS	2030TG
Global river TP load (Gmol yr^{-1})	312	349	366	384	372	380
Global river RP load (Gmol yr^{-1})	113	133	151	175	159	169
TP retained (Gmol yr^{-1})	22	42	61	67	62	66
RP retained (Gmol yr^{-1})	9	18	29	36	31	35
Fraction of global TP load retained (%)	7	12	17	17	17	17
Fraction of global RP load retained (%)	8	14	19	21	19	21
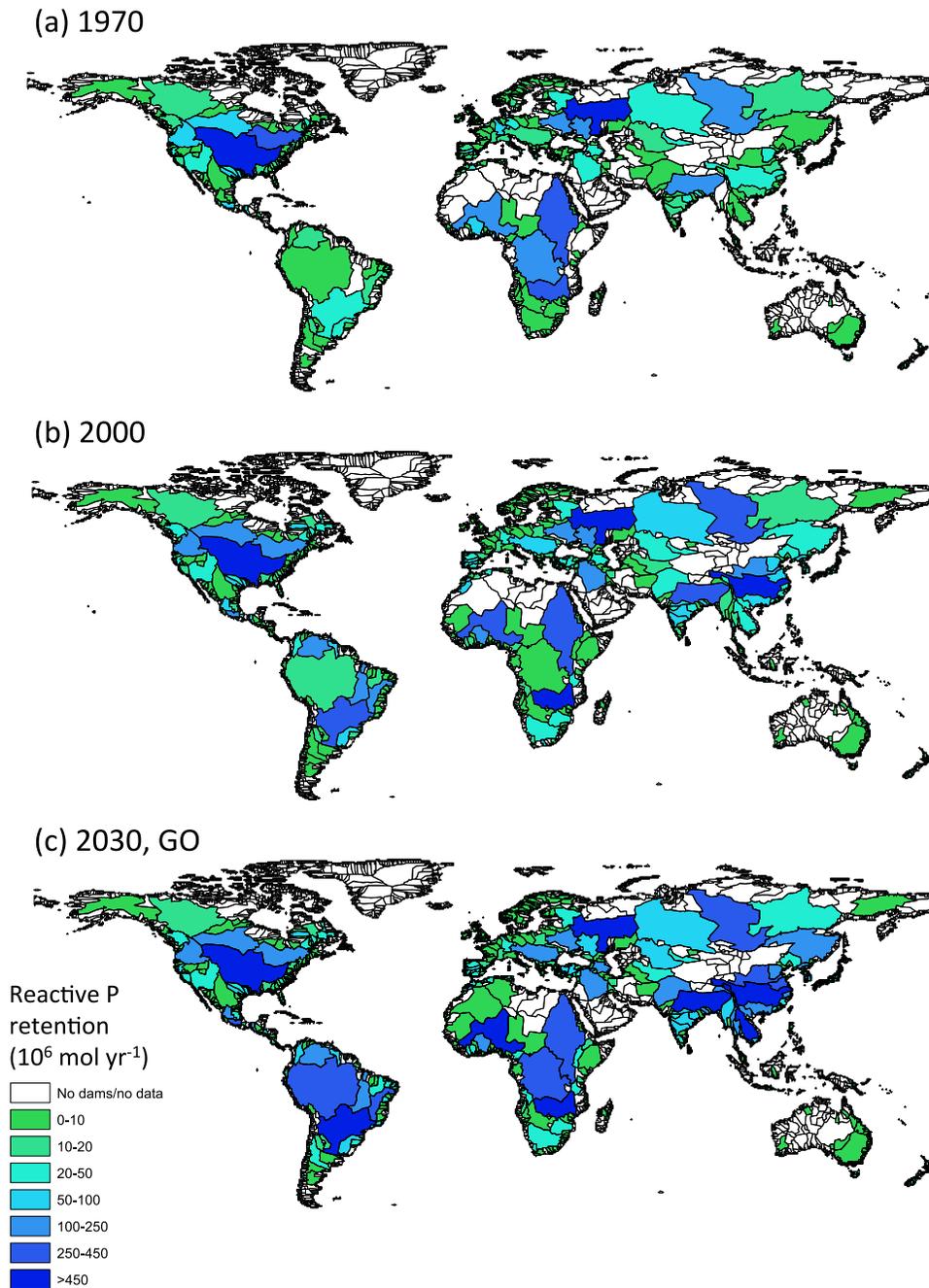
Figure 4.2: Reactive phosphorus (RP) retention by dams in individual watersheds in (a) 1970, (b) 2000, and (c) 2030 under the Global Orchestration (GO) scenario. The 2030 RP retentions assume that all dams currently planned or under construction will be completed by 2030 (Zarfl et al., 2015). The GO scenario predicts the highest global river P load by 2030 and, hence, yields the largest relative changes in P retention.

relatively small number of large reservoirs, including the 180 km^3 Lake Kariba along the Zambezi River, and the cascade of reservoirs on the Volga River, including the Volgograd, Rybinsk and Kuybyshev Reservoirs, each exceeding 25 km^3 in volume.

4.3.3 Projected P retention by dams: 2030

Estimates of retention of P in dam reservoirs in 2030 are calculated by combining the four MEA scenarios (Seitzinger et al., 2010) with the added retention capacity of new hydroelectric dams with generation capacities ≥1 MW that are projected to be completed by 2030 (Zarfl et al., 2015). The corresponding global TP retentions fall between 61 and 67 Gmol yr^{-1}, or 17% of the global riverine TP loads (Table 4.1). The RP retentions are in the range 29-36 Gmol yr^{-1}. Currently available global projections of river damming do not include smaller reservoirs or reservoirs whose main function is not electricity production. My projections are therefore likely at the lower end of the potential increase in P retention by 2030.

Over the next 15 years, South America, central Africa, and Southeast Asia will experience the greatest growth in P retention by river damming (Figure 4.2c, Table 4.2). By 2030, the largest single increase in dam P retention will occur in the Yangtze basin, with up to 2.6 Gmol yr^{-1} more RP retained behind 142 new dams. The Yangtze alone will then account for roughly a quarter of the additional mass of RP retained globally. Large increases in TP and RP are also projected for the drainage basins of the Mekong, Salween, and Ganges-Brahmaputra Rivers. In the Mekong River basin, 121 new dams will increase RP retention by 0.7 Gmol yr^{-1}. Together, the basins of the Amazon, Paraná and Tocantins Rivers in South America will retain an additional 0.7 Gmol yr^{-1} RP because of the construction of 616 new dams. In Africa, the Zaire and Zambezi river basins will experience significant increases in P retention due to the construction of 30 new dams. The retention of RP by dams in the basin of the Kura River, which empties into the Caspian Sea, should increase by 0.2 Gmol yr^{-1} upon completion of 14 new dams.

4.4 Discussion

Nutrient enrichment and damming are major anthropogenic pressures on river-floodplain systems and receiving water bodies. By building dams, humans further modify the fluxes and speciation of nutrients along the river continuum (Friedl and Wüest, 2002; Maavara et al., 2014; Van Cappellen and Maavara, 2016). In particular, retention in reservoirs can greatly reduce the delivery of P to downstream areas and the coastal zone, influencing regional nutrient limitation patterns, trophic

Table 4.2: Top 10 watersheds ranked according to the annual mass of reactive phosphorus (RP) retained in their dam reservoirs, for 1970, 2000, and 2030 (GO scenario). Number of reservoirs, river RP load and RP retention are provided. An expanded list with the top 150 watersheds for year 2000 can be found in the Appendix C (Dataset S2). Only reservoirs listed in the GRanD database and, for 2030, reservoirs under construction or planned for completion by 2030, are included.

Rank	Watershed	Number of reservoirs	RP load (10^6 mol/yr)	RP retained (10^6 mol/yr)	% retention
1970					
1	Mississippi	546	2700	1805	66.9
2	Volga	15	1423	676	47.5
3	Zambezi	13	734	390	53.1
4	Nile	7	581	376	64.7
5	St. Lawrence	162	1896	337	17.8
6	Dnepr	5	466	298	63.9
7	Yenisei	3	773	280	36.2
8	Niger	17	602	247	41.0
9	Zaire	6	2574	221	8.6
10	Ganges-Brahmaputra	43	6044	152	2.5
2000					
1	Mississippi	700	1880	920	48.9
2	Zambezi	50	863	531	61.5
3	Volga	17	1320	500	37.9
4	Yangtze	358	3758	480	12.8
5	Paraná	70	2410	357	14.8
6	Ganges-Brahmaputra	83	8961	322	3.6
7	Yenisei	6	840	267	31.8
8	Niger	52	687	262	38.1
9	Nile	10	624	239	38.3
10	Dnepr	6	438	202	46.1
2030 (GO scenario)					
1	Yangtze	500	8327	2898	34.8
2	Mississippi	700	2294	1124	49.0
3	Paraná	418	3912	676	17.3
4	Mekong	140	3283	650	19.8
5	Zambezi	65	884	649	73.4
6	Ganges-Brahmaputra	483	10 006	621	6.2
7	Niger	74	1422	568	39.9
8	Volga	17	1334	506	37.9
9	Zaire	20	2462	417	16.9
10	Huang He	51	1033	402	38.9

conditions and food web dynamics (Friedl and Wüest, 2002; Nixon, 2003; Teodoru and Wehrli, 2005). For example, the drop in primary production due to the near-complete cessation of P supply to the offshore Nile delta region, following the completion of the Aswan High Dam in 1964, is believed to be at the origin of the collapse of the local fishery industry (Nixon, 2003). Here, I extend the existing studies on individual reservoirs and watersheds by performing spatially explicit assessments of the global impacts of damming on the riverine P fluxes for the period 1970-2030.

Post-World War II dam construction was particularly intense in North America and Europe, with more than one third of all dams globally located in the United States by 1970 (Lehner et al., 2011). The geographical hub of dam construction started to shift during the last 30 years of the 20th century. This trend continues to the present day, as new regional economies develop and the need for non-fossil fuel-based energy sources becomes more critical. Current and near-future damming hotspots include western China, the Himalayas and Andes, Brazil, Southeast Asia, and the Balkans, where collectively more than 3000 major hydropower dams (>1 MW generating capacity) are under construction or planned (Grill et al., 2015; Zarfl et al., 2015). As a consequence, the global distribution of TP and RP retention by dams in the 21st century will depart significantly from that of the second half of the 20th century.

The global river TP load has at least doubled since pre-human times (Compton et al., 2000; Filippelli, 2002; Meybeck, 1982). That is, 50% or more of the average TP flux in rivers is now of anthropogenic origin. In addition, anthropogenic sources deliver relatively more reactive P to rivers than natural sources (Compton et al., 2000). From an ecological health perspective, riverine RP is more relevant than TP, because RP represents the P pool that is potentially available for biological assimilation. Although on average individual dam reservoirs retain more than 40% of the inflowing TP and RP, river damming itself had not offset global anthropogenic P enrichment of rivers by the end of the last century. In 2000, the model-predicted worldwide retention of TP by dam reservoirs only represented 12% of the global riverine TP load (Table 4.1), because (1) not all TP entering rivers passes through dam reservoirs, and (2) the majority of TP retention currently occurs in smaller reservoirs characterized by relatively short water residence times (≤ 0.5 years) and, correspondingly, relatively low retention efficiencies (Figure AC1).

From 1970 to 2000, the fraction of the global river TP load sequestered in reservoirs increased from 7 to 12% (Table 4.1). This increase is attributed to the construction of about 2500 new dams during the last three decades of the 20th century, 65% of which have water residence times greater than 6 months (16) and corresponding average TP retentions in excess of 25% (Figure AC1). By

2030, the retained TP fraction is projected to rise up to 17% of the global river TP load, notwithstanding the much higher number of dams (3782) projected to be built between 2000 and 2030. The more modest increase in post-2000 TP retention per dam, compared to the previous 30-year period, reflects the predominance of hydroelectric dams currently under construction or planned. Hydropower reservoirs generally have shorter water residence times, and correspondingly lower retention efficiencies, than reservoirs of similar size that are primarily used for irrigation or flood control. Of the dams under construction or planned, 63% have reservoirs with water residence times ≤0.1 years (2). In comparison, only 13% of the reservoirs currently included in the GRanD database have water residence times ≤0.1 years.

The combined effects of anthropogenic nutrient enrichment and damming on P export fluxes to the coastal zone are illustrated in Figure 4.3. The decreases in TP and RP export between 1970 and 2000 observed for Europe are mainly due to the approximately 10% drop in river TP loading following legislation to curb phosphate use in detergents and upgrades to wastewater treatment plants (Ludwig et al., 2009; Van Drecht et al., 2009). For the same time period, TP export in South America also decreased. However, in this case, damming caused the decline in TP export, as anthropogenic TP loading actually increased. In contrast to TP, RP export in South America increased from 1970 to 2000, because (1) RP made up much of the additional anthropogenic P released to rivers, and (2) RP tends to be retained less efficiently than UPP in reservoirs. Little change in TP and RP export fluxes are observed for North America, while in all other cases, TP and RP exports increased from 1970 to 2000. Thus, at the global scale, the accelerating anthropogenic P release to rivers during the last decades of the 20th century exceeded the added retention capacity of new dams.

Among the four MEA scenarios, the Global Orchestration (GO) and Adapting Mosaic (AM) yield the largest and lowest riverine TP and RP loads in 2030, respectively (Table 4.1). Assuming that either (1) no new dam construction takes place after 2000, or (2) all dams under construction or planned will be completed by 2030, export fluxes calculated using the GO and AM river loads show that, with the exception of Europe, North America and Australia plus Oceania, the building of new dams in the 2000-2030 period should reduce the export of TP (Figure 4.3 and Figure AC2). For Africa and Europe, TP export fluxes are predicted to be lower than in 2000, while for Asia, North America and South America TP export fluxes under the AM scenario would remain close to their 2000 values. The current surge in dam construction would therefore appear to be able to largely offset the ongoing and future increases in anthropogenic TP inputs to river systems.
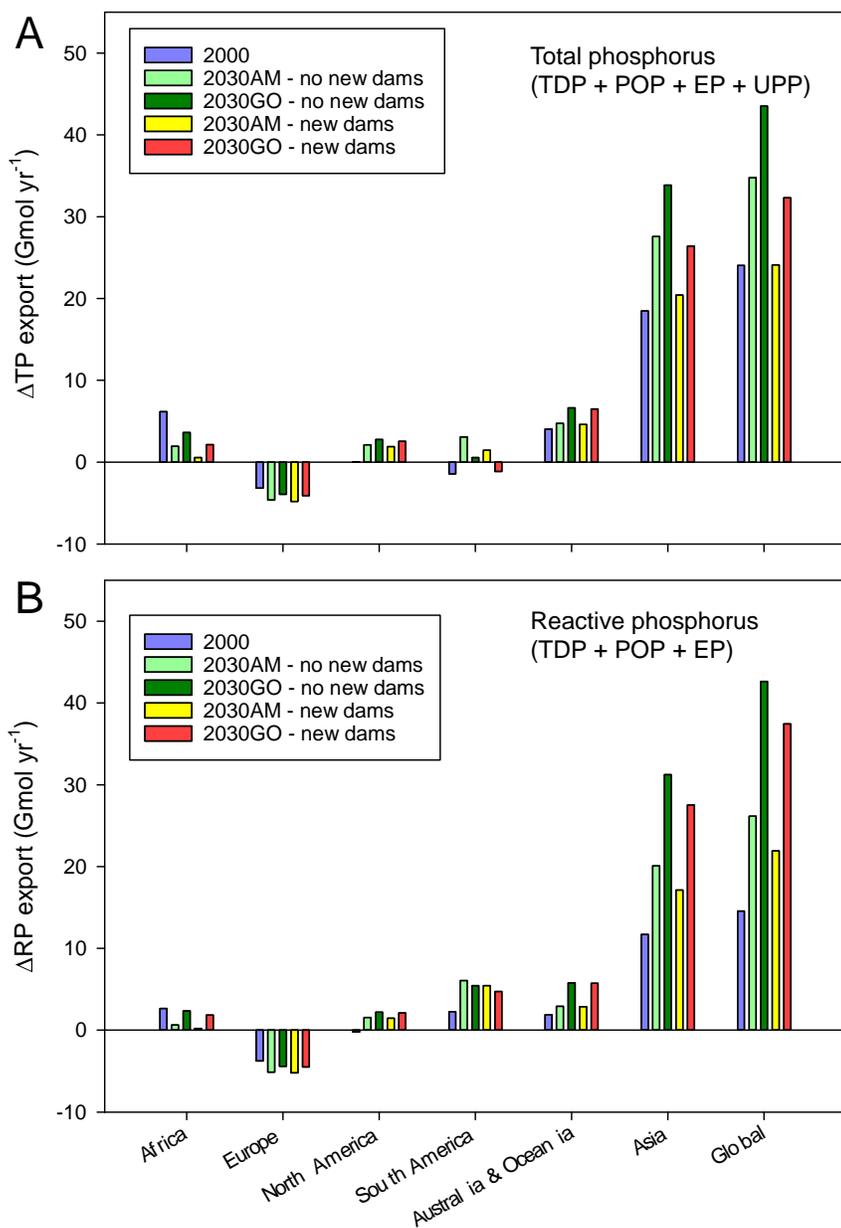
Figure 4.3: Changes in riverine export fluxes of (a) TP and (b) RP to the coastal zone, relative to the corresponding 1970 values. Export fluxes are calculated by subtracting P retained by dam reservoirs in a watershed from the no-dam river P load predicted by the Global-NEWS model. The 2030 scenarios with "no new dams" only account for retention by dams currently in the GRanD database, while the 2030 scenarios with "new dams" include the GRanD dams plus those planned to be completed by 2030, as compiled by Zarfl et al. (2015).

The global export of RP follows a different trajectory, however (Figure 4.3b). In contrast to TP, even with the construction of new dams, the 2030 export fluxes of RP for South America, Asia and Australia and Oceania are predicted to substantially exceed the corresponding fluxes in 2000, even under the AM scenario. These upward trends for RP are due principally to the fact that anthropogenic sources are mostly delivering reactive P phases to river systems. Hence, for South America, Asia and Australia and Oceania combined, the RP fraction of the river TP load is estimated to grow from 34% in 2000 to 43% in 2030. Therefore, in spite of the massive dam building activity now and in the near future, global anthropogenic RP loading is projected to continue to outpace RP retention until at least 2030. Under the GO scenario, global RP export is expected to be 21% higher in 2030 than in 2000. Such a large global increase in RP export would likely further exacerbate cultural eutrophication of surface water bodies.

My estimations of TP and RP retention in reservoirs imply that global river damming represents a major anthropogenic perturbation of the continental P cycle. Dams also influence river fluxes of other nutrients, including nitrogen and silicon (Si) (Harrison et al., 2009; Maavara et al., 2014). Because retention efficiencies by reservoirs differ from one nutrient element to another (Donald et al., 2015; Maavara et al., 2014; Maavara et al., 2015a), the presence of dams may modify nutrient stoichiometry along rivers and thereby affect nutrient limitation and food-web dynamics in river-fed aquatic ecosystems. The existing evidence suggests dams generally remove P more efficiently than N and Si (Donald et al., 2015; Maavara et al., 2015a). Damming could therefore be one factor explaining the trend toward more widespread P limitation of coastal waters (Elser et al., 2007; Howarth and Marino, 2006). Given the importance of P as a key, and often limiting, nutrient, as well as the rapid pace of global damming, there is an urgent need to better understand the effects of dams on riverine P fluxes, and to fully determine the associated environmental impacts.

4.5 Materials and Methods

The biogeochemical processes controlling P cycling in surface water bodies are relatively well understood. The existing knowledge base is thus used to build a P mass balance model that captures the key transformations responsible for changes in P speciation between river inflow and dam outflow (Figure 4.1). Note that the model does not account for spatial trends within a reservoir, or for sub-annual variability in P dynamics. It is not designed to provide a detailed representation of any particular reservoir, but rather to perform first-order estimations of annual P sequestration by dams at the river basin scale or higher.

The model assumes that P is supplied to a reservoir via river inflow. For each of the P pools considered in the model (TDP, POP, EP, and UPP), the input is computed as

$$F_i^{in} = Q \times [TP]_{in} \times \alpha_i^{in} \qquad (4.3)$$

where Q is the volumetric river discharge, $[TP]_{in}$ the TP concentration of the inflow, and α_i^{in} the fraction of species i in inflowing TP. The fluxes redistributing P between the TDP, POP and EP pools, the burial fluxes of the particulate forms of POP, EP and UPP, and the outflow fluxes of the four pools of P are all assumed to obey first-order kinetics with respect to the corresponding source pool mass. Burial is defined as the transfer of P below the topmost, active surface layer of sediment, where mineralization and desorption processes remobilize part of the deposited POP and EP. The pools in Figure 4.1 are therefore partly located within the water column and partly within the upper, active sediment layer.

4.5.1 Monte Carlo analysis: Model parameters

The P mass balance model contains 13 adjustable parameters (Table 4.3). Based on the available literature, probability density functions (PDFs) are assigned to 11 parameters, while fixed values are imposed to the remaining two (Table 4.3). Monte Carlo simulations are carried out by randomly generating 6000 different parameter combinations from the imposed PDFs. Each individual model run is performed with Runge-Kutta 4 integration and 0.01 year time steps, for the length of time elapsed since dam closure (i.e., if the dam is 20 years old, the model is run for 2000 time steps). The model-predicted R_{TP} and R_{RP} values exhibit positive trends with the hydraulic residence time, τ_r (Figure AC1), as expected from the literature (Brett and Benjamin, 2008; Hejzlar et al., 2006; Kõiv et al., 2011). The trends are fitted to the classical Vollenweider model for P sequestration in lakes (Equation 4.2).

Details on how the parameter ranges and distributions are selected are given below. It is important to emphasize that sections 4.5.1.1 through 4.5.1.4 deal with assigning values to the rate constants (in yr^{-1}) of the processes controlling the cycling of P in reservoirs, not to the corresponding fluxes (in mol yr^{-1}). In the model, the effluxes out of the reservoir are inversely related to the water residence time, that is, in-reservoir fluxes (or rates) increase with water residence time as the corresponding processes act over longer time scales. In turn, I assume that the rate constants are independent of the water residence time, in order to avoid duplication of the water residence time effect on the rates/fluxes.

4.5.1.1 Permanent burial

The rate constant for burial of particulate P, k_{burial}, is the most sensitive parameter governing model-predicted TP retentions (Section 4.5.3). The probability function assigned to k_{burial} is obtained by fitting a gamma function to burial rate constants reported for 61 lakes and reservoirs gathered from literature sources (Table 4.3). The resulting gamma distribution reproduces the observed range of R_{TP} values of the reservoirs included in Dataset S1 (Appendix C).

4.5.1.2 Primary productivity

Phosphorus uptake and assimilation via primary productivity (F_{12}) is, in general, the main in-reservoir process leading to RP retention. The imposed range of k_{up} is based on annually averaged, whole-reservoir primary production rates reported in the literature (Imboden and Gächter, 1978; Imboden, 1974; Maavara et al., 2014; Snodgrass and O'Melia, 1975). Note that these rates are typically lower than those derived from short-term microcosm incubations (Cotner and Wetzel, 1992; Hudson et al., 2000). The k_{up} range reproduces the TDP retentions and their corresponding TP retentions calculated for the 16 reservoirs with available TDP budgets of Dataset S1 (Appendix C).

4.5.1.3 Mineralization

Mineralization of organic P (F_{21}) is modeled using a fixed value of 7 yr^{-1} for the rate constant, k_{miner}, based on the references in Table 4.3 (Griffin and Ferrara, 1984; Katsev et al., 2006; Malmaeus et al., 2006; Slomp and Van Cappellen, 2007). Results of the model sensitivity analysis (Section 4.5.3, Table 4.4) show no change (<0.1% difference) in model outcome for variations in k_{miner} of ±10%.

4.5.1.4 Sorption

Sorption and desorption cover a wide range of processes with widely different kinetics. The sensitivity analysis indicates that R_{TP} and R_{RP} are relatively insensitive to the absolute values assigned to the rate constants k_{sorb} and k_{desorb} (Table 4.4), but rather depend on their ratio. Hence, the sorption rate constant is fixed, while the desorption rate constant is varied over a sufficiently broad range in order to simulate conditions ranging from net P sorption ($k_{sorb}>k_{desorb}$) to net desorption ($k_{sorb}<k_{desorb}$).

In general, phosphate sorption is stronger under oxygenated conditions than in the absence of oxygen (Katsev et al., 2006). As a first order approach to determine the likelihood that the bottom waters of a reservoir become anoxic, I use the average water depth: in analogy with lakes (Gorham and Boyce, 1989), I assume that reservoirs with average water depth >7 m are more prone to undergo

stratification and, hence, have a higher potential for anoxia than shallower reservoirs. A lower k_{sorb} value (0.5 yr^{-1}) is assigned when water depth >7m, and a higher value (1.5 yr^{-1}) when water depth ≤7m.

4.5.1.5 Riverine P inputs

The distribution of TP in world average river water is: 9% TDP, 4% POP, 72% UPP and 15% EP (Berner and Berner, 1995; Compton et al., 2000; Meybeck, 1982; Meybeck, 1993). These proportions imply that, on average, about 20% of particulate P (PP) is reactive. Gamma probability functions are used to represent the proportions of the reactive pools of P delivered by rivers into reservoirs (α^{in}_i): α^{in}_i values vary between 0 and 1, with mean values equal to the world average values given above.

4.5.2 Global phosphorus retention estimates

4.5.2.1 1970 and 2000 Retentions

To generate the 1970 and 2000 global TP and RP retentions in reservoirs, Equations 4.1 and 4.2 are scaled up by spatially intersecting the GRanD database (Lehner et al., 2011) with the 1970 and 2000 P river loads calculated by the Global-NEWS model (Harrison et al., 2010; Maavara et al., 2014; Mayorga et al., 2010). For the 1970 calculations, all dams built in 1971 and later are removed from the GRanD database. For each reservoir, the TP and RP inputs from the reservoir's watershed are computed as

$$X_{in,i} = W \times Y \tag{4.4}$$

where $X_{in,i}$ is the TP or RP influx to reservoir i in units of mol yr^{-1}, W is the upstream watershed area (km^2) listed in the GRanD database, and Y is the RP or TP yield of the watershed in units of mol P $km^{-2} yr^{-1}$. Note that the Y values in Equation 4.4 are obtained after inactivating the Global-NEWS model's built-in damming function.

Equation 4.4 assumes uniform RP and TP yields throughout a given catchment (Harrison et al., 2012; Jansen et al., 2010). The amounts of TP or RP retained annually in the reservoir are then calculated as

$$X_{ret,i} = X_{in,i} - X_{out,i} = R_X \times X_{in,i} \tag{4.5}$$

Table 4.3: Parameter ranges and distributions used in Monte Carlo analysis. PDF = probability distribution function. See text for details. Note that σ values listed in the PDF parameter column are unrelated to the nutrient loss parameter σ in Equation 4.2.

Parameter	Range	Accuracy	PDF equation	PDF parameters	Assumptions/notes	Ref.
Volume	0.001-180 km^3	High	Pareto: $$y = \left(\frac{1}{\sigma}\right)\left(1 + k\frac{x-\theta}{\sigma}\right)^{-1-\frac{1}{k}}$$	$\sigma = 0.0556487$, $k = 1.39388$, $\theta = 0$	PDF fitted to GRanD database reservoir volume distribution, binned according to Freedman-Diaconis rule.	(Lehner et al., 2011)
Discharge	0.01-150 km^3 yr^{-1}	High	Pareto: $$y = \left(\frac{1}{\sigma}\right)\left(1 + k\frac{x-\theta}{\sigma}\right)^{-1-\frac{1}{k}}$$	$\sigma = 0.0511971$, $k = 2.12464$, $\theta = 0$	PDF fitted to GRanD database reservoir discharge distribution, binned according to Freedman-Diaconis rule.	(Lehner et al., 2011)
Inflowing TP concentration	0.001-800μM (1000-8x10^8 mol km^{-3})	High	Lognormal: $$y = \frac{1}{x\sigma\sqrt{2\pi}}exp\left\{\frac{-(\ln x - \mu)^2}{2\sigma^2}\right\}$$	$\mu = 15.148$, $\sigma = 1.24707$	PDF fitted to reservoir P budget database according to Freedman-Diaconis rule.	Dataset S1 (Appendix C)
Proportion TDP (α^{in}_{TDP})	0-1	Moderate	Gamma: $$y = \frac{\left(\frac{1}{b^a\Gamma(a)}x^{a-1}e^{\frac{-x}{b}}\right)}{20}$$	a = 1.2, b = 1.5	Gamma PDF constrained using world average proportions of each species (TDP = 0.09, POP = 0.04, EP = 0.15, UPP = 0.72). Mean of Monte Carlo outputs will equal these constrained means, but full range of proportions possible in outcome.	(Berner and Berner, 1995; Compton et al., 2000; Meybeck, 1982; Meybeck, 1993)
Proportion POP (α^{in}_{POP})				a = 0.8, b = 1.0		
Proportion EP (α^{in}_{EP})				a = 3.0, b = 1.0		
Proportion UPP (α^{in}_{UPP})			$\alpha^{in}_{UPP} = 1 - (\alpha^{in}_{TDP} + \alpha^{in}_{POP} + {}^{in}\alpha_{EP})$	N/A		
k_{desorb}	0.01-2 yr^{-1}	Low	Uniform	N/A	Sorption is held constant while desorption can vary. k_{sorb} is 1.5 yr^{-1} if reservoir depth is less than or equal to 7m, and 0.5 yr^{-1} if greater than 7m.	(Gorham and Boyce, 1989)
k_{sorb}	0.5 or 1.5 yr^{-1}	Low	N/A	N/A		
k_{burial}	0.01-60 yr^{-1}	Moderate	Gamma: $$y = \frac{1}{b^a\Gamma(a)}x^{a-1}e^{\frac{-x}{b}}$$	a = 0.2, b = 13	61 values, binned according to Freedman-Diaconis rule, crosschecked for suitability of range against Dataset S1 data.	(Duras and Hejzlar, 2001; Imboden and Gächter, 1978; Imboden, 1974; James and Barko, 1997; Krogerus and Ekholm, 2003; Larsen and Mercier, 1976; Moosmann et al., 2006; Snodgrass and O'Melia, 1975)
k_{up}	0.08-200 yr^{-1}	Moderate	Uniform	N/A	Range constrained using literature values, checked against Dataset S1 data.	(Imboden and Gächter, 1978; Imboden, 1974; Maavara et al., 2014; Snodgrass and O'Melia, 1975)
Reservoir age (i.e. model run-time)	0.05-1000 years	High	Lognormal: $$y = \frac{1}{x\sigma\sqrt{2\pi}}exp\left\{\frac{-(\ln x - \mu)^2}{2\sigma^2}\right\}$$	$\mu = 3.88106$, $\sigma = 0.46671$	PDF fitted to GRanD database reservoir age distribution, binned according to Freedman-Diaconis rule.	(Lehner et al., 2011)
k_{miner}	7 yr^{-1}	Moderate	N/A	N/A	Model insensitive to changes in this parameter.	(Cotner and Wetzel, 1992; Gorham and Boyce, 1989; Griffin and Ferrara, 1984; Malmaeus et al., 2006; Slomp and Van Cappellen, 2007)

where R_X is defined by Equation 4.1. Because Global-NEWS estimates the yields of dissolved organic P (DOP), dissolved inorganic P (DIP) and particulate P (PP), the corresponding RP yield is calculated as the sum of DOP and DIP, plus 20% of PP (Compton et al., 2000; Meybeck, 1982).

The GRanD database accounts for ≥76% of the estimated global volume of reservoirs worldwide. The bulk of the reservoirs not included in the GRanD database are relatively small, <1 km^2 in size (Lehner et al., 2011). Those reservoirs in the GRanD database that are smaller than 1 km^2 have a median water residence time of 0.6 years. I therefore assume that the missing reservoirs receive approximately 24% of the global riverine TP and RP inputs and have water residence times of 0.6 years. The missing reservoirs then account for an additional 14 Gmol TP yr^{-1} and 6 Gmol RP yr^{-1} retained in 2000. For the 1970 calculations, I assume the number of missing reservoirs is half that in 2000, because 1970 was roughly midway through the first post-WWII boom in dam construction (Grill et al., 2015; Zarfl et al., 2015). I thus estimate that in 1970 the missing reservoirs account for an additional 7 Gmol TP yr^{-1} and 3 Gmol RP yr^{-1}.

4.5.2.2 2030 Retentions

With the recently published database of hydroelectric dams under construction or planned (Grill et al., 2015; Zarfl et al., 2015), it is possible to estimate the projected increases in TP and RP retentions by the year 2030, under the assumption that all planned dams will be completed (Grill et al., 2015). The database contains 3782 dams with hydropower production capacities of 1 MW or greater. Projected hydropower production capacities and dam discharges are given in Zarfl et al. (2015), while reservoir volumes are estimated using a linear regression between hydroelectric capacity and reservoir volume established by Grill et al. (2015). I overlay the global map of new reservoirs with the Global-NEWS model output in order to estimate nutrient retention by the new dams constructed between 2000 and 2030, as done for existing reservoirs using the GRanD database.

I use the four Millennium Ecosystem Assessment scenarios as incorporated into the Global-NEWS model by Seitzinger et al. (2010). As before, the Global-NEWS model is run after turning off the built-in damming function. The four scenarios, TechnoGarden (TG), Global Orchestration (GO), Adapting Mosaic (AM), and Order through Strength (OS), yield different river P loads depending on whether society follows a proactive approach to environmental management (TG and AM) or a reactive approach (OS and GO), and whether the world becomes increasingly globalized (GO and TG) or regionalized (AM and OS) (Garnier et al., 2010).

The 3782 dams planned or under construction will be built on 344 rivers, that is, dam cascades are the norm for the current surge in damming. This is accounted for in the retention estimates by applying, the following equation to all dam reservoirs in a watershed, except the most upstream one (for which Equation 4.4 is used),

$$X_{in,i} = [(W_i - W_{i-1}) \times Y] + X_{i-1,out} \tag{4.6}$$

where W_{i-1} is the catchment surface area of the reservoir immediately upstream of reservoir i, and $X_{i-1,out}$ is the TP or RP flux out of the reservoir immediately upstream of reservoir i.

4.5.3 Uncertainty and sensitivity analyses

To approximate the uncertainties on global dam P retention estimates associated with the mechanistic modeling approach, I fitted gamma functions to the R_{TP} and R_{RP} distributions produced by the 6000 Monte Carlo simulations of the model (Figure AC1). A second Monte Carlo analysis was then carried out to calculate global P retentions in which, for each reservoir in GRanD, R_{TP} and R_{RP} values were randomly selected from the corresponding gamma distributions. A total of 20 simulations were carried out, yielding ±7% standard deviations on the average global TP and RP retentions. Note that these relatively modest uncertainties do not account for the errors associated with the model structure, the Global-NEWS output and the GRanD database. Model uncertainties on the global TP and RP retentions of the 2030 MEA scenarios are ±20% higher than those of 1970 and 2000, because dams added between 2000 and 2030 tend to have shorter water residence times (95% have $\tau_r \leq 2$ years) than dams built before 2000. The ±20% error estimate is based on the drop in goodness-of-fit of Equation 4.2 when only using the results of the Monte Carlo analysis for τ_r between 0 and 2 years.

A sensitivity analysis is performed by varying the "default" parameter values listed in Table 4.4 by ±10%, and running 150 model iterations per parameter value. Discharge and volume (and therefore surface area and depth) vary according to the ranges and distributions described in Table 4.3, in order to quantify parameter sensitivity over a range of hydraulic residence times. The sensitivity to the proportions of the different pools making up the total river P load is assessed using variable α^{in}_i values reflecting the range of uncertainty in global river P export to the oceans (Table 4.4). To test the model's sensitivity to initial conditions, the output using initial species concentrations of 0 mol km^{-3} are compared to the global averages for rivers from the Global River Chemistry Database (GloRiCh).

For each set of 150 iterations, R_{TP} and R_{RP} are plotted against the hydraulic residence time and fitted to Equation 4.2 to determine the corresponding changes in σ. Results show that k_{burial} and the α^{in}_i

values are the most sensitive model parameters. The imposed variations in initial conditions, reservoir age, inflowing TP concentration and the other rate constants have little or no effects on R_{TP}, and generally somewhat larger effects on R_{RP} (Table 4.4).

Table 4.4: Summary of the sensitivity analysis of the mass balance P model. The calculated responses refer to the relative change in the rate constant σ in Equation 4.2.

Parameter	Default parameter	Adjustment	TP response	RP response
inflow TP concentration	7.4 µM (GloRiCh average)	±10%	< ±0.1%	< ±0.1%
k_{desorb}	1 yr^{-1}	±10%	±0.2%	±1%
k_{sorb}	1 yr^{-1}	±10%	±0.1%	±1%
k_{up}	4 yr^{-1}	±10%	±0.5%	±2%
k_{burial}	2.6 yr^{-1}	±10%	±10%	±9%
k_{min}	7 yr^{-1}	±10%	±0.1%	±0.5%
Reservoir age	40 yr	=10 years	< ±0.1%	< ±0.1%
Species inflow proportions (α_i^{in})	POP = 0.04, TDP = 0.09, UPP = 0.72, EP = 0.15	All species = 0.25	+14%	+0.4%
		POP = 0.04, TDP = 0.05, UPP = 0.73, EP = 0.18	-2.7%	-9%
Initial conditions	0 µM	= GloRiCh averages	< ±0.1%	+0.2%
		= influx	< ±0.1%	+0.4%

Chapter 5

Global perturbation of organic carbon cycling by river damming

This chapter is modified from:

5.1 Summary

The damming of rivers represents one of the most far-reaching human modifications of the flows of water and associated matter from land to sea. Dam reservoirs are hotspots of sediment accumulation, primary productivity (P) and carbon mineralization (R) along the river continuum. Here I show that for the period 1970-2030, global carbon mineralization in reservoirs exceeds carbon fixation ($P<R$); the global P/R ratio, however, varies significantly, from 0.20 to 0.58 because of the changing age distribution of dams. I further estimate that at the start of the 21st Century, in-reservoir burial plus mineralization eliminated 4.0 ± 0.9 Tmol yr^{-1} (48 ± 11 Tg C yr^{-1}) or 13% of total organic carbon (OC) carried by rivers to the oceans. Because of the ongoing boom in dam building, in particular in emerging economies, this value could rise to 6.9 ± 1.5 Tmol yr^{-1} (83 ± 18 Tg C yr^{-1}) or 19% by 2030.

5.2 Introduction

Rivers act as reactive conduits connecting the continental and oceanic carbon (C) cycles: they annually deliver around 1.0 Pg C (83 Tmol) to the sea, about half under the form of total organic carbon (OC) (Battin et al., 2009; Cole et al., 2007; Regnier et al., 2013; Syvitski et al., 2005; Ver et al., 1999). Humans, however, have profoundly altered the balance between carbon fixation, mineralization and OC burial along the river continuum, not only by increasing the loadings of OC and nutrients to rivers but also through the massive building of dams (Cole et al., 2007; Grill et al., 2015; Tranvik et al., 2009; Vitousek et al., 1997). Globally, there are over 16 million dams, with more than 50,000 large dams having heights exceeding 15 m (Lehner et al., 2011). Over the next few decades, many new dams will be built, primarily for energy production. The number of large hydroelectric dams, which currently represent about 20% of large dams, is expected to double in the next 15-20 years (Lehner et al., 2011; Zarfl et al., 2015). All the available evidence suggests that river damming significantly changes riverine OC export to the ocean (Regnier et al., 2013).

Upon dam closure, increased water residence time, improved light conditions, nutrient retention and sediment trapping in the impounded reservoir amplify primary productivity and promote the burial of autochthonous and allochthonous OC (Downing et al., 2008; Mendonça et al., 2012a; Mulholland and Elwood, 1982; Skalak et al., 2013). The construction of a dam also causes flooding and subsequent degradation of submerged biomass and soil organic matter within the reservoir (Barros et al., 2011; Catalan et al., 2016; Fearnside, 1995). These processes modify the downstream transfer of OC and nutrients, and thus the trophic state of the river system, as indicated by the decrease in pCO_2 observed in many rivers after dam closure (Garnier and Billen, 2007; Jones et al.,

2003; Lauerwald et al., 2015; Wang et al., 2007). However, the global-scale changes in riverine OC fluxes due to damming remain poorly quantified (Mendonça et al., 2012a). Only OC burial in the largest 600-700 reservoirs has been estimated (Mayorga et al., 2010), while global estimations of in-reservoir photosynthetic carbon fixation and mineralization are highly uncertain (Barros et al., 2011; Cole et al., 2007; Regnier et al., 2013).

In this study, I present a worldwide analysis of decadal trends in riverine OC fluxes that explicitly accounts for reservoirs as a dynamic compartment of the C cycle on the continents (Le Quéré et al., 2015; Regnier et al., 2013). I use a spatially explicit modelling approach to predict global in-reservoir primary production (P), mineralization (R) and burial of OC, from 1970 to 2050, in order to assess the evolving role of dams in the riverine export of OC to the oceans. I predict that dams decreased OC delivery to the oceans by 13% in 2000, with this value increasing to 19% by 2030. My analysis further reveals that, during the period 1970-2030, worldwide reservoir respiration exceeds primary production ($P<R$), because of the continual addition of new dams. Should dam construction become negligible after 2030, dam reservoirs could globally become net autotrophic (i.e., $P>R$) by the middle of the century.

5.3 Methods

5.3.1 Dam databases

The Global Reservoirs and Dams (GRanD) database provides the most comprehensive compilation of data on dams and reservoirs, including reservoir volume, surface area, water discharge through the dam, and date of dam closure (Lehner et al., 2011). GRanD includes reservoirs with surface areas greater than 0.1 km^2 and is near complete for reservoirs larger than 10 km^2. The 6862 reservoirs in GRanD (Lehner et al., 2011) represent 77% of the estimated global reservoir volume of 8069 km^3. Small reservoirs with surface areas down to 0.0001 km^2 make up the remaining volume. My global estimates of carbon fixation, mineralization and burial for years 1970 and 2000 are based on the dams listed in GRanD (with closure dates preceding either 1970 or 2000), hence including a much larger number of reservoirs than previous estimates (Lehner and Döll, 2004; Seitzinger et al., 2005; Vörösmarty et al., 2003). For the 2030 and 2050 projections, GRanD is augmented with the database compiled by Zarfl et al. (2015) which contains over 3,700 hydroelectric dams with generating capacities ≥ 1 MW that are now under construction or planned to be completed by 2030. I assume that

these dams will account for most of the increase in global reservoir volume in the first half of the 21st Century.

5.3.2 Modelling approach

Dams under operation at the selected time points (1970, 2000, 2030 and 2050) are extracted from the dam databases. I assume that all the dams in the database of Zarfl et al. (2015) will be completed by 2030, and that the ongoing dam building boom will end by 2030, beyond which no major further dam construction will take place. In-reservoir organic carbon (OC) transformations and burial rates are simulated using a simple, biogeochemical mass balance (or box) model (Figure 5.1). The parameters of the kinetic expressions representing the in-reservoir processes are assigned probability density functions (PDF) that take into account each parameter's inter- and intra-reservoir variability at the annual timescale. The PDFs are derived from available data on photosynthetic C fixation, OC mineralization and OC burial in lentic systems. A similar approach was previously applied to predict global-scale phosphorus and nutrient silicon retention in dam reservoirs (Maavara et al., 2014; Maavara et al., 2015b).

A virtual database of model reservoirs is generated by performing 6000 Monte Carlo (MC) simulations with rate parameters selected randomly from their corresponding PDFs. From this virtual database, global relationships are derived that predict burial, mineralization, and photosynthesis rates from the reservoir's hydraulic residence time. The global relationships are applied to a real-world database that includes existing reservoirs (GRanD) (Lehner et al., 2011) in 1970 and 2000, and reservoirs under construction or planned to be completed by 2030 (Zarfl et al., 2015). Together with the DOC and POC loads to reservoirs obtained from the Global-NEWS model, the burial, mineralization, and photosynthesis fluxes in the reservoirs of all major watersheds worldwide are then simulated for four selected time points (1970, 2000, 2030 and 2050). The MC analysis also yields estimates of the uncertainties on the OC fluxes associated with parameter variability.

The Global-NEWS model is well suited for the proposed modelling approach: it differentiates between POC and DOC, it implicitly accounts for in-stream OC losses, and it has been used to hindcast nutrient loads to watersheds in the years 1970 and 2000, and to forecast the 2030 and 2050 loads according to the Millennium Ecosystem Assessment (MA) scenarios (Mayorga et al., 2010; Seitzinger et al., 2010). Global-NEWS predicts sediment, OC and nutrient yields based on land use and land cover (e.g., wetlands, cropland, and grasslands), climate variables (including temperature and precipitation), geomorphological parameters (including slope and lithology), and anthropogenic
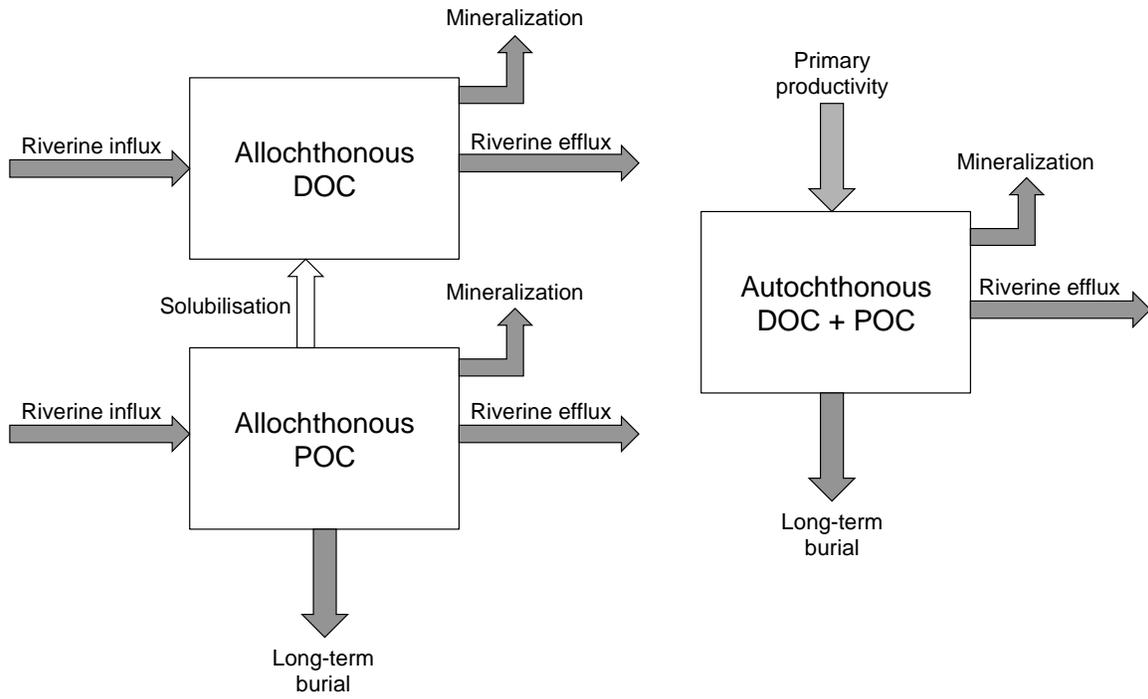
Figure 5.1: Mechanistic model of in-reservoir organic carbon cycling.

alterations (including consumptive water usage). The MA scenarios are storylines for a future world that will become either more globalized (Global Orchestration, GO, and TechnoGarden, TG) or regionalized (Adapting Mosaic, AM, and Order from Strength, OS), and take either a proactive (TG and AM) or reactive approach to environmental management (GO and OS) (Seitzinger et al., 2010). Each of the MA scenarios assumes changing land uses, climate regimes, and anthropogenic perturbations, which in turn modify the fluxes of sediments, OC and nutrients delivered to river systems.

A caveat of Global-NEWS is the lack of representation of extreme hydrological events with a low recurring probability but potentially large contributions to long-term riverine fluxes. These events are not captured by the Global-NEWS model itself or by the observed data it was trained on. These events can involve geomorphologic processes such as landslides, which mobilize the carbon stored in the entire soil horizon plus the standing biomass. Such events, which can be related to extreme weather phenomena (e.g. tropical cyclones) or earthquakes, have been described for steep catchments in the sub-tropics (e.g. Taiwan (West et al., 2011)) and temperate regions (e.g. New Zealand (Hilton et al., 2011)). Their contributions to OC mobilization at the global scale remain to be quantified.

In my modeling approach, reservoir infilling due to sedimentation is not taken into account. Vörösmarty et al. (1997) estimate that sedimentation has reduced the volume of reservoirs in the United States by up to 2 km^3, that is, only ~0.2% of the total US reservoir volume. While reservoir infilling may vary significantly from one reservoir to another, the effect of sediment accumulation on water residence time likely represents a relatively minor source of uncertainty on the impact of dams on the global riverine OC flux.

5.3.3 Mass balance model

The mass balance model for in-reservoir allochthonous and autochthonous OC cycling is shown in Figure 5.1. Riverine inflow fluxes of allochthonous particulate and dissolved OC (POC and DOC) are calculated by multiplying inflow concentrations (mol km^{-3}) by the river discharge (Q, km^3 yr^{-1}) through the dam. Assuming inflow of water to a reservoir equals the outflow through the dam, values for Q are retrieved from the GRanD database (Lehner et al., 2011), augmented with the database of hydroelectric dams of Zarfl et al. (2015) for the 2030 and 2050 projections. Outflow fluxes of OC through the dam are obtained by multiplying the in-reservoir POC and DOC masses (mol) by the flushing rate, ρ (yr^{-1}), which is equal to Q/V where V is the reservoir volume in km^3. The key role of ρ (or its inverse, the water residence time) in material mass balances of reservoirs is well-established (Maavara et al., 2014; Tranvik et al., 2009; Vollenweider, 1975; Vörösmarty et al., 2003).

Except for primary production, the fluxes (F, mol yr^{-1}) describing the in-reservoir OC processes assume first-order kinetics with respect to the mass (M, mol) of the OC pool from which the flux originates:

$$F = k \times M \tag{5.1}$$

where k is the first-order rate constant (yr^{-1}). Primary production of autochthonous POC (P, mol yr^{-1}) is assumed to be phosphorus limited (Hecky and Kilham, 1988; Schindler, 1977; Smith et al., 1999), according to

$$P = P_{\max} \frac{[TDP]}{K_{s} + [TDP]} \tag{5.2}$$

where P_{max} is the maximum value of P under nutrient saturated conditions, $[TDP]$ the concentration of total dissolved phosphorus in the reservoir, and K_s the half-saturation TDP concentration. For each reservoir and time point, $[TDP]$ is extracted from the previously published global reservoir phosphorus model (Maavara et al., 2015b). The mass balance equations for the various OC pools are solved using the Runge-Kutta 4 integration scheme with 0.01-year time steps, and run for the length of time since dam closure (i.e., if the dam is 10 years old, the model is run for 1000 time steps).

5.3.4 Model parameterization

For each parameter value a probability density function (PDF) is derived from data reported in the literature (Table 5.1). For the river inflow DOC concentration I impose the gamma distribution proposed by Sobek et al. (2007) based on data for 7500 lakes. This is justified as the mean and range of DOC concentrations in rivers are comparable to those observed in lakes (Meybeck, 1988; Spitzy and Leenheer, 1991). For the inflow POC concentrations, a generalized Pareto distribution yields the highest log-likelihood when fitted to the POC concentrations derived by applying the Global-NEWS loads and discharge values to the GRanD reservoirs (Lehner et al., 2011; Mayorga et al., 2010). Similarly, the PDFs for reservoir volume, discharge, latitude, altitude and age (i.e. years since dam closure) are the functions that were found to best fit the observed distributions in the GRanD database (Table 5.1). Reservoirs in GRanD further yield the following relationship between surface area (*SA,* km^2) and volume:

$$SA = 42.264 \times V^{0.8183} \tag{5.3}$$

Table 5.1: Probability distribution functions (PDFs) used in the Monte Carlo analysis. Note that parameters a and b are unrelated to those used in Equations 5.8, 5.9 and 5.12, 5.13.

Parameter	Range, units	PDF equation	PDF parameters	Ref.
Volume (V)	0.001-180 km^3	Pareto: $$y = \left(\frac{1}{\sigma}\right)\left(1 + k\frac{x - \theta}{\sigma}\right)^{-1-\frac{1}{k}}$$	$\sigma = 0.0556487$, $k = 1.39388$, $\theta = 0$	(Lehner et al., 2011)
Discharge (Q)	0.01-150 km^3 yr^{-1}	Pareto: $$y = \left(\frac{1}{\sigma}\right)\left(1 + k\frac{x - \theta}{\sigma}\right)^{-1-\frac{1}{k}}$$	$\sigma = 0.0511971$, $k = 2.12464$, $\theta = 0$	(Lehner et al., 2011)
Latitude	-90.00 – 90.00°	Normal: $$y = \frac{1}{\sigma\sqrt{2\pi}}e^{\frac{-(x-\mu)^2}{2\sigma^2}}$$	$\sigma = 35.5964$, $\mu = 12.1614$	(Lehner et al., 2011)
Altitude	-33 – 4515 m	Lognormal: $$y = \frac{1}{x\sigma\sqrt{2\pi}}exp\left\{\frac{-(\ln x - \mu)^2}{2\sigma^2}\right\}$$	$\sigma = 1.11179$, $\mu = 5.71949$	(Lehner et al., 2011)
Inflow DOC concentration	0.001 – 1x10^5 ppm	Gamma: $$y = \frac{1}{b^a\Gamma(a)}x^{a-1}e^{\frac{-x}{b}}$$	$a = 1.218$, $b = 5.886$	(Sobek et al., 2007)
Inflow POC concentration	0.1 – 10 000 µM	Pareto: $$y = \left(\frac{1}{\sigma}\right)\left(1 + k\frac{x - \theta}{\sigma}\right)^{-1-\frac{1}{k}}$$	$\sigma = 0.991719$, $k = 208.827$, $\theta = 0$	(Lehner et al., 2011; Mayorga et al., 2010)
Half-saturation constant (K_s)	2.0x10^5 – 6.3x10^6 mol TDP km^{-3}	Uniform	N/A	(Ahlgren, 1977, 1978; Holm and Armstrong, 1981; Lehman, 1976; Nalewajko and Lean, 1978; Nyholm, 1977; Reynolds, 1988; Tilman and Kilham, 1976; van Liere and Mur, 1979)
k_{bur}	1 – 15 yr^{-1}	Uniform	N/A	(Dean and Gorham, 1998; Jørgensen, 1976; Kastowski et al., 2011; Mulholland and Elwood, 1982; Sobek et al., 2009)
k_{20}	0.256 – 1.825 yr^{-1}	Normal: $$y = \frac{1}{\sigma\sqrt{2\pi}}e^{\frac{-(x-\mu)^2}{2\sigma^2}}$$	$\sigma = 0.685027$, $\mu = 0.174299$	(Catalan et al., 2016; Hanson et al., 2014; Hanson et al., 2011)
Autochthonous k_{20} scaling factor	1 – 6 (unitless)	Normal: $$y = \frac{1}{\sigma\sqrt{2\pi}}e^{\frac{-(x-\mu)^2}{2\sigma^2}}$$	$\sigma = 1$, $\mu = 3$	(Catalan et al., 2016; Koehler et al., 2012; Sobek et al., 2009)

In the MC analysis, *SA* values from Equation 3.1 are multiplied by a random number between 0.1 and 10, thus allowing deviations in SA by ± one order of magnitude from Equation 3.1. I compute *SA* from *V*, rather than vice versa, because *V* is the primary size variable used to calculate the water residence times in the up-scaling procedure.

Mineralization fluxes include the contributions of biological respiration processes, as well as photochemical degradation (Hanson et al., 2014; Hanson et al., 2011; Tranvik et al., 2009). The temperature dependence of the allochthonous POC and DOC mineralization (biological respiration and photochemical degradation) rate constants, $k_{\text{min,allo}}$, is assumed to follow the same expression as that derived by Hanson (Hanson et al., 2014; Hanson et al., 2011) from a compilation of ecosystem-scale mineralization rates of allochthonous DOC in lakes:

$$k_{\text{min,allo}} = k_{20} \times \theta^{(T-20)} \tag{5.4}$$

where *T* is the average water temperature (°C), k_{20} is the rate constant at 20°C, and θ is a dimensionless coefficient equal to 1.07 (Hanson et al., 2014). The PDF of k_{20} in Table 5.1 is directly derived from the data of Hanson et al. (Hanson et al., 2014; Hanson et al., 2011). While the same k_{20} PDF is applied to both allochthonous DOC and POC (Hanson et al., 2014), the k_{20} values for POC and DOC are allowed to vary independently in the MC analysis. This approach allows for reactivities of allochthonous POC that in some cases are higher, in others lower, than those of allochthonous DOC, as has been reported for lentic systems (Cardoso et al., 2014; Ostapenia et al., 2009).

In-reservoir produced autochthonous OC tends to be more labile than allochthonous OC (Koehler et al., 2012; Sobek et al., 2009). The k_{20} value for autochthonous OC is therefore multiplied by a variable scaling factor. An average 3-times higher autochthonous k_{20} yields the best fit of my model-predicted total carbon mineralization rate constants to the rate constants compiled by Catalan et al. (2016) across a wide range of aquatic ecosystems and climate zones. To capture the range of the Catalan et al. (2016) rate constant data (with the exception of 4 outliers, 3 of which are from the same small streams), the autochthonous scaling factor is assumed to follow a normal distribution between 1 and 6 (Table 5.1). With this range of the scaling factor, the model-generated total OC mineralization rate constants reproduce the range of observed rate constants of Catalan et al. (2016) (Figure AD1). Because of its greater lability, autochthonous OC exported through a dam is assumed to be mineralized before reaching a downstream reservoir.

The reservoir water temperature *T* is computed as a function of latitude and altitude following Hart and Rayner (1994). For 2030 and 2050, the average air temperature increases predicted by Fekete et al. (2010) for each individual MA scenario are converted to reservoir water temperature increases

using the relationship of Lauerwald et al. (2015), and added to the temperature predicted with the Hart and Rayner equation (Table 5.2).

The half saturation constant K_s in Equation 5.2 is represented by a uniform PDF ranging from 2.0 x 10^7 to 7.0 x 10^8 mol km^{-3} in units of total dissolved phosphorus (Ahlgren, 1977, 1978; Holm and Armstrong, 1981; Lehman, 1976; Nalewajko and Lean, 1978; Nyholm, 1977; Reynolds, 1988; Tilman and Kilham, 1976; van Liere and Mur, 1979). The maximum primary production P_{max} in Equation 5.2 is estimated with:

$$P_{max} = B \times P_{Chl} \times V \times M \times D_f \qquad (5.5)$$

where B is the average annual depth-integrated chlorophyll concentration in the reservoir (mg Chl-a km^{-3}), P_{Chl} is the maximum, annually integrated, chlorophyll-specific carbon fixation rate (mol C (mg Chl-a)$^{-1}$ yr^{-1}), M is a dimensionless metabolic correction factor for water temperature, and D_f is the yearly proportion of ice-free days. The value of P_{Chl} is fixed at 0.15 mol C (mg Chl-a)$^{-1}$ yr^{-1}, which is equivalent to 2.5 g C (g Chl-a)$^{-1}$ hr^{-1}, assuming an annual average of 12 hours daylight per 24 hours (Behrenfeld and Falkowski, 1997a, b; Falkowski, 1981; Platt, 1986); M is equal to 1 at water temperatures $\geq 28°C$, and decreases at lower temperatures with a Q_{10} of 2 (Lewis Jr, 2011); the duration of ice cover required to estimate D_f is calculated from latitude following Williams et al. (2004); B is updated in each model iteration using the relationship provided by Reynolds (2006):

$$B = \left(\frac{1}{k_c}\right)\left[0.75\left(\frac{PP}{RP}\right)\left(\frac{DL}{24}\right)ln\left(\frac{0.7\,I_{o,max}}{0.5\,I_k}\right)\left(\frac{1}{Z_{mix}}\right) - (K_{dw} + K_{dp} + K_{dg})\right] \qquad (5.6)$$

where k_c is the absorbance of photosynthetically active radiation (PAR) per unit of chlorophyll (fixed at 0.014 m^2 (mg Chl-a)$^{-1}$ globally (Lewis Jr, 2011)), PP/RP is the ratio of maximum gross photosynthesis to algal respiration per unit chlorophyll, fixed at 15 (Reynolds and Maberly, 2002), DL is the hours of daylight, fixed annually at 12 hours per day (Reynolds, 2006), $I_{o,max}$ is the maximum site-specific PAR (μmol m^{-2} s^{-1}), I_k is the PAR at the onset of photosaturation, fixed at 120 μmol m^{-2} s^{-1}) (Reynolds, 2006), Z_{mix} is the reservoir mixing depth (m), and $K_{dw} + K_{dp} + K_{dg}$ is the nonalgal PAR attenuation (m^{-1}). The value of $I_{o,max}$ is calculated for each reservoir based on the annually averaged latitude-specific values provided by Lewis Jr (2011) assuming linear interpolation between the latitudinal bands provided; Z_{mix} is estimated based on the empirical relationship with lake fetch (Lewis Jr, 2011), where fetch is assumed to be equal to the diameter of a circle with the same area as the reservoir; PAR attenuation in pure water, $K_{dw,}$, is fixed at 0.13 m^{-1}, PAR attenuation by inorganic suspended particulate matter (tripton), K_{dp}, is fixed at 0.06 m^{-1} , and that by dissolved

organic matter (gilvin), K_{dg}, is calculated for each reservoir with the relationship proposed by Lewis Jr (2011):

$$\ln K_{dg} = -4.44 + 1.80 \times \ln[DOC] - 0.149 \times (\ln[DOC])^2 \tag{5.7}$$

where $[DOC]$ in ppm is generated using the same PDF as for inflow $[DOC]$ (Sobek et al., 2007). A t-test shows that B values generated in the MC analysis are statistically indistinguishable ($p < 0.05$) from values found in the literature (Behrenfeld and Falkowski, 1997a; Lewis Jr, 2011; Reynolds, 2006).

The burial rate constant, k_{bur}, is an effective parameter describing the long-term retention of POC with the sediments accumulating in the reservoir, that is, the POC that is not remineralized or otherwise remobilized and exported over the reservoir's lifetime. The value of k_{bur} aggregates all the factors controlling the POC burial efficiency other than the water residence time, including sedimentation rate, reservoir morphology (which controls deposition patterns), oxygen exposure time, temperature, and sediment resuspension events (Sobek et al., 2009). The upper and lower bounds for the uniform k_{bur} distribution, 1 and 15 yr^{-1} respectively, are based on published rate constants (Jørgensen, 1976) and values back-calculated from global and regional datasets of OC accumulation rates in lakes and reservoirs (Dean and Gorham, 1998; Kastowski et al., 2011; Mulholland and Elwood, 1982; Sobek et al., 2009). More studies quantifying burial rate constants in a diversity of reservoir settings will be needed to further delineate the form of the k_{bur} PDF. The rate constant for allochthonous POC solubilisation to DOC is kept fixed at 0.1 yr^{-1}, as the model is insensitive to this parameter (see Section 5.3.6) (Rotter et al., 2008).

5.3.5 Global upscaling

Global regression relationships are obtained from the MC analysis by carrying out 6000 iterations with the 1970 and 2000 parameter values each, plus 6000 additional iterations for each of the MA scenarios in 2030 and 2050 taking into account the projected changes in air temperature. For all time points and MA scenarios considered, the water residence time, τ_r, provides the best predictor for the fate of allochthonous OC entering a reservoir. The in-reservoir burial and mineralization fluxes, $F_{i,bur}$ and $F_{i,min,}$ produced by the MC simulations are fitted to

$$F_{i,bur} = F_{i,in} \times a_i \left[1 - \frac{1}{1 + \alpha_i \times \tau_r} \right] \tag{5.8}$$

and

$$F_{i,\text{min}} = F_{i,\text{in}} \times b_i \left[1 - \frac{1}{1 + \beta_i \times T \times \tau_r} \right] \qquad (5.9)$$

where the subscript i stands for allochthonous POC or DOC (POC only in the case of burial), in stands for inflow, T is average annual reservoir water temperature (°C), α_i and β_i are first-order rate coefficients describing loss due to burial and mineralization, respectively, and a_i and b_i are dimensionless coefficients. The best-fit values of α_i, β_i, a_i and b_i are given in Table AD1. Note that Eqs. (8) and Eq. (9) are formally similar to the equation derived by Vollenweider (1975) to describe phosphorus cycling in lakes, though scaled with a_i and b_i to account for the separation of loss fluxes into mineralization and burial, rather than lumped together as in Vollenweider's derivation.

The inflows of allochthonous DOC and POC, $F_{i,\text{in}}$, are estimated by spatially overlaying the GRanD reservoirs (Lehner et al., 2011) onto the Global-NEWS watersheds. Global-NEWS is used because it generates spatially explicit riverine OC and phosphorus yields for the four MA scenarios. The projected MA global average air temperature increases are 0.91-1.09°C in 2030 and 1.29-2.11°C in 2050, relative to 2000. These projections are similar to the temperature increases of the Representative Concentration Pathways scenarios RCP4.0 and RCP6.5 (IPCC, 2013). Reservoir water temperature, T, is calculated for each reservoir in GRanD using the relationship with latitude and altitude derived by Hart and Rayner (1994). For the 2030 and 2050 scenarios, an increase in water temperature is added to each reservoir based on the average latitude-specific temperature increases predicted by Fekete et al. (2010).

All reservoirs are spatially routed to account for dams that occur longitudinally in series, and dams on tributaries as illustrated in Figure 5.2. The total influx (mol yr^{-1}) of allochthonous POC or DOC to a reservoir k is then given by:

$$F_{k,\text{in}} = \sum_1^n F_{k-1,\text{out}} + (W_k - \sum_1^n W_{k-1}) \times Y_k \qquad (5.10)$$

where $\sum_1^n F_{k-1,\text{out}}$ is the sum of the fluxes of allochthonous POC or DOC leaving all dams immediately upstream of reservoir k on tributaries 1 to n, W_k is the total upstream watershed area
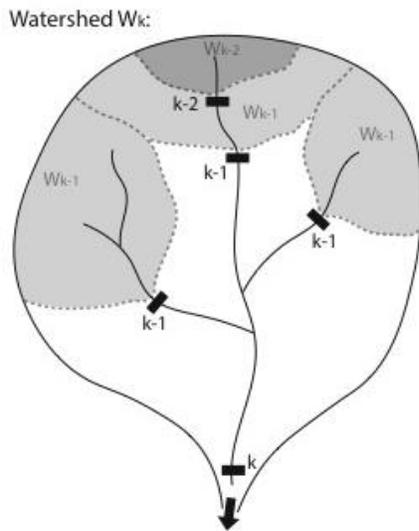
Figure 5.2: Schematic representation of the breakdown of a hypothetical watershed into the sub-watersheds that are hydrologically connected to the dam reservoirs in the watershed; k represents the most downstream dam, k-1 the next dam upstream, and so on. The corresponding sub-watershed for dam k is W_k, W_{k-1} for dam k-1, and so on. The figure helps explain the routing procedure described in Equation 5.10.

(km^2), $\sum_1^n W_{k-1}$ is the sum of the upstream watershed areas of dams *k-1*, and Y_k is the POC or DOC yield (mol km^{-2} yr^{-1}) in the undammed, $(W_k - \sum_1^n W_{k-1})$, watershed area downstream of dams *k-1*. In other words, the OC loads leaving all upstream reservoirs are added to the OC load entering the river from its undammed upstream watershed area.

In Global-NEWS, carbon and nutrient loads from landscapes to rivers are empirically adjusted to match the fluvial DOC and POC export fluxes measured at the mouths of large rivers. To reconcile my estimates of OC elimination in reservoirs with the observed OC export fluxes to the coastal ocean, the Global-NEWS allochthonous OC loads to rivers are recalibrated. As an initial hypothesis I impose the original Global-NEWS DOC and POC loads to calculate in-reservoir elimination fluxes and export fluxes to the coastal ocean. The loads are then iteratively adjusted until they reproduce the Global-NEWS coastal OC export fluxes for 1970 and 2000. For the 2030 and 2050 scenarios, which are based on projections rather than calibrated to data, I apply the same correction factor to any given watershed as that for 2000. On average, the revised OC loads to watersheds differ only by ±1.3% from the original Global-NEWS estimates.

The combined outputs of the MC analyses of reservoir OC and phosphorus models yield the following relationship between in-reservoir primary production, *P*, and the inflow flux of total dissolved phosphorus, TDP_{in} (mol yr^{-1}):

$$P = e^{10.5042 \pm 0.0939} TDP_{in}^{0.5938 \pm 0.0085} \quad (R^2 = 0.48) \tag{5.11}$$

where the uncertainty associated with each parameter corresponds to ± one standard deviation (see Model sensitivity and uncertainty). Equation 5.11 is then used in relationships of the form of Equations 5.8 and 5.9 to describe the fractions of in-reservoir produced autochthonous OC that are buried and mineralized:

$$F_{j,\text{bur}} = P \times a_j \left[1 - \frac{1}{1 + \alpha_j \times \tau_r} \right] \tag{5.12}$$

and

$$F_{j,\text{min}} = P \times b_j \left[1 - \frac{1}{1 + \beta_j \times T \times \tau_r} \right] \tag{5.13}$$

where the subscript *j* stands for burial and mineralization of autochthonous OC. The values of the parameters α_j, β_j, a_j and b_j are listed in Table AD1.

The initial amount of degradable soil and biomass OC flooded after closure of a dam, TOC_0, is estimated from global soil (Hiederer and Köchy, 2011) and biomass carbon (Ruesch and Gibbs, 2008) maps, scaled to the surface area of the reservoir. The decay of the flooded OC follows:

$$TOC(t) = TOC_0\, e^{-k_{\text{min,flood}}t} \tag{5.14}$$

where t is the number of years since dam closure. I assume the same temperature function (i.e., $\theta^{(T-20)}$) for $k_{\text{min,flood}}$ as in Equation 5.4 and adjust the pre-function coefficient k_{20} so as to reproduce the decay time scale of flooded soil organic matter typically observed after dam closure (10-15 years) (Barros et al., 2011; Teodoru et al., 2012). The resulting expression is then:

$$k_{\text{min,flood}} = 2.21 \times 1.07^{(T-20)} \tag{5.15}$$

The Strahler stream orders of the GRanD reservoirs (Table AD2) are estimated with the empirical scaling law relating stream order to catchment area derived by Lauerwald et al. (2015). This scaling law is derived from the HydroSHEDS stream network for 3rd order streams and higher (Lehner and Grill, 2013), and extrapolated for the two lowest stream orders that are not represented in HydroSHEDS (Lauerwald et al., 2015). To test the validity of the scaling law, I have compared calculated stream orders with actual stream orders from the HydroSHEDS stream network for all dammed streams and rivers in Europe (n=2192) and South America (n=1602), yielding statistically significant R^2 values of 0.90 and 0.87, respectively.

5.3.6 Model sensitivity and uncertainty

Sensitivity analyses are performed separately for in-reservoir allochthonous and autochthonous OC cycling. The effects on burial and mineralization fluxes of changing one parameter value at the time are summarized in Tables AD3 and AD4. In most cases, the parameter is varied ±10% from the assigned "default" value in 100 iterations, the results of which are compared to the burial and mineralization fluxes obtained using the default value. Reservoir volume and discharge (and hence water residence time) are varied according to the distributions in Table 5.1. Sensitivity to initial conditions is assessed by comparing the results of model runs with the initial reservoir DOC, POC and TOC masses set equal to either 0 or 1×10^6 mol. Two reservoir ages are tested: 10 and 40 years. Sensitivity to a 1°C increase in global air temperature is determined, which is equivalent to a water temperature increase of 0.82°C. Not surprisingly, allochthonous and autochthonous OC burial fluxes are most sensitive to the rate constant of burial k_{bur} while mineralization fluxes are most sensitive to

k_{20} and latitude, given the dependence of k_{min} on temperature, which is in turn related to latitude, and to a lesser degree, altitude (Tables AD3 and AD4).

A bootstrap analysis is used to estimate the uncertainties associated with primary productivity P calculated with Equation 5.11: sampling with replacement was conducted drawing 5000 samples from the 6000 model runs generated in the Monte Carlo (MC) analysis, and fitted to a power law as in Equation 5.11. After 5000 iterations, the bootstrap analysis yields the standard deviation estimates for each parameter in Equation 5.11. When scaled up globally, the uncertainty on P translates into uncertainties in the mineralization and burial fluxes of autochthonous OC of ±15%.

The total uncertainties in the global reservoir OC burial and mineralization are assessed as follows. Burial and mineralization fluxes predicted by the 6000 MC iterations are binned according to water residence times as shown in Figure AD2. Gamma functions are fitted to the distributions of fluxes in each bin. A second MC analysis is then carried out in which, for each GRanD reservoir, the burial and mineralization fluxes are randomly selected from the gamma functions. A total of 20 simulations yields ±8% standard deviation on the global OC fluxes for allochthonous DOC mineralization, ±15% for allochthonous POC mineralization, and ±12% for allochthonous burial. For autochthonous OC fluxes, this analysis yields ±2% and ±3% standard deviation for mineralization and burial fluxes, respectively. Combined with the ±15% error associated with the Global-NEWS OC loads to rivers, I estimate uncertainties on the order of ±23%, ±30%, and ±27%, for allochthonous DOC mineralization, and allochthonous POC mineralization and burial, respectively. For the global values of autochthonous OC burial and mineralization, I estimate an uncertainty on the global fluxes of ±32% for mineralization and ±33% for burial. The higher uncertainties for autochthonous OC reflect the uncertainty in estimates of P (see above). Note that the estimated uncertainties in the burial and mineralization fluxes are those associated with the mass balance modeling approach, and do not account for inaccuracies and omissions in the GRanD or future dam databases.

5.4 Results and Discussion

5.4.1 Organic carbon cycling in reservoirs

The results for 1970 and 2000 record the impacts of the first boom in dam construction that began after World War II (Vörösmarty and Sahagian, 2000). During the last three decades of the 20th Century, the number of dams increased by more than 70%, while the total reservoir storage volume increased from about 3500 to nearly 6200 km³. The global input of allochthonous OC to reservoirs

grew from 3.8 ± 0.6 Tmol yr^{-1} (46 Tg C yr^{-1}) in 1970 to 6.6 ± 1.0 Tmol yr^{-1} (79 Tg C yr^{-1}) in 2000 (Figure 5.3), because of the doubling of the catchment area upstream of dams combined with the rising anthropogenic OC loading to rivers. At the same time, in-reservoir production of autochthonous OC grew from 0.65 ± 0.20 to 1.2 ± 0.4 Tmol yr^{-1} (7.8 to 14.4 Tg C yr^{-1}). As expected, the larger supply of allochthonous OC and higher in-reservoir C fixation caused a significant increase in the amount of OC trapped behind dams: from 1.1 ± 0.3 Tmol yr^{-1} (13 Tg C yr^{-1}) buried in 1970 to 2.2 ± 0.6 Tmol yr^{-1} (26 Tg C yr^{-1}) in 2000. In contrast, the estimated global OC mineralization rates in 1970 and 2000 are nearly identical, around 2.5-3.0 Tmol yr^{-1} (30-36 Tg C yr^{-1}). The reason is that in 1970 over 70% of in-reservoir mineralization was associated with the respiration of flooded biomass and soil OC in recently impounded reservoirs. In the 1960s alone, 1405 GRanD dams were built worldwide (Lehner et al., 2011). However, because of the slow-down in dam construction toward the end of the 20th Century, with just 405 GRanD dams completed in the 1990s, flooded OC contributed only about 30% of reservoir mineralization in 2000.

The second boom in dam construction started shortly after the turn of the 21st Century (Zarfl et al., 2015). The new dams, however, tend to have shorter water residence times than those built in the last century because, for the majority of them, the primary purpose is hydropower production. Reservoirs of hydroelectric dams typically have smaller volumes and faster flows than the storage reservoirs of the 20th century. In 2000, the median water residence time of reservoirs was about 8 months, for post-2000 dams it is on the order of 1 month. Of the dams under construction or planned to be completed by 2030, 7% have water residence times under 5 days, compared with just 3% in 2000. As a result, mean OC burial and mineralization efficiencies are predicted to be lower for the post-2000 dam reservoirs. For instance, I estimate that, in 2000, 40 and 12% (0.48 ± 0.16 and 0.14 ± 0.04 Tmol yr^{-1} of 0.65 ± 0.20 Tmol yr^{-1}) of autochthonous OC produced in reservoirs were buried and mineralized, respectively, compared to 32 and 10% (0.98 ± 0.32 and 0.30 ± 0.10 Tmol yr^{-1} of 3.0 ± 0.60 Tmol yr^{-1}) predicted for 2030. In turn, this implies an increase in the fraction of autochthonous OC transferred downstream of dams, from 48% (0.58 ± 0.2 of 0.65 ± 0.20 Tmol yr^{-1}) in 2000 to 58% (1.7 ± 0.6 of 3.0 ± 0.6 Tmol yr^{-1}) in 2030. The relatively small changes in OC fluxes between 2030 and 2050 are a direct consequence of the assumption that damming stops after 2030. Although it is unlikely that damming activity will cease abruptly, a slowing down in dam construction can be expected by 2030, at which time fragmentation by dams will already affect more than 90% of the total river volume on Earth (Grill et al., 2015).
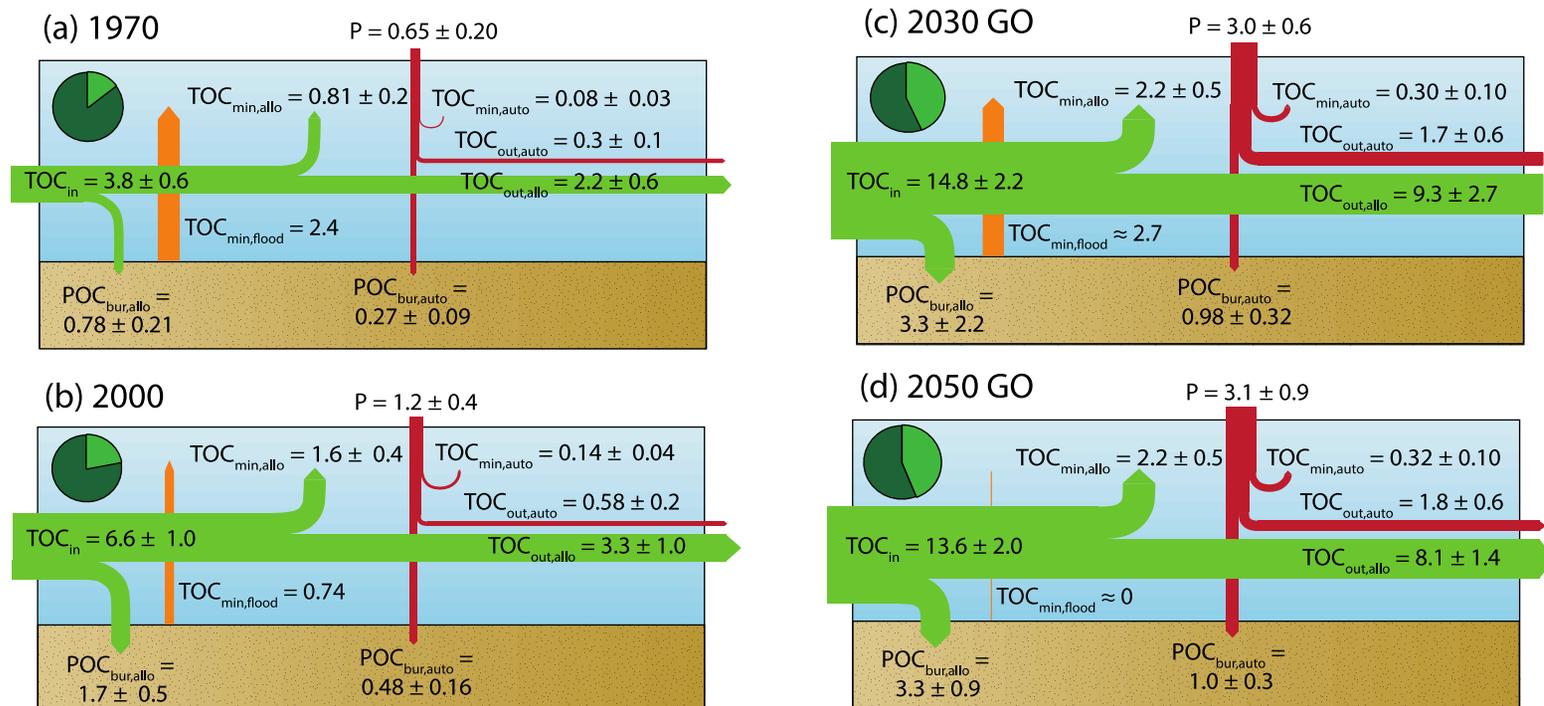
Figure 5.3: Globally integrated organic carbon (OC) budgets of reservoirs in 1970, 2000, 2030 and 2050 (Global Orchestration scenario). All fluxes are given in units of Tmol yr^{-1} and rounded to 2 significant digits. Fluxes shown are the aggregated values for reservoirs worldwide. TOC_{in}: global influx of particulate organic carbon (POC) plus dissolved organic carbon (DOC) to dam reservoirs (note: the routing procedure avoids double counting OC passing through cascades of dams, see Figure 5.2). *P*: primary production. TOC_{out}: global efflux of POC plus DOC exiting dam reservoirs, without double counting TOC that passes through multiple dams. Subscripts: *bur*: burial; *min*: mineralization; *flood*: flooded terrestrial biomass and soil organic carbon; *allo*: allochthonous; *auto*: autochthonous; *out*: outflow. Errors assigned to TOC_{in} reflect the uncertainties associated with the Global-NEWS model yield estimates. Other error estimates include those associated with the model parameterization, upscaling, and errors in Global-NEWS, see Methods. Pie charts in top left of each panel represent the proportion of POC plus DOC loaded to global rivers that passes through at least one dam (shown in light green) before reaching the coastal zone.

Table 5.2: Summary of fluxes predicted in the model, and relevant global damming parameters. Note that several database entries have been removed in this analysis. These include Canadian oil sands tailings dams, barrages or diversion canals with no proper reservoirs, including the Farakka Barrage on the Ganges, and the five planned dams in Chilean Patagonia that have been cancelled.

Flux (Tmol yr^{-1}) or parameter	1970	2000	2030 GO	2030 AM	2030 TG	2030 OS	2050 GO	2050 AM	2050 TG	2050 OS
POC export to coast	11	12	11	12	11	11	11	11	11	11
DOC export to coast	13	14	14	14	14	14	14	14	14	14
POC load to watersheds	12	14	15	16	15	15	15	15	15	15
DOC load to watersheds	14	16	17	17	17	17	17	17	17	17
POC load to reservoirs	1.4-1.5	2.5	5.4	5.5	5.5	5.5	6.0	6.0	5.4	5.5
DOC load to reservoirs	2.3-2.4	4.1	9.4	6.8	9.5	6.9	7.6	7.6	9.3	9.0
Number of dams	3987-4393	6846	10547	10547	10547	10547	10547	10547	10547	10547
Total reservoir volume (km^3)	3371-3573	6191	8503	8503	8503	8503	8503	8503	8503	8503
Dammed catchment area (10^7 km^2)	2.2– 2.4	3.5	4.7	4.7	4.7	4.7	4.7	4.7	4.7	4.7
Dammed % of total catchment area	17-18	27	36	36	36	36	36	36	36	36
Air temperature increase relative to year 2000	N/A	N/A	1.09	1.02	0.91	1.0	2.11	1.86	1.29	1.82
$POC_{bur,allo}$	0.75 – 0.81	1.7	3.3	3.5	3.4	3.4	3.3	3.3	3.2	3.4
$POC_{bur,auto}$	0.26-0.28	0.48	0.98	0.88	0.93	0.91	1.0	1.0	0.94	0.91
$POC_{bur,tot}$	1.0-1.1	2.2	4.3	4.4	4.3	4.3	4.3	4.3	4.1	4.3
$POC_{min,allo}$	0.08 – 0.09	0.27	0.37	0.39	0.37	0.38	0.40	0.38	0.36	0.40
$DOC_{min,allo}$	0.71 - 0.73	1.3	1.8	1.8	1.7	1.7	1.8	1.8	1.8	1.8
$TOC_{min,auto}$	0.08	0.14	0.30	0.26	0.29	0.27	0.32	0.32	0.30	0.29
$TOC_{min,flooded}$	2.4	0.74	2.7	2.7	2.7	2.7	0	0	0	0
$TOC_{min,tot}$	3.3	2.5	5.2	5.2	5.1	5.1	2.5	2.5	2.5	2.5
P	0.63-0.67	1.2	3.0	2.7	2.9	2.8	3.1	3.1	2.9	2.8
TOC load to watersheds + P	26-27	31	35	36	35	35	35	35	35	35
Total load eliminated	1.9-2.0	4.0	6.8	6.9	6.7	6.7	6.8	6.8	6.6	6.8
% eliminated	7	13	19	19	19	19	19	19	19	19

5.4.2 Production versus mineralization

During the 1970-2030 period, reservoirs remain globally net heterotrophic with OC mineralization (R) exceeding primary production (P) (Figure 5.3, Table 5.2). The global P/R ratio, however, is highly variable, with values ranging from 0.20 in 1970 to 0.58 in 2030. The low P/R value in 1970 reflects the large contribution to R of mineralization of flooded terrestrial OC behind recently completed dams. Because flooded OC degrades on relatively short timescales ($\leq$10 years), decreasing exponentially as the reservoir ages (Barros et al., 2011; Catalan et al., 2016), global reservoir P/R depends on the pace at which new dams are constructed. The 3763 dams currently under construction or planned to be completed within the next two decades are expected to flood 80 Tmol (960 Tg C) of degradable OC (see Section 5.3). The exact timing of the degradation of the flooded OC is difficult to predict as the completion dates for most of the new dams are uncertain (Zarfl et al., 2015). I estimate that on average roughly 2.7 Tmol (32 Tg C) of flooded OC will be mineralized annually over the 2000-2030 period. If, as assumed in the 2050 projection, new dam construction becomes negligible after 2030, the mineralization of flooded OC will slow down rapidly, and the global reservoir P/R ratio could climb to values exceeding 1, reaching 1.24 in 2050. That is, reservoirs could become net autotrophic.

While mineralization of flooded OC has the greatest impact on the trophic state of a reservoir in the years following dam closure, mineralization of OC derived from the upstream catchment and that of OC produced in situ continue over the lifetime of the reservoir. On a global scale, mineralization of allochthonous OC exceeds that of autochthonous OC by a factor of 7-11, because the input of allochthonous OC is much greater than in-reservoir photosynthetic carbon fixation. Global reservoir OC mineralization, however, is primarily driven by the world's larger reservoirs that are usually associated with higher stream orders, i.e. with the larger rivers that receive the flow from many tributaries (Figure 5.4). In fact, my model predicts that, on average, for Strahler stream orders smaller than 5, in-reservoir productivity sustained by anthropogenic phosphorus loading exceeds mineralization, i.e., P/R>1.

The predicted net mineralization fluxes of reservoirs (i.e., $R - P$) can be compared to reported carbon evasion rates, as the latter are primarily driven by in-reservoir OC mineralization. Barros et al. (2011) estimate that reservoirs annually emit 4.2 Tmol of carbon to the atmosphere (51 Tg yr^{-1}). Regnier et al. (2013) propose a CO_2 evasion of 26 Tmol yr^{-1} (320 Tg C yr^{-1}) for lakes and reservoirs combined. Correcting the latter value using a regionalized lake to reservoir surface area ratio
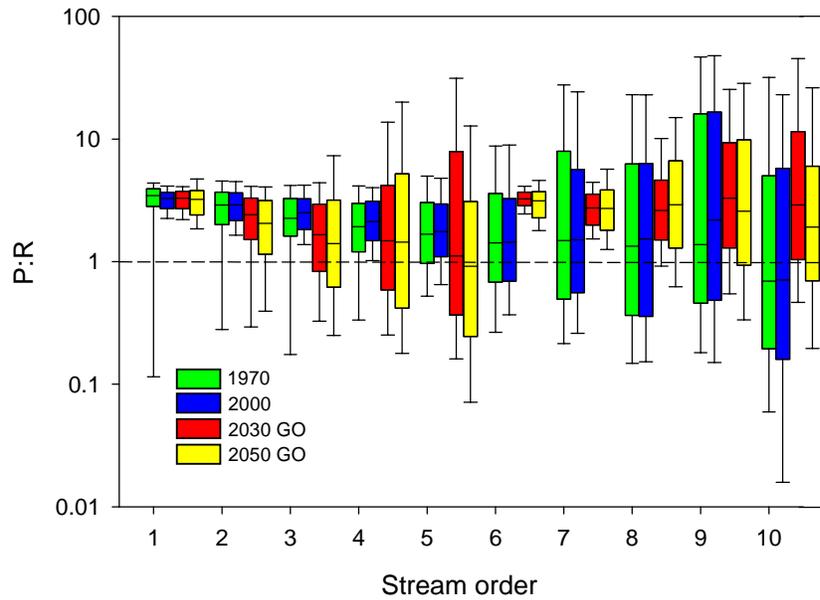
Figure 5.4: Distributions of P:R ratios of reservoirs included in the GRanD and Zarfl et al.'s (2015) databases as a function of Strahler stream order, for 1970, 2000, 2030 (GO scenario), and 2050 (GO scenario). Solid lines represent median values, box edges represent 1 standard deviation and whiskers represent 1st and 3rd quartile. For clarity, outliers have been removed.

(Lehner and Döll, 2004) then yields a global evasion flux from reservoirs alone of 3.3 Tmol yr-1 (40 Tg C yr^{-1}). These CO_2 evasion fluxes are of the same order of magnitude as my net mineralization fluxes for the period 1970-2000 (1.3-2.6 Tmol yr^{-1} or 16-32 Tg yr^{-1}). The CO_2 evasion flux from reservoirs of St Louis et al. (2000) is much larger: 23 Tmol yr^{-1} (280 Tg C yr^{-1}). Their estimate, however, is based on a limited set of CO_2 evasion rates that are scaled to a total reservoir surface area of 1.5 million km², that is, more than three times the surface area of the GRanD reservoirs.

5.4.3 Organic carbon burial

Around 75% of OC accumulating in reservoir sediments is allochthonous. Reservoirs along large, higher-order rivers are preferential sites of OC accumulation: I estimate that more than half of OC burial takes place in reservoirs on 8th order or higher rivers, although they only represent about 10% of all reservoirs worldwide (Figure 5.5). These reservoirs tend to intercept the rivers carrying the highest OC loads. Globally, OC burial in reservoirs is expected to reach 4.3 ± 1.2 Tmol yr^{-1} (52 Tg C yr^{-1}) by 2030, that is, a 4-fold increase relative to 1970 (Figure 5.3). The increase in OC burial correlates with the growing number of dams and, to a lesser extent, the increasing OC loading to rivers. The latter primarily reflects changes in land use and land cover that cause increased soil erosion (Regnier et al., 2013).

The predicted global net mineralization to burial ratio for reservoirs in 2000 is 1.1, which is comparable to the value of 1.5 of Cole et al. (2007) for inland waters. Nonetheless, my global reservoir OC burial fluxes tend to fall below previously published values. For example, Mulholland and Elwood (1982) estimate that reservoirs globally accumulate 17 Tmol yr^{-1} of OC (200 Tg C yr^{-1}) using burial rates from Europe and North America, Dean and Gorham (1998) obtain a value of 13 Tmol yr^{-1} (160 Tg C yr^{-1}) by extrapolating average values of sedimentation rate, OC concentration and bulk density to the global reservoir surface area, while the similarly large estimate of Stallard (1998) of 24 Tmol yr^{-1} (290 Tg C yr^{-1}) is calibrated using parameters from reservoirs in the United States. The discrepancy is likely due to two reasons. First, my fluxes only account for reservoirs in the GRanD (Lehner et al., 2011) and Zarfl et al. (2015) data bases and, hence, ignore the contributions of the large number of small reservoirs. Second, the earlier estimates rely on empirical extrapolations from data on small numbers of reservoirs with uneven geographical coverage, mostly concentrated in temperate climate zones (Mulholland and Elwood, 1982; Pacala et al., 2007). As a result they probably over-predict burial OC rates, because they do not account for the high mineralization rates in the tropics. Further note that the C burial rate of 1-3 Pg C yr^{-1} (83 – 250 Tmol yr^{-1}) for reservoirs
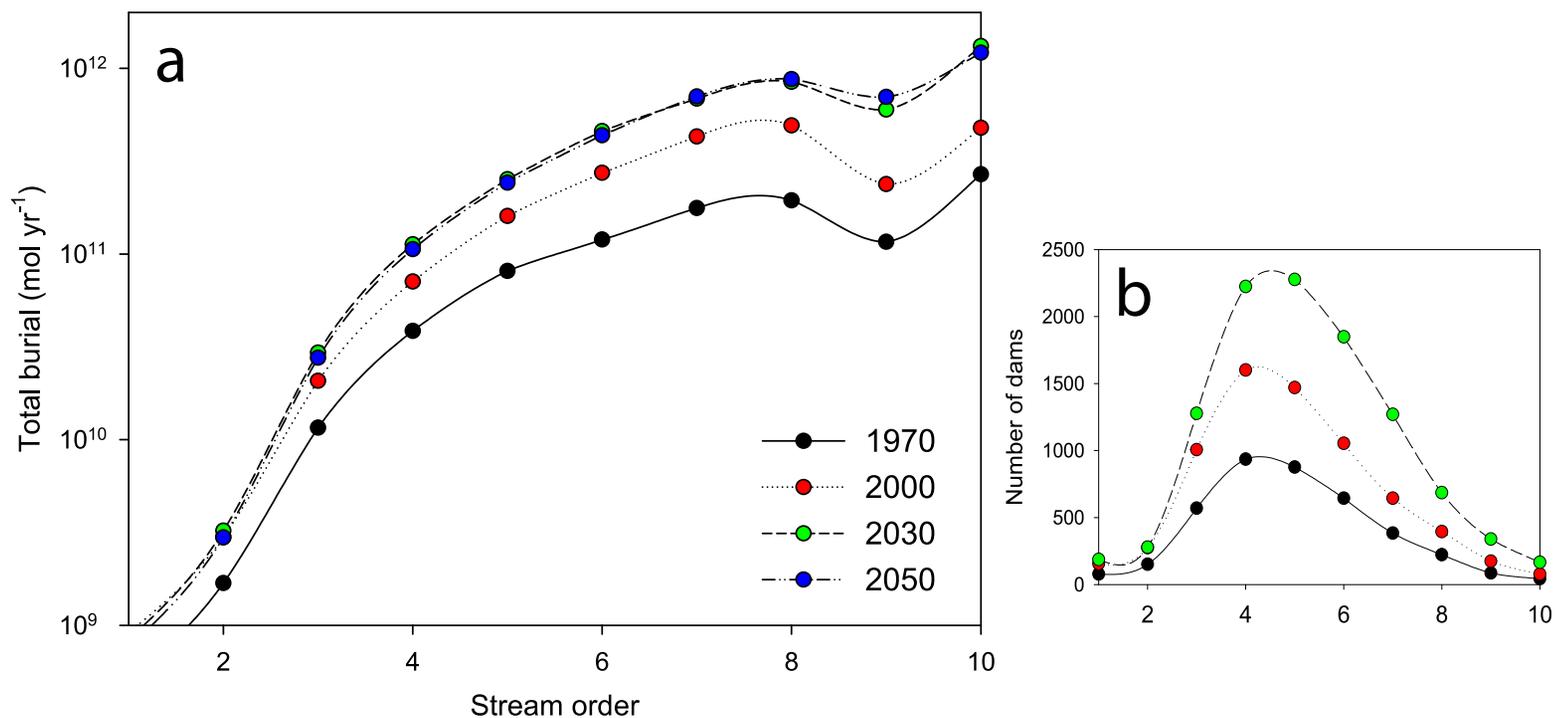
Figure 5.5: (a) Global OC burial (autochthonous + allochthonous) in dam reservoirs as a function of Strahler stream order. The 2030 and 2050 OC burial estimates correspond to the Global Orchestration (GO) Millennium Assessment (MA) scenario. (b) Distribution of dams according to the Strahler stream order on which they are located. Note that the number of dams in 2050 is assumed to be equal to that in 2030. See Table AD2 for the assignment of Strahler stream orders.

reported by Syvitski et al. (2005) includes inorganic carbon, while my estimates only account for OC burial.

5.4.4 Regional hotspots

From 1970 to 2000, reservoirs in the Mississippi, Niger, and Ganges River basins buried most OC (Figure 5.6): together, they accounted for 31 and 25% of global OC burial by dams in 1970 and 2000, respectively (Supplementary Data 1). In 1970, the highest in-reservoir OC elimination occurred in the Mississippi River basin, where 192 Gmol of OC (2.3 Tg C yr^{-1}) were buried and 305 Gmol (3.7 Tg C yr^{-1}) mineralized annually. By 2000, OC mineralization in reservoirs of the Paraná and Zambezi River basins overtook the Mississippi River basin. The estimated 631 Gmol yr^{-1} (7.6 Tg C yr^{-1}) mineralized in 70 dam reservoirs along the Paraná River and its tributaries in year 2000 reflect degradation of flooded material following construction of new dams at the end of the 20th century, including the 11 km long Eng Sérgio Motta Dam. The high mineralization in the Zambezi basin is due in large part to Lake Kariba, the world's largest reservoir by volume. Other hotspots of reservoir OC burial include the basins of the Danube in Europe, the Ganges and Mekong in central and Southeast Asia, the Yenisei in Russia, the large Chinese rivers, and the Tocantins in South America. The OC burial hotspots generally coincide with OC mineralization hotspots (Figure 5.6). One notable exception is the Mackenzie River basin where in 1970 relatively low OC burial fluxes coexisted with high OC mineralization rates. The latter are explained by the large pulse in mineralization of flooded soil OC and biomass in Williston Lake, the seventh largest reservoir globally by volume, following completion of the W.A.C. Bennett Dam in 1968.

Damming is increasingly focused in river catchments of Asia, South America, Africa and the Balkans (Figure 5.7). The Amazon, Yangtze and Ganges basins are expected to remain the primary hotspots for reservoir OC burial and mineralization. In the Amazon basin, with the planned completion of 184 new dams by 2030, OC burial will increase 38-fold to 290 Gmol yr^{-1} (3.5 Tg C yr^{-1}), or 7% of global reservoir OC accumulation. For the Yangtze River basin, the estimated 2030 reservoir OC burial and mineralization fluxes are 172 and 152 Gmol yr^{-1} (2.1 and 1.8 Tg C yr^{-1}). The corresponding total OC removal by reservoirs (172 + 152 = 324 Gmol yr^{-1}) agrees well with the reduction in riverine OC flux since the 1950s of 408 ± 158 Gmol yr^{-1}, derived independently by Li et al. (2015) using sediment core data from the lower reaches of the Yangtze River. These authors ascribe the drop in OC flux to the construction of dams in the Yangtze River basin, which started in the 1950s. Note that I use my estimate for 2030 rather than 2000, in order to account for the very large dams built after 2000, including the Three Gorges Reservoir dam.
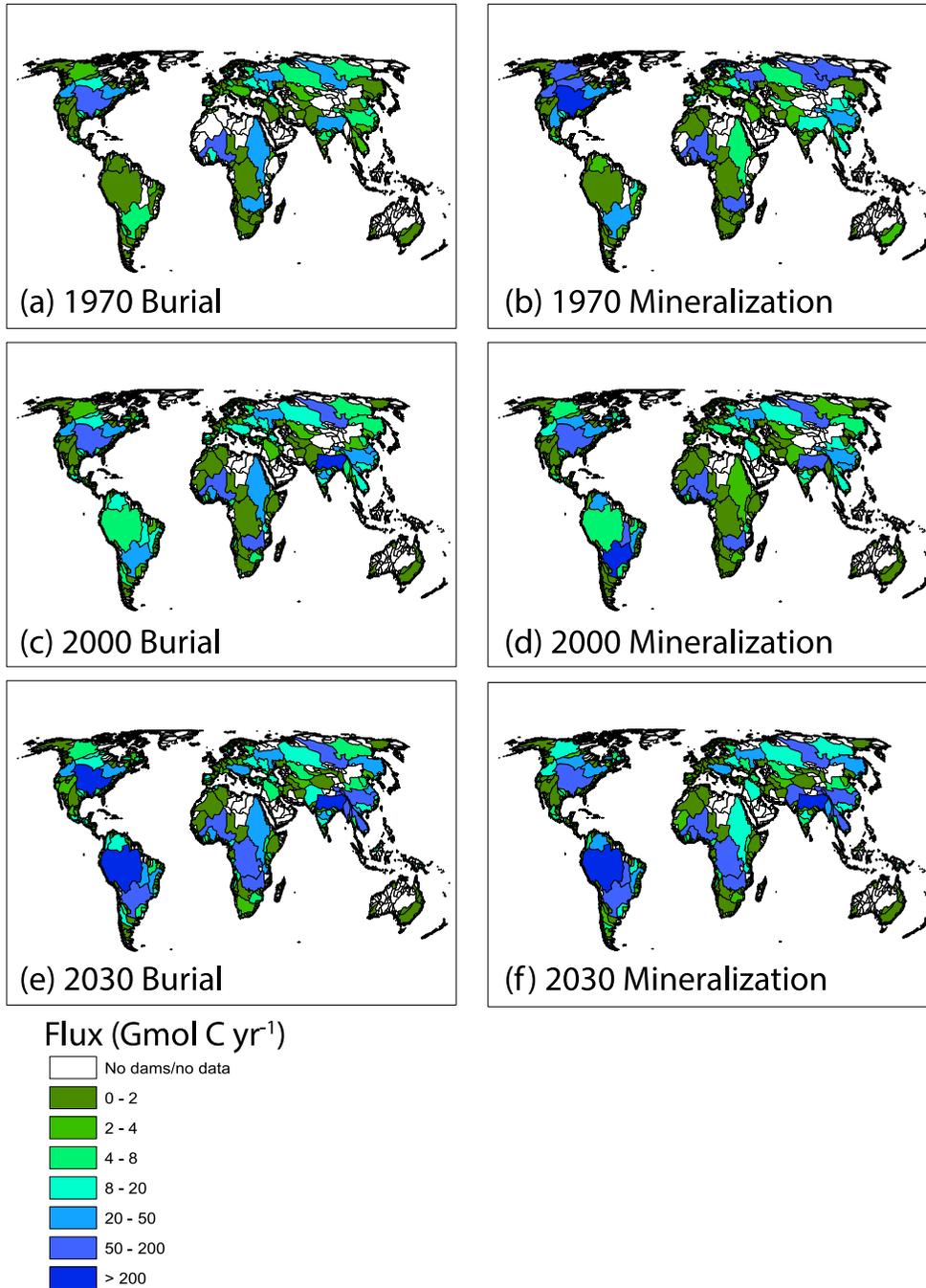
Figure 5.6: Mineralization and burial fluxes of OC in reservoirs of the main river basins of the world, for 1970 (a and b), 2000 (c and d), and 2030 GO scenario (e and f), in units of Gmol yr^{-1}. To estimate the 2030 mineralization fluxes of flooded OC for dams without defined completion dates or completion dates that can be estimated based on start dates (n = 2925), I randomly assigned completion dates to evenly space dam closures over time between 2000 and 2030. The uncertainty associated with this procedure does not substantially affect the 2030 spatial trends.
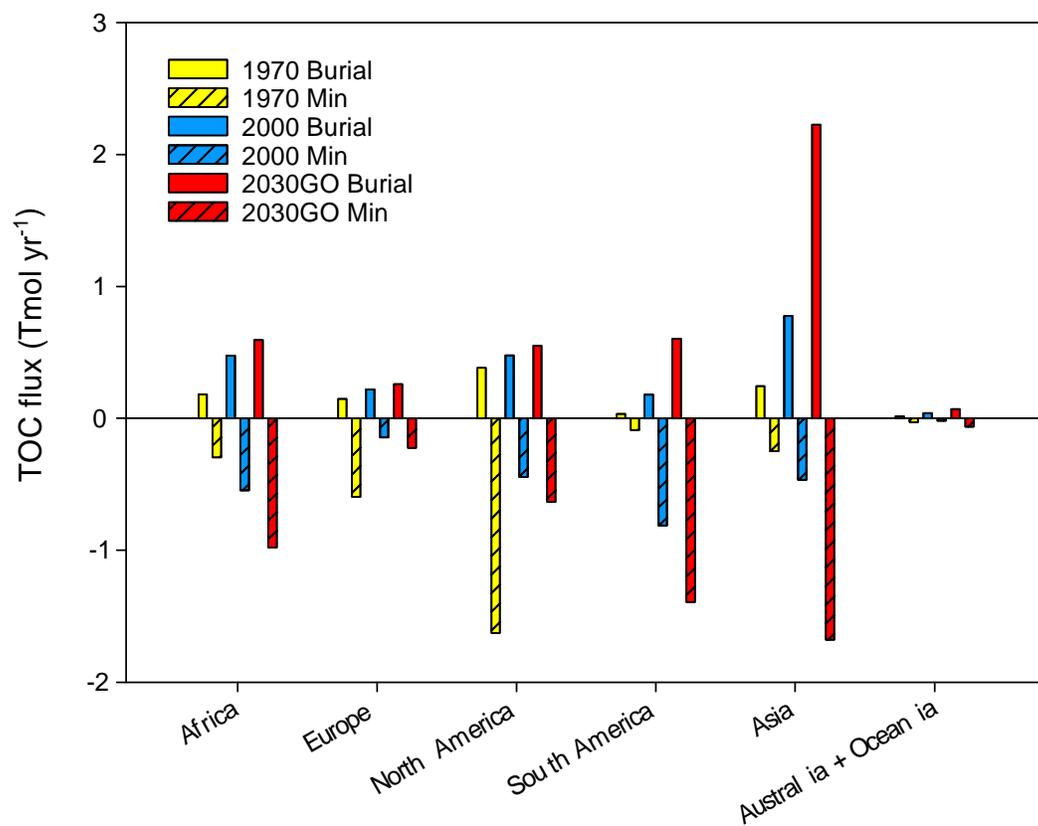
Figure 5.7: Global OC burial and mineralization in reservoirs, for 1970, 2000, and 2030 (GO scenario). Mineralization fluxes are shown as negative values for clarity.

The Congo (Zaire) basin may experience a major surge in dam construction over the next 20-30 years. Of the 15 new dams planned or under construction, the most notable is the proposed Grand Inga Dam, which could surpass the Three Gorges Dam in terms of hydroelectric generating capacity. When built, the new reservoirs in the Congo basin would collectively bury and mineralize on the order of 68 and 113 Gmol yr^{-1} (0.82 and 1.4 Tg C yr^{-1}), respectively. New dams in the basins of the Mekong, Paraná, Salween and Tocantins rivers are also predicted to contribute substantially to reservoir OC respiration in 2030, largely as a result of the degradation of recently flooded soil and biomass OC (Figure 5.6, Supplementary Data 1). Increases to OC mineralization fluxes in tropical reservoirs are also expected between 2000 and 2030 due to warmer water temperatures, particularly in the 0-10°S latitude band (Figure AD3).

Most existing regional carbon flux estimations for inland water bodies do not separate dam reservoirs from lakes. Hence, the corresponding fluxes provide upper limits that I can compare with my values for reservoirs alone. For instance, the U.S. Climate Change Science Program (Pacala et al., 2007) estimate that inland waters in North America buried 1.9 Tmol yr^{-1} (23 Tg C yr^{-1}) in 2003. As expected, my reservoir-only OC burial flux for North America in 2000 is smaller, on the order of 0.3 Tmol yr^{-1}. Similarly, in Russia, where reservoirs make up around 12% of the total inland water surface area (Lauerwald et al., 2015; Lehner and Döll, 2004), my estimate of in-reservoir net mineralization represents about 13% of the value of 0.98 Tmol yr^{-1} (12 Tg C yr^{-1}) reported by Dolman et al. (2012) for all Russian inland waters together.

5.4.5 Organic carbon export to the global coastal zone

Dam reservoirs modify the riverine export of OC to the coastal ocean: primary production adds new OC to the river system, while burial and mineralization eliminate OC. At the global scale, dams represent a net sink for riverine OC, as burial and mineralization of allochthonous and autochthonous OC together exceed in-reservoir production for the entire 1970-2050 period. The evolution over time of the global reservoir OC sink is closely related to the changing fraction of the world's river catchment area located upstream of dams: 18% in 1970, 27% in 2000, and 36% in 2030 and 2050 (Table 5.2), which in turn determines the proportion of the global OC load that enters dam reservoirs (Figure 5.1). As more and more catchment area leads into dam reservoirs, an increasing proportion of riverine OC is eliminated. In particular, the larger dams in lowland areas near the coast have the greatest potential to eliminate OC as they intercept the loads generated throughout the catchment. These dams thus play a disproportionate role in OC burial and mineralization along the aquatic continuum.

According to my calculations, in 2000, dams lowered the OC export to the global coastal zone via rivers by 13%: 7% through sequestration of OC in reservoir sediments and 6% through in-reservoir mineralization (Table 5.2). For comparison, for the same period, dams decreased riverine export of reactive silicon and phosphorus by only 5 and 12%, respectively (Maavara et al., 2014; Maavara et al., 2015b). All other factors equal, by eliminating OC more efficiently than nutrients, river damming should enhance carbon fixation over mineralization in the receiving waters. With the ongoing rise in the number of dams, riverine OC export in 2030 could be 19% lower than if no new dams were built after 2000 (12% due to burial and 7% to mineralization). Therefore, in all but one of the MA scenarios, the current boom in dam construction could even cause a net decrease in OC export to the coastal zone between 2000 and 2030, despite the increased anthropogenic loading of OC to watersheds (Table 5.2). Through its large impact on the delivery of riverine OC, damming therefore represents a major anthropogenic forcing on the trophic conditions and carbon balance of the coastal ocean.

Chapter 6

River damming: Driver or inhibitor of coastal Si limitation?

6.1 Summary

In this chapter I calculate the dam-driven changes to N:P:Si ratios delivered from rivers to coastal zones worldwide, for year 1970, 2000 and 2050. To differentiate between the temporal changes from anthropogenic nutrient loading and river damming, I compared results from scenarios with dams and scenarios in which all dams are removed from the river network. In general, P is eliminated most efficiently from the water column, followed by Si, followed by N. Trends in anthropogenic nutrient loading suggest that N:P ratios are decreasing over time. Damming therefore mitigates the consequential increase in N-limitation, to some extent. Results further indicate that in P-limited rivers, damming serves to protect against Si-limitation via preferential elimination of P. This was the dominant situation in year 2000. By 2050, when N-limitation will increase in prominence, the subsequent occurrence of Si-limitation will increase, due to preferential elimination of Si from N in dam reservoirs.

6.2 Coastal nutrient ratios

Human nutrient enrichment of rivers represents a global threat to coastal ecosystems (Anderson et al., 2008; Anderson et al., 2002; Cloern, 2001). Increased anthropogenic loadings of the nutrient elements phosphorus (P) and nitrogen (N) are causing severe coastal eutrophication worldwide (Nixon, 1995). Changes in the relative loadings of nutrients may further greatly alter the structure of coastal ecosystems. For example, when the availability of P and N increases relative to that of nutrient silicon (Si), coastal diatom communities, which rely on the supply of riverine Si for growth (Billen and Garnier, 2007; Officer and Ryther, 1980), may be out-competed by non-siliceous plankton, including dinoflagellates and cyanobacteria, hence promoting the incidence of harmful algal blooms (Billen et al., 1991; Garnier et al., 2010).

Another major human perturbation of river systems is damming. We are now in the midst of the largest boom in dam construction since the decades following the Second World War (Lehner et al., 2011; Zarfl et al., 2015). Efforts to catalogue ongoing dam building estimate that approximately 3700 hydroelectric dams with generating capacities of 1 MW or greater are currently under construction or planned to be completed by 2030, effectively doubling the number of hydroelectric dams in this category (Grill et al., 2015; Zarfl et al., 2015). By 2030 up to 93% of rivers on Earth will be fragmented by dams (Grill et al., 2015). Damming modifies nutrient fluxes along the river continuum (Friedl and Wüest, 2002). For instance, burial of reactive Si in sediments accumulating within reservoirs may exacerbate Si limitation in downstream water bodies (Humborg et al., 2000; Humborg et al., 1997; Ittekkot et al., 2000). In

contrast to P and N, which have large anthropogenic sources, the supply of Si to rivers depends primarily on slow, natural rock weathering processes (Struyf et al., 2009; Turner et al., 2003).

In Chapter 3 and 4 I quantified the impacts of river damming on the fluxes of nutrient P and Si delivered to the coastal zones, and a concurrent study has quantified the impacts of damming on N fluxes (Akbarzadeh et al., in preparation for submission to PNAS; Maavara et al., 2014; Maavara et al., 2015b). According to these studies, dams on average reduce the riverine fluxes of reactive Si (RSi = dissolved Si + reactive particulate Si), reactive P (RP = total dissolved P + reactive particulate P), and total N (TN) by 21, 43 and 12%, respectively. Similar preferential elimination of P over Si, and of Si over N, has been reported for individual reservoirs (Bartoszek and Koszelnik, 2016; Donald et al., 2015; Garnier et al., 1999; Grantz et al., 2014; Maavara et al., 2015a). Damming alone would thus increase the N:P and N:Si ratios delivered to the world's coastal zones. Primary productivity in unperturbed coastal environments tends to be N limited, that is, the availability of N, rather than P or Si, controls the extent of algal growth (Howarth and Marino, 2006). The changes in relative riverine nutrient supplies due to damming therefore have the potential to reduce N limitation of coastal productivity.

In this study, I analyze how anthropogenic nutrient enrichment and damming are changing TN:RP:RSi ratios exported from watersheds to the coastal zone. In particular, I examine the hypothesis that nutrient processing in reservoirs may increase N:P and N:Si in river water discharged to coasts. To this end, I calculate spatially explicit TN:RP:RSi ratios of river water reaching the land-ocean interface and compare those to the Redfield-Brzezinski molar ratios (C:N:P:Si = 106:15:1:20), which describe nutrient uptake by marine phytoplankton (Brzezinski, 1985; Conley et al., 1989; Redfield, 1934). The nutrient species included in my ratios include species that are bioavailable or can easily become bioavailable to coastal phytoplankton communities. Previous global analyses of ratios in river discharge delivered to the coastal zone use ratios of dissolved Si (DSi) to total P (TP) to TN loads (Garnier et al., 2010). This approach compares species of vastly different reactivities (e.g. highly bioavailable DSi with unreactive detrital mineral P), and excludes reactive pools like reactive particulate Si. The effects of damming on individual riverine nutrient fluxes are derived from single-element (P, N, and Si) models presented in Chapters 3 and 4 (Akbarzadeh et al., in preparation for submission to PNAS; Maavara et al., 2014; Maavara et al., 2015b). I perform the calculations for the years 1970, 2000 and 2050 using existing and planned dams that are included in available databases (Lehner et al., 2011; Zarfl et al., 2015). To distinguish between the effects of river damming and changing

anthropogenic nutrient loads on N:P:Si ratios, I examine hypothetical scenarios in which dams are removed or nutrient loads kept constant.

The results show that damming does decrease the prevalence of N-limitation in river water delivered to coastal zones, relative to undammed conditions (Table 6.1). For year 2000, results show that 32,000 km^3 yr^{-1} of river discharge, or 90% of the 35,800 km^3 yr^{-1} estimated global discharge, is more P-limited in the scenario with damming than in the scenario where dams are excluded, due to preferential elimination of P over N in reservoirs. Despite the widespread shift towards P-limitation, the presence of dams causes only 123 km^3 yr^{-1} (0.35%) of river discharge to coasts to cross the 16:1 N:P threshold from N-limitation into P-limitation. With dams, 861 km^3 yr^{-1} (2.4%) of coastal zones receive N-limited water, without dams, 985 km^3 yr^{-1} (2.8%).

The temporal changes indicate that anthropogenic nutrient emissions and river damming have opposite effects on N:P ratios delivered to coastal zones: nutrient emissions are driving N:P ratios down, while damming drives these ratios up. The extent of the modulating effect of damming on N:P ratios is dependent on the number of dams worldwide, and thus increases over time (Figure 6.1). Our estimations project that in 2050, 2760 km^3 yr^{-1} (8%) river discharge to coastal zones receive N-limited water, compared with 4980 km^3 yr^{-1} (14%) in the no-dam scenario. The higher year 2050 no-dam prominence of N-limitation than in year 2000 indicates that the overall anthropogenic emissions of TN are increasing at a greater rate than RP. The dam-driven rise in N:P modulates, to some extent, the decreasing N:P caused by disproportionate increases in P emissions, resulting in only a small increase in the global proportion of coastal zones receiving N-limited discharge between 2000 and 2050 (Figure 6.1). The global N:P ratio of rivers discharging to the coasts is 16 in year 2050, or at the threshold for N-limitation. Without dams, this ratio would be 13, clearly N-limited.

The concurrent effects of anthropogenic nutrient emissions and river damming on N:P ratios play a critical role in determining whether coastal river discharge will additionally become Si-limited. Coastal zones receiving river water with N:P ratios greater than 16 (P-limited) generally tend to be "protected" from Si-limitation by river damming, because of preferential retention of P over Si in reservoirs, which drives Si:P ratios up. This is evident in the year 2000 P-limited discharge, where more discharge is also Si-limited in the no-dams scenario than in the scenario with dams. On the other hand, coastal zones receiving river water with N:P ratios below 16 (N-limited) have a tendency to shift towards Si-limitation, as reservoirs eliminate N less efficiently than Si under most conditions, thus driving Si:N ratios down. In year 2000, when P-limitation is predominant in coastal discharge, damming drives a shift towards Si-limitation in only 2380 km^3

Table 6.1: Magnitude of discharge (km^3 yr^{-1}), classified based on nutrient limitation, in scenarios with and without dams included, for year 2000 and 2050.

Year, scenario	P+Si limited	P limited, Si non-limited	N+Si limited	N limited, Si non-limited
2000, no dams	1860	32,520	720	260
2000, dams	1590	32,610	720	140
2050, TG no dams	1490	28,560	260	4720
2050, TG dams	1750	30,520	760	2000

yr^{-1} (7%) of coastal discharge, usually corresponding to regions with TN:RP < 16, compared with a shift away from Si-limitation in 30,210 km^3 yr^{-1} (85%) of coastal discharge, usually corresponding to regions with TN:RP > 16. Of the N-limited discharge, 84% is also Si-limited, compared with only 5% of the P-limited discharge (Table 6.1). These data suggest that in year 2000, damming may have served to mitigate Si-limited coastal eutrophication in the majority of the world's coastal zones.

The ability for damming to protect coastal discharge from Si-limitation depends on the TN:RP ratios in the river water reaching the coasts. In year 2000, rivers were predominantly P-limited and thus protected from Si-limitation via preferential reservoir elimination of P over Si. As ongoing anthropogenic nutrient emissions drive TN:RP ratios down, ongoing damming will cause a shift towards Si-limitation of river waters exported to the coastal zone (Table 6.1). By 2050, damming will drive a shift towards Si-limitation in 21,110 km^3 yr^{-1} (60%) of coastal discharge, compared with no-dam scenarios. Compared with year 2000, an additional 201 km^3 yr^{-1} discharge will become Si-limited by 2050, largely as a result of the shift towards N-limitation (Table 6.1). Relative to the 2050 no-dam scenario, a total of 760 km^3 yr^{-1} discharge becomes Si-limited, 66% of which is also N-limited. It is also worth noting that the P-limited rivers no longer act as protectors from Si-limitation, with an increase in Si and P limited discharge in the scenario with dams compared with the scenario without. This difference arises due to rising P loads to rivers, compared with relatively constant Si loads; though Si is removed less effectively from the water column by dams, P concentrations are sufficiently high that even modest removal of Si by dams is sufficient to push the Si:P ratio across the threshold into Si limitation. The coastal shift towards Si-limitation in year 2050 will take place primarily in China, Southeast Asia, South America and Africa (Figure 6.2), where there is a concurrent increase in anthropogenic nutrient loading, primarily in the form of P, as well as dam construction.

Previous research has hypothesized that damming promotes Si-limitation in coastal zones due to rising anthropogenic P and N emissions, combined with Si retention in reservoirs (Garnier et al., 2010; Humborg et al., 2006; Humborg et al., 2008). Here I show that dam-driven Si-limitation in coastal river discharge typically develops in river systems that are N-limited, due to preferential elimination of reactive Si over N in reservoirs. For P-limited river waters, the preferred P elimination in reservoirs serves to protect coastal systems from Si-limitation. Global river discharge was overwhelmingly P-limited in year 2000 and damming was thus a mitigating factor with regard to coastal Si-limitation. I further propose that anthropogenic nutrient emissions
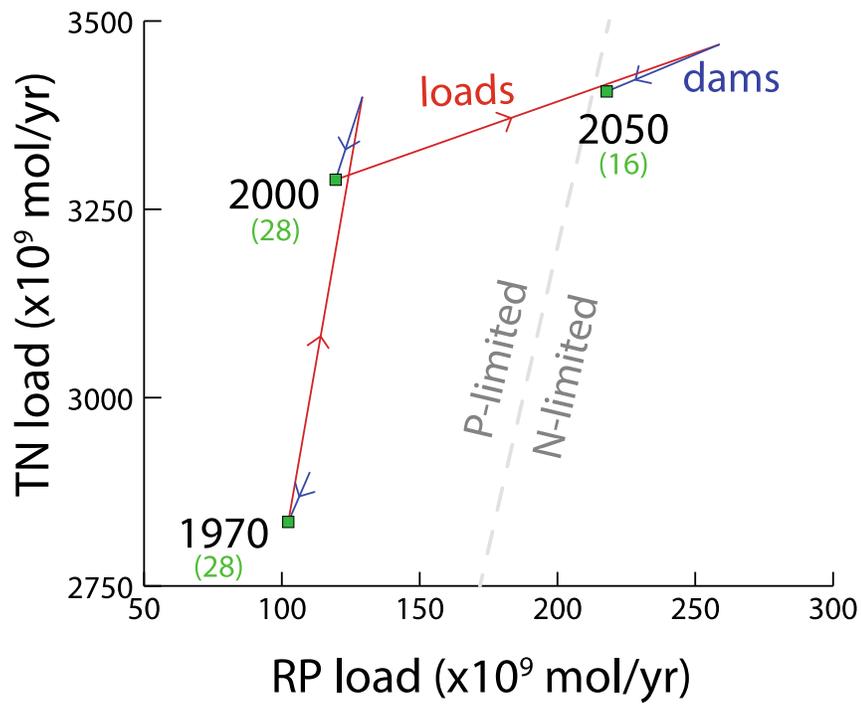
Figure 6.1: RP and TN load changes over time, broken down into the load to rivers (red) and the removal by damming (blue). Green numbers in brackets indicate the TN:RP ratio at each time point. 16:1 P:N limitation threshold is shown as grey dashed line.

are currently decreasing riverine N:P ratios worldwide, this is, disproportionately rising P loads are causing a shift of river discharge towards N-limitation, which in turn implies that dams may be shifting from being protectors of coastal Si-limitation, to drivers of coastal Si-limitation. Nutrient management strategies in heavily dammed watersheds that focus on reducing N loads without considering P loads may therefore inadvertently exacerbate the potential for coastal Si limitation.
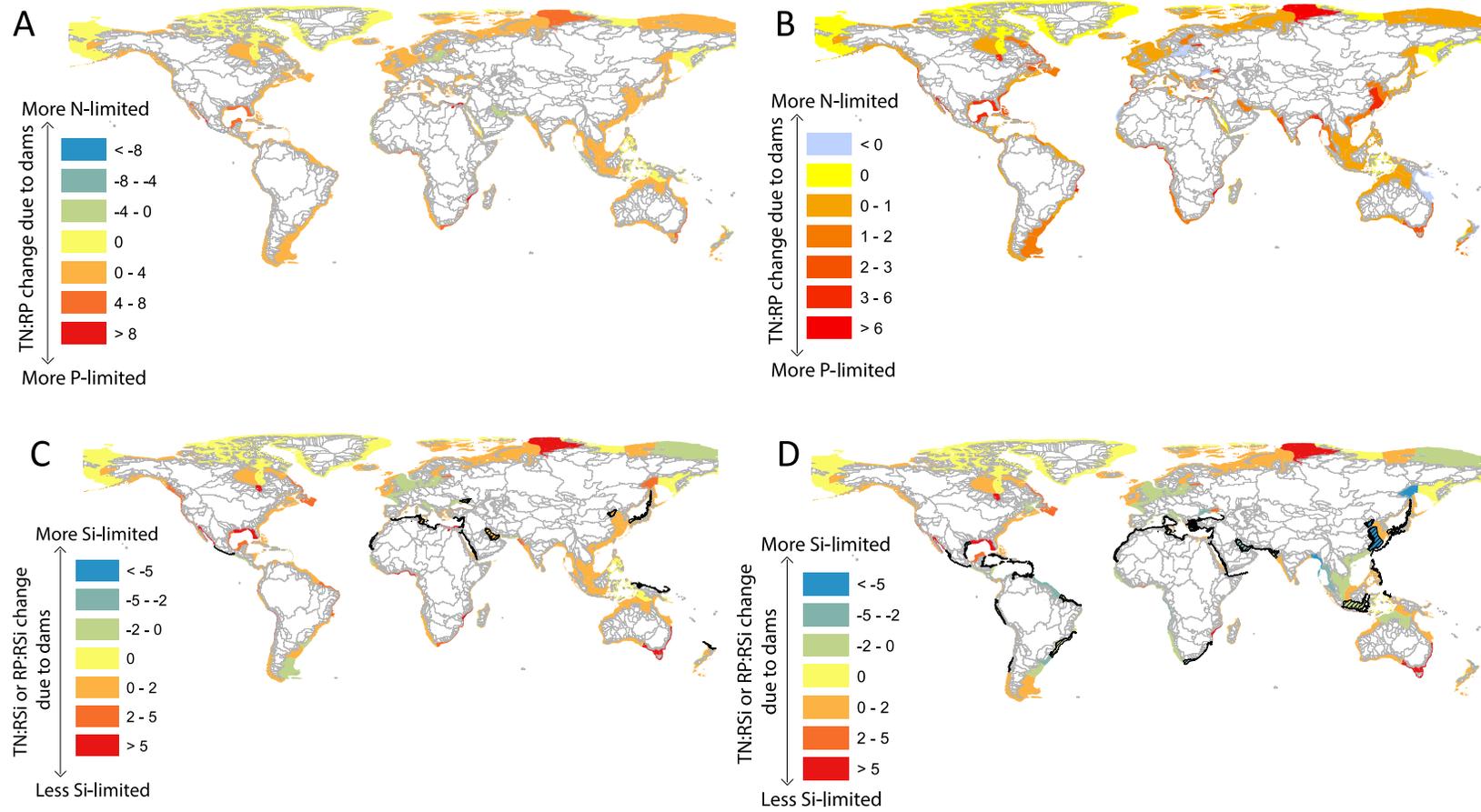
Figure 6.2: Changes in TN:RP ratios (A and B) when dams are introduced, compared with no-dam scenarios, for year 2000 (A) and 2050 (B); and changes in TN:RSi or RP:RSi ratios (C and D) when dams are introduced, compared with no-dam scenarios, for year 2000 (C) and 2050 (B). In C and D, N-limited regions are indicated with a black outline and diagonal lines.

6.3 Methods

Reservoir nutrient elimination, R_X, is defined as:

$$R_X = \frac{X_{in} - X_{out}}{X_{in}} \times 100\% \qquad\qquad\qquad (6.1)$$

where X_{in} is the flux of nutrient X delivered to the reservoir via the river inflow (mol yr^{-1}) and X_{out} is the flux of nutrient X exiting the reservoir via the dam(s) (mol yr^{-1}). In the case of N, fixation results on average in an additional 10% increase in TN delivered to a given reservoir (Akbarzadeh et al., in preparation), which is largely responsible for the comparatively low R_N calculated with Equation 6.1. Fixation is not included within X_{in} because I quantify the overall change to riverine N fluxes from damming; for an in-depth analysis of the importance of reservoir fixation within the context of the global N cycle, refer to Akbarzadeh et al. (in preparation for submission to PNAS).

Riverine TN, RP and RSi loads (mol yr^{-1}) to coastal zones were calculated by subtracting total watershed-specific reservoir elimination, predicted in Chapters 3 and 4 (Maavara et al., 2014; Maavara et al., 2015b) and in Akbarzadeh et al. (in preparation for submission to PNAS), from no-dam loads to coastal zones predicted by the Global-NEWS model (Mayorga et al., 2010). No-dam loads to coastal zones were calculated using the Global-NEWS model output, with the model's built-in damming retention variable removed. Year 2050 no-dam RP and TN loads are taken from the Millennium Ecosystem Assessment scenario application of the Global-NEWS, for the TechnoGarden scenario (Seitzinger et al., 2010). Year 2050 RSi no-dam loads are assumed equal to year 2000 no-dam loads.

Exorheic watersheds were grouped according to which sea basin shelf they drained into by spatially intersecting the outlets of the STN-30p drainage networks (Vörösmarty et al., 2000) with the COSCAT/MARCAT continental shelves segmentation (Laruelle et al., 2013), using a 0.5° buffer zone around the shelves to ensure overlap with the coarse STN-30p dataset. Riverine nutrient loads were summed. Note that the nutrient loads discharged to coastal zones do not account for estuarine or oceanic reactions or mixing processes, including desorption of P from metal oxides in saline waters or mixing with the open ocean. The STN-30p data used is available online here: http://www.wsag.unh.edu/Stn-30/stn-30.html and the COSCAT dataset is available in Laruelle et al. (2013). Ratios were calculated using these summed loads.

Chapter 7

Conclusions and Perspectives

7.1 Summary of major findings

In this thesis I quantified both the absolute and relative changes to global Si, P and organic C (OC) loads delivered to the coastal ocean from damming (Table 7.1). Through use of a case study focused on Lake Diefenbaker (Chapter 2), and global-scale models (Chapters 3-6), I showed that damming drives a decoupling of nutrient cycles, via preferential elimination of P from the water column, followed by Si, over N. My results indicate that river damming modulates decreases in N:P ratios from anthropogenic loading in rivers discharging to the coastal zone. Despite this mitigating effect, 2760 km^3 yr^{-1} of river discharge will be N-limited by 2050, compared with only 980 km^3 yr^{-1} in 2000. The consequence of this shift will be a 9% increase in the proportion of coastal Si-limitation, due to the preferential retention of Si over N in reservoirs. I showed that dams bury unreactive P and Si species more efficiently than bioavailable species. In the case of P, the average arithmetic reservoir burial efficiency for total P (TP) exceeds reactive P (RP) by only 1%. Despite this minor difference, the overall load reduction of RP delivered to the coast is 14%, compared with only 12% for TP, indicating that a greater proportion of the global RP load passes through dams than TP. In the case of Si, the preferential retention of reactive Si (RSi) over dissolved Si (DSi) is reflected at the global scale, with double the proportion of the global riverine RSi load eliminated.

Through use of a coupled organic carbon-phosphorus model (Chapter 5), I showed that damming is promoting increased autotrophy in reservoirs, through higher P availability and longer water residence times. Simultaneously, heterotrophic processes are increasing, with the magnitude of the global mineralization flux largely dependent on the flooding of soil organic matter and biomass following new dam construction. The ratio of primary production to mineralization thus varies annually depending on the age distribution of dams worldwide. However, if all dam construction ends, long-term in-reservoir primary productivity fluxes will eventually outpace mineralization fluxes, indicating that reservoir systems worldwide will be predominantly autotrophic. Similarly, reservoir OC burial fluxes may eventually exceed the magnitude of mineralization fluxes.

Table 7.1: Year 2000 global model-predicted reservoir nutrient elimination fluxes and efficiencies. OC values were developed in collaboration with Ronny Lauerwald and Pierre Regnier (Maavara et al., 2017), and TN values obtained from Akbarzadeh et al. (in preparation for submission to PNAS). *Values in brackets represent the percentage of riverine load to coasts eliminated in the GRanD reservoirs alone, with the routing protocol implemented in Chapter 5; global extrapolation calculations for small reservoirs missing from GranD are excluded in order to allow for direct comparison with N and OC calculations, where no extrapolation for small reservoirs was done.

Nutrient	Species	Average reservoir elimination efficiency	Reservoir elimination flux (mol yr^{-1})	Percent of global load to coasts eliminated*
Silicon	DSi	0.13	1.63×10^{11}	2.6% (1.8%)
	RSi	0.21	3.72×10^{11}	5.3% (3.6%)
Phosphorus	TP	0.44	4.2×10^{11}	12% (12%)
	RP	0.43	1.8×10^{11}	14% (21%)
Nitrogen	TN	0.12	2.2×10^{11}	6%
Organic carbon	TOC	0.76	4.0×10^{12}	13%

7.2 Future work

The immediate continuation of the research presented in this thesis should focus on two areas: (1) improving estimates of nutrient loading to water bodies along the entire land-ocean aquatic continuum (LOAC); and (2) performing an assessment of the role of small reservoirs (< 0.1 km^3) in nutrient transformations and retention.

7.2.1 Improving biogeochemical modelling along the LOAC

The research presented in Chapters 3-6 in this thesis relies heavily on the Global-NEWS model, and is therefore constrained by the assumptions and limitations of said model. The most notable limitation is the spatial resolution of Global-NEWS, which lumps watershed nutrient yields into a single value, calibrated for the river mouth (Mayorga et al., 2010; Seitzinger et al., 2005). To improve the estimates of nutrient loads to individual reservoirs, a higher spatial resolution is needed. At present, the single watershed-scale nutrient yield is most accurate for predicting retention and elimination in reservoirs close to the coast, with increasing uncertainty in reservoirs further upstream, as distance from the location of calibration increases.

The hybrid approach I follow of integrating Global-NEWS loads with separate reservoir databases to calculate elimination presents several limitations. For example, in Chapter 5 it was impossible to integrate the autochthonous and allochthonous models together into the reservoir routing routine, as I was unable to quantify the extent of autochthonous mineralization in-stream between reservoirs, and Global-NEWS does not provide any information regarding the reactivity of dissolved and particulate OC (DOC and POC) loads. The consequence of this limitation was that I had to assume that autochthonous OC transported downstream of a reservoir was highly labile and was emitted in gaseous form before reaching a downstream reservoir. An improved modeling approach should utilize a globally routed hydrological network to quantify allochthonous and autochthonous fluxes along the entire LOAC. This approach would provide a means of tracking both the reactivity and speciation of nutrients and carbon loads that are delivered to reservoirs, retained or eliminated, and transported downstream.

In this thesis I have shown that river damming results in the decoupling of nutrient cycles through preferential elimination of P over Si and N in reservoirs. In Chapter 6 I quantified how these changes affect coastal nutrient limitation. However, this decoupling likely affects aquatic ecosystems along the entire LOAC. It is also likely that there are mechanisms in lakes, wetlands, and rivers that drive

nutrient cycle decoupling. Using mechanistic nutrient and carbon models coupled to a global hydrological network would enable the quantification of each of these fluxes. As a suggestion, future work could apply the Raven hydrological modelling framework (website: http://www.civil.uwaterloo.ca/jrcraig/Raven/Main.html) to all major watersheds on Earth, and incorporate a modified RIVE biogeochemical model component. The Raven modelling framework is a modular, object-oriented code that allows for flexible spatial and temporal discretization of watershed hydrological processes. The freely available model framework allows the user to decide which hydrological processes to include, easy parameter manipulation, and user-defined output. The model is ideal for global application as the code is already optimized to run efficiently. By coupling the Raven model hydrology with processes accounted for in the RIVE biogeochemical model (Billen et al., 1994; Garnier et al., 2006), it will be possible to predict major nutrient species fluxes and ecological community compositions throughout the aquatic continuum. This will enable the quantification of the drivers of nutrient cycle decoupling, and identification of hotspots for these processes and predict the likelihood of eutrophication. Using the Raven framework, the user can track sequential changes to nutrient loads from headwaters to the ocean.

While the Raven model was developed originally for watershed scale modelling, model inputs are available at the global scale, including high-resolution land use cover information, lithology, a complete stream network, with lakes, wetlands, and reservoirs, and climate (Hartmann and Moosdorf, 2012; Lauerwald et al., 2015; Lehner and Döll, 2004; Lehner and Grill, 2013; Lehner et al., 2011). A major advantage to using Raven in combination with RIVE is that the models are structured in such a way that development can begin with a simple model framework, and upgrade as needed. This approach will enable the determination of the level of detail needed to adequately predict processes at the global scale. This type of meta-analysis has never been undertaken, and so it is unclear to what extent existing global models are adequately parameterized. In addition, rather than constraining fixed rate constants for nutrient and phytoplankton transformations, the model should apply the Monte Carlo approach I used in Chapters 3-5 to account for variability in rate constants in the biogeochemical RIVE model component. In other words, the model should constrain distributions of rate constants and run Monte Carlo analyses to account for the possible outcomes using a range of values. It will also be possible to correlate certain rate constants (e.g. respiration) with latitude, as I did in Chapter 5. The model's biogeochemical output can be validated using the Global River Chemistry (Glorich) database (Hartmann et al., 2014) which contains more than 20 000 river

chemistry data points. Hydrological output can be calibrated and validated using discharge measurements available through local and national conservation authorities.

7.2.2 Quantifying the role of small reservoirs

A body of literature is emerging that indicates that reservoirs <0.1 km^2 may have disproportionately high rates of biogeochemical transformations (Downing, 2010), despite accounting for only about 4% of the total reservoir surface area (Lehner et al., 2011). Catalan et al. (2016) show that OC decomposition rate constants increase as water residence time decreases. (Note that water residence time generally correlates positively with surface area of a water body.) They show that this relationship results in decreasing OC mineralization rate constants along the LOAC, due to break down of highly reactive material in headwater streams with low residence times and subsequent downstream transport of the less labile material to larger water bodies with higher residence times. Cheng and Basu (2017) found similar inverse relationships between elimination of TP, TN, nitrate, and phosphate and water residence time in reservoirs, lakes, and wetlands. When they upscaled this relationship to the wetland size distribution in the Des Moines Lobe of the prairie pothole region in Iowa, they found that 50% of the TN elimination takes place in wetlands smaller than $10^{2.5}$ m^2.

At present, a spatially explicit estimate of reservoir nutrient and carbon transformation in small reservoirs is impossible to conduct within acceptable uncertainty bounds. There exists no complete database of the ~16.7 million reservoirs worldwide (Lehner et al., 2011). Previous estimates of nutrient retention or elimination in small reservoirs have relied on size distribution functions, typically Pareto, applied randomly to river systems worldwide (Downing et al., 2006; Harrison et al., 2012; Harrison et al., 2009). These studies provide a foundation for future research investigating the relative importance of small reservoirs in global nutrient cycling. However, due to their lack of integration within watershed routing networks, predicting nutrient loads to these reservoirs is highly uncertain, and subsequent calculations of the magnitude of elimination fluxes are unreliable. It additionally becomes impossible to incorporate the changes in reactivity along the LOAC, as shown by Catalan et al. (2016), into these calculations. Future research should focus on developing a viable means of predicting the locations and basic physical characteristics of small reservoirs worldwide.

7.3 Moving towards responsible dam construction

It is unlikely that humans will stop building dams. As the effects of climate change worsen worldwide, the need for flood control and reliable water storage solutions will increase. I have shown

that if we maintain the status quo and continue to build dams without considering the impacts to nutrient cycling, we can expect widespread changes to coastal nutrient ratios, potentially driving increased prevalence of harmful algal blooms (HABs). By trapping nutrients and carbon in reservoirs, dam construction is also pushing primary production fluxes upstream. That is, nutrients that would normally promote photosynthesis in downstream or coastal environments are being trapped further upstream, driving increased photosynthesis and nutrient recycling on the continents. I have provided evidence that this worldwide shift is taking place, and quantified the extent to which we can expect nutrient cycles to be altered.

Responsible dam construction and management can be achieved by mitigating the tradeoffs between the environmental and social consequences with the service provided by the dam. The research I have presented in this thesis provides both challenges and opportunities with regard to these tradeoffs. I identified the consequences of dam construction on nutrient loads and ratios along the LOAC, including the coastal zone, the consideration of which will represent a new challenge for dam managers. With about 40% of the global population reliant on marine fisheries for at least 15% of their protein (FAO, 2002), $80 billion USD in gross revenue from marine fishing, and up to $235 billion USD in employment and ancillary services (Dyck and Sumaila, 2010; Sumaila et al., 2011), the reorganization of coastal nutrient limitation could have harmful consequences to the world economy.

Beginning in the 1990s, nutrient management has focused on reducing N loads due to the predominance of N-limitation worldwide (Boesch, 2002; Howarth and Marino, 2006; NRC, 2000). However, studies have identified many coastal zones as P-limited, N or P co-limited, or alternating between N and P limitation seasonally (e.g. the Chesapeake Bay and portions of the Gulf of Mexico) (Malone et al., 1996; Rabalais et al., 2002). As a result, there is an evolving view that reduction of N and P together are necessary to mitigate many coastal eutrophication problems (Conley, 1999; Conley et al., 2009; Howarth and Marino, 2006). The results I presented in Chapter 6 indicate that if N:P ratios continue to decrease, damming is and will continue to increase the predominance of Si-limitation in coastal zones worldwide. Watershed management authorities can either attempt to manage the dams in such a way that will maintain nutrient ratios transported, or respond to dam-driven changes in nutrient ratios by implementing nutrient loading management regimes. Given that this thesis presents the first global summary of the decoupling of nutrient ratios due to river damming, the science exploring solutions to managing nutrient ratios exported through dams is nonexistent. As

a result, modifying nutrient loading management strategies to account for the effects of damming will likely be an easier solution. Local-scale studies evaluating the potential for increasing coastal Si-limitation should be undertaken to determine if regulating N, P or Si loads will be more effective in reducing coastal eutrophication.

From a more positive standpoint, dam construction may present opportunities to alleviate eutrophication or excess nutrient problems. This has already been done through the construction of "pre-dams," i.e. small upstream dams, which reduce nutrient loads to the reservoirs of concern in order to mitigate eutrophication (Benndorf and Pütz, 1987; Pütz and Benndorf, 1998). Along these lines, it may be further possible to use dams to mitigate coastal eutrophication problems, particularly when P is the limiting nutrient. In order for this approach to be successful, an integrated watershed management approach is needed, to optimize the nutrient loads and ratios along the entire LOAC, rather than merely driving eutrophication problems further upstream to the pre-reservoirs. Future research could additionally focus on identifying more sophisticated dam operational regimes to regulate downstream nutrient loads.

A major aspect missing from most dam construction plans is a long-term strategy for dam and reservoir management, which may ultimately include the removal of a dam after a set period of time. Hydroelectricity generated from damming may currently represent a relatively straightforward, responsible solution to reducing greenhouse gas emissions in places like China and India. However, as technologies with fewer environmental and social consequences (e.g. solar, wind) increase in efficiency and decrease in cost, continuing to use electricity generated from dammed rivers will no longer be the most responsible solution. Policy-makers should be prepared to deconstruct dams after they have fulfilled their purpose to mitigate cumulative environmental costs. The question of dam removal has arisen with increasing regularity in the media in recent years, particularly following the Oroville Dam near-disaster in California in February 2017, when a mismanaged dam nearly failed and resulted in the evacuation of nearly 200,000 downstream residents. It is becoming clear that dams have a finite lifespan, after which they become too costly to maintain or they are no longer needed for their original purpose. However, dam removal is still generally considered a radical solution, and as a result the existing body of literature on the topic of dam removal currently lacks meaningful quantification of the consequences to nutrient cycling along the LOAC. As dam deconstruction becomes a priority, particularly in North America and Europe where most dams are over 50 years old, quantifying the consequences to biogeochemical cycling along the LOAC should be a focus.

Bibliography

Abirhire, O., North, R.L., Hunter, K., Vandergucht, D.M., Sereda, J. and Hudson, J.J. (2015) Environmental factors influencing phytoplankton communities in Lake Diefenbaker, Saskatchewan, Canada. Journal of Great Lakes Research 41, 118-128.

Ahlgren, G. (1977) Growth of oscillatoria agardhii in chemostat culture: 1. nitrogen and phosphorus requirements. Oikos, 209-224.

Ahlgren, G. (1978) Growth of Oscillatoria agardhii in chemostat culture. 2. Dependence of growth constants on temperature, Symposium: Experimental Use of Algal Cultures in Limnology 26-28 October 1976, Sandefjord, Norway. Internationale Vereinigung fur Theoretische und Angewandte Limnologie, Mittelungen.

Akbarzadeh, Z., Maavara, T., Slowinski, S. and Van Cappellen, P. (in preparation for submission to PNAS) Damming modifies global nitrogen cycling along the river continuum.

Anderson, D.M., Burkholder, J.M., Cochlan, W.P., Glibert, P.M., Gobler, C.J., Heil, C.A., Kudela, R.M., Parsons, M.L., Rensel, J.J. and Townsend, D.W. (2008) Harmful algal blooms and eutrophication: examining linkages from selected coastal regions of the United States. Harmful Algae 8, 39-53.

Anderson, D.M., Glibert, P.M. and Burkholder, J.M. (2002) Harmful algal blooms and eutrophication: nutrient sources, composition, and consequences. Estuaries 25, 704-726.

Anderson, D.M., Hoagland, P., Kaoru, Y. and White, A.W. (2000) Estimated annual economic impacts from harmful algal blooms (HABs) in the United States.

Ansar, A., Flyvbjerg, B., Budzier, A. and Lunn, D. (2014) Should we build more large dams? The actual costs of hydropower megaproject development. Energy Policy 69, 43-56.

Apostol, I., Miller, K.J., Ratto, J. and Kelner, D.N. (2009) Comparison of different approaches for evaluation of the detection and quantitation limits of a purity method: a case study using a capillary isoelectrofocusing method for a monoclonal antibody. Analytical biochemistry 385, 101-106.

Arai, H. and Fukushima, T. (2012) Silicon budget of eutrophic Lake Kasumigaura, Japan. Journal of soils and sediments 12, 1501-1507.

Barão, L., Clymans, W., Vandevenne, F., Meire, P., Conley, D. and Struyf, E. (2014) Pedogenic and biogenic alkaline-extracted silicon distributions along a temperate land-use gradient. European Journal of Soil Science 65, 693-705.

Barbieri, A. and Mosello, R. (1992) Chemistry and trophic evolution of Lake Lugano in relation to nutrient budget. Aquat. Sci. 54, 219-237.

Bargu, S., Silver, M.W., Ohman, M.D., Benitez-Nelson, C.R. and Garrison, D.L. (2012) Mystery behind Hitchcock's birds. Nat. Geosci. 5, 2-3.

Barros, N., Cole, J.J., Tranvik, L.J., Prairie, Y.T., Bastviken, D., Huszar, V.L., Del Giorgio, P. and Roland, F. (2011) Carbon emission from hydroelectric reservoirs linked to reservoir age and latitude. Nat. Geosci. 4, 593-596.

Bartoszek, L. and Koszelnik, P. (2016) The qualitative and quantitative analysis of the coupled C, N, P and Si retention in complex of water reservoirs. SpringerPlus 5, 1157.

Bates, S., Bird, C.J., Freitas, A.d., Foxall, R., Gilgan, M., Hanic, L.A., Johnson, G.R., McCulloch, A., Odense, P. and Pocklington, R. (1989) Pennate diatom Nitzschia pungens as the primary source of domoic acid, a toxin in shellfish from eastern Prince Edward Island, Canada. Canadian Journal of Fisheries and Aquatic Sciences 46, 1203-1215.

Battin, T.J., Luyssaert, S., Kaplan, L.A., Aufdenkampe, A.K., Richter, A. and Tranvik, L.J. (2009) The boundless carbon cycle. Nat. Geosci. 2, 598-600.

Beale, E. (1962) Some uses of computers in operational research. Industrielle Organisation 31, 27-28.

Behrenfeld, M.J. and Falkowski, P.G. (1997a) A consumer's guide to phytoplankton primary productivity models. Limnology and Oceanography 42, 1479-1491.

Behrenfeld, M.J. and Falkowski, P.G. (1997b) Photosynthetic rates derived from satellite-based chlorophyll concentration. Limnology and oceanography 42, 1-20.

Benndorf, J. and Pütz, K. (1987) Control of eutrophication of lakes and reservoirs by means of pre-dams—I. Mode of operation and calculation of the nutrient elimination capacity. Water research 21, 829-838.

Berner, E.K. and Berner, R.A. (1995) Global Environment: Water, Air, and Geochemical Cycles. Prentice Hall, New Jersey.

Betsill, M. and Hoffmann, M.J. (2011) The contours of "cap and trade": the evolution of emissions trading systems for greenhouse gases. Review of Policy Research 28, 83-106.

Beusen, A., Van Beek, L., Bouwman, L., Mogollón, J. and Middelburg, J. (2015) Coupling global models for hydrology and nutrient loading to simulate nitrogen and phosphorus retention in surface water–description of IMAGE–GNM and analysis of performance. Geoscientific model development 8, 4045-4067.

Beusen, A.H., Bouwman, A.F., Van Beek, L.P., Mogollón, J.M. and Middelburg, J.J. (2016) Global riverine N and P transport to ocean increased during the 20th century despite increased retention along the aquatic continuum. Biogeosciences 13, 2441.

Beusen, A.H.W., Bouwman, A.F., Durr, H.H., Dekkers, A.L.M. and Hartmann, J. (2009) Global patterns of dissolved silica export to the coastal zone: Results from a spatially explicit global model. Global Biogeochemical Cycles 23, 13.

Beusen, A.H.W., Dekkers, A.L.M., Bouwman, A.F., Ludwig, W. and Harrison, J. (2005) Estimation of global river transport of sediments and associated particulate C, N, and P. Global Biogeochemical Cycles 19, 19.

Billen, G. and Garnier, J. (2007) River basin nutrient delivery to the coastal sea: Assessing its potential to sustain new production of non-siliceous algae. Marine Chemistry 106, 148-160.

Billen, G., Garnier, J. and Hanset, P. (1994) Modelling phytoplankton development in whole drainage networks: the RIVERSTRAHLER model applied to the Seine river system, Phytoplankton in Turbid Environments: Rivers and Shallow Lakes. Springer, pp. 119-137.

Billen, G., Lancelot, C., Meybeck, M., Mantoura, R., Martin, J.-M. and Wollast, R. (1991) N, P and Si retention along the aquatic continuum from land to ocean, Ocean Margin Processes in Global Change, 1. John Wiley & Sons, pp. 19-44.

Boesch, D.F. (2002) Challenges and opportunities for science in reducing nutrient over-enrichment of coastal ecosystems. Estuaries and Coasts 25, 886-900.

Brett, M.T. and Benjamin, M.M. (2008) A review and reassessment of lake phosphorus retention and the nutrient loading concept. Freshwater Biology 53, 194-211.

Brunskill, G., Povoledo, D., Graham, B. and Stainton, M. (1971) Chemistry of surface sediments of sixteen lakes in the Experimental Lakes Area, northwestern Ontario. Journal of the Fisheries Board of Canada 28, 277-294.

Brzezinski, M. (1985) The Si: C: N ratio of marine diatoms: interspecific variability and the effect of some environmental variables. Journal of phycology 21, 347-357.

Brzezinski, M.A., Phillips, D.R., Chavez, F.P., Friederich, G.E. and Dugdale, R.C. (1997) Silica production in the Monterey, California, upwelling system. Limnology and Oceanography 42, 1694-1705.

Buchan, A., LeCleir, G.R., Gulvik, C.A. and González, J.M. (2014) Master recyclers: features and functions of bacteria associated with phytoplankton blooms. Nature Reviews Microbiology 12, 686-698.

Cardoso, S.J., Enrich-Prast, A., Pace, M.L. and Roland, F. (2014) Do models of organic carbon mineralization extrapolate to warmer tropical sediments? Limnology and Oceanography 59, 48-54.

Carlson, R.E. and Simpson, J. (1996) A coordinator's guide to volunteer lake monitoring methods. North American Lake Management Society 96, 96.

Catalan, N., Marce, R., Kothawala, D.N. and Tranvik, L.J. (2016) Organic carbon decomposition rates controlled by water retention time across inland waters. Nature Geosci 9, 501-504.

Cheng, F.Y. and Basu, N.B. (2017) Biogeochemical hotspots: Role of small water bodies in landscape nutrient processing. Water Resources Research in press.

Cloern, J.E. (2001) Our evolving conceptual model of the coastal eutrophication problem. Marine ecology progress series 210, 223-253.

Cole, J.J., Prairie, Y.T., Caraco, N.F., McDowell, W.H., Tranvik, L.J., Striegl, R.G., Duarte, C.M., Kortelainen, P., Downing, J.A. and Middelburg, J.J. (2007) Plumbing the global carbon cycle: Integrating inland waters into the terrestrial carbon budget. Ecosystems 10, 172-185.

Compton, J., Mallinson, D., Glenn, C., Filippelli, G., Follmi, K., Shields, G. and Zanin, Y. (2000) Variations in the global phosphorus cycle. SEPM Special Publication 66, 21-33.

Conley, D., Schelske, C. and Stoermer, E. (1993) Modification of the biogeochemical cycle of silica with eutrophication. Marine Ecology Progress Series 101, 179-192.

Conley, D.J. (1997) Riverine contribution of biogenic silica to the oceanic silica budget. Limnology and Oceanography 42, 774-777.

Conley, D.J. (1998) An interlaboratory comparison for the measurement of biogenic silica in sediments. Marine Chemistry 63, 39-48.

Conley, D.J. (1999) Biogeochemical nutrient cycles and nutrient management strategies, Man and River Systems. Springer, pp. 87-96.

Conley, D.J., Kilham, S.S. and Theriot, E. (1989) Differences in Silica Content Between Marine and Freshwater Diatoms. Limnology and Oceanography 34, 205-213.

Conley, D.J., Paerl, H.W., Howarth, R.W., Boesch, D.F., Seitzinger, S.P., Havens, K.E., Lancelot, C. and Likens, G.E. (2009) Controlling eutrophication: nitrogen and phosphorus. Science 323, 1014-1015.

Conway, H., Parker, J., Yaguchi, E. and Mellinger, D. (1977) Biological utilization and regeneration of silicon in Lake Michigan. Journal of the Fisheries Board of Canada 34, 537-544.

Cook, P.L., Aldridge, K., Lamontagne, S. and Brookes, J. (2010) Retention of nitrogen, phosphorus and silicon in a large semi-arid riverine lake system. Biogeochemistry 99, 49-63.

Cornelis, J.-T., Delvaux, B., Georg, R., Lucas, Y., Ranger, J. and Opfergelt, S. (2011) Tracing the origin of dissolved silicon transferred from various soil-plant systems towards rivers: a review. Biogeosciences 8, 89-112.

Cornwell, J.C. and Banahan, S. (1992) A silicon budget for an Alaskan arctic lake. Hydrobiologia 240, 37-44.

Correll, D.L. (1998) The role of phosphorus in the eutrophication of receiving waters: A review. Journal of environmental quality 27, 261-266.

Cotner, J. and Wetzel, R. (1992) Uptake of dissolved inorganic and organic phosphorus compounds by phytoplankton and bacterioplankton. Limnology and oceanography 37, 232-243.

Crutzen, P.J. (2006) The "anthropocene", Earth system science in the anthropocene. Springer, pp. 13-18.

Dai, J., Sun, M.-Y., Culp, R.A. and Noakes, J.E. (2009) A laboratory study on biochemical degradation and microbial utilization of organic matter comprising a marine diatom, land grass, and salt marsh plant in estuarine ecosystems. Aquatic ecology 43, 825-841.

Davis, C.C., Chen, H.-W. and Edwards, M. (2002) Modeling silica sorption to iron hydroxide. Environmental science & technology 36, 582-587.

Dean, W.E. and Gorham, E. (1998) Magnitude and significance of carbon burial in lakes, reservoirs, and peatlands. Geology 26, 535-538.

Deemer, B.R., Harrison, J.A., Li, S., Beaulieu, J.J., DelSontro, T., Barros, N., Bezerra-Neto, J.F., Powers, S.M., dos Santos, M.A. and Vonk, J.A. (2016) Greenhouse Gas Emissions from Reservoir Water Surfaces: A New Global Synthesis. BioScience 66, 949-964.

Dickson, E. (1975) A silica budget for Lough Neagh 1970–1972. Freshwater Biology 5, 1-1.

Dolman, A., Shvidenko, A., Schepaschenko, D., Ciais, P., Tchebakova, N., Chen, T., Van Der Molen, M., Belelli Marchesini, L., Maximov, T. and Maksyutov, S. (2012) An estimate of the terrestrial carbon budget of Russia using inventory-based, eddy covariance and inversion methods. Biogeosciences 9, 5323-5340.

Donald, D.B., Parker, B.R., Davies, J.-M. and Leavitt, P.R. (2015) Nutrient sequestration in the Lake Winnipeg watershed. Journal of Great Lakes Research 41, 630-642.

Donk, E. and Kilham, S.S. (1990) Temperature effects on silicon‐and phosphorus‐limited growth and competitive interactions among three diatoms. Journal of Phycology 26, 40-50.

Downing, J., Prairie, Y., Cole, J., Duarte, C., Tranvik, L., Striegl, R., McDowell, W., Kortelainen, P., Caraco, N. and Melack, J. (2006) The global abundance and size distribution of lakes, ponds, and impoundments. Limnology and Oceanography 51, 2388-2397.

Downing, J.A. (2010) Emerging global role of small lakes and ponds. Limnetica 29, 0009-0024.

Downing, J.A., Cole, J.J., Middelburg, J.J., Striegl, R.G., Duarte, C.M., Kortelainen, P., Prairie, Y.T. and Laube, K. (2008) Sediment organic carbon burial in agriculturally eutrophic impoundments over the last century. Global Biogeochemical Cycles 22, GB1018.

Duan, S., Xu, F. and Wang, L.-J. (2007) Long-term changes in nutrient concentrations of the Changjiang River and principal tributaries. Biogeochemistry 85, 215-234.

Dubourg, P., North, R.L., Hunter, K., Vandergucht, D.M., Abirhire, O., Silsbe, G.M., Guildford, S.J. and Hudson, J.J. (2015) Light and nutrient co-limitation of phytoplankton communities in a large reservoir: Lake Diefenbaker, Saskatchewan, Canada. Journal of Great Lakes Research 41, 129-143.

Dumont, E., Harrison, J., Kroeze, C., Bakker, E. and Seitzinger, S. (2005) Global distribution and sources of dissolved inorganic nitrogen export to the coastal zone: Results from a spatially explicit, global model. Global Biogeochemical Cycles 19.

Duras, J. and Hejzlar, J. (2001) The Effect of Outflow Depth on Phosphorus Retention in a Small, Hypertrophic Temperate Reservoirwith Short Hydraulic Residence Time. International review of hydrobiology 86, 585-601.

Dürr, H.H., Meybeck, M., Hartmann, J., Laruelle, G.G. and Roubeix, V. (2011) Global spatial distribution of natural riverine silica inputs to the coastal zone. Biogeosciences 8, 597-620.

Dyck, A.J. and Sumaila, U.R. (2010) Economic impact of ocean fish populations in the global fishery. Journal of Bioeconomics 12, 227-243.

Elser, J.J., Bracken, M.E., Cleland, E.E., Gruner, D.S., Harpole, W.S., Hillebrand, H., Ngai, J.T., Seabloom, E.W., Shurin, J.B. and Smith, J.E. (2007) Global analysis of nitrogen and phosphorus limitation of primary producers in freshwater, marine and terrestrial ecosystems. Ecology Letters 10, 1135-1142.

Falkowski, P.G. (1981) Light-shade adaptation and assimilation numbers.

Falkowski, P.G., Barber, R.T. and Smetacek, V. (1998) Biogeochemical controls and feedbacks on ocean primary production. Science 281, 200-206.

FAO (2002) The state of world fisheries and aquaculture, 2002. United Nations Food & Agriculture Org.

Fearnside, P.M. (1995) Hydroelectric dams in the Brazilian Amazon as sources of 'greenhouse' gases. Environmental Conservation 22, 7-19.

Fekete, B.M., Vörösmarty, C.J. and Lammers, R.B. (2001) Scaling gridded river networks for macroscale hydrology: Development, analysis, and control of error. Water Resources Research 37, 1955-1967.

Fekete, B.M., Wisser, D., Kroeze, C., Mayorga, E., Bouwman, L., Wollheim, W.M. and Vörösmarty, C. (2010) Millennium Ecosystem Assessment scenario drivers (1970–2050): Climate and hydrological alterations. Global Biogeochemical Cycles 24, GB0A12.

FEMA (2016) Benefits of Dams. United States Department of Homeland Security.

Ferris, J.A. and Lehman, J.T. (2007) Interannual variation in diatom bloom dynamics: roles of hydrology, nutrient limitation, sinking, and whole lake manipulation. Water research 41, 2551-2562.

Filippelli, G.M. (2002) The Global Phosphorus Cycle. Reviews in Mineralogy and Geochemistry 48, 391-425.

Friedl, G., Teodoru, C. and Wehrli, B. (2004) Is the Iron Gate I reservoir on the Danube River a sink for dissolved silica? Biogeochemistry 68, 21-32.

Friedl, G. and Wüest, A. (2002) Disrupting biogeochemical cycles-Consequences of damming. Aquat. Sci. 64, 55-65.

Frings, P.J., Clymans, W., Jeppesen, E., Lauridsen, T.L., Struyf, E. and Conley, D.J. (2014) Lack of steady-state in the global biogeochemical Si cycle: emerging evidence from lake Si sequestration. Biogeochemistry 117, 255-277.

Fryxell, G.A., Villac, M.C. and Shapiro, L.P. (1997) The occurrence of the toxic diatom genus Pseudo-nitzschia (Bacillariophyceae) on the West Coast of the USA, 1920–1996: a review. Phycologia 36, 419-437.

Galloway, J.N., Dentener, F.J., Capone, D.G., Boyer, E.W., Howarth, R.W., Seitzinger, S.P., Asner, G.P., Cleveland, C., Green, P. and Holland, E. (2004) Nitrogen cycles: past, present, and future. Biogeochemistry 70, 153-226.

Garibaldi, L., Mezzanotte, V., Brizzio, M.C., Rogora, M. and Mosello, R. (1999) The trophic evolution of Lake Iseo as related to its holomixis. Journal of limnology 58, 10-19.

Garnier, J., Beusen, A., Thieu, V., Billen, G. and Bouwman, L. (2010) N:P:Si nutrient export ratios and ecological consequences in coastal seas evaluated by the ICEP approach. Global Biogeochemical Cycles 24, 12.

Garnier, J. and Billen, G. (2007) Production vs. Respiration in river systems: An indicator of an "ecological status". Science of the Total Environment 375, 110-124.

Garnier, J., Leporcq, B., Sanchez, N. and Philippon, X. (1999) Biogeochemical mass-balances (C, N, P, Si) in three large reservoirs of the Seine Basin (France). Biogeochemistry 47, 119-146.

Garnier, J., Sferratore, A., Meybeck, M., Billen, G. and Dürr, H. (2006) Modeling silicon transfer processes in river catchments. The Silicon Cycle. Human Perturbations and Impacts on Aquatic Systems 66, 139-162.

Geddes, M. (1984) Limnology of Lake Alexandrina, River Murray, South Australia, and the effects of nutrients and light on the phytoplankton. Marine and Freshwater Research 35, 399-415.

Gibson, C., Wang, G. and Foy, R. (2000) Silica and diatom growth in Lough Neagh: the importance of internal recycling. Freshwater Biology 45, 285-293.

Goedkoop, W. and Johnson, R.K. (1996) Pelagic-benthic coupling: Profundal benthic community response to spring diatom deposition in mesotrophic Lake Erken. Limnology and Oceanography 41, 636-647.

Gorham, E. and Boyce, F.M. (1989) Influence of Lake Surface Area and Depth Upon Thermal Stratification and the Depth of the Summer Thermocline. Journal of Great Lakes Research 15, 233-245.

Goto, N., Iwata, T., Akatsuka, T., Ishikawa, M., Kihira, M., Azumi, H., Anbutsu, K. and Mitamura, O. (2007) Environmental factors which influence the sink of silica in the limnetic system of the large monomictic Lake Biwa and its watershed in Japan. Biogeochemistry 84, 285-295.

Grantz, E.M., Haggard, B.E. and Scott, J.T. (2014) Stoichiometric imbalance in rates of nitrogen and phosphorus retention, storage, and recycling can perpetuate nitrogen deficiency in highly-productive reservoirs. Limnology and Oceanography 59, 2203-2216.

Griffin, T.T. and Ferrara, R.A. (1984) A Multicomponent Model of Phosphorus Dynamics in Reservoirs. Wiley Online Library.

Grill, G., Lehner, B., Lumsdon, A.E., MacDonald, G.K., Zarfl, C. and Liermann, C.R. (2015) An index-based framework for assessing patterns and trends in river fragmentation and flow regulation by global dams at multiple scales. Environmental Research Letters 10, 015001.

Hallegraeff, G.M. (1993) A review of harmful algal blooms and their apparent global increase*. Phycologia 32, 79-99.

Hanson, P.C., Buffam, I., Rusak, J.A., Stanley, E.H. and Watras, C. (2014) Quantifying lake allochthonous organic carbon budgets using a simple equilibrium model. Limnology and Oceanography 59, 167-181.

Hanson, P.C., Hamilton, D.P., Stanley, E.H., Preston, N., Langman, O.C. and Kara, E.L. (2011) Fate of allochthonous dissolved organic carbon in lakes: a quantitative approach. PloS one 6, e21884.

Harrison, J.A., Bouwman, A., Mayorga, E. and Seitzinger, S. (2010) Magnitudes and sources of dissolved inorganic phosphorus inputs to surface fresh waters and the coastal zone: A new global model. Global Biogeochemical Cycles 24.

Harrison, J.A., Frings, P.J., Beusen, A.H.W., Conley, D.J. and McCrackin, M.L. (2012) Global importance, patterns, and controls of dissolved silica retention in lakes and reservoirs. Global Biogeochemical Cycles 26, 12.

Harrison, J.A., Maranger, R.J., Alexander, R.B., Giblin, A.E., Jacinthe, P.-A., Mayorga, E., Seitzinger, S.P., Sobota, D.J. and Wollheim, W.M. (2009) The regional and global significance of nitrogen removal in lakes and reservoirs. Biogeochemistry 93, 143-157.

Harrison, J.A., Seitzinger, S.P., Bouwman, A.F., Caraco, N.F., Beusen, A.H.W. and Vorosmarty, C.J. (2005) Dissolved inorganic phosphorus export to the coastal zone: Results from a spatially explicit, global model. Global Biogeochemical Cycles 19, 17.

Hart, R. and Rayner, N. (1994) Temperature-related distributions of Metadiaptomus and Tropodiaptomus (Copepoda: Calanoida), particularly in southern Africa. Hydrobiologia 272, 77-86.

Hartmann, J., Jansen, N., Dürr, H.H., Harashima, A., Okubo, K. and Kempe, S. (2010) Predicting riverine dissolved silica fluxes to coastal zones from a hyperactive region and analysis of their first-order controls. International Journal of Earth Sciences 99, 207-230.

Hartmann, J., Lauerwald, R. and Moosdorf, N. (2014) A brief overview of the GLObal RIver CHemistry Database, GLORICH. Procedia Earth and Planetary Science 10, 23-27.

Hartmann, J., Levy, J. and Kempe, S. (2011) Increasing dissolved silica trends in the Rhine River: an effect of recovery from high P loads? Limnology 12, 63-73.

Hartmann, J. and Moosdorf, N. (2012) The new global lithological map database GLiM: A representation of rock properties at the Earth surface. Geochem. Geophys. Geosyst. 13, 37.

Hayes, N.M., Deemer, B.R., Corman, J.R., Razavi, N.R. and Strock, K.E. (2017) Key differences between lakes and reservoirs modify climate signals: A case for a new conceptual model. Limnology and Oceanography Letters 2, 47-62.

Hecker, M., Khim, J.S., Giesy, J.P., Li, S.-Q. and Ryu, J.-H. (2012) Seasonal dynamics of nutrient loading and chlorophyll A in a northern prairies reservoir, Saskatchewan, Canada. Journal of Water Resource and Protection 4, 180.

Hecky, R., Bootsma, H., Mugidde, R. and Bugenyi, F. (1996) Phosphorus pumps, nitrogen sinks, and silicon drains: plumbing nutrients in the African Great Lakes. The limnology, climatology and paleoclimatology of the East African lakes. Gordon and Breach, 205-233.

Hecky, R. and Kilham, P. (1988) Nutrient limitation of phytoplankton in freshwater and marine environments: A review of recent evidence on the effects of enrichment. Limnology and Oceanography 33, 796-822.

Hecky, R., Mugidde, R., Ramlal, P., Talbot, M. and Kling, G. (2010) Multiple stressors cause rapid ecosystem change in Lake Victoria. Freshwater Biology 55, 19-42.

Heisler, J., Glibert, P.M., Burkholder, J.M., Anderson, D.M., Cochlan, W., Dennison, W.C., Dortch, Q., Gobler, C.J., Heil, C.A. and Humphries, E. (2008) Eutrophication and harmful algal blooms: a scientific consensus. Harmful algae 8, 3-13.

Hejzlar, J., Šámalová, K., Boers, P. and Kronvang, B. (2006) Modelling phosphorus retention in lakes and reservoirs. Water, Air, & Soil Pollution: Focus 6, 487-494.

Hermoso, V. (2017) Freshwater ecosystems could become the biggest losers of the Paris Agreement. Global Change Biology.

Hiederer, R. and Köchy, M. (2011) Global soil organic carbon estimates and the Harmonized World Soil Database. Publications Office of the EU, Luxembourg.

Hilton, R.G., Meunier, P., Hovius, N., Bellingham, P.J. and Galy, A. (2011) Landslide impact on organic carbon cycling in a temperate montane forest. Earth Surface Processes and Landforms 36, 1670-1679.

Hoffman, D.A., Tramutt, P.R. and Heller, F.C. (1967) Water quality study of Lake Mead.

Hofmann, A., Roussy, D. and Filella, M. (2002) Dissolved silica budget in the North basin of Lake Lugano. Chemical Geology 182, 35-55.

Holm, N.P. and Armstrong, D.E. (1981) Role of nutrient limitation and competition in controlling the populations of Asterionella formosa and Microcystis aeruginosa in semicontinuous culture. Limnology and Oceanography 26, 622-634.

Holz, J.C., Hoagland, K.D., Spawn, R.L., Popp, A. and Andersen, J.L. (1997) Phytoplankton community response to reservoir aging, 1968–92. Hydrobiologia 346, 183-192.

Hongve, D. (1994) Nutrient metabolism (C, N, P, and Si) in the trophogenic zone of a meromictic lake. Hydrobiologia 277, 17-39.

Horn, H. and Horn, W. (2000) Sedimentation–the main Loss Factor in Waters Dominated by Diatoms. Results of Long-Term Investigations. International review of hydrobiology 85, 191-208.

Houghton, R., Hackler, J. and Lawrence, K. (1999) The US carbon budget: contributions from land-use change. Science 285, 574-578.

Howarth, R.W. and Marino, R. (2006) Nitrogen as the limiting nutrient for eutrophication in coastal marine ecosystems: evolving views over three decades. Limnology and Oceanography 51, 364-376.

Hudson, J.J., Taylor, W.D. and Schindler, D.W. (2000) Phosphate concentrations in lakes. Nature 406, 54-56.

Hudson, J.J. and Vanderguoht, D.M. (2015) Spatial and temporal patterns in physical properties and dissolved oxygen in Lake Diefenbaker, a large reservoir on the Canadian prairies. Journal of Great Lakes Research 41, 22-33.

Hughes, H., Bouillon, S., André, L. and Cardinal, D. (2012) The effects of weathering variability and anthropogenic pressures upon silicon cycling in an intertropical watershed (Tana River, Kenya). Chemical geology 308, 18-25.

Humborg, C., Conley, D.J., Rahm, L., Wulff, F., Cociasu, A. and Ittekkot, V. (2000) Silicon retention in river basins: Far-reaching effects on biogeochemistry and aquatic food webs in coastal marine environments. Ambio 29, 45-50.

Humborg, C., Ittekkot, V., Cociasu, A. and Bodungen, B.v. (1997) Effect of Danube River dam on Black Sea biogeochemistry and ecosystem structure.

Humborg, C., Pastuszak, M., Aigars, J., Siegmund, H., Morth, C.M. and Ittekkot, V. (2006) Decreased silica land-sea fluxes through damming in the Baltic Sea catchment - significance of particle trapping and hydrological alterations. Biogeochemistry 77, 265-281.

Humborg, C., Smedberg, E., Medina, M.R. and Morth, C.M. (2008) Changes in dissolved silicate loads to the Baltic Sea - The effects of lakes and reservoirs. J. Mar. Syst. 73, 223-235.

Hvistendahl, M. (2008) China's Three Gorges Dam: An Environmental Catastrophe? Scientific American 25.

ICOLD (2007) Dams and the World's Water: An Education Book that Explains how Dams Help to Manage the World's Water. International Commission on Large Dams, Paris, France.

Iler, R.K. (1979) The Chemistry of Silica: Solubility, Polymerization, Colloid and Surface Properties and Biochemistry of Silica. Wiley, New York.

Imboden, D. and Gächter, R. (1978) A dynamic lake model for trophic state prediction. Ecological Modelling 4, 77-98.

Imboden, D.M. (1974) Phosphorus model of lake eutrophication. Limnol. Oceanogr 19, 297-304.

IPCC (2013) Summary for Policymakers, in: Stocker, T., Qin, D., Plattner, G.-K., Alexander, L., Allen, S., Bindoff, N., Bréon, F.-M., Church, J., Cubasch, U., Emori, S. (Eds.), Climate Change 2013: The Physical Science Basis. Contribution of Working Group I to the Fifth Assessment Report of the Intergovernmental Panel on Climate Change. Cambridge University Press, New York, NY, USA.

ISAG, I.S.A.G. (2000) Report on the acid deposition monitoring of EANET during the preparatory phase —Its results, major constraints and ways to overcome them. http://www.eanet.asia/product/rep_pre_chapter.pdf.

Ittekkot, V., Humborg, C. and Schäfer, P. (2000) Hydrological Alterations and Marine Biogeochemistry: A Silicate Issue? Silicate retention in reservoirs behind dams affects ecosystem structure in coastal seas. BioScience 50, 776-782.

James, W.F. and Barko, J.W. (1997) Net and gross sedimentation in relation to the phosphorus budget of Eau Galle Reservoir, Wisconsin. Hydrobiologia 345, 15-20.

Jansen, N., Hartmann, J., Lauerwald, R., Durr, H.H., Kempe, S., Loos, S. and Middelkoop, H. (2010) Dissolved silica mobilization in the conterminous USA. Chemical Geology 270, 90-109.

Jónasson, P., Lastein, E. and Rebsdorf, A. (1974) Production, insolation, and nutrient budget of eutrophic Lake Esrom. Oikos, 255-277.

Jones, J.B., Stanley, E.H. and Mulholland, P.J. (2003) Long-term decline in carbon dioxide supersaturation in rivers across the contiguous United States. Geophysical Research Letters 30, 1495.

Jørgensen, S.E. (1976) A eutrophication model for a lake. Ecological Modelling 2, 147-165.

Kareiva, P., Marvier, M. and McClure, M. (2000) Recovery and management options for spring/summer chinook salmon in the Columbia River Basin. Science 290, 977-979.

Kastowski, M., Hinderer, M. and Vecsei, A. (2011) Long‑term carbon burial in European lakes: Analysis and estimate. Global Biogeochemical Cycles 25.

Katsev, S., Tsandev, I., L'Heureux, I. and Rancourt, D.G. (2006) Factors controlling long-term phosphorus efflux from lake sediments: Exploratory reactive-transport modeling. Chemical Geology 234, 127-147.

Kelly, V.J. (2001) Influence of reservoirs on solute transport: a regional‑scale approach. Hydrological Processes 15, 1227-1249.

Kimmel, B.L. and Groeger, A.W. (1986) Limnological and Ecological Changes Associated with Reservoir Aging, in: Hall, G.E., Van Den Avyle, M.J. (Eds.), Reservoir Fisheries Management: Strategies for the 80's. Reservoir Committee, Southern Division American Fisheries Society, Bethesda, Maryland, pp. 103-109.

Koehler, B., Wachenfeldt, E., Kothawala, D. and Tranvik, L.J. (2012) Reactivity continuum of dissolved organic carbon decomposition in lake water. Journal of Geophysical Research: Biogeosciences (2005–2012) 117.

Kõiv, T., Nõges, T. and Laas, A. (2011) Phosphorus retention as a function of external loading, hydraulic turnover time, area and relative depth in 54 lakes and reservoirs. Hydrobiologia 660, 105-115.

Kopáček, J., Turek, J., Hejzlar, J., Kaňa, J. and Porcal, P. (2006) Element fluxes in watershed-lake ecosystems recovering from acidification: Plešné Lake, the Bohemian Forest, 2001–2005. Biologia 61, S427-S440.

Koszelnik, P. and Tomaszek, J.A. (2008) Dissolved silica retention and its impact on eutrophication in a complex of mountain reservoirs. Water Air Soil Pollut. 189, 189-198.

Krause, J.W., Nelson, D.M. and Brzezinski, M.A. (2011) Biogenic silica production and the diatom contribution to primary production and nitrate uptake in the eastern equatorial Pacific Ocean. Deep Sea Research Part II: Topical Studies in Oceanography 58, 434-448.

Krogerus, K. and Ekholm, P. (2003) Phosphorus in settling matter and bottom sediments in lakes loaded by agriculture. Hydrobiologia 492, 15-28.

Kunz, M.J., Anselmetti, F.S., Wüest, A., Wehrli, B., Vollenweider, A., Thüring, S. and Senn, D.B. (2011) Sediment accumulation and carbon, nitrogen, and phosphorus deposition in the large tropical reservoir Lake Kariba (Zambia/Zimbabwe). Journal of Geophysical Research: Biogeosciences 116.

Lafrancois, B.M., Magdalene, S. and Johnson, D.K. (2009) Recent water quality trends and a comparison to sediment-core records for two riverine lakes of the Upper Mississippi River basin: Lake St. Croix and Lake Pepin. Journal of Paleolimnology 41, 603-622.

Lal, H. (2010) Nutrient credit trading—a market-based approach for improving water quality. Advances in Nitrogen Management for Water Quality (Delgado JA, Follett RF, eds.). Ankeny, IA: Soil and Water Conservation Society.

Landres, P.B., Morgan, P. and Swanson, F.J. (1999) Overview of the use of natural variability concepts in managing ecological systems. Ecological Applications 9, 1179-1188.

Langenberg, V.T., Nyamushahu, S., Roijackers, R. and Koelmans, A.A. (2003) External nutrient sources for Lake Tanganyika. Journal of Great Lakes Research 29, 169-180.

Larsen, D. and Mercier, H. (1976) Phosphorus retention capacity of lakes. Journal of the Fisheries Board of Canada 33, 1742-1750.

Laruelle, G.G., Durr, H.H., Lauerwald, R., Hartmann, J., Slomp, C.P., Goossens, N. and Regnier, P.A.G. (2013) Global multi-scale segmentation of continental and coastal waters from the watersheds to the continental margins. Hydrol. Earth Syst. Sci. 17, 2029-2051.

Laruelle, G.G., Roubeix, V., Sferratore, A., Brodherr, B., Ciuffa, D., Conley, D.J., Durr, H.H., Garnier, J., Lancelot, C., Phuong, Q.L.T., Meunier, J.D., Meybeck, M., Michalopoulos, P.,

Moriceau, B., Longphuirt, S.N., Loucaides, S., Papush, L., Presti, M., Ragueneau, O., Regnier, P., Saccone, L., Slomp, C.P., Spiteri, C. and Van Cappellen, P. (2009) Anthropogenic perturbations of the silicon cycle at the global scale: Key role of the land-ocean transition. Global Biogeochemical Cycles 23, 17.

Lauerwald, R., Hartmann, J., Moosdorf, N., Durr, H.H. and Kempe, S. (2012) Retention of dissolved silica within the fluvial system of the conterminous USA. Biogeochemistry 112, 637-659.

Lauerwald, R., Laruelle, G.G., Hartmann, J., Ciais, P. and Regnier, P.A. (2015) Spatial patterns in CO_2 evasion from the global river network. Global Biogeochemical Cycles 29, 534-554.

Lazzaretti-Ulmer, M.A. and Hanselmann, K.W. (1999) Seasonal variation of the microbially regulated buffering capacity at sediment-water interfaces in a freshwater lake. Aquat. Sci. 61, 59-74.

Le Quéré, C., Andrew, R.M., Canadell, J.G., Sitch, S., Korsbakken, J.I., Peters, G.P., Manning, A.C., Boden, T.A., Tans, P.P. and Houghton, R.A. (2016) Global carbon budget 2016. Earth System Science Data 8, 605.

Le Quéré, C., Moriarty, R., Andrew, R.M., Canadell, J.G., Sitch, S., Korsbakken, J.I., Friedlingstein, P., Peters, G.P., Andres, R.J., Boden, T.A., Houghton, R.A., House, J.I., Keeling, R.F., Tans, P., Arneth, A., Bakker, D.C.E., Barbero, L., Bopp, L., Chang, J., Chevallier, F., Chini, L.P., Ciais, P., Fader, M., Feely, R.A., Gkritzalis, T., Harris, I., Hauck, J., Ilyina, T., Jain, A.K., Kato, E., Kitidis, V., Klein Goldewijk, K., Koven, C., Landschützer, P., Lauvset, S.K., Lefèvre, N., Lenton, A., Lima, I.D., Metzl, N., Millero, F., Munro, D.R., Murata, A., Nabel, J.E.M.S., Nakaoka, S., Nojiri, Y., O'Brien, K., Olsen, A., Ono, T., Pérez, F.F., Pfeil, B., Pierrot, D., Poulter, B., Rehder, G., Rödenbeck, C., Saito, S., Schuster, U., Schwinger, J., Séférian, R., Steinhoff, T., Stocker, B.D., Sutton, A.J., Takahashi, T., Tilbrook, B., van der Laan-Luijkx, I.T., van der Werf, G.R., van Heuven, S., Vandemark, D., Viovy, N., Wiltshire, A., Zaehle, S. and Zeng, N. (2015) Global Carbon Budget 2015. Earth Syst. Sci. Data 7, 349-396.

Le Thi Phuong, Q., Billen, G., Garnier, J., Théry, S., Fézard, C. and Minh, C.V. (2005) Nutrient (N, P) budgets for the Red River basin (Vietnam and China). Global biogeochemical cycles 19.

Lehman, J.T. (1976) Ecological and nutritional studies on Dinobryon Ehrenb.: Seasonal periodicity and the phosphate toxicity problem. Limnology and Oceanography 21, 646-658.

Lehner, B. and Döll, P. (2004) Development and validation of a global database of lakes, reservoirs and wetlands. J. Hydrol. 296, 1-22.

Lehner, B. and Grill, G. (2013) Global river hydrography and network routing: baseline data and new approaches to study the world's large river systems. Hydrological Processes 27, 2171-2186.

Lehner, B., Liermann, C.R., Revenga, C., Vorosmarty, C., Fekete, B., Crouzet, P., Doll, P., Endejan, M., Frenken, K., Magome, J., Nilsson, C., Robertson, J.C., Rodel, R., Sindorf, N. and Wisser, D. (2011) High-resolution mapping of the world's reservoirs and dams for sustainable river-flow management. Frontiers in Ecology and the Environment 9, 494-502.

Lerman, A., Mackenzie, F.T. and Ver, L.M. (2004) Coupling of the perturbed C-N-P cycles in industrial time. Aquat. Geochem. 10, 3-32.

Lewis Jr, W.M. (2011) Global primary production of lakes: 19th Baldi Memorial Lecture. Inland Waters 1, 1-28.

Li, G., Wang, X.T., Yang, Z., Mao, C., West, A.J. and Ji, J. (2015) Dam-triggered organic carbon sequestration makes the Changjiang (Yangtze) river basin (China) a significant carbon sink. Journal of Geophysical Research: Biogeosciences 120, 39-53.

Likens, G. (1985) An ecosystem approach to aquatic ecology, Mirror Lake and its environment. New York, Springer-Verlag.

Loucaides, S., Van Cappellen, P., Roubeix, V., Moriceau, B. and Ragueneau, O. (2012) Controls on the recycling and preservation of biogenic silica from biomineralization to burial. Silicon 4, 7-22.

Lucas, B.T., Liber, K. and Doig, L.E. (2015a) Reconstructing diatom and chironomid assemblages to infer environmental spatiotemporal trends within Lake Diefenbaker, a narrow river-valley reservoir on the Canadian Prairies. Journal of Great Lakes Research 41, 45-55.

Lucas, B.T., Liber, K. and Doig, L.E. (2015b) Spatial and temporal trends in reservoir physicochemistry and phosphorus speciation within Lake Diefenbaker, a Great Plains reservoir, as inferred from depositional sediments. Journal of Great Lakes Research 41, 67-80.

Ludwig, W., Dumont, E., Meybeck, M. and Heussner, S. (2009) River discharges of water and nutrients to the Mediterranean and Black Sea: major drivers for ecosystem changes during past and future decades? Progress in Oceanography 80, 199-217.

Maavara, T., Dürr, H.H. and Van Cappellen, P. (2014) Worldwide retention of nutrient silicon by river damming: From sparse data set to global estimate. Global Biogeochemical Cycles 28, 842-855.

Maavara, T., Hood, J.L.A., North, R.L., Doig, L.E., Parsons, C.T., Johansson, J., Liber, K., Hudson, J.J., Lucas, B.T., Vandergucht, D.M. and Van Cappellen, P. (2015a) Reactive silicon dynamics in a large prairie reservoir (Lake Diefenbaker, Saskatchewan). Journal of Great Lakes Research 41, 100-109.

Maavara, T., Lauerwald, R., Regnier, P. and Van Cappellen, P. (2017) Global Perturbation of Organic Carbon Cycling by River Damming. Nature communications 8, 15347.

Maavara, T., Parsons, C.T., Ridenour, C., Stojanovic, S., Dürr, H.H., Powley, H.R. and Van Cappellen, P. (2015b) Global phosphorus retention by river damming. Proc Natl Acad Sci U.S.A. 112, 15603-15608.

Mackenzie, F.T., Ver, L.M. and Lerman, A. (2002) Century-scale nitrogen and phosphorus controls of the carbon cycle. Chemical Geology 190, 13-32.

Malmaeus, J.M., Blenckner, T., Markensten, H. and Persson, I. (2006) Lake phosphorus dynamics and climate warming: A mechanistic model approach. Ecological Modelling 190, 1-14.

Malone, T.C., Conley, D.J., Fisher, T.R., Glibert, P.M., Harding, L.W. and Sellner, K.G. (1996) Scales of nutrient-limited phytoplankton productivity in Chesapeake Bay. Estuaries 19, 371-385.

Mayorga, E., Seitzinger, S.P., Harrison, J.A., Dumont, E., Beusen, A.H.W., Bouwman, A.F., Fekete, B.M., Kroeze, C. and Van Drecht, G. (2010) Global Nutrient Export from WaterSheds 2 (NEWS 2): Model development and implementation. Environ. Modell. Softw. 25, 837-853.

McClain, M.E., Boyer, E.W., Dent, C.L., Gergel, S.E., Grimm, N.B., Groffman, P.M., Hart, S.C., Harvey, J.W., Johnston, C.A. and Mayorga, E. (2003) Biogeochemical hot spots and hot moments at the interface of terrestrial and aquatic ecosystems. Ecosystems 6, 301-312.

McGinnis, D.F., Bocaniov, S., Teodoru, C., Friedl, G., Lorke, A. and Wuest, A. (2006) Silica retention in the Iron Gate I reservoir on the Danube River: The role of side bays as nutrient. River Res. Appl. 22, 441-456.

McManus, D.P., Gray, D.J., Li, Y., Feng, Z., Williams, G.M., Stewart, D., Rey-Ladino, J. and Ross, A.G. (2010) Schistosomiasis in the People's Republic of China: the era of the Three Gorges Dam. Clinical microbiology reviews 23, 442-466.

Mendonça, R., Kosten, S., Sobek, S., Barros, N., Cole, J.J., Tranvik, L. and Roland, F. (2012a) Hydroelectric carbon sequestration. Nat. Geosci. 5, 838-840.

Mendonça, R., Roland, F., Pacheco, F., Vidal, L.O., Barros, N. and Kosten, S. (2012b) Greenhouse gas emissions from hydroelectric reservoirs: what knowledge do we have and what is lacking? INTECH Open Access Publisher.

Meybeck, M. (1982) Carbon, nitrogen, and phosphorus transport by world rivers. Am. J. Sci. 282, 401-450.

Meybeck, M. (1988) How to establish and use world budgets of riverine materials, Physical and chemical weathering in geochemical cycles. Springer, pp. 247-272.

Meybeck, M. (1993) C, N, P and S in rivers: from sources to global inputs, in: Wollast, R., Mackenzie, F.T., Chou, L. (Eds.), Interactions of C, N, P and S Biogeochemical Cycles and Global Change. Springer, pp. 163-193.

Michel, T.J., Saros, J.E., Interlandi, S.J. and Wolfe, A.P. (2006) Resource requirements of four freshwater diatom taxa determined by in situ growth bioassays using natural populations from alpine lakes. Hydrobiologia 568, 235-243.

Moosmann, L., Gächter, R., Müller, B. and Wüest, A. (2006) Is phosphorus retention in autochthonous lake sediments controlled by oxygen or phosphorus? Limnology and Oceanography 51, 763-771.

Mosley, L.M., Zammit, B., Leyden, E., Heneker, T.M., Hipsey, M.R., Skinner, D. and Aldridge, K.T. (2012) The impact of extreme low flows on the water quality of the Lower Murray River and Lakes (South Australia). Water Resources Management 26, 3923-3946.

Mulholland, P.J. and Elwood, J.W. (1982) The role of lake and reservoir sediments as sinks in the perturbed global carbon cycle. Tellus 34, 490-499.

Müller, B., Berg, M., Pernet-Coudrier, B., Qi, W. and Liu, H. (2012) The geochemistry of the Yangtze River: Seasonality of concentrations and temporal trends of chemical loads. Global Biogeochemical Cycles 26.

Müller, B., Maerki, M., Schmid, M., Vologina, E.G., Wehrli, B., Wüest, A. and Sturm, M. (2005) Internal carbon and nutrient cycling in Lake Baikal: sedimentation, upwelling, and early diagenesis. Global and Planetary Change 46, 101-124.

Muvundja, F.A., Pasche, N., Bugenyi, F.W., Isumbisho, M., Müller, B., Namugize, J.-N., Rinta, P., Schmid, M., Stierli, R. and Wüest, A. (2009) Balancing nutrient inputs to Lake Kivu. Journal of Great Lakes Research 35, 406-418.

Nalewajko, C. and Lean, D. (1978) Phosphorus kinetics--algal growth relationships in batch cultures, Symposium: Experimental Use of Algal Cultures in Limnology 26-28 October 1976, Sandefjord, Norway. Internationale Vereinigung fur Theoretische und Angewandte Limnologie, Mittelungen.

Nelson, D.M., Tréguer, P., Brzezinski, M.A., Leynaert, A. and Quéguiner, B. (1995) Production and dissolution of biogenic silica in the ocean: revised global estimates, comparison with regional data and relationship to biogenic sedimentation. Global Biogeochemical Cycles 9, 359-372.

Nilsson, C. and Berggren, K. (2000) Alterations of Riparian Ecosystems Caused by River Regulation: Dam operations have caused global-scale ecological changes in riparian ecosystems. How to protect river environments and human needs of rivers remains one of the most important questions of our time. BioScience 50, 783-792.

Nixon, S.W. (1995) Coastal marine eutrophication: a definition, social causes, and future concerns. Ophelia 41, 199-219.

Nixon, S.W. (2003) Replacing the Nile: Are Anthropogenic Nutrients Providing the Fertility Once Brought to the Mediterranean by a Great River? Ambio 32, 30-39.

North, R., Johansson, J., Vandergucht, D., Doig, L., Liber, K., Lindenschmidt, K., Baulch, H. and Hudson, J. (2015) Evidence for internal phosphorus loading in a large prairie reservoir (Lake Diefenbaker, Saskatchewan). J. Great Lakes Res. in review.

NRC (2000) Clean coastal waters: understanding and reducing the effects of nutrient pollution. National Academies Press.

Nyholm, N. (1977) Kinetics of phosphorus-limited growth. Biotechnology and Bioengineering 19, 467-472.

Officer, C. and Ryther, J. (1980) The possible importance of silicon in marine eutrophication. Marine Ecology Progress Series 3, 83-91.

Ohlendorf, C. and Sturm, M. (2008) A modified method for biogenic silica determination. Journal of Paleolimnology 39, 137-142.

Opfergelt, S., Eiriksdottir, E.S., Burton, K.W., Einarsson, A., Siebert, C., Gislason, S.R. and Halliday, A.N. (2011) Quantifying the impact of freshwater diatom productivity on silicon isotopes and silicon fluxes: Lake Myvatn, Iceland. Earth Planet. Sci. Lett. 305, 73-82.

Ostapenia, A.P., Parparov, A. and Berman, T. (2009) Lability of organic carbon in lakes of different trophic status. Freshwater biology 54, 1312-1323.

P'yankova, L. (1994) Central Asia in the Bronze Age: sedentary and nomadic cultures. Antiquity 68, 355-372.

Pacala, S., Birdsey, R.A., Bridgham, S.D., Conant, R.T., Davis, K., Hales, B., Houghton, R.A., Jenkins, J.C., Johnston, M., Marland, G. and Paustian, K. (2007) The Carbon Cycle of North American in a Global Context, in: King, A.W., Dilling, L., Zimmerman, G.P., Fairman, D.M., Houghton, R.A., Marland, G., Rose, A.Z., Wilbanks, T.J. (Eds.), The First State of the Carbon Cycle Report (SOCCR): The North American Carbon Budget and Implications for the Global Carbon Cycle. National Oceanic and Atmospheric Administration, National Climatic Data Centre, Asheville, NC, USA, pp. 21-28.

Perl, T.M., Bédard, L., Kosatsky, T., Hockin, J.C., Todd, E.C. and Remis, R.S. (1990) An outbreak of toxic encephalopathy caused by eating mussels contaminated with domoic acid. New England Journal of Medicine 322, 1775-1780.

Platt, T. (1986) Primary production of the ocean water column as a function of surface light intensity: algorithms for remote sensing. Deep Sea Research Part A. Oceanographic Research Papers 33, 149-163.

Poff, N.L., Olden, J.D., Merritt, D.M. and Pepin, D.M. (2007) Homogenization of regional river dynamics by dams and global biodiversity implications. Proceedings of the National Academy of Sciences 104, 5732-5737.

Pomeroy, J. and Shook, K. (2012) Review of Lake Diefenbaker operations: 2010–2011. Final Report to the Saskatchewan Watershed Authority. http://www.usask.ca/hydrology/papers/Pomeroy_Shook_2012.pdf.

Pütz, K. and Benndorf, J. (1998) The importance of pre-reservoirs for the control of eutrophication of reservoirs. Water Science and Technology 37, 317-324.

Quilbé, R., Rousseau, A.N., Duchemin, M., Poulin, A., Gangbazo, G. and Villeneuve, J.-P. (2006) Selecting a calculation method to estimate sediment and nutrient loads in streams: application to the Beaurivage River (Québec, Canada). J. Hydrol. 326, 295-310.

Rabalais, N.N., Turner, R.E. and Wiseman Jr, W.J. (2002) Gulf of Mexico hypoxia, AKA" The dead zone". Annual Review of ecology and Systematics, 235-263.

Ran, X., Yu, Z., Yao, Q., Chen, H. and Guo, H. (2013) Silica retention in the Three Gorges reservoir. Biogeochemistry 112, 209-228.

Raymond, P.A., Hartmann, J., Lauerwald, R., Sobek, S., McDonald, C., Hoover, M., Butman, D., Striegl, R., Mayorga, E., Humborg, C., Kortelainen, P., Durr, H., Meybeck, M., Ciais, P. and Guth, P. (2013) Global carbon dioxide emissions from inland waters. Nature 503, 355-359.

Redfield, A. (1934) On the proportions of organic derivatives in sea water and their relation to the composition of plankton. University Press of Liverpool.

Redshaw, C., Mason, C., Hayes, C. and Roberts, R. (1988) Nutrient budget for a hypertrophic reservoir. Water research 22, 413-419.

Regnier, P., Friedlingstein, P., Ciais, P., Mackenzie, F.T., Gruber, N., Janssens, I.A., Laruelle, G.G., Lauerwald, R., Luyssaert, S., Andersson, A.J., Arndt, S., Arnosti, C., Borges, A.V., Dale, A.W., Gallego-Sala, A., Godderis, Y., Goossens, N., Hartmann, J., Heinze, C., Ilyina, T., Joos, F., LaRowe, D.E., Leifeld, J., Meysman, F.J.R., Munhoven, G., Raymond, P.A., Spahni, R., Suntharalingam, P. and Thullner, M. (2013) Anthropogenic perturbation of the carbon fluxes from land to ocean. Nat. Geosci. 6, 597-607.

REN21 (2016) Renewables 2016 Global Status Report. Paris.

Reynolds, C. (1988) Functional morphology and the adaptive strategies of freshwater phytoplankton. Cambridge University Press, Cambridge.

Reynolds, C. and Maberly, S. (2002) A simple method for approximating the supportive capacities and metabolic constraints in lakes and reservoirs. Freshwater Biology 47, 1183-1188.

Reynolds, C.S. (2006) The ecology of phytoplankton. Cambridge University Press.

Rotter, B., Barry, D., Gerhard, J. and Small, J. (2008) Parameter and process significance in mechanistic modeling of cellulose hydrolysis. Bioresource technology 99, 5738-5748.

Ruesch, A. and Gibbs, H. (2008) New global biomass carbon map for the year 2000 based on IPCC Tier-1 methodology. Oak Ridge National Laboratory's Carbon Dioxide Information Analysis Center, Oak Ridge, TN, USA.

Ruttenberg, K. (2003) The global phosphorus cycle. Treatise on Geochemistry 8, 585-643.

Ryves, D.B., Battarbee, R.W., Juggins, S., Fritz, S.C. and Anderson, N.J. (2006) Physical and chemical predictors of diatom dissolution in freshwater and saline lake sediments in North America and West Greenland. Papers in the Geosciences, 5.

Saccone, L., Conley, D., Koning, E., Sauer, D., Sommer, M., Kaczorek, D., Blecker, S. and Kelly, E. (2007) Assessing the extraction and quantification of amorphous silica in soils of forest and grassland ecosystems. European Journal of Soil Science 58, 1446-1459.

Sadeghian, A., de Boer, D., Hudson, J.J., Wheater, H. and Lindenschmidt, K.-E. (2015) Lake Diefenbaker temperature model. Journal of Great Lakes Research 41, 8-21.

Salvia-Castellvi, M., Dohet, A., Vander Borght, P. and Hoffmann, L. (2001) Control of the eutrophication of the reservoir of Esch-sur-Sûre (Luxembourg): evaluation of the phosphorus removal by predams. Hydrobiologia 459, 61-71.

Sauer, D., Saccone, L., Conley, D.J., Herrmann, L. and Sommer, M. (2006) Review of methodologies for extracting plant-available and amorphous Si from soils and aquatic sediments. Biogeochemistry 80, 89-108.

Schelske, C.L. (1985) Biogeochemical silica mass balances in Lake Michigan and Lake Superior. Biogeochemistry 1, 197-218.

Schelske, C.L. and Stoermer, E.F. (1971) Eutrophication, silica depletion, and predicted changes in algal quality in Lake Michigan. Science 173, 423-424.

Schindler, D. (1977) Evolution of phosphorus limitation in lakes. Science 195, 260-262.

Schindler, D.W., Hecky, R., Findlay, D., Stainton, M., Parker, B., Paterson, M., Beaty, K., Lyng, M. and Kasian, S. (2008) Eutrophication of lakes cannot be controlled by reducing nitrogen input: results of a 37-year whole-ecosystem experiment. Proceedings of the National Academy of Sciences 105, 11254-11258.

Scholin, C.A., Gulland, F., Doucette, G.J., Benson, S., Busman, M., Chavez, F.P., Cordaro, J., DeLong, R., De Vogelaere, A. and Harvey, J. (2000) Mortality of sea lions along the central California coast linked to a toxic diatom bloom. Nature 403, 80-84.

Seitzinger, S.P., Harrison, J.A., Dumont, E., Beusen, A.H.W. and Bouwman, A.F. (2005) Sources and delivery of carbon, nitrogen, and phosphorus to the coastal zone: An overview of Global

Nutrient Export from Watersheds (NEWS) models and their application. Global Biogeochemical Cycles 19, GB4S01.

Seitzinger, S.P., Mayorga, E., Bouwman, A.F., Kroeze, C., Beusen, A.H.W., Billen, G., Van Drecht, G., Dumont, E., Fekete, B.M., Garnier, J. and Harrison, J.A. (2010) Global river nutrient export: A scenario analysis of past and future trends. Global Biogeochemical Cycles 24, GB0A08.

Seitzinger, S.P., Styles, R.V., Boyer, E.W., Alexander, R.B., Billen, G., Howarth, R.W., Mayer, B. and Van Breemen, N. (2002) Nitrogen retention in rivers: model development and application to watersheds in the northeastern USA, The Nitrogen Cycle at Regional to Global Scales. Springer, pp. 199-237.

Sferratore, A., Billen, G., Garnier, J., Smedberg, E., Humborg, C. and Rahm, L. (2008) Modelling nutrient fluxes from sub-arctic basins: Comparison of pristine vs. dammed rivers. J. Mar. Syst. 73, 236-249.

Skalak, K.J., Benthem, A.J., Schenk, E.R., Hupp, C.R., Galloway, J.M., Nustad, R.A. and Wiche, G.J. (2013) Large dams and alluvial rivers in the Anthropocene: The impacts of the Garrison and Oahe Dams on the Upper Missouri River. Anthropocene 2, 51-64.

Slomp, C.P. and Van Cappellen, P. (2007) The global marine phosphorus cycle: sensitivity to oceanic circulation. Biogeosciences 4, 155-171.

Smil, V. (2000) Phosphorus in the environment: natural flows and human interferences. Annual Review of Energy and the Environment 25, 53-88.

Smith, V.H., Joye, S.B. and Howarth, R.W. (2006) Eutrophication of freshwater and marine ecosystems. Limnology and Oceanography 51, 351-355.

Smith, V.H., Tilman, G.D. and Nekola, J.C. (1999) Eutrophication: impacts of excess nutrient inputs on freshwater, marine, and terrestrial ecosystems. Environmental pollution 100, 179-196.

Snodgrass, W.J. and O'Melia, C.R. (1975) Predictive model for phosphorus in lakes. Environmental science & technology 9, 937-944.

Soballe, D. and Kimmel, B. (1987) A large-scale comparison of factors influencing phytoplankton abundance in rivers, lakes, and impoundments. Ecology 68, 1943-1954.

Sobek, S., Durisch-Kaiser, E., Zurbrügg, R., Wongfun, N., Wessels, M., Pasche, N. and Wehrli, B. (2009) Organic carbon burial efficiency in lake sediments controlled by oxygen exposure time and sediment source. Limnology and Oceanography 54, 2243-2254.

Sobek, S., Tranvik, L.J., Prairie, Y.T., Kortelainen, P. and Cole, J.J. (2007) Patterns and regulation of dissolved organic carbon: An analysis of 7,500 widely distributed lakes. Limnology and Oceanography 52, 1208-1219.

Spitzy, A. and Leenheer, J. (1991) Dissolved organic carbon in rivers. Biogeochemistry of major world rivers, 213-232.

St Louis, V.L., Kelly, C.A., Duchemin, É., Rudd, J.W. and Rosenberg, D.M. (2000) Reservoir Surfaces as Sources of Greenhouse Gases to the Atmosphere: A Global Estimate Reservoirs are sources of greenhouse gases to the atmosphere, and their surface areas have increased to the point where they should be included in global inventories of anthropogenic emissions of greenhouse gases. BioScience 50, 766-775.

Stallard, R.F. (1998) Terrestrial sedimentation and the carbon cycle: coupling weathering and erosion to carbon burial. Global Biogeochemical Cycles 12, 231-257.

Stehfest, E., van Vuuren, D., Bouwman, L. and Kram, T. (2014) Integrated assessment of global environmental change with IMAGE 3.0: Model description and policy applications. Netherlands Environmental Assessment Agency (PBL).

Strokal, M., Kroeze, C., Wang, M. and Ma, L. (2017) Reducing future river export of nutrients to coastal waters of China in optimistic scenarios. Science of The Total Environment 579, 517-528.

Struyf, E. and Conley, D.J. (2009) Silica: an essential nutrient in wetland biogeochemistry. Frontiers in Ecology and the Environment 7, 88-94.

Struyf, E., Smis, A., Van Damme, S., Garnier, J., Govers, G., Van Wesemael, B., Conley, D., Batelaan, O., Frot, E. and Clymans, W. (2010) Historical land use change has lowered terrestrial silica mobilization. Nature communications 1, 129.

Struyf, E., Smis, A., Van Damme, S., Meire, P. and Conley, D.J. (2009) The global biogeochemical silicon cycle. Silicon 1, 207-213.

Sumaila, U.R., Cheung, W.W., Lam, V.W., Pauly, D. and Herrick, S. (2011) Climate change impacts on the biophysics and economics of world fisheries. Nature climate change 1, 449-456.

Syvitski, J.P., Vörösmarty, C.J., Kettner, A.J. and Green, P. (2005) Impact of humans on the flux of terrestrial sediment to the global coastal ocean. Science 308, 376-380.

Tavernini, S., Pierobon, E. and Viaroli, P. (2011) Physical factors and dissolved reactive silica affect phytoplankton community structure and dynamics in a lowland eutrophic river (Po river, Italy). Hydrobiologia 669, 213-225.

Teodoru, C., Dimopoulos, A. and Wehrli, B. (2006) Biogenic silica accumulation in the sediments of Iron Gate I reservoir on the Danube River. Aquat. Sci. 68, 469-481.

Teodoru, C. and Wehrli, B. (2005) Retention of sediments and nutrients in the Iron Gate I Reservoir on the Danube River. Biogeochemistry 76, 539-565.

Teodoru, C.R., Bastien, J., Bonneville, M.-C., del Giorgio, P.A., Demarty, M., Garneau, M., Hélie, J.-F., Pelletier, L., Prairie, Y.T., Roulet, N.T., Strachan, I.B. and Tremblay, A. (2012) The net carbon footprint of a newly created boreal hydroelectric reservoir. Global Biogeochemical Cycles 26, GB2016.

Teubner, K. and Dokulil, M.T. (2002) Ecological stoichiometry of TN: TP: SRSi in freshwaters: nutrient ratios and seasonal shifts in phytoplankton assemblages. Archiv fur Hydrobiologie 154, 625-646.

Thieu, V., Billen, G. and Garnier, J. (2009) Nutrient transfer in three contrasting NW European watersheds: the Seine, Somme, and Scheldt Rivers. A comparative application of the Seneque/Riverstrahler model. Water research 43, 1740-1754.

Thornton, J., Steel, A. and Rast, W. (1996) Reservoirs, in: Chapman, D.V. (Ed.), Water quality assessments: a guide to the use of biota, sediments and water in environmental monitoring, 2 ed. World Health Organization Press, CRC.

Tilman, D. and Kilham, S.S. (1976) Phosphate and silicate growth and uptake kinetics of the diatoms Asterionella formosa and Cyclotella meneghiniana in batch and semi-continuous culture. Journal of Phycology 12, 375-383.

Tran, N.N. (1995) The geology of Vietnam: A brief summary and problems. 静岡大学地球科学研究報告 22, 1-9.

Tranvik, L.J., Downing, J.A., Cotner, J.B., Loiselle, S.A., Striegl, R.G., Ballatore, T.J., Dillon, P., Finlay, K., Fortino, K. and Knoll, L.B. (2009) Lakes and reservoirs as regulators of carbon cycling and climate. Limnology and Oceanography 54, 2298-2314.

Tréguer, P., Nelson, D., Van Bennekom, A., Demaster, D., Leynaert, A. and Quéguiner, B. (1995) The silica balance in the world ocean: a reestimate. Science 268, 375.

Tréguer, P. and Pondaven, P. (2000) Global change: Silica control of carbon dioxide. Nature 406, 358-359.

Triplett, L.D. (2008) Two Rivers, Two Lakes, Two Legacies: Anthropogenic Alterations to Silica Cycling and Heavy Metal Loading in Lake St. Croix and Lake Pepin, USA. ProQuest.

Triplett, L.D., Engstrom, D.R. and Conley, D.J. (2012) Changes in amorphous silica sequestration with eutrophication of riverine impoundments. Biogeochemistry 108, 413-427.

Turner, R.E., Rabalais, N.N., Justic, D. and Dortch, Q. (2003) Global patterns of dissolved N, P and Si in large rivers. Biogeochemistry 64, 297-317.

Valiela, I. (2013) Marine ecological processes. Springer Science & Business Media.

Van Cappellen, P. (2003) Biomineralization and global biogeochemical cycles. Reviews in mineralogy and geochemistry 54, 357-381.

Van Cappellen, P., Dixit, S. and van Beusekom, J. (2002) Biogenic silica dissolution in the oceans: Reconciling experimental and field-based dissolution rates. Global Biogeochemical Cycles 16, 23-21-23-10.

Van Cappellen, P. and Maavara, T. (2016) Rivers in the Anthropocene: Global scale modifications of riverine nutrient fluxes by damming. Ecohydrology and Hydrobiology 16, 106-111.

Van Cappellen, P. and Qiu, L. (1997) Biogenic silica dissolution in sediments of the Southern Ocean. II. Kinetics. Deep Sea Research Part II: Topical Studies in Oceanography 44, 1129-1149.

Van Drecht, G., Bouwman, A., Harrison, J. and Knoop, J. (2009) Global nitrogen and phosphate in urban wastewater for the period 1970 to 2050. Global Biogeochemical Cycles 23.

van Liere, L. and Mur, L.R. (1979) Growth kinetics of Oscillatoria agardhii Gomont in continuous culture, limited in its growth by the light energy supply. Journal of General Microbiology 115, 153-160.

Ver, L.M.B., Mackenzie, F.T. and Lerman, A. (1999) Biogeochemical responses of the carbon cycle to natural and human perturbations: Past, present, and future. Am. J. Sci. 299, 762-801.

Vitousek, P.M., Mooney, H.A., Lubchenco, J. and Melillo, J.M. (1997) Human domination of Earth's ecosystems. Science 277, 494-499.

Vollenweider, R.A. (1975) Input-output models with special reference to the phosphorus loading concept in limnology. Schweizerische Zeitschrift für Hydrologie 37, 53-84.

Vörösmarty, C., Fekete, B., Meybeck, M. and Lammers, R. (2000) Geomorphometric attributes of the global system of rivers at 30-minute spatial resolution. J. Hydrol. 237, 17-39.

Vörösmarty, C.J., Meybeck, M., Fekete, B., Sharma, K., Green, P. and Syvitski, J.P. (2003) Anthropogenic sediment retention: Major global impact from registered river impoundments. Global and Planetary Change 39, 169-190.

Vörösmarty, C.J. and Sahagian, D. (2000) Anthropogenic disturbance of the terrestrial water cycle. BioScience 50, 753-765.

Vörösmarty, C.J., Sharma, K.P., Fekete, B.M., Copeland, A.H., Holden, J., Marble, J. and Lough, J.A. (1997) The storage and aging of continental runoff in large reservoir systems of the world. Ambio 26, 210-219.

Wakatsuki, T. and Masunaga, T. (2009) Dissolved silica dynamics and phytoplankton population in Citarum watershed, Indonesia. International journal of food, agriculture and environment 7, 655-661.

Wang, F., Wang, Y., Zhang, J., Xu, H. and Wei, X. (2007) Human impact on the historical change of CO2 degassing flux in River Changjiang. Geochemical Transactions 8, 1-10.

Wang, F., Yu, Y., Liu, C., Wang, B., Wang, Y., Guan, J. and Mei, H. (2010) Dissolved silicate retention and transport in cascade reservoirs in Karst area, Southwest China. Science of the Total Environment 408, 1667-1675.

Water Office, W. (2014) Real-time Hydrometric Data. http://www.wateroffice.ec.gc.ca/.

WCD, W.C.o.D. (2000) Dams and Development: A New Framework for Decision-making: the Report of the World Commission on Dams. Earthscan.

Welch, H.E. and Legault, J.A. (1986) Precipitation chemistry and chemical limnology of fertilized and natural lakes at Saqvaqjuac, NWT. Canadian Journal of Fisheries and Aquatic Sciences 43, 1104-1134.

West, A., Lin, C.-W., Lin, T.-C., Hilton, R., Liu, S.-H., Chang, C.-T., Lin, K.-C., Galy, A., Sparkes, R. and Hovius, N. (2011) Mobilization and transport of coarse woody debris to the oceans triggered by an extreme tropical storm. Limnology and oceanography 56, 77-85.

Wetz, M.S., Hales, B. and Wheeler, P.A. (2008) Degradation of phytoplankton-derived organic matter: Implications for carbon and nitrogen biogeochemistry in coastal ecosystems. Estuarine, Coastal and Shelf Science 77, 422-432.

Weyhenmeyer, G. (2004) Synchrony in relationships between the North Atlantic Oscillation and water chemistry among Sweden's largest lakes. Limnol. Oceanogr 49, 1191-1201.

Wilhelmus, B., Bernhardt, M. and Neuman, P. (1978) Vergleichende untersuchungen uber die phosphoreleminierung von vorsperren - Verminderung der algenentwicklung in speicherbecken und talsperren, deutscher verein gas wasser-fach. Schriftenr. Wasser 16, 140-176.

Williams, G., Layman, K.L. and Stefan, H.G. (2004) Dependence of lake ice covers on climatic, geographic and bathymetric variables. Cold Regions Science and Technology 40, 145-164.

Winemiller, K., McIntyre, P., Castello, L., Fluet-Chouinard, E., Giarrizzo, T., Nam, S., Baird, I., Darwall, W., Lujan, N. and Harrison, I. (2016) Balancing hydropower and biodiversity in the Amazon, Congo, and Mekong. Science 351, 128-129.

WSA, W.S.A. (2012) State of Lake Diefenbaker. Saskatchewan, Canada, https://www.wsask.ca/Global/Lakes and Rivers/Dams and Reservoirs/Operating Plans/Developing an Operating Plan for Lake Diefenbaker/State of Lake Diefenbaker Report - October 19 2012.pdf.

Wu, J., Huang, J., Han, X., Xie, Z. and Gao, X. (2003) Three-Gorges dam--experiment in habitat fragmentation? Science 300, 1239-1240.

Zarfl, C., Lumsdon, A., Berlekamp, J., Tydecks, L. and Tockner, K. (2015) A global boom in hydropower dam construction. Aquat. Sci. 77, 161-170.

Znachor, P., Visocká, V., Nedoma, J. and Rychtecký, P. (2013) Spatial heterogeneity of diatom silicification and growth in a eutrophic reservoir. Freshwater Biology 58, 1889-1902.

Appendix A

Supplementary Material: Chapter 2

Table AA1: Concentrations of PRSi interlaboratory comparison standards reported in literature reference and concentrations determined from extractions in this study. Note: Only alkaline extraction results are presented due to conclusions made by Saccone et al. (2007) regarding the ineffectiveness of acid extractions.

Sample ID	Reference PRSi (mean ± SD, wt. % as SiO_2)	Observed PRSi (this study, wt. % as SiO_2)
Chesapeake Bay Still Pond[1]	2.82 ± 1.17	1.61
Chesapeake Bay R-64[1]	6.49 ± 2.09	6.59
Yellowstone Lake[1]	38.2 ± 9.48	38.77
HBEF Sample D[2]	1.79 ± 0.014 (Na_2CO_3 extraction) 1.42 (NaOH extraction)	1.42
Great Plains Grasslands Sample SH6[2]	0.43 ± 0.2 (Na_2CO_3 extraction) 0.94 (NaOH extraction)	1.33

References: [1]Conley (1998); [2]Saccone et al. (2007)

Alternative flux calculations

In addition to the ratio estimator flux calculation presented in the text, five methods were tested to calculate DSi influxes and effluxes in Lake Diefenbaker. These methods broadly fall into three categories: averaging estimators (methods A-D), ratio estimators (method E), and regression methods (method F). Each method is summarized below, the calculated fluxes are presented (Table AA2), and a brief discussion is given to justify my choice of method in the DSi budget calculation. A full summary of the merits and assumptions of each method is provided in Quilbé et al., 2006.

(1) Averaging estimators:

A. $F_s = \bar{C} \cdot \bar{Q} \cdot n$

where F_s is the flux (mol yr^{-1}), $\bar{C}$ is the arithmetic mean concentration for the days Q and C are both measured (mol km^{-3}), $\bar{Q}$ is the arithmetic mean discharge for the days Q and C are both measured (mol day^{-1}), and n is the total number of days over the period of flux estimation (i.e. 365 days).

B. $F_w = \bar{C} \cdot \mu_Q \cdot n$

with

$\mu_Q = \frac{\sum_{i=1}^{n} Q_i}{n}$

where F_w is the flux (mol yr^{-1}), μ_Q is the arithmetic mean of all flow measurements collected year-round (km^3 day^{-1}) and Q_i is the discharge on day i (km^3 day^{-1}).

C. $F_a = \overline{CQ} \cdot n$

where F_a is the flux (mol yr^{-1}), and $\overline{CQ}$ is the arithmetic average of the fluxes calculated on days where C and Q were both measured (mol day^{-1}).

D. $F_c = \overline{CQ} \cdot \frac{\mu_Q}{\bar{Q}} \cdot n$

where F_c is the flux (mol yr^{-1}).

(2) Ratio estimators:

154

E. $F_{re} = F_c \cdot \left(\dfrac{1 + \frac{1}{n_d} \cdot \frac{S_{CQ}}{\overline{CQ} \cdot \overline{Q}}}{1 + \frac{1}{n_d} \cdot \frac{S_{Q^2}}{\overline{Q}^2}} \right)$

where F_{re} is the flux (mol yr^{-1}), F_c is the flux calculated according to equation d, n_d is number of days C and Q were both measured, S_{CQ} is the covariance between flux and discharge on days concentrations measurements were taken, and S_{Q^2} is the variance of the flux on days concentration measurements were taken.

(3) Regression methods:

F. This method involves finding an empirical relationship between available daily Q and C data and applying this method to all the remaining days of the year where Q is available in order to estimate C. The method is useful only if there is a statistically significant relationship between C and Q with an R^2 that exceeds 0.5. Quilbé et al. (2006) indicate that the most commonly used equation is the log-log linear regression curve:

$$log_{10}(C) = a + b \cdot log_{10}(Q)$$

where a and b are constants. Once C is found for n days, annual flux, F_l, can be calculated according to:

$$F_l = \sum_{i=1}^{n} C_i Q_i$$

Methods A-C yield unreliable results (Table AA2). They are largely dependent on the assumption that the averages of the concentration values collected represent the annual average. As a result, sampling biases have a large effect on the flux calculation. Method D is less biased than A-C, and yields the same result as method E, which multiplies F_c by a correcting ratio accounting for the covariance between discharge and flux. Method E is unbiased and an ideal method if method F (regression method) yields poor relationships between concentration and discharge (Quilbé et al., 2006).

The similar outcomes of methods D and E indicate that there is little correlation between concentration and discharge at any location. The regression analysis in method F confirms this conclusion. Linear, logarithmic and exponential regressions do not yield statistically significant

155

(p<0.05) fits with R^2 that exceed 0.5 for any of the inflow or outflow locations. In addition, SSR and SCC show an increasing trend in concentration with discharge, while both outlets show a decreasing trend in concentration with discharge, likely as a consequence of reservoir Si cycling. While I may opt for fitting different curves at each location, this approach is speculative and would require a larger dataset for establishing the required statistical power.

Table AA2: Annual DSi fluxes and retentions calculated using each of the above-described methods, in addition to the flow-weighting method presented in the text.

Calculation method	Annual influx (mol yr^{-1})	Annual efflux (mol yr^{-1})	DSi retention
A	1.46×10^9	7.60×10^8	0.48
B	7.66×10^8	7.47×10^8	0.02
C	1.75×10^9	6.73×10^8	0.61
D	9.12×10^8	6.61×10^8	0.28
E	9.12×10^8	6.42×10^8	0.30

Appendix B
Supplementary Material: Chapter 3

Statistical analyses

ANOVA analysis indicates that reservoirs are much more predominantly eutrophic than lakes (p<0.05), indicating the systems have increased in productivity relative to their previous state as an undammed river stretch. This relationship may be more a function of land-use in the lake catchments versus reservoir catchments. Additional data is needed on catchment use before this trend can be suitably explored. It is also found that oligotrophic reservoirs tend to have lower retention (R_{DSi}=0.013) than eutrophic reservoirs (R_{DSi}=0.3088). Trophic status is not related to pH, though it is related to residence time, with oligotrophic lakes tending to have longer residence times than eutrophic lakes. It is hypothesized that this relationship is primarily due to the dilution effect of nutrients in lakes with large volumes (and thus large residence times).

A significant (p<0.05) relationship is obtained in a one-way ANOVA test of bedrock lithology and DSi retention in the dataset of all 44 lakes and reservoirs. The highest retention is observed in metamorphic and crystalline felsic igneous bedrock such as gneiss and granite (R_{Si}≈0.62, n=20), while the lowest retention is observed in carbonate-rich rocks (R_{Si}≈0.28, n=11) and quartz-rich sandstones (R_{Si}≈0.04, n=4). Mixed sedimentary bedrock including shale, mudstone, diamictite, and conglomerate show moderate retention (R≈0.5, n=10). ANOVA analysis shows no relationship (p>0.05) between bedrock lithology and reservoirs alone, suggesting that water passes through reservoirs too quickly to be influenced by chemical effects arising from bedrock lithology. I am reluctant to make any firm conclusions about the role of bedrock lithology on R_D in lentic systems due to the relatively poor distribution of lithologies present in the dataset compared with the global distribution (Figure 3.1). Not surprisingly, a significant relationship is also found between bedrock lithology and pH, with carbonate and sandstone bedrocks tending towards alkaline and metamorphic and granitic rocks tending towards acidic.

Climate, represented by precipitation and temperature, does not seem to play much of a role in influencing retention, though there may be some relationship between R_{DSi} and annual temperature, as indicated by the results of a linear regression model (p<0.05). However, bedrock lithology and temperature and precipitation are not statistically independent of each other, suggesting the climate relationship may be a relic of the geological effect. The relationship between reservoir age and retention remains unclear due to the uncertainty regarding the

regularity and extent of sediment dredging in individual reservoirs. However, a weak trend may be present indicating decreasing DSi retention with reservoir age, suggesting dissolution of deposited sediments into solution is occurring, allowing for the export of DSi. This relationship emerges more clearly in the mechanistic model and is discussed in more detail in section 3.5.3.

Regression models indicate exponential decay trends relating R_D to reservoir volume and depth. Statistically significant R^2 values do not exceed 0.3 for any of these relationships (the best fit being depth) (Table AB2). Instead, the statistical analyses indicate that R_D is most closely related to the water residence time (τ_r). Retention of DSi in lakes exhibits an exponential growth to a maximum with the water residence time (Figure AB3a), given by:

$$R_D = 0.7679 \times (1 - e^{-1.1210\tau_r}); R^2 = 0.61, \text{p<0.05, n=24} \qquad \text{(AB1)}$$

where τ_r is expressed in units of years. The reservoirs in the calibration data set not only tend to have shorter water residence times than the lakes, they also follow a distinctly separate trend with respect to τ_r. The following lognormal relationship (Figure AB3b) is obtained for all reservoirs:

$$R_D = \frac{0.2219}{\tau_r} \exp\left[-0.5\left(\frac{\ln(\tau_r/0.5507)}{0.6573}\right)^2\right]; R^2 = 0.8154, \text{p<0.0001, n=18} \qquad \text{(AB2)}$$

The robustness of Equation AB2 was tested by performing 10 rounds of cross-validation with randomly generated training sets of 70% of the data and using the remaining 30% for validation. The average standard error for the lognormal fits was over five times lower than for a linear regression model (0.30 versus 1.60), hence supporting the log-normal distribution. It is unclear as to whether the shape represented by Equation AB2 is a "true" process-justified relationship in reservoirs. While some argument can be made justifying the peaks and valleys in the curve arising as a result of different rates of dissolution, sedimentation and export in each reservoir (which can be reproduced to some degree using the mechanistic model), I chose not to pursue this relationship in the global estimate.

Table AB1: Summary data for lakes used to calibrate retention model. References: (1) Welch and Legault (1986); (2) Likens (1985); (3) Hongve (1994); (4) Kopáček et al. (2006); (5) Cornwell and Banahan (1992); (6) Jónasson et al. (1974); (7) Barbieri and Mosello (1992); (8) Hofmann et al. (2002); (9) Lazzaretti-Ulmer and Hanselmann (1999); (10) Lafrancois et al. (2009); (11) Triplett et al. (2012); (12) Triplett (2008); (13) Garibaldi et al. (1999); (14) Arai and Fukushima (2012); (15) Goto et al. (2007); (16) Jens Hartmann – personal communication; (17) Conley et al. (1993); (18) Weyhenmeyer (2004); (19) Muvundja et al. (2009); (20) Schelske (1985); (21) Hecky et al. (1996); (22) Müller et al. (2005); (23) Langenberg et al. (2003).

Latitude	Lake name	Location	Bedrock lithology	Trophic status	Surface area (km^2)	Mean depth (m)	pH	Climate	Residence time (years)	R_D	Reference
63.6	Jade	Canada	Gneiss, carbonate	Oligo	0.036	1.82	5.90	Arctic	0.85	0.92	1
63.6	Far	Canada	Gneiss, carbonate	Oligo	0.037	3.61	6.15	Arctic	2.93	0.80	1
63.6	Spring	Canada	Gneiss, carbonate	Oligo	0.069	2.71	6.20	Arctic	1.63	0.57	1
63.6	P&N	Canada	Gneiss, carbonate	Oligo	0.071	3.28	6.40	Arctic	2.9	0.73	1
43.6	Mirror	USA	Mixed metamorphic	Oligo	0.15	5.75	6.36	Temperate	1.02	0.65	2
49.65	Rawson (Lake 239)	Canada	Plutonic (felsic)	Eu	0.56	10.18	4.92	Temperate	10.8	0.44	2
60.15	Nordbytjernet	Norway	Mixed metamorphic	Oligo	0.28	9.9	7.60	Subarctic	1.4	0.45	3
48.78	Plesne Lake	Czech Republic	Mixed metamorphic	Meso	0.75	0.82	5.00	Temperate	0.8	0.24	4
68.6	Toolik Lake	Alaska	Mixed sedimentary	Oligo	1.5	7	6.80	Arctic	1	0.17	5
56	Lake Esrum	Denmark	Mixed sedimentary	Eu	17.3	12.3	8.30	Subarctic	9.6	0.65	6
46	Lake Lugano	Switzerland/Italy	Gneiss, carbonate	Eu	27.5	171	7.60	Temperate	12	0.785	7, 8, 9
44.9	St. Croix	USA	Sandstone	Meso	35	14	7.82	Temperate	0.1	0.038	10, 11, 12
44.4	Pepin	USA	Sandstone	Eu	103	8.9	8.10	Temperate	0.05	-0.11	10,11, 12
45.43	Lake Iseo	Italy	Carbonate	Eu	61	123	7.70	Temperate	4.2	0.84	13
36	Lake Kasumigaura	Japan	Mixed sedimentary	Eu	168	4	8.14	Subtropical	0.57	0.56	14
35.2	Lake Biwa	Japan	Mixed igneous, carbonate	Meso	670	41	7.90	Subtropical	5	0.8	15, 16
59.5	Malaren	Sweden	Plutonic (felsic)	Meso	1140	13	7.53	Subarctic	3	0.83	17, 18
58.5	Vattern	Sweden	Plutonic (felsic)	Oligo	1900	40	7.60	Subarctic	58	0.94	17, 18
-2	Kivu	Africa	Mixed metamorphic	Oligo	2700	245	9.00	Tropical	100	0.53	19
44	Michigan	USA	Mixed sedimentary	Meso	5800	84	8.40	Temperate	100	0.80	20
47.3	Superior	Canada	Mixed igneous, metamorphic	Oligo	82367	148	7.35	Subarctic	191	0.7	20
-12.2	Malawi	Africa	Mixed metamorphic	Meso	29600	292	7.90	Tropical	140	0.96	21
53	Baikal	Russia	Mixed igneous, carbonate	Oligo	31475	740	7.10	Arctic	330	0.76	22
-6.3	Tanganyika	Africa	Mixed metamorphic	Oligo	32900	570	8.40	Tropical	440	0.98	23

Table AB2: Summary statistics of variables used in calibration dataset. Note that hydraulic load is calculated as Discharge/Surface area.

| Dataset	Independent variable	Dependent variable	Test	p-value, R^2 (if applicable)	Significant?
Lakes and reservoirs	Lake vs reservoir	R_D	Independent samples t-test	7.172×10^{-6}	Yes
		Water residence time	Independent samples t-test	0.01947	Yes
		Hydraulic load	Independent samples t-test	0.02336	Yes
		Trophic status	Independent samples t-test	0.02547	Yes
	Bedrock lithology	R_D	1-way ANOVA	0.00814	Yes
		pH	1-way ANOVA	0.0655	No
	Trophic status	R_D	1-way ANOVA	0.143	No
		pH	1-way ANOVA	0.162	No
		Water residence time	1-way ANOVA	0.0347	Yes
		Climate	1-way ANOVA	0.005	Yes
	Climate	R_D	1-way ANOVA	0.0227	Yes
	pH	R_D	Linear regression	$p=0.608$, $R^2=0.006314$	No
Reservoirs only	Bedrock lithology	R_D	1-way ANOVA	0.788	No
	Trophic status	R_D	1-way ANOVA	0.0913	Yes
	pH	R_D	Linear regression	$p=0.234$, $R^2=0.07769$	No
	Climate	R_D	1-way ANOVA	0.171	No
	Water residence time	R_D	Non-linear regression	$p<0.0001$, $R^2=0.8154$	Yes
	Volume	R_D	Non-linear regression	$p<0.0001$, $R^2=0.16124$	No
	Hydraulic load	R_D	Linear regression	$p<0.0001$, $R^2 = 0.2846$	No
	Depth	R_D	Non-linear regression	$R^2 = 0.2729$, $p<0.0001$	No
	Reservoir age	R_D	Linear regression	0.7071	No
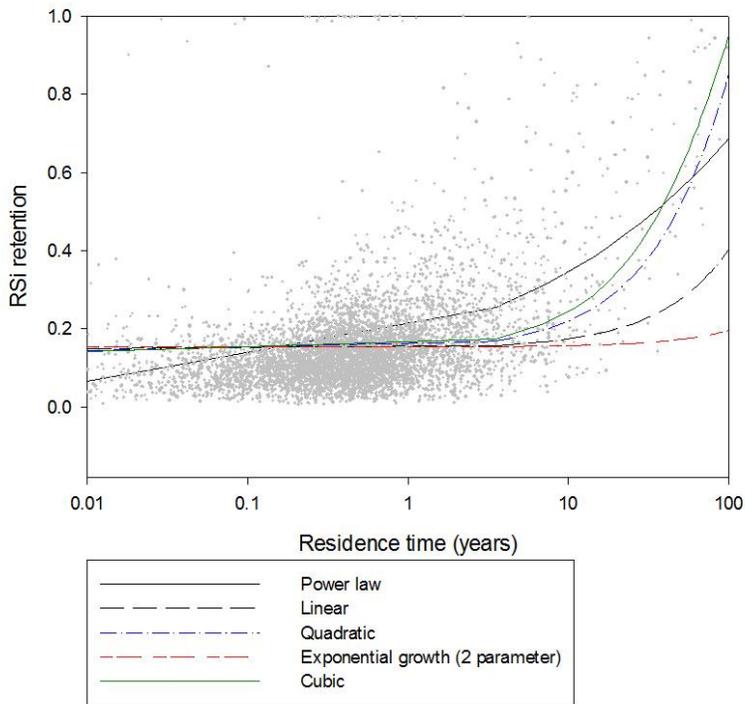
Figure AB1: Monte Carlo output for RSi retention plotting as a function of residence time. Most relevant statistically significant ($p < 0.05$) regression analyses trend lines are shown. R^2 values for power law, linear, quadratic, exponential growth and cubic curves are 0.31, 0.11, 0.24, 0.04 and 0.27, respectively. Because my focus in the chapter is RSi retention, I therefore apply a power law relationship to DSi retention for consistency.
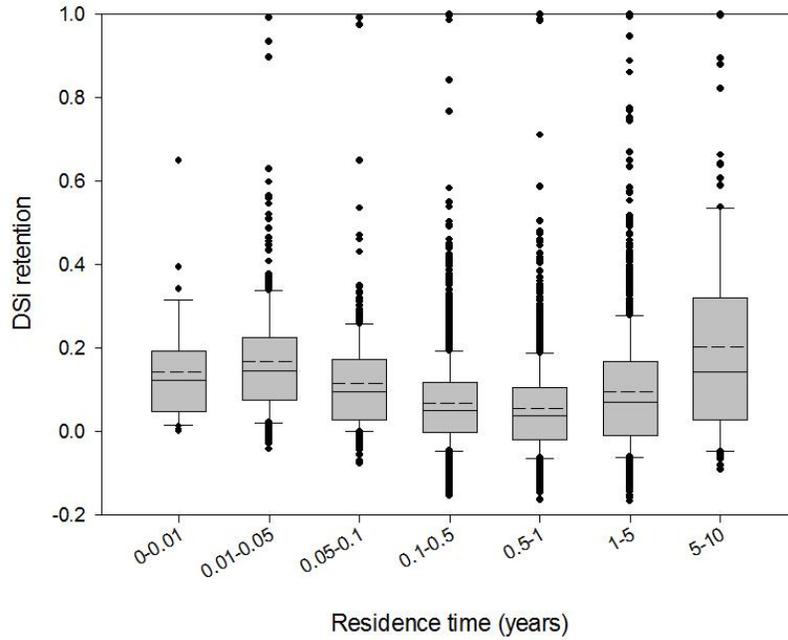
Figure AB2: Monte Carlo output for DSi retention. Solid lines are median, dashed lines are means for each box. The edges of each box represent the 1st and 3rd quartiles, and the whiskers are standard deviations. Retentions of 1 at lower residence times arise primarily in small reservoirs (i.e. low volume, low surface area) with extremely high productivity (i.e. up to an order of magnitude higher R_{max} than that calculated using Equation 3.4).
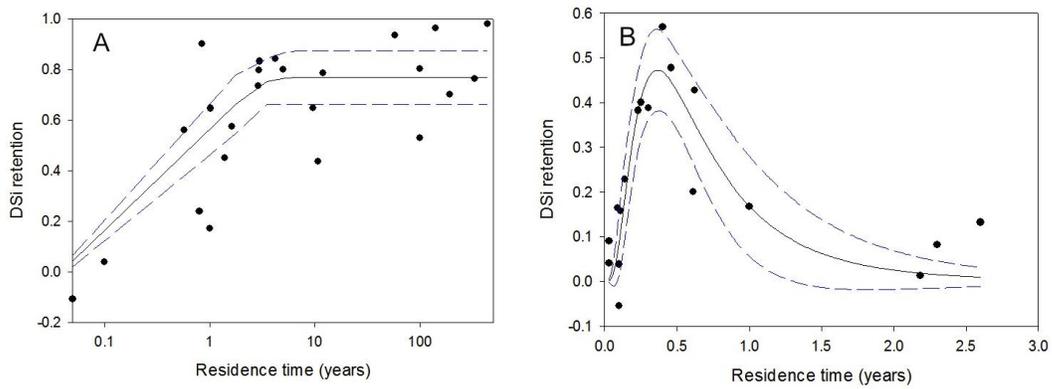
Figure AB3: a) Lake and b) reservoir DSi retentions predicted using Equations AB1 and AB2, respectively. Dashed lines indicated 95% confidence intervals.

Appendix C

Supplementary Material: Chapter 4

Derivation of nutrient loss parameter (σ)

The following is an abbreviated derivation of that originally provided by Vollenweider (1975), used to predict nutrient retention in lakes. The mass balance for a (non-volatile) substance in a lake or reservoir is:

$$\sum_{i=1}^{i} m_i - m_w - \sum_{s=1}^{s} m_s - \frac{dM_w}{dt} = 0 \qquad \text{(AC1)}$$

where M_w is the total mass of the substance in the lake/reservoir of volume V, m_i is the inflow flux of the substance to the lake/reservoir via the i-th river, m_w is the outflow flux of the substance, and $\sum_{s=1}^{s} m_s = S$ represents all processes removing the substance from the lake/reservoir water column, other than through the outflowing river.

In the case of P, Equation (AC1) applies to the total mass, or to the mass of any given compound or pool of compounds. Vollenweider (1975) explicitly states that, "if, e.g. the substances in question would be ortho-phosphate only, then $\sum_{s=1}^{s} m_s$ would contain also all transformations of PO_4 to other P-compounds." Thus, for TP in my mechanistic model (Figure 4.1), the $\sum_{s=1}^{s} m_s = S$ term includes the burial fluxes of POP, EP and UPP. For RP, the term includes the same burial fluxes, with the exception of burial of UPP ($F_{4,\text{bur}}$). Thus, we can expect numerically different $\sum_{s=1}^{s} m_s = S$ terms for TP and RP.

Assuming a first-order dependence, as in my model, $S = \sigma \times M_w$, Vollenweider then obtains

$$\frac{dM_w}{dt} = \sum_{i=1}^{i} q_i[m_i] - q_w[m_w] - \sigma \times M_w \qquad \text{(AC2)}$$

where q_i is the inflow to the lake/reservoir via the i-th river, q_w is the outflow from the lake/reservoir, and $[m_i]$ and $[m_w]$ are the inflow and outflow concentrations of the substance of interest. For a perfectly mixed lake/reservoir, $[m_w]$ is equal to the average water column concentration, or $[m_w] = M_w/V$. In Equation (AC2), σ is the first-order rate constant for the total in-lake/in-reservoir removal flux S. In other words, σ accounts for all in-reservoir processes that remove the substance of interest from the water column.

By dividing all terms by V and solving the ordinary differential equation for steady state, we have:

164

$$m_w = \frac{m_i}{1 + \sigma \times \tau_r} \qquad\qquad (AC3)$$

where τ_r is the water residence time. Defining nutrient retention as:

$$R_m = \frac{m_i - m_w}{m_i} \qquad\qquad (AC4)$$

and substituting equation AC3 into AC4, we arrive at:

$$R_m = 1 - \frac{1}{1 + \sigma \times \tau_r} \qquad\qquad (AC5)$$

which is Equation 4.2. The equation applies to both RP and TP, but with σ values that are specific for RP and TP.
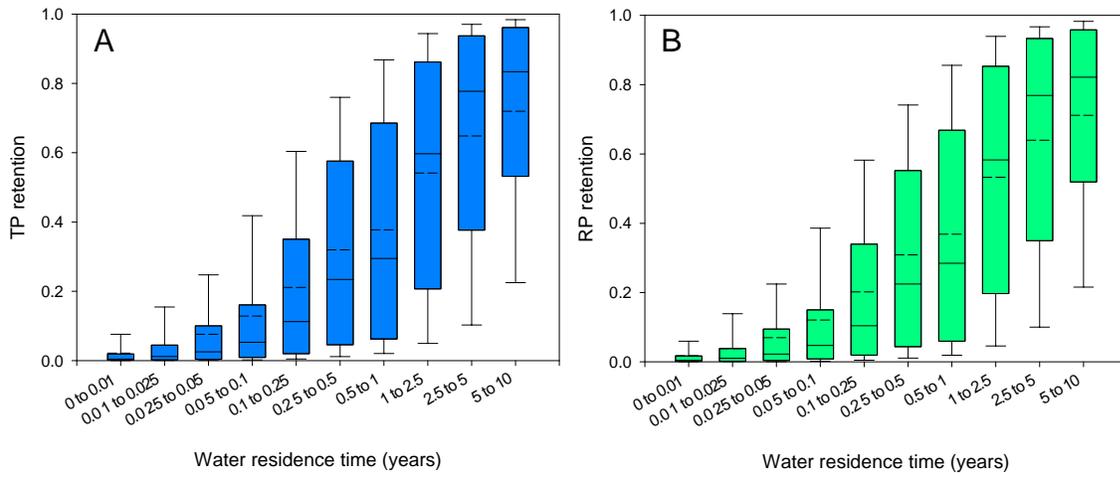
Figure AC1: Box-plots for (a) R_{TP} and (b) R_{RP} predicted by 6000 Monte Carlo simulations of the mass balance P model, plotted against the hydraulic residence time. Solid line within boxes indicates median, dashed line indicates mean, edges of boxes indicate 1st and 3rd quartiles, and whiskers are standard deviations.
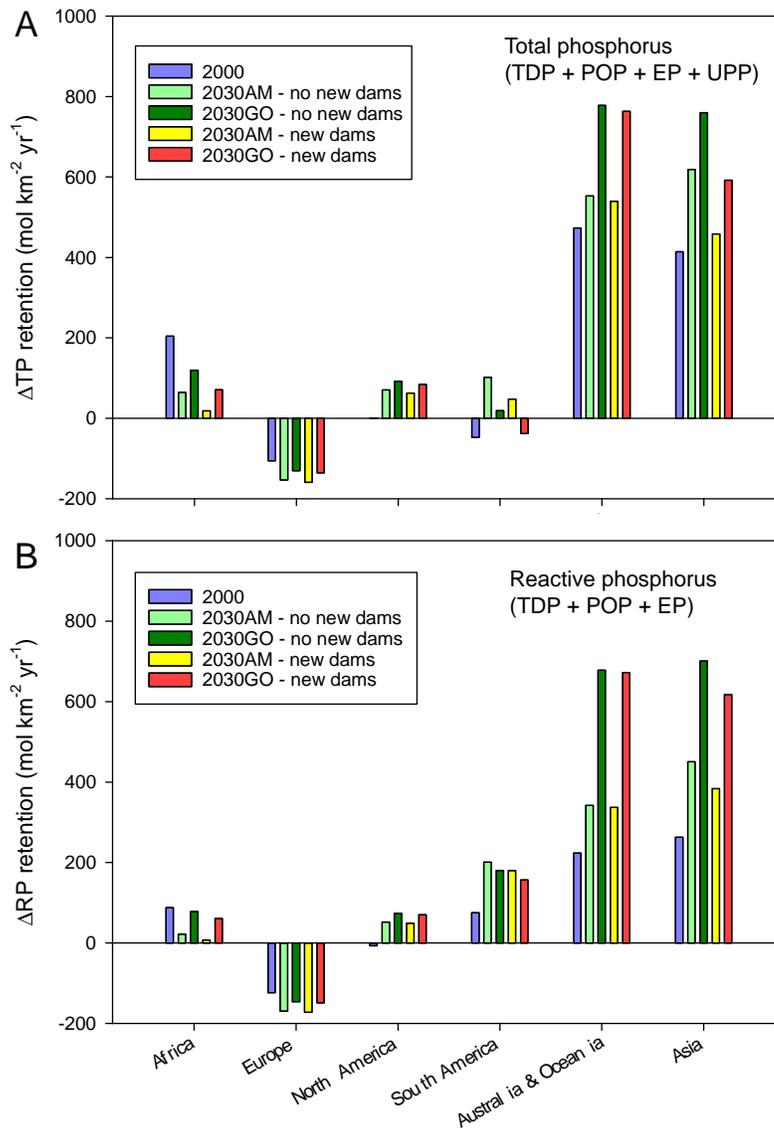
Figure AC2: Changes in net river export of (a) TP and (b) RP from the continents, normalized by the continental surface areas, relative to the corresponding 1970 values. Net export is defined as the difference between P loads to watersheds and P retained in reservoirs. The 2030 scenarios with "no new dams" consider only retention behind the GRanD database dams in the year 2000, while the 2030 scenarios with "new dams" consider both GRanD database dams (year 2000), plus new dams projected to be completed by 2030 (Zarfl et al., 2015).

Chapter 4 datasets

Datasets cited in Chapter 4 are available at the following link:

http://www.pnas.org/content/112/51/15603?tab=ds

The captions for each dataset are as follows:

Dataset S1: Literature database of P retention in dam reservoirs.

Dataset S2: Top 150 watersheds in terms of RP mass retained in dam reservoirs for year 2000.

Appendix D

Supplementary Material: Chapter 5

Table AD1: Parameters used to fit Equations 5.8, 5.9 and 5.12, 5.13 for all scenarios with statistically significant ($p<0.05$) R^2 values given.

Scenario	$POC_{bur,allo}$	$POC_{min,allo}$	$DOC_{min,allo}$	$POC_{bur,auto}$	$TOC_{min,auto}$
1970, 2000	$a = 0.8679$	$b = 0.1086$	$b = 1$	$a = 0.7505$	$b = 0.2428$
	$\alpha = 8.401$	$\beta = 0.2728$	$\beta = 0.0391$	$\alpha = 9.658$	$\beta = 0.3773$
	$R^2 = 0.82$	$R^2 = 0.25$	$R^2 = 0.74$	$R^2 = 0.60$	$R^2 = 0.25$
2030 AM	$a = 0.8635$	$b = 0.1119$	$b = 1$	$a = 0.7404$	$b = 0.2466$
	$\alpha= 8.279$	$\beta = 0.2791$	$\beta = 0.04084$	$\alpha = 9.995$	$\beta = 0.3728$
	$R^2 = 0.82$	$R^2 = 0.25$	$R^2 = 0.47$	$R^2 = 0.63$	$R^2 = 0.27$
2030 GO	$a = 0.8628$	$b = 0.1136$	$b = 1$	$a = 0.7417$	$b = 0.2463$
	$\alpha = 8.511$	$\beta = 0.2648$	$\beta = 0.04121$	$\alpha = 9.831$	$\beta = 0.3858$
	$R^2 = 0.82$	$R^2 = 0.26$	$R^2 = 0.34$	$R^2 = 0.62$	$R^2 = 0.25$
2030 OS	$a = 0.8672$	$b = 0.1089$	$b = 1$	$a = 0.7426$	$b = 0.2469$
	$\alpha = 8.439$	$\beta = 0.2835$	$\beta = 0.03818$	$\alpha = 10.05$	$\beta = 0.3667$
	$R^2 = 0.82$	$R^2 = 0.25$	$R^2 = 0.75$	$R^2 = 0.63$	$R^2 = 0.26$
2030 TG	$a = 0.8675$	$b = 0.1124$	$b = 1$	$a = 0.7402$	$b = 0.2471$
	$\alpha = 8.273$	$\beta = 0.2547$	$\beta = 0.03804$	$\alpha = 9.792$	$\beta = 0.4003$
	$R^2 = 0.82$	$R^2 = 0.25$	$R^2 = 0.80$	$R^2 = 0.62$	$R^2 = 0.25$
2050 AM	$a = 0.8593$	$b = 0.1180$	$b = 1$	$a = 0.7374$	$b = 0.2528$
	$\alpha = 8.447$	$\beta = 0.2547$	$\beta= 0.03969$	$\alpha = 9.881$	$\beta = 0.3802$
	$R^2 = 0.81$	$R^2 = 0.25$	$R^2 = 0.61$	$R^2 = 0.62$	$R^2 = 0.26$
2050 GO	$a = 0.8581$	$b = 0.1177$	$b = 1$	$a = 0.7375$	$b = 0.2523$
	$\alpha = 8.390$	$\beta = 0.2803$	$\beta = 0.03998$	$\alpha = 9.645$	$\beta = 0.3911$
	$R^2 = 0.81$	$R^2 = 0.25$	$R^2 = 0.71$	$R^2 = 0.63$	$R^2 = 0.26$
2050 OS	$a = 0.8605$	$b = 0.1167$	$b = 1$	$a = 0.7277$	$b = 0.261$
	$\alpha = 8.405$	$\beta = 0.2687$	$\beta = 0.03978$	$\alpha = 10.17$	$\beta = 0.3401$
	$R^2 = 0.82$	$R^2 = 0.27$	$R^2 = 0.60$	$R^2 = 0.59$	$R^2 = 0.26$
2050 TG	$a = 0.8626$	$b = 0.1135$	$b = 1$	$a = 0.7411$	$b = 0.2493$
	$\alpha = 8.368$	$\beta = 0.2723$	$\beta = 0.04036$	$\alpha = 9.569$	$\beta = 0.4009$
	$R^2 = 0.82$	$R^2 = 0.27$	$R^2 = 0.53$	$R^2 = 0.63$	$R^2 = 0.26$

Table AD2: Estimated stream order and corresponding upstream catchment area.

Stream order	Upstream catchment area (km^2)
1	<4
2	<15
3	<60
4	<250
5	<1000
6	<4000
7	<16000
8	<63000
9	<250000
10	<1x10^6

Table AD3: Model sensitivity analysis for autochthonous OC. % change represents the differences in global burial and mineralization fluxes, relative to the values obtained with the default parameters. Sensitivity of parameters used to calculate P is discussed in the Section 5.3.6.

Parameter	Default value	Imposed change	Burial % change	Min % change
Age	40 years	Set to 10 years	<1%	<1%
Latitude	35.0°	±10%	±4%	±9%
Elevation	300m	±10%	<1%	<1%
k_{bur}	7 yr^{-1}	±10%	±5%	±5%
Initial TOC mass	0 mol	Set to 1x10^6 mol	No effect	No effect
Temperature	19.6°C	+0.82°C	<1%	+2%
k_{20}	3 yr^{-1}	±10%	±3%	±8%

Table AD4: Model sensitivity analysis for allochthonous OC. % change represents the differences in global burial and mineralization fluxes, relative to the values obtained with the default parameters.

| Parameter	Default value	Imposed change	Burial % change	DOC min % change	POC min % change
Age	40 years	Set to 10 years	No effect	No effect	No effect
Inflow POC concentration	10 µM	±10%	No effect	No effect	No effect
Inflow DOC concentration	5.71 ppm	±10%	No effect	No effect	No effect
Latitude	35.0°	±10%	±1%	±4%	±8%
Elevation	300m	±10%	<1%	<1%	<1%
k_{bur}	7 yr^{-1}	±10%	±3%	No effect	±6%
k_{hyd} (hydrolysis rate constant)	0.1 yr^{-1}	±10%	<1%	No effect	<1%
Initial POC and DOC mass	0 mol	Both set to 1x10^6 mol	No effect	No effect	No effect
Temperature	19.6°C	+0.82°C	<1%	+1%	+2%
k_{20}	1 yr^{-1}	±10%	±9%	±9%	±4%
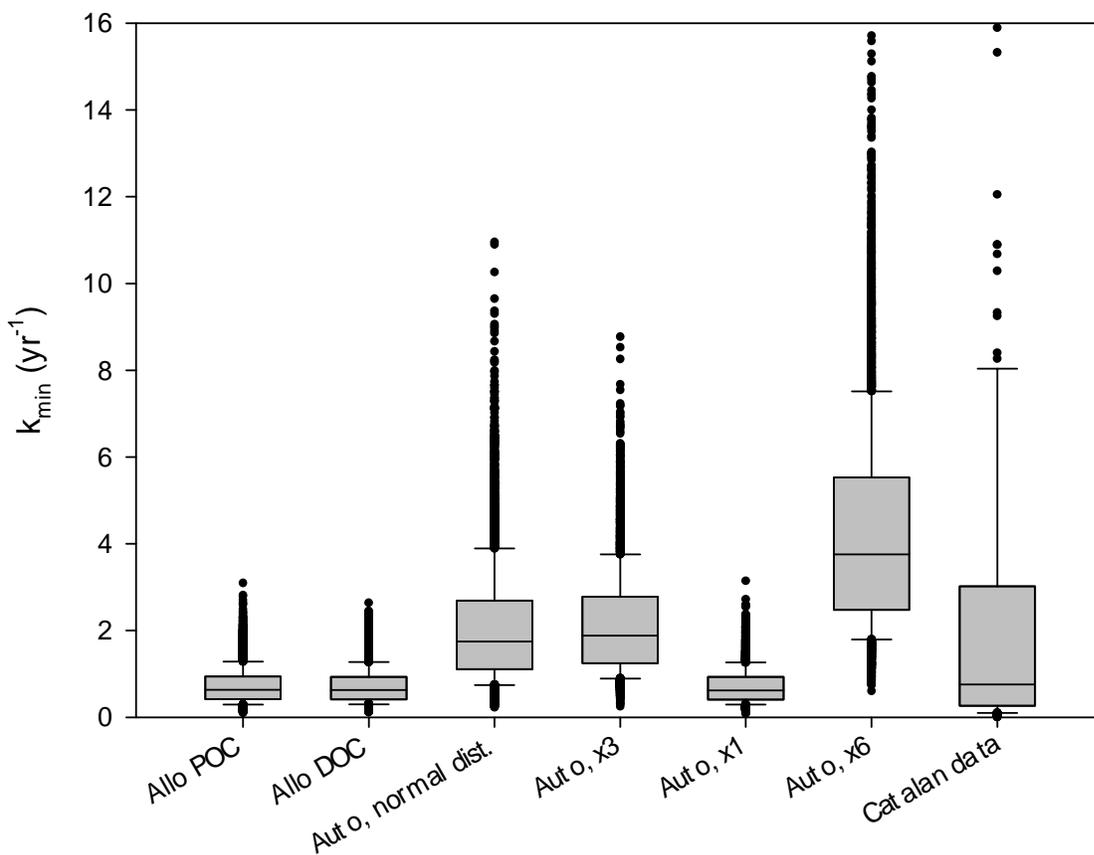
Figure AD1: Comparison between k_{min} values generated by the Monte Carlo (MC) procedure used in my model and the k_{min} values obtained independently by Catalan et al. (2016) from a global data compilation. The first three boxes to the left show the output of the MC analysis with the default model constraints (Table AD1). The boxes labelled "Auto, x3", "Auto, x1", and "Auto, x6" show additional outputs of MC analyses where the reactivity of autochthonous OC is assumed to be 3 times higher, equal, and 6 times higher than that of allochthonous OC, respectively. The last box shows the k_{min} distribution of Catalan et al., which lumps together values for POC and DOC, and for allochthonous and autochthonous OC. For clarity, extreme outliers of the Catalan data are not shown. Note that the default scaling factor of 3 used in the OC reservoir model (i.e., imposing a mean k_{min} value 3 times higher for autochthonous than allochthonous OC) is consistent with the observed k_{min} distribution of Catalan et al., while this is not the case for the lower (equal reactivity) or higher (6 times higher) scaling factors. Solid lines represent median values, box edges represent 1 standard deviation and whiskers represent 1st and 3rd quartile.

172
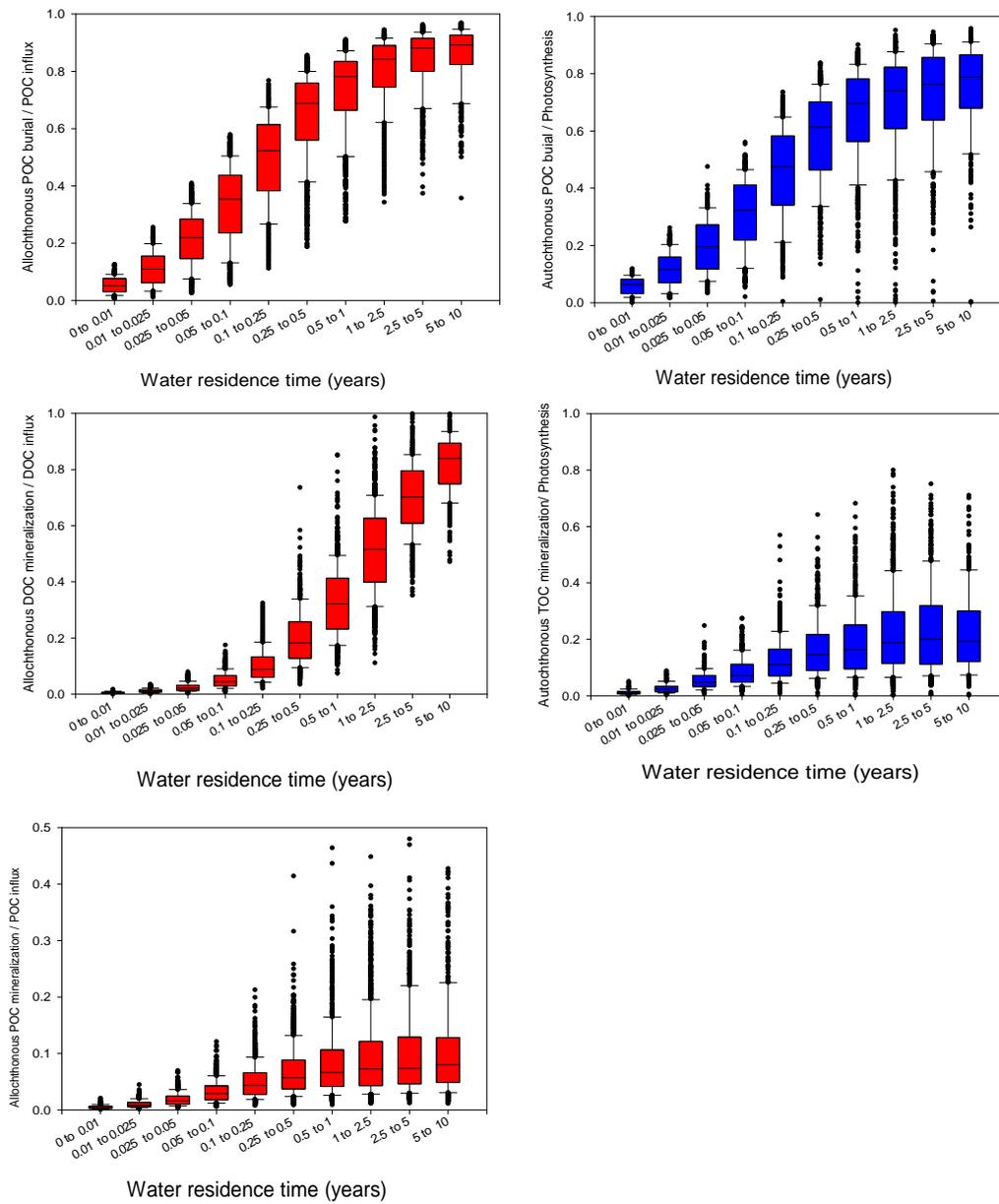
Figure AD2: Relative allochthonous and autochthonous burial and mineralization fluxes (normalized by P or POC or DOC influx) generated by the 6000 Monte Carlo iterations for years 1970 and 2000, and binned by water residence time. Solid lines represent median values, box edges represent 1 standard deviation and whiskers represent 1st and 3rd quartile.
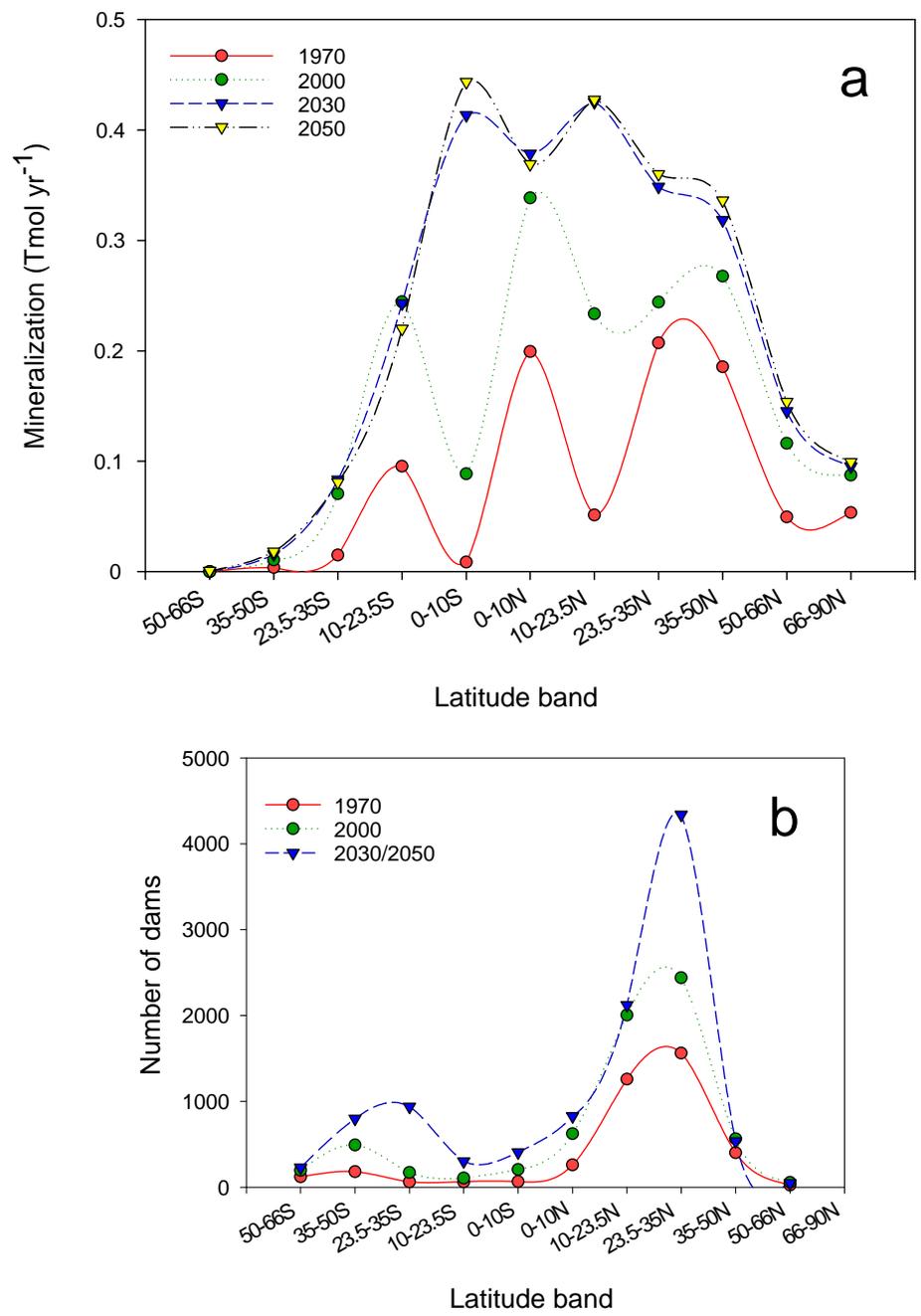
Figure AD3: (a) Reservoir OC mineralization fluxes by latitude band, excluding short-term degradation of flooded material, and (b) distribution of dams by latitude. Note that the number of dams in 2050 is assumed to be equal to that in 2030.

Chapter 5 dataset

Supplementary Data 1 is available in the Supplementary Material for Maavara et al. (2017)